2013

A Molecular-Level View of the Sorting of Lipidated Peptides and the Origin of Cholesterol's Condensing Effect in Fluid Bilayers

Trevor Daly
Lehigh University

A Molecular-Level View of the Sorting of Lipidated Peptides and the Origin of Cholesterol's Condensing Effect in Fluid Bilayers

by

Trevor A. Daly

A Dissertation

Presented to the Graduate and Research Committee

of Lehigh University

in Candidacy for the Degree of

Doctor of Philosophy

in

Chemistry

Lehigh University

2013

Approved and recommended for acceptance as a dissertation in partial fulfillment of the requirements for the degree of Doctor of Philosophy

Trevor A. Daly
A Molecular-Level View of the Sorting of Lipidated Peptides and the Origin of Cholesterol's Condensing Effect in Fluid Bilayers

_____

Defense Date

_____

Steven L. Regen, Ph. D.
Dissertation Director

Approved Date

Committee Members:

_____

Robert A. Flowers II, Ph. D.

_____

Kerney Jebrell Glover, Ph. D.

_____

Linda J. Lowe-Krentz, Ph. D.

ACKNOWLEDGMENTS

I wish to express my gratitude to the faculty of Lehigh University for their contributions to my graduate education, especially Dr. Steven Regen for his mentorship, guidance, and patience throughout my graduate career. I would also like to thank the members of my dissertation committee, Dr. Linda Lowe-Krentz, Dr. Robert Flowers, and Dr. K. Jebrell Glover for their assistance. I would also like to thank Dr. Paulo Almeida (University of North Carolina, Wilmington) for his contributions to the studies discussed in this disssertation.

Special thanks to all of the past and present members of the Regen group, whose help, advice, and friendship have been invaluable. Particular gratitude is due to Dr. Vaclav Janout, Dr. Serhan Turkyilmaz, and Dr. Ravil Petrov for numerous insightful conversations.

Finally, I thank my family for their love and encouragement. None of this work would have been possible without the constant support of my parents, William and Lucille Daly, my wife Shamina Chasteen, and my children, Isaiah and Shane Daly.

TABLE OF CONTENTS

LIST OF FIGURES

LIST OF TABLES

LIST OF SCHEMES

LIST OF ABBREVIATIONS

25-OH	25-hydroxy cholesterol
7β-OH	7β-hydroxy cholesterol
AEDP	3-((2-aminoethyl)dithio)propionic acid
AFM	atomic force microscopy
Boc	*tert*-butyl carbamate
CHAPS	3-[(3-cholamidopropyl)dimethylammonio]-1-propanesulfonate
CTB	cholera toxin subunit B
DCC	*N,N′*-dicyclohexylcarbodiimide
DIPEA	*N,N*-diisopropylethylamine
DLS	dynamic light scattering
DMPC	1,2-myristoyl-*sn*-glycero-3-phosphocholine
DOPC	1,2-oleoyl-*sn*-glycero-3-phosphocholine
DPPC	1,2-palmitoyl-*sn*-glycero-3-phosphocholine
DPPE	1,2-palmitoyl-*sn*-glycero-3-phosphoethanolamine
DPPG	1,2-palmitoyl-*sn*-glycero-3-phosphoglycerol
DSC	differential scanning calorimetry
DSPC	1,2-stearoyl-*sn*-glycero-3-phosphocholine
DTT	dithiothreitol
EDC	1-ethyl-3-(3-dimethylaminopropyl)carbodiimide
EDTA	Ethylenediaminetetraacetic acid
FCS	fluorescence correlation spectroscopy
FRAP	fluorescence return after photobleaching
FRET	Förster resonance energy transfer
GDP	guanosine diphosphate
GP	generalized polarization

GPI	glycosylphosphatidylinositol
GPMV	giant plasma membrane vesicle
GTP	guanosine triphosphate
GUV	giant unilamellar vesicle
HOBT	Hydroxybenzotriazole
HPLC	high performance liquid chromatography
HR-ESI	high resolution electrospray ionization
l_d	liquid disordered
l_o	liquid ordered
LUV	large unilamellar vesicle
MALDI	matrix assisted laser desorption ionization
MS	mass spectroscopy
NHS	*N*-hydroxysuccinimide
NMR	nuclear magnetic resonance
NNR	nearest neighbor recognition
NSOM	near-field scanning optical microscopy
PC	phosphocholine
PE	phosphoethanolamine
POPC	1-palmitoyl-2-oleyol-*sn*-glycero-3-phosphocholine
STED	stimulated emission depletion microscopy
TCEP	*tris*(2-carboxyethyl)phosphine
TEA	triethylamine
TFA	trifluoroacetic acid
THF	tetrahydrofuran
TLC	thin layer chromatography
TOF	time of flight
TRIS	*tris*(hydroxymethyl)aminomethane

ABSTRACT

The lateral organization of lipids in cell membranes is one of the most vexing problems facing chemists, biologists, and biophysicists today. Among the techniques used to probe membrane organization, the Nearest Neighbor Recognition (NNR) method developed in our laboratory is unique in its ability to provide quantitative, molecular level information about the interactions between lipids in a bilayer. The NNR method was applied to two problems of biological relevance: "lipid sorting," *i.e*. the partitioning of membrane components into discrete domains, and the origin of cholesterol's condensing effect.

Lipid sorting was probed by measuring the free energy of interaction between a mimic of the known raft associating peptide motif [(myristoyl)GlyCys(palmitoyl)], as well as an analogous peptide bearing an unsaturated acyl chain, and mimics of 1,2-dipalmitoyl-sn-glycero-3-phosphocholine (DPPC) and cholesterol. The NNR results, which represent the first direct measurement of lipidated peptide-lipid interaction energies, were then used in Monte Carlo simulations to produce a physical picture of the partitioning of the peptide between liquid ordered (l_o) and liquid disordered (l_d) domains in a model membrane. The peptide motif [(myristoyl)GlyCys(palmitoyl)] mixed ideally across both domains, while the analogous peptide bearing an unsaturated acyl chain was found to have a slight preference for l_d domains. The lack of a clear preference for the l_o phase suggests that hydrophobic interactions between lipidated proteins and membrane lipids may be less important than previously hypothesized for lipid sorting, with other factors such as hydrogen bonding potentially playing a greater role.

The origin of cholesterol's condensing effect was revealed via the use of NNR measurements to compare the relative condensing power of three sterols: cholesterol, coprostanol, and dihydrocholesterol. Contrary to what is predicted by the widely accepted "umbrella model," coprostanol was found to be a weaker condensing agent than the other sterols, despite its larger cross-sectional area. To explain this observation, we propose a "template model" for cholesterol's condensing effect, wherein the rigid planar core acts as a template upon which the acyl chains of phospholipids can extend and condense, maximizing hydrophobic contact.

Chapter 1

Introduction

1.1 Membrane Structure

Cellular membranes consist of a complex mixture of lipids and proteins. Classically, the arrangement of these components has been described by the "fluid mosaic" model.[1] In this model, the lipids of the membrane form a homogenous fluid bilayer. The lipids diffuse rapidly in the plane of the bilayer, but diffusion from one leaflet to the other is slow. Unlike earlier models which described all of the membrane proteins as forming monolayers encasing both sides of the lipid bilayer, the fluid mosaic model calls for two distinct classes of membrane proteins: *peripheral proteins*, which are bound to the exterior of the bilayer, and *integral proteins,* which are inserted directly into the phospholipid matrix, and may span one or both leaflets of the bilayer.

When it was first proposed in 1972, the fluid mosaic model gained widespread acceptance. In recent years, however, it has been largely replaced by a "lipid raft" model.[2,3] In this view of membrane organization, the lipid bilayer is not a homogenous mixture. Nanoscale domains rich in cholesterol, sphingolipids, other high-melting lipids, and certain proteins, float like rafts in a sea of low-melting lipids. Lipid rafts have been suggested to be the site of cellular signaling events, as they would allow proteins to be brought into close proximity.[4,5]

Because lipid rafts in cell membranes are thought to be too small (10-100 nm in diameter)[3] to be resolved optically, evidence for their existence is mostly inferential. Detergent resistance experiments, in which fractions of membrane lipids enriched in sphingolipids, cholesterol, and certain membrane proteins are shown to resist extraction

by cold detergents, provided the initial evidence for the presence of discrete membrane domains.[6] Detergent resistance experiments are frequently used to measure the affinity of specific lipids or proteins for raft domains.[7,8] However, due to the destructive nature of such experiments and the low temperatures used (typically 4 ^{o}C) there are lingering questions as to whether detergent resistance correlates to native membrane organization.[9]

More recently, advances in microscopy technologies have provided evidence for transient, nanoscale domains in cellular membranes.[3,10] Eggeling and coworkers have used Stimulated Emission Depletion Microscopy (STED) in Fluorescence Correlation Spectroscopy (FCS) experiments to show that sphingolipids in live cells become transiently trapped in domains with an estimated radius of less than 20 nm.[11] The use of STED achieves a smaller focal volume than tradition FCS experiments, permitting the resolution of nanometer scale domains. Similar techniques using Near-Field Scanning Optical Microscopy (NSOM) have also been used to detect the entrapment of sphingolipids in nanoscale domains in live cells.[12] Additional studies using advanced Förster Resonance Energy Transfer (FRET) and Fluorescence Return After Photobleaching (FRAP) techniques have detected clustering of certain lipid anchored proteins in cholesterol dependent nanoscale domains in cell membranes.[13,14] Taken together, these findings represent the strongest evidence yet for the existence of raft-like domains in live cells.

While lipid rafts in cells remain a controversial idea, phase separation in model membranes is well-studied. Phase diagrams have been published for model systems consisting of binary and ternary mixtures of lipids.[15] Phase separation on a large enough scale to be visualized by fluorescence microscopy has been seen in model membranes

prepared from pure lipids. Many of these systems exhibit coexisting fluid phases, called the liquid disordered (l_d) and liquid ordered (l_o) phases. The liquid ordered phase, like the putative lipid rafts in live cells, is enriched in cholesterol and characterized by slower lateral diffusion of lipids, a thicker membrane, and more fully extended lipid acyl chains than the l_d phase. For this reason, the l_o phase is considered a useful model of a lipid raft. It should be noted, however, that l_o domains are distinct from lipid rafts, and raft associating proteins have been shown to be excluded from l_o domains in certain model systems.[16,17]

A complete understanding of the origin of phase separation in both cells and model membranes depends on the precise measurement of lipid-lipid interactions in the membrane. Among the numerous techniques used to study lipid interactions in model membranes, including differential scanning calorimetry, fluorescence resonance energy transfer, isothermal titration calorimetry, and analyses of phase diagrams, the Nearest Neighbor Recognition (NNR) method is unique in its ability to quantitatively measure interaction energies without relying on comparison to theoretical curves.[15] Nearest Neighbor Recognition experiments are sensitive enough to measure differences in interaction energy of tens of calories per mole. Nearest Neighbor Recognition thus has unique potential for gaining insight into the molecular level organization of model membranes.

1.2 The Nearest Neighbor Recognition Method

The NNR method was developed in our laboratory as a tool to measure molecular interaction energies between lipids in a phospholipid bilayer.[18] This method, depicted in

Scheme 1, measures the thermodynamic tendency of two lipids to become nearest neighbors. Dimers consisting of two lipid molecules (**A** and **B**) connected via a disulfide bond are incorporated into a bilayer and allowed to undergo thiolate-disulfide exchange, resulting in an equilibrium mixture of the heterodimer (**AB**) and the two homodimers (**AA** and **BB**). This equilibrium is governed by an equilibrium constant, *K*, given by the equation $K = [AB]^2/([AA][BB])$. If lipids **A** and **B** mix ideally, this will result is a statistical distribution of dimers, reflected by a *K* value of 4. If hetero-association is favored, however, K will be greater than 4, and if homo-association is favored *K* is less than 4. Furthermore, taking statistical considerations into account, the nearest neighbor interaction free energies between **A** and **B** are then given by $\omega_{AB} = -\frac{1}{2}RT \ln(K/4)$. Values of ω_{AB} are the primary information sought in NNR experiments, and can be used in Monte Carlo simulations to produce a physical picture of membrane organization.

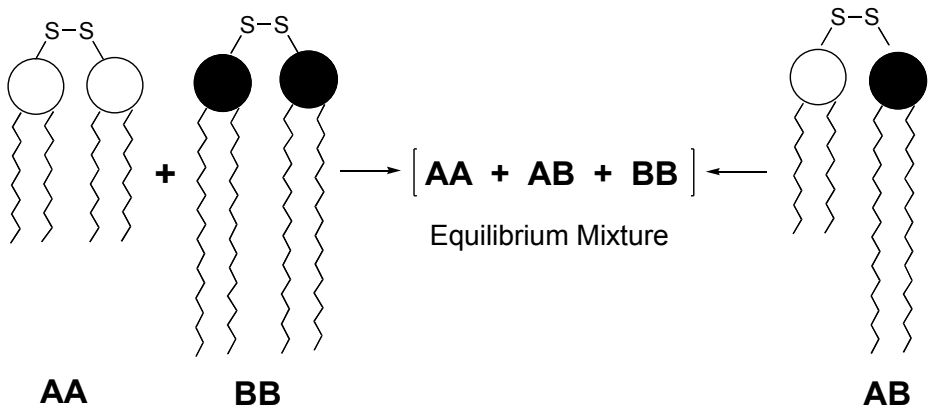

Scheme 1: Stylized illustration of the NNR method

The NNR method is unique in its ability to provide quantitative measurements of nearest neighbor interaction free energies in model membranes, and is sensitive enough to measure energy differences as small as tens of calories per mole.

In addition to measurements of ω_{AB}, NNR has been shown to be useful as a "chemical sensor" to probe the state of a membrane.[19] When small amounts (~5 mol%) of exchangeable lipid dimers are included in a host membrane of non-exchangeable lipids, the resulting *K* value is very sensitive to changes in the structure of the host membrane. For example, NNR experiments were conducted in host membranes consisting of 1,2-dipalmitoyl-*sn*-glycero-3-phosphocholine (DPPC) and cholesterol using the exchangeable lipids shown in Figure 1, **cho** (an exchangeable mimic of cholesterol) and **16PL** (an exchangeable mimic of a 16 carbon phospholipid).

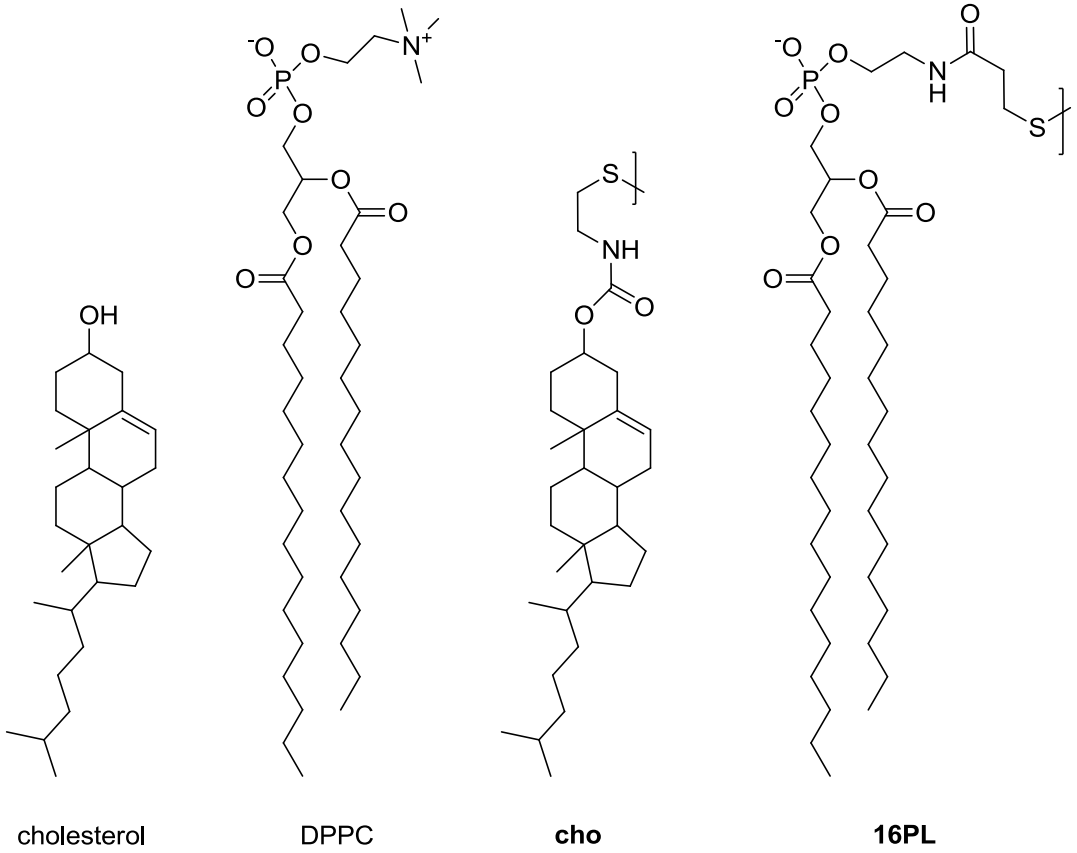

Figure 1: Structures of cholesterol, DPPC, and exchangeable lipids **cho** and **16PL**

As shown in Figure 2, the observed *K* values were found to be dependent on the cholesterol content of the host membrane.[19] At sterol concentrations below 14 mol%,

when the host membrane is in the liquid disordered phase (l_d), a K of ~3.7 was observed, while host membranes in the liquid ordered phase (l_o) exhibited a K of ~5.5. The observed K value can therefore be considered a measure of the compactness of the host membrane, with a more condensed membrane having in a larger value K. This "chemical sensor" application of NNR makes it a sensitive tool for detecting changes in the organization of a phospholipid membrane.

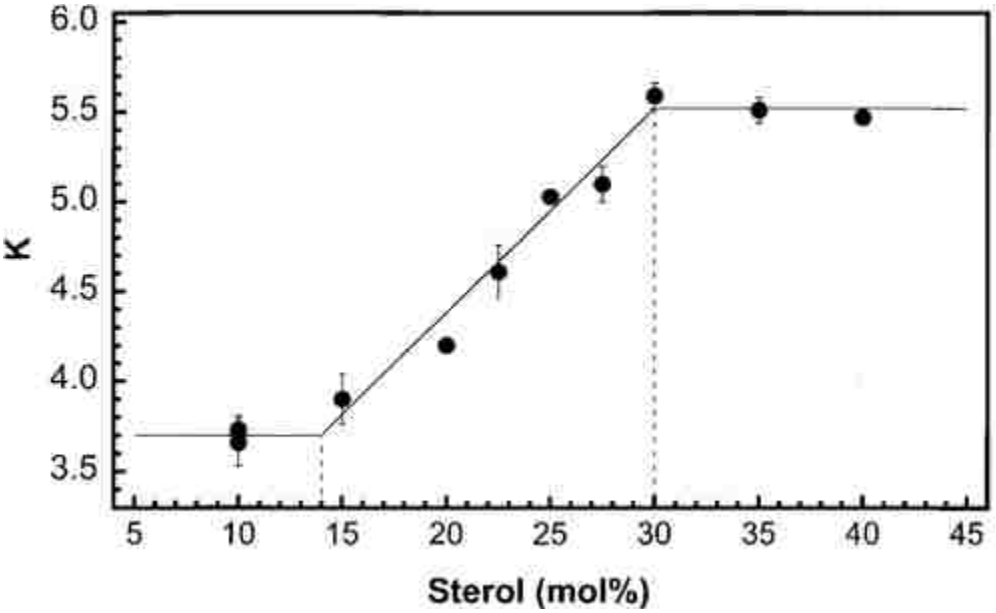

Figure 2: Plot of K versus the mol % of total sterol present in bilayers made from 95 mol % of non-exchangeable lipids (i.e., DPPC plus varying percentages of cholesterol) and 5 mol % of exchangeable lipids (2.5 mol % of **cho** and 2.5 mol % of **16PL**)[19]

In recent years, NNR has been applied to a variety of biologically relevant questions, including the detection of cross-talk in membranes,[20] the mechanism of action of general anesthetics,[21-23] and the effect of oxidative stress on membrane fluidity.[24] In this thesis, two significant problems of biological relevance, lipid sorting of peripheral proteins, and the origin of cholesterol's condensing effect, have been investigated using the NNR method.

Chapter 2

Lipid Sorting

2.1 Background

An estimated 25-40% of eukaryotic proteins are membrane bound.[25] These proteins are divided into two classes: integral proteins, having one or more transmembrane domains that penetrate one or both of the membrane leaflets, and peripheral proteins, which are otherwise soluble proteins anchored to the membrane by a covalently attached hydrophobic moiety. Among the most common anchors (shown in Figure 3) are (i) myristoylation – attachment of a 14 carbon acyl chain to an N-terminal glycine residue via an amide bond, (ii) S-acylation (palmitoylation) – a thioester bond attaching an acyl chain, typically 16 carbons long, to the sulfur of a cysteine residue, (iii) prenylation – a 15 carbon (farnesylation) or 20 carbon (geranylgeranylation) isoprenoid unit linked via a thioether bond to a cysteine residue, and (iv) cholesteroylation – a cholesterol moiety found on the carboxyl group of a C-terminal glycine residue.[26] In addition, peripheral proteins can be anchored to the membrane by glycosylphosphatidylinositol (GPI) anchors,[27] a conserved oligosaccharide core coupled to a phosphoinositide moiety bearing two or three acyl chains (Figure 4). The oligosaccharide core may also be modified with additional branching sugars or ethanolamine phosphate groups. Among these lipid anchors, palmitoylation is unique in that it is dynamically controlled (*i.e.* the palmitoyl chain is added and removed enzymatically and is not present for the entire lifetime of the protein).[26]

Lipid Anchor	Amino Acid Modified	Structure
myristic acid	N-terminal glycine	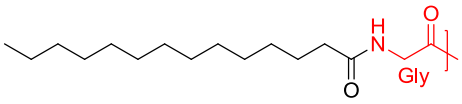
palmitic acid	cysteine	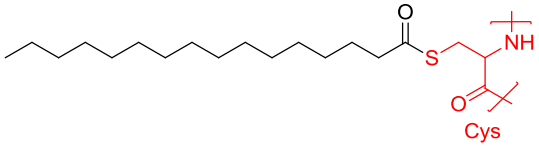
farnesyl group	C-terminal cysteine	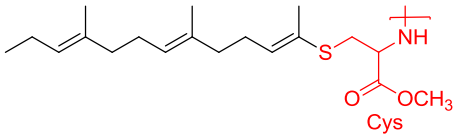
geranylgeranyl group	C-terminal cysteine	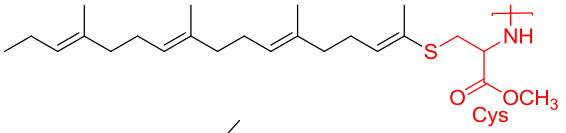
cholesterol group	C-terminal glycine	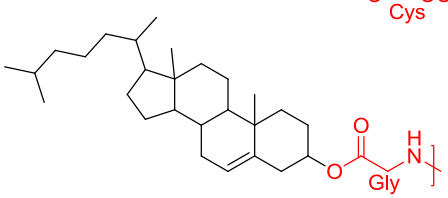

Figure 3: Structures of several common membrane anchors (figure adapted from ref. **26**)

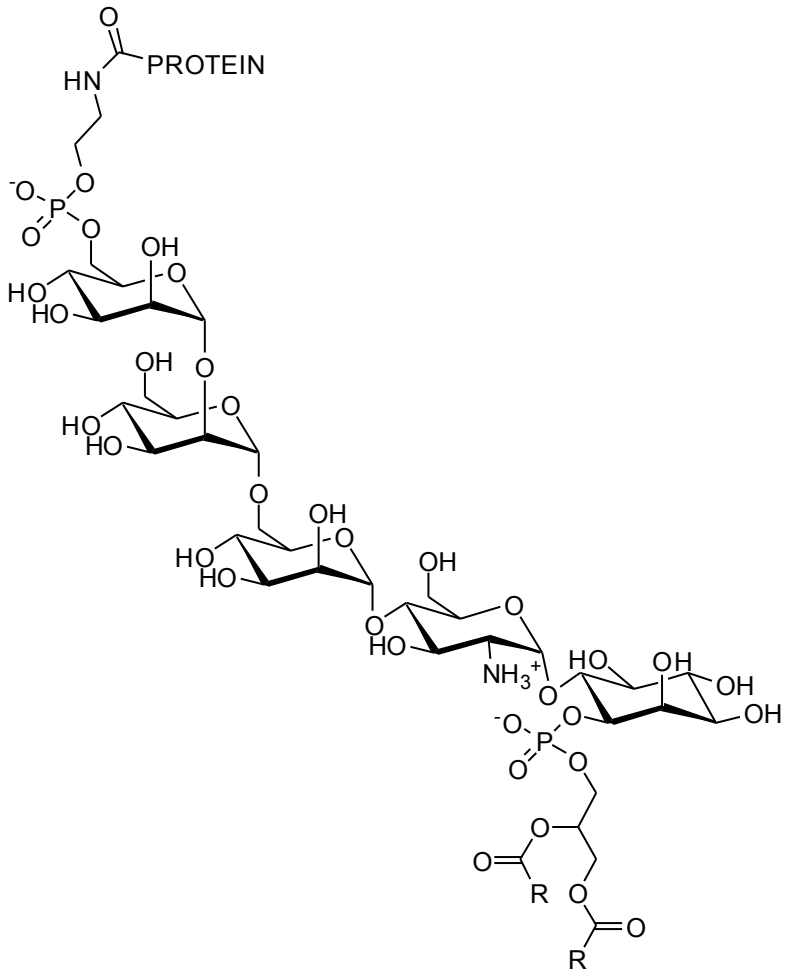

Figure 4: Structure of a GPI anchored protein. R=a saturated acyl chain. The 2-OH position on the inositol ring may also be acylated with a palmitoyl chain

Due to the diversity of anchor structures and the enzymatic control of palmitoylation, it has been suggested that along with conferring membrane association to proteins, these anchors act to direct proteins to specific regions of the cell for proper functioning. Achieving an understanding of the processes by which these lipid anchors of membrane proteins serve to separate and direct proteins to their targeted domains (*i.e.* lipid sorting) is a major problem facing biochemists and biophysicists today.

The earliest evidence for raft association of membrane proteins came from detergent resistance experiments (see Section 1.1). [7,8] Detergent resistance has been used

extensively as an indicator of raft affinity in both live cells and model membranes for a large variety of proteins, including GPI anchored proteins, palmitoylated proteins, and cholesterol anchored proteins (for a review see reference 28). Despite its widespread use, detergent resistance has several drawbacks as a method for measuring raft association. Because of the destructive nature of detergent resistance experiments, it is not clear to what extent the composition of the detergent resistant fraction represents the native lipid rafts.[9] The low temperatures used in detergent resistance experiments also call their relevance to physiological membranes into question.[9] Detergent resistance varies depending on the detergent extraction procedure used as well. Some GPI anchored proteins, for example, have been shown to be resistant to extraction by Triton X-100, but not 3-[(3-cholamidopropyl)dimethylammonio]-1-propanesulfonate (CHAPS).[29] Finally, detergent resistance experiments are qualitative measures of raft association, no quantitative partition coefficient can be obtained.

A complementary approach to detergent resistance involves the use of fluorescence microscopy to visualize domain partitioning in model membranes. Giant unilamellar vesicles (GUVs), typically prepared from a ternary mixture of cholesterol, a high-melting lipid such as DPPC or sphingomyelin, and a low melting lipid such as POPC, exhibit phase separation into large scale (micrometer sized) l_o and l_d domains.[30] Partitioning of fluorescently labeled proteins can thus be directly visualized in these systems. Large scale phase separation can also be induced in model systems through the cross-linking of known raft components to form large domains. Cross-linking of the ganglioside GM_1 by the pentavalent ligand cholera toxin subunit B (CTB), for example, has been used to induce the formation of large l_o domains in model membranes that show

no phase separation in the absence of CTB.[16,31] Like detergent resistance, fluorescence microscopy has found widespread use as a tool to gauge raft partitioning of many proteins, including palmitoylated and farnesylated peripheral protiens,[32,33] transmembrane domains,[34-36] and GPI anchored proteins.[37]

The composition of simple model systems may be a poor mimic of the rich compositional diversity found in cell membranes. Recently, Giant Plasma Membrane Vesicles (GPMVs)[38] and Plasma Membrane Spheres (PMSs),[31] model systems prepared by chemically separating some or all of the membrane from an intact cell, have been used for fluorescence microscopy experiments. These systems offer raft-like domains compositionally similar to those thought to exist in live cells, and thus represent the best available model system. However, there is some ambiguity in the results of experiments in these systems, as the phase separation properties of the model systems depend strongly on the method of preparation,[39] and significant differences in the partitioning of some anchored proteins has been observed even in different GPMVs prepared by identical methods.[40] In addition, fluorescence microscopy experiments in GUVs, GPMVs, and PMSs all rely on micron-sized domains which can be readily visualized. The relevance such domains may have to nanoscale lipid rafts remains unclear.

Several other techniques are less commonly used to probe lipid sorting in both model membranes and live cells. Atomic Force Microscopy has been used to visualize the clustering of proteins in l_d domains in supported bliayers.[41] As noted above (see Section 1.1), recent advances in FRET, FRAP, and FCS have been used to track sorting of GPI anchored proteins into raft-like domains. Fluorescence quenching assays have been used to probe the relative affinity of a variety of small lipidated peptides toward l_o

domains in model membranes.[42] Recently, Chao and Daniel have reported the use of a micro fluidic device to measure the kinetics of the sorting of lipid probes between supported bilayers of l_o and l_d membranes.[43] The diversity of available techniques places the concept of lipid sorting on firmer ground, but all of these techniques suffer from some of the same inherent drawbacks as detergent resistance experiments and microscopy in GUVs, including the reliance on micron sized domains and the inability to determine a partition coefficient.

To see how all of these techniques can be applied to gain insight into protein functioning via studies of lipid sorting, let us consider the Ras family of GTPase proteins as a "case study." The Ras GTPases are a family of peripheral membrane proteins involved in signal transduction.[44] Misregulated Ras signaling has been implicated in ~30% of human cancers.[41] These enzymes hydrolyze guanosine triphosphate (GTP), producing guanosine diphosphate (GDP). Three Ras isoforms are common in mammalian cells, H-Ras, N-Ras, and K-Ras. These isoforms have homologous GTP binding regions (called the *G-domain*), and differ only in the *hypervariable region*, the 23 C-terminal residues. The hypervariable region is comprised of the signal sequence for the attachment of the membrane anchors, as well as a linker region that connects the membrane anchor region to the G-domain. All three isoforms have a farnesyl anchor, N-Ras and H-Ras also have additional palmitoylation sites. The hypervariable domain of K-Ras also includes a polybasic region of six consecutive lysine residues. These differences in the structure of the part of the protein that interacts with the membrane suggest that the various isoforms may sort into different membrane domains.

To examine the sorting of Ras proteins, Hancock and coworkers conducted a series of studies using detergent resistance, as well as a similar separation technique based on fractionation of membrane proteins over a sucrose gradient.[45,46] It was discovered that H-Ras associates with rafts when it is in its inactivated (GDP bound) state, but in its activated (GTP bound) form is excluded from rafts. Conversely, K-Ras remains outside of rafts, regardless of bound nucleoside.[45,46] These detergent resistance results were confirmed using an immuno-imaging procedure in which the distribution of Ras proteins on the membrane surface was visualized by electron microscopy of gold nanoparticles attached to anti-Ras antibodies.[45,46] More recently, the preference of K-Ras for non-raft domains has been confirmed using both fluorescence microscopy in GUVs and AFM studies in model membranes.[32] Fluorescence microscopy, surface plasmon resonance, and AFM have also shown N-Ras to favor disordered domains regardless of the GTP/GDP binding state, or palmitoylation state.[33,47] Unlike K-Ras, however, N-Ras was shown to form clusters at the interface of l_o and l_d domains in AFM experiments. The differences in the hypervariable regions therefore dictate that the three isoforms cluster in three distinct regions of the cell. Taken together, these results can explain how, despite their conserved G-domain, these three proteins can have different signal outputs.

While studies like those done the Ras family of proteins can improve our understanding of protein function via a study of lipid sorting, there is still remarkably little understanding of the basic mechanistic principles of lipid sorting. Because of the qualitative nature of most of the methods for measuring protein partitioning between domains, very little work has been done to determine how the structure of specific lipid

anchors influences lipid sorting. In one such investigation, Silvius and coworkers used a fluorescence quenching assay in model membranes, as well as detergent resistance experiments in cells, to measure the relative partitioning of several small lipidated peptides.[42] In this study, small peptides bearing a variety of lipid anchors were fluorescently labeled and incorporated in model membranes containing TEMPO-DOPC, a lipid bearing a quenching group which is known to partition into disordered domains. For each lipidated peptide, plots of fluorescence intensity as a function of TEMPO-DOPC concentration were prepared, where the shape of such "quenching curves" is indicative of the partitioning of the fluorescent lipid. Partitioning of the probe into l_o domains results in upward concavity in the quenching curve, while partitioning into l_d domains results in downward concavity. Based on the shape of their fluorescence quenching curves, several lipidated probes were ranked by their relative preference for the l_o phase. It was found that both the structure of the lipid anchors and the spacing between anchors influenced the partitioning of the peptides. A tripeptide consisting of an N-terminal glycine acylated with a myristoyl chain, followed by a palmitoylated cysteine residue and another glycine bearing the fluorescent tag, ([(myristoyl)GlyCys(palmitoyl)Gly]-caBim, Figure 5) was found to be the smallest motif which could be demonstrated to consistently prefer l_o domains in both fluorescence quenching and detergent resistance experiments. It should be noted that while it does measure the *relative* affinity for the l_o phase for the peptides, the fluorescence quenching technique does not provide an absolute partition coefficient. In addition, this method relies on a "top down" measurement of the fluorescence of entire liposomes, and as such does not provide any insight into the molecular level interactions that drive lipid sorting.

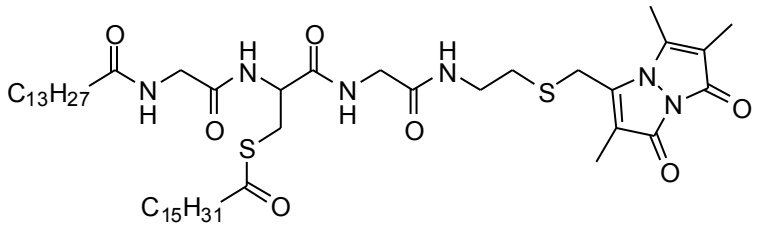

Figure 5: Structure of [(myristoyl)GlyCys(palmitoyl)Gly]-caBim

The aim of the work reported in this thesis was to develop a quantitative approach to lipid sorting by taking a "bottom up" approach to the measurement of peptide partitioning. Molecular interaction energies between lipidated peptides and lipids were measured using the NNR method. These energy measurements give insight into the interactions that are thought to drive lipid sorting. The measured interaction energies were then used in Monte Carlo Simulations to provide a physical picture of membrane organization. *This combination of NNR measurement and Monte Carlo simulation is a powerful new tool for the study of lipid sorting, which allows the quantitative determination of partition coefficients and is not limited to macroscale phase separated models.*

2.2 Experimental Design

The experimental approach described in this chapter details how NNR experiments were expected to measure the energetics of interaction between lipidated peptides, cholesterol, and phospholipids in both l_o and l_d host membranes. The resulting energy measurements can then be used in Monte Carlo simulations to provide a physical picture of membrane organization in a simulated membrane containing coexisting and l_o and l_d domains, as well as a quantitative partition coefficient to describe the distribution

of the peptide between domains. In designing these experiments, variables to consider include (*i*) the choice of lipidated peptides to examine, (*ii*) the choice of host membranes to use for NNR experiments, and (*iii)* the choice of exchangeable lipids. For each of these variables, we sought to choose the simplest possible substrate, expected to produce the greatest possible partitioning.

Our choice of lipidated peptide was inspired by the work of Silvius *et. al*, who found a peptide of the structure [(myristoyl)GlyCys(palmitoyl)Gly] to be the minimal motif that ensures partitioning into the l_o phase in model membranes (see Section 2.1).[42] This motif has been observed in the protein $p56^{lck}$, as well as in the *src* family of kinases.[42] The presence of this motif in the *src* related kinase *Fyn* has been shown to be necessary for the proteins to associate with detergent resistant fractions in COS-1 cells.[48] The exchangeable dipeptide, **Pep1**, (Figure 6) that we have chosen to study is therefore a mimic of this motif. In **Pep1**, the thioester has been replaced by a thioether to allow greater stability under NNR conditions.

In order to assess the effect of unsaturation in the lipid anchors on peptide partitioning a second dipeptide, **Pep2**, bearing a permanent kink in its C14 chain, was also chosen. Because double bonds undergo *cis/trans* isomerization under NNR conditions, a cyclopropyl group was used to "lock in" a permanent kink.[49]

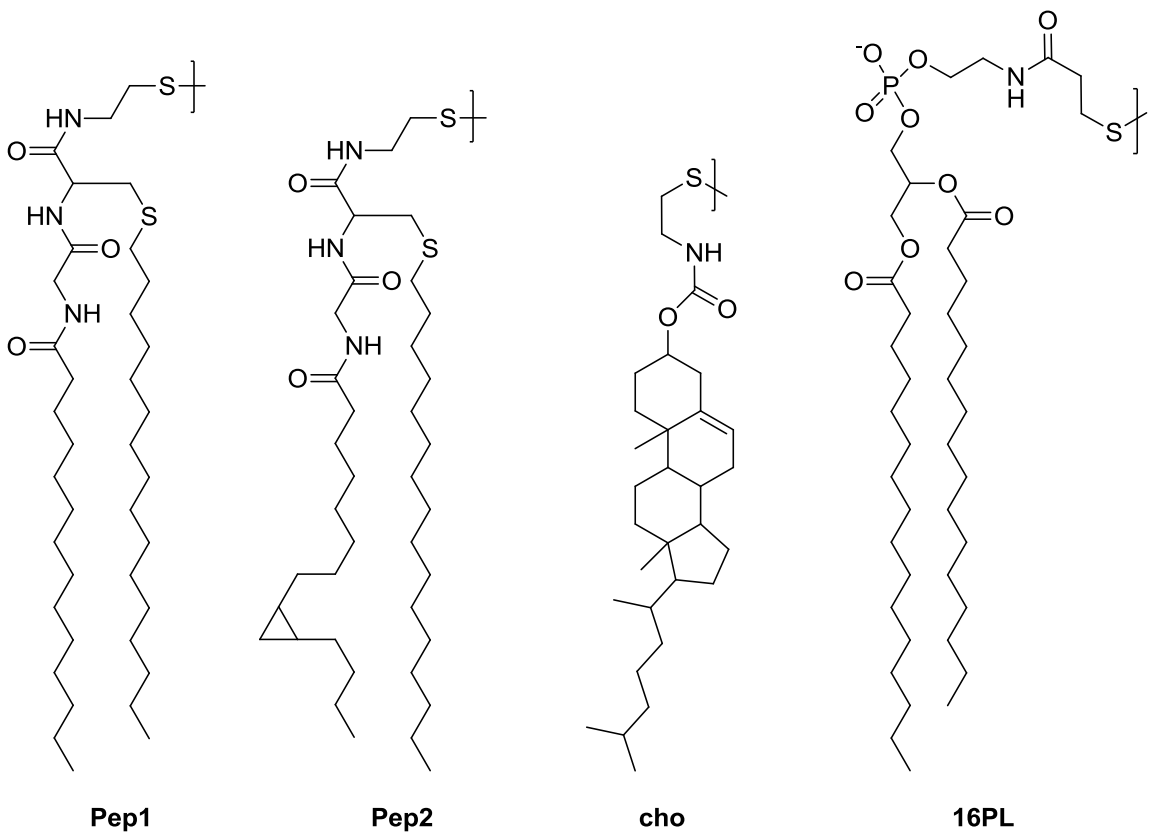

Figure 6: Structures of exchangeable lipids used in NNR studies

The NNR reactions were conducted in host membranes of DPPC and cholesterol. The phase diagram of this system is well understood,[50] and allows convenient access to both l_o and l_d membranes at 45 ^{o}C depending on cholesterol content. In addition, this system is of interest because at intermediate cholesterol concentrations discrete l_o micro domains, roughly analogous to putative lipid rafts, are thought to be present but have never been directly observed.[51-53] For measuring the interaction of **Pep1** and **Pep2** with DPPC and cholesterol, **cho** and **16PL** were used in NNR reactions. These lipids have previously been shown to be excellent mimics of cholesterol and DPPC, respectively, with **cho** having condensing behavior nearly identical to cholesterol, and **16PL** having a transition temperature of 41.9 ^{o}C (compared to 41.5 ^{o}C for cholesterol).[54,55] NNR

reactions conducted in DPPC/cholesterol host membranes using the four exchangeable lipids shown in Figure 6 provide a simple system for measuring the interactions of small lipidated peptides with lipids in l_o and l_d membranes.

Nearest neighbor interaction energies, however, are not the only data necessary to model the organization of a membrane using Monte Carlo simulations. Because both **Pep1** and **Pep2** resemble phospholipids, having a polar headgroup and two acyl chain tails, they might be expected to exhibit phase transition behavior in a bilayer similar to phospholipids. In order to model their behavior in a bilayer, it is therefore necessary to estimate their transition temperatures. Differential Scanning Calorimetry (DSC) experiments were thus carried out to measure the phase transition properties of the heterodimers {**Pep1-16PL**} and {**Pep2-16PL**}, as well as **Pep1a** and **Pep2a**, non-exchangeable monomer mimics of **Pep1** and **Pep2** (Figure 7).

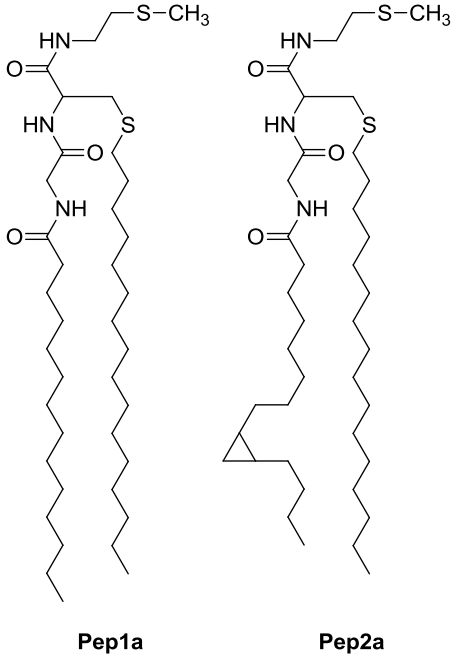

Figure 7: Structures of **Pep1a** and **Pep2a**.

2.3 Results[56]

2.3.1 Synthesis of Dimers

The homodimer {**Pep1-Pep1**} was synthesized as shown in Scheme 2. Alkylation of boc-cysteine with bromohexadecane, followed by deprotection and condensation with cystamine afforded **2**, which was then coupled with a myristoyl glycine (**3**) to give {**Pep1-Pep1**}. As shown in Scheme 3, {**Pep1-cho**} was prepared using a similar strategy. Activation of cholesterol with N,N' disuccinimidyl carbonate and subsequent reaction with cystamine afforded **4**, which was then coupled, sequentially with alkylated boc-cysteine and **3** to produce the desired heterodimer.

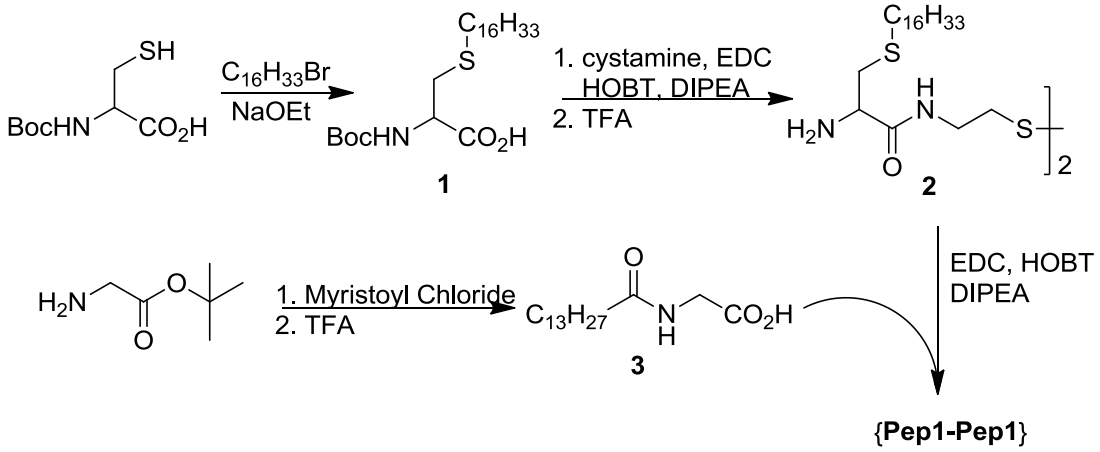

Scheme 2: Synthesis of {**Pep1-Pep1**}

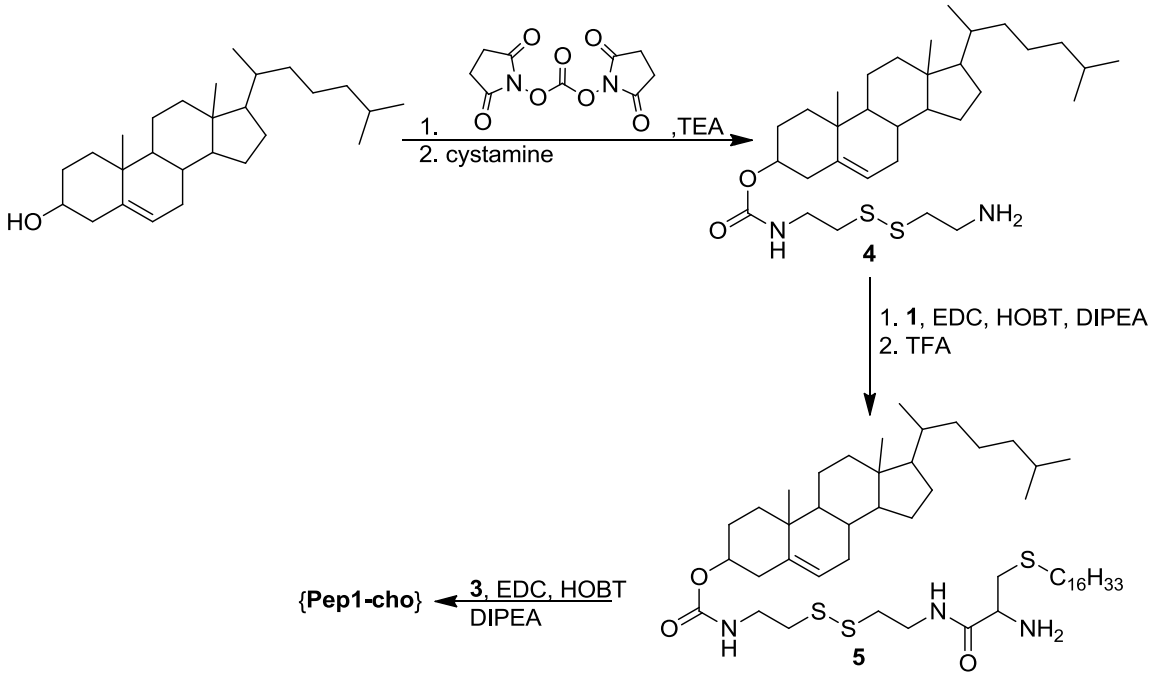

Scheme 3: Synthesis of {**Pep1-cho**}

To prepare the heterodimer {**Pep1-16PL**}, the homodimer {**Pep1-Pep1**} was first reduced with *tris*(2-carboxyethyl)phosphine hydrochloride salt (TCEP) to make the thiol monomer, which was then reacted with an activated form of 1,2-dipalmitoyl-*sn*-glycero-3-phosphoethanolamine (DPPE) (**6**), producing the desired heterodimer (Scheme 4).

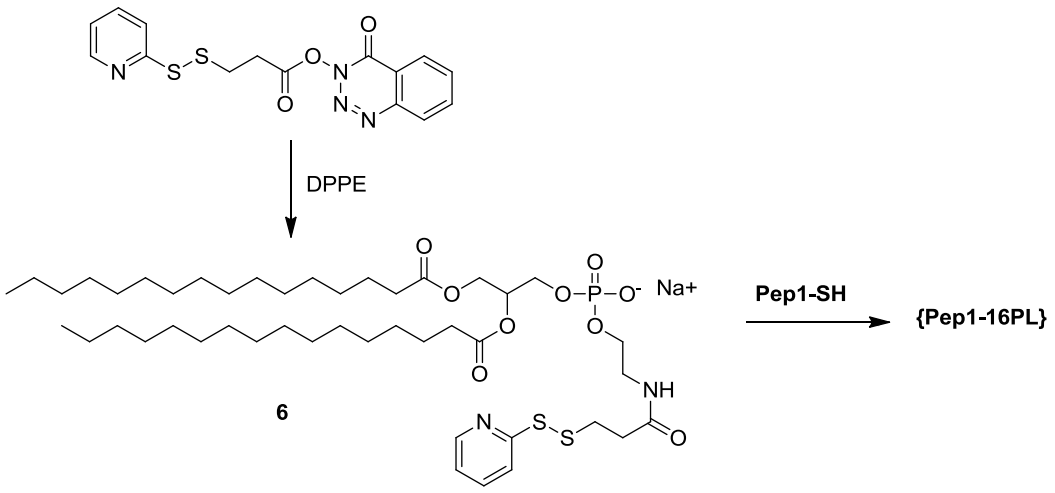

Scheme 4: Synthesis of {**Pep1-16PL**}

The homodimer {**Pep2-Pep2**} was synthesized using similar methods. A cyclopropyl derivative of myristeoleic acid (**7**) was prepared via a Simmon's Smith reaction using the procedure of Charette *et al.*[57] Coupling of **2** with boc-glycine, followed by deprotection and reaction with **7** gave {**Pep2-Pep2**} (Scheme 5).

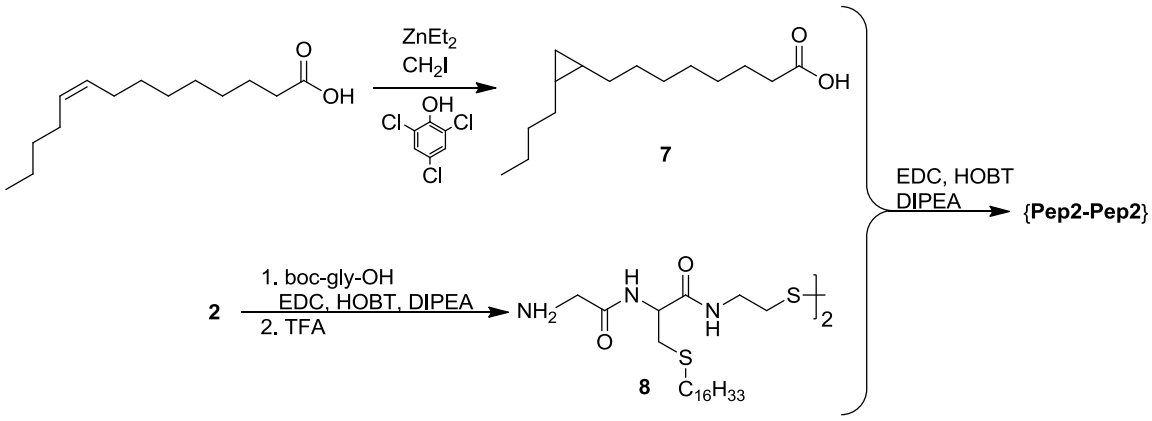

Scheme 5: Synthesis of {**Pep2-Pep2**}

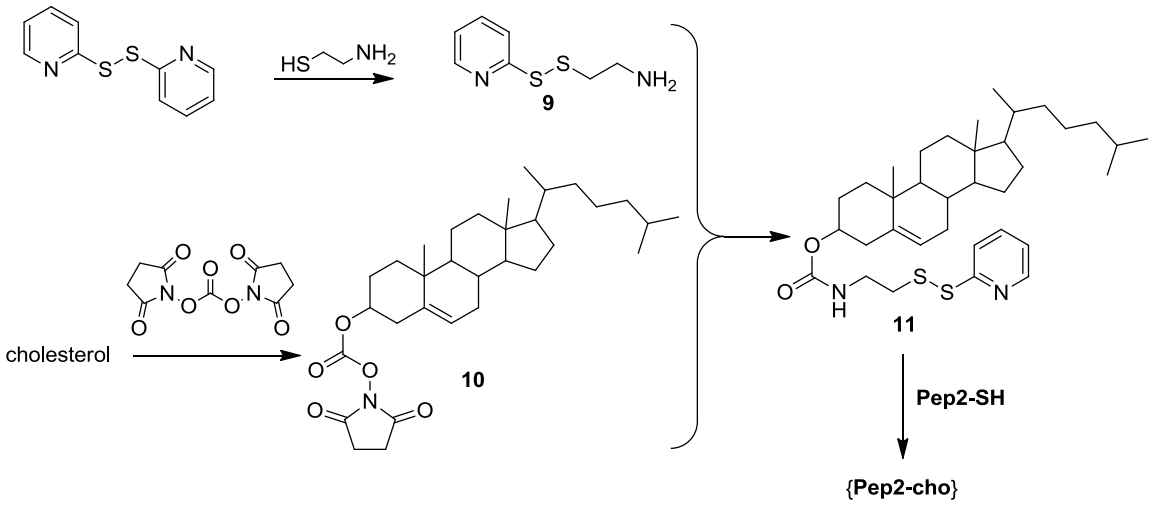

Scheme 6: Synthesis of {**Pep2-cho**}

The synthesis of {**Pep2-cho**} is shown in Scheme 6. Activation of cholesterol with N,N' disuccinimidyl carbonate, to give **10**, and subsequent condensation with **9** afforded the activated disulfide **11**. The homodimer {**Pep2-Pep2**} was reduced with TCEP and combined with **11**, giving the final heterodimer, {**pep2-cho**}.

Like {**Pep1-16**}, {**Pep2-16**} was prepared via reaction of the peptide thiol monomer with **6**. The remaining dimers used in these studies, {**cho-cho**}, {**16PL-16PL**}, and {**16PL-cho**} were synthesized in our laboratory by Dr. Wen-Hua Chen using previously reported procedures.[19,55]

2.3.2 Calibration of Chromatographic Systems

All NNR reactions performed using {**16PL-cho**} were analyzed using the previously published calibration curve.[21] For the other dimer pairs, the chromatographic systems were calibrated by repeating the NNR sample preparation technique using samples of known dimer concentration and using the same HPLC conditions as the NNR samples (see Section 5.2 for experimental procedures). For the chromatographic system used for **{Pep1-cho}** reactions, the system was found to respond as follows: For **{Pep1-Pep1}**, 1016685 x $n_{\{Pep1\text{-}Pep1\}}$ + 696011 = *Signal* (R^2= 0.9988); for **{Pep1-cho}** 752027 x $n_{\{Pep1\text{-}cho\}}$ + 491569 = *Signal n* (R^2 =0.9982); for **{cho-cho}** 579558 x $n_{\{cho\text{-}cho\}}$ + 213952 = *Signal* (R^2 = 0.9975), where *signal* is the area of the chromatographic peaks for the dimers and *n* is the number of moles of dimers. The calibration curve for these dimers is shown in Figure 8.

Figure 9 shows the calibration curve for the chromatographic system used for **{Pep1-16PL}** reactions, which was found to respond as follows: For **{Pep1-Pep1}**, 359579 x $n_{\{Pep1\text{-}Pep1\}}$ + 94387 = *Signal* (R^2= 0.9903); for **{Pep1-16PL}** 778799 x $n_{\{Pep1\text{-}16PL\}}$ + 289723 = *Signal n* (R^2 =0.9957); for **{16PL-16PL}** 1040969 x $n_{\{16PL\text{-}16PL\}}$ + 274274 = *Signal* (R^2 = 0.9974).

For the chromatographic system used for **{Pep2-cho}** reactions, the system was found to respond as follows: For **{Pep2-Pep2}**, 997621 x $n_{\{Pep2\text{-}Pep2\}}$ + 979954 = *Signal* (R^2= 0.9953); for **{Pep2-cho}** 723232 x $n_{\{Pep2\text{-}cho\}}$ + 398744 = *Signal n* (R^2 =0.9969); for **{cho-cho}** 446355 x $n_{\{cho\text{-}cho\}}$ + 281227 = *Signal* (R^2 = 0.9961). The calibration curve for these dimers is shown in Figure 10.

Finally, as shown in Figure 11, the chromatographic system used for **{Pep2-16PL}** reactions was found to respond as follows: For **{Pep2-Pep2}**, 427519 x $n_{\{Pep2\text{-}Pep2\}}$ + 167174 = *Signal* (R^2= 0.9990); for **{Pep2-16PL}** 652968 x $n_{\{Pep2\text{-}16PL\}}$ + 31632 = *Signal n* (R^2 =0.9989); for **{16PL-16PL}** 1037098 x $n_{\{16PL\text{-}16PL\}}$ + 365839 = *Signal* (R^2 = 0.9966).

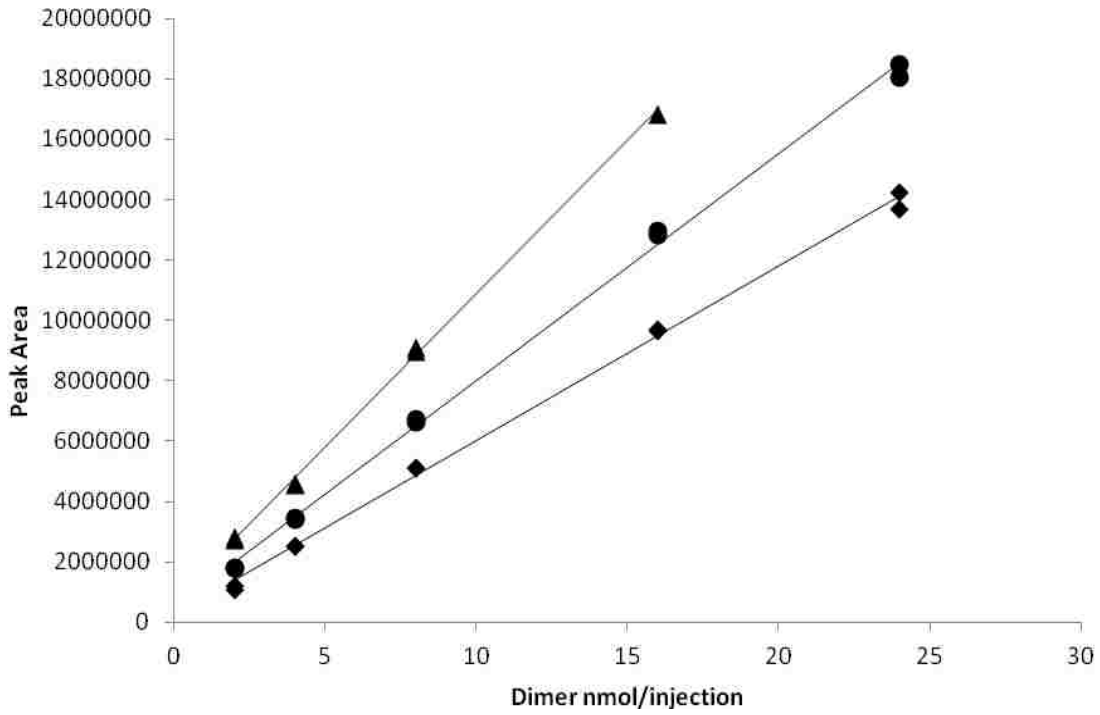

Figure 8: Peak area plotted as a function of nmol/injection for dimers {**cho-cho**} (♦),{**Pep1-cho**} (●), and {**Pep1-Pep1**} (▲).

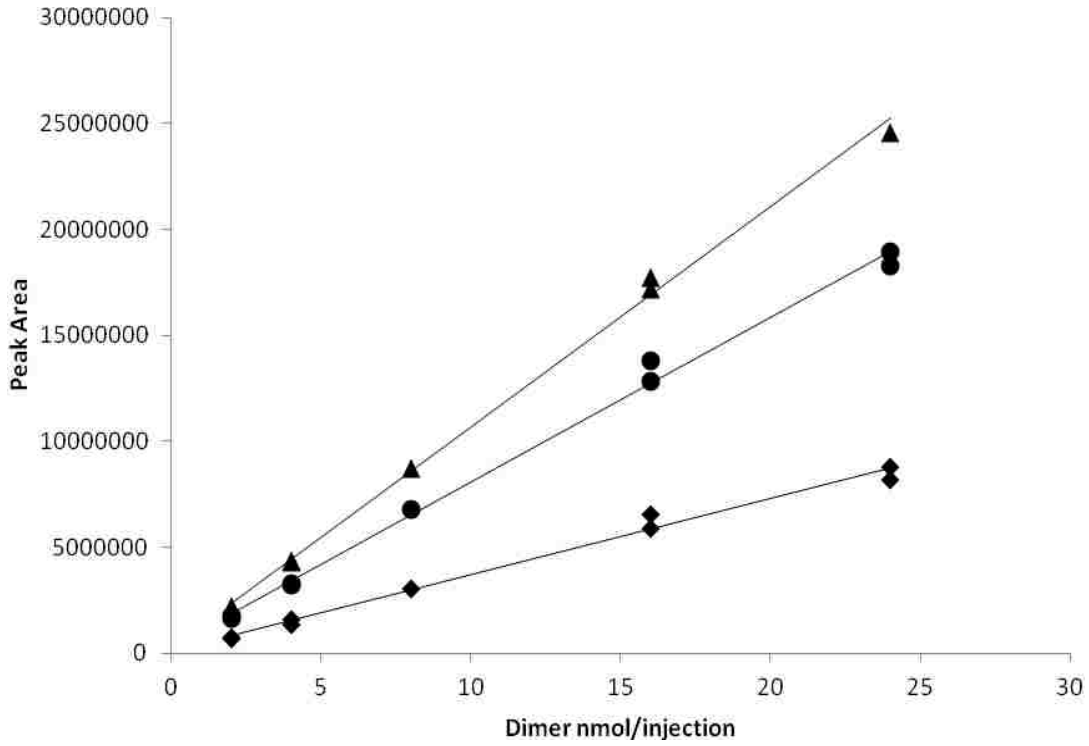

Figure 9: Peak area plotted as a function of nmol/injection for dimers {**16PL-16PL**} (♦),{**Pep1-16PL**} (●), and {P**ep1-Pep1**} (▲).

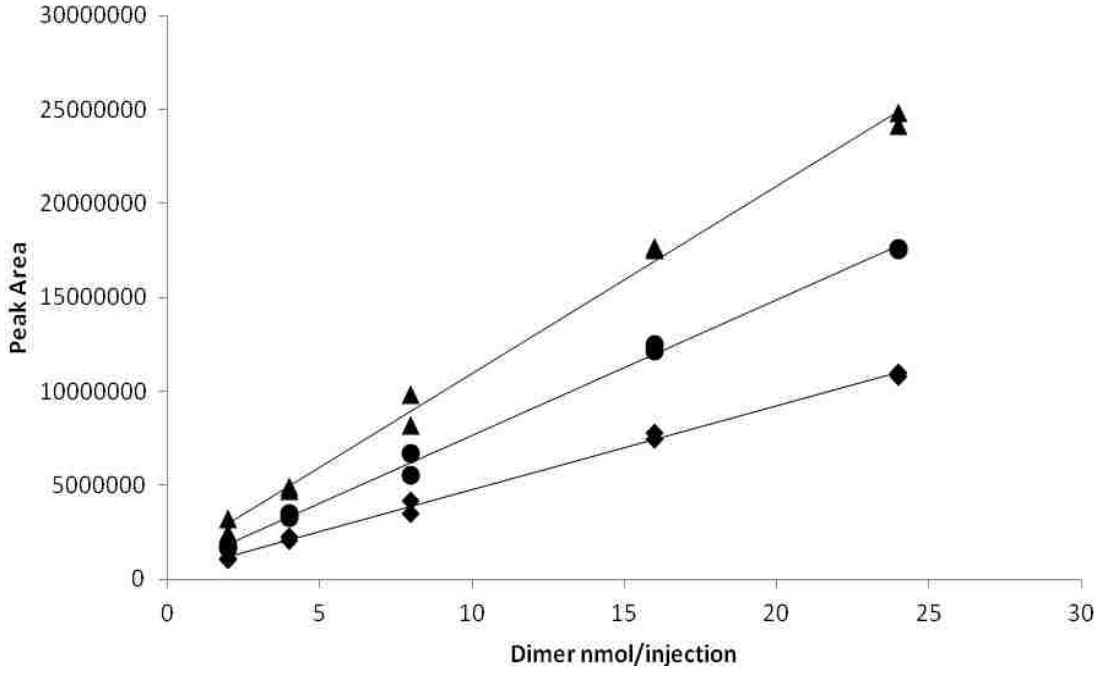

Figure 10: Peak area plotted as a function of nmol/injection for dimers {**cho-cho**} (♦),{**Pep2-cho**} (●), and {**Pep2-Pep2**} (▲).

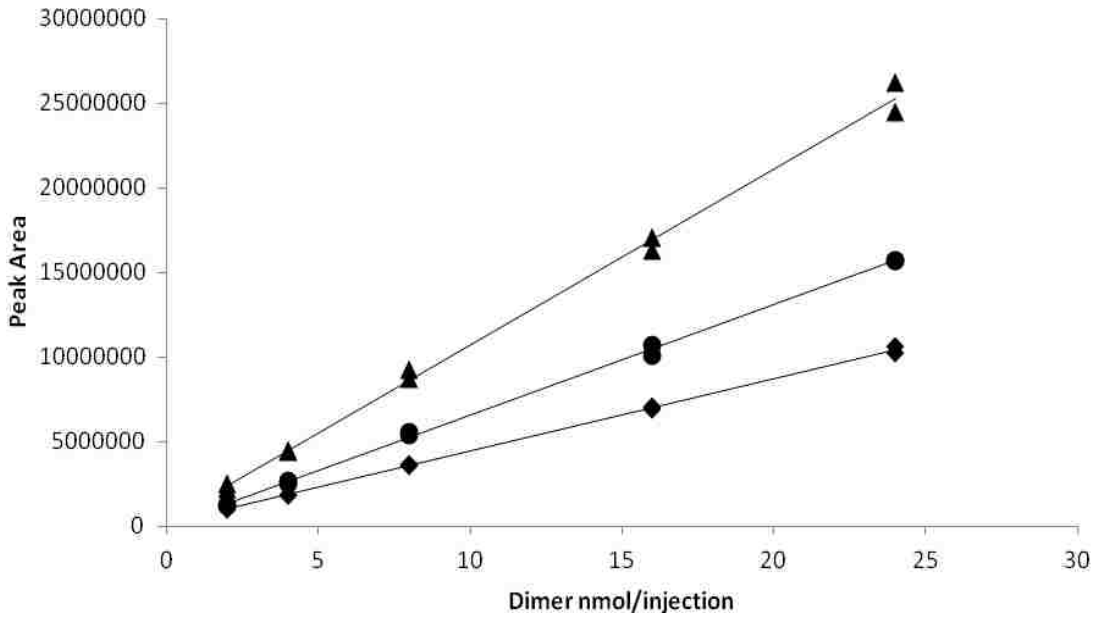

Figure 11: Peak area plotted as a function of nmol/injection for dimers {**16PL-16PL**} (♦),{**Pep2-16PL**} (●), and {**Pep2-Pep2**} (▲).

2.3.3 Epimerization of {Pep1-Pep1}

A typical HPLC chromatogram for an NNR reaction starting from {**Pep1-cho**} is shown in Figure 12. The peak at retention time ~32 minutes, which is the homodimer {**Pep1-Pep1**}, is overlapping with a second peak, rendering it impossible to integrate accurately. In order to quantify the concentration of all three dimers in the sample and obtain a reliable measurement of *K*, it was therefore necessary to determine the source of this second peak.

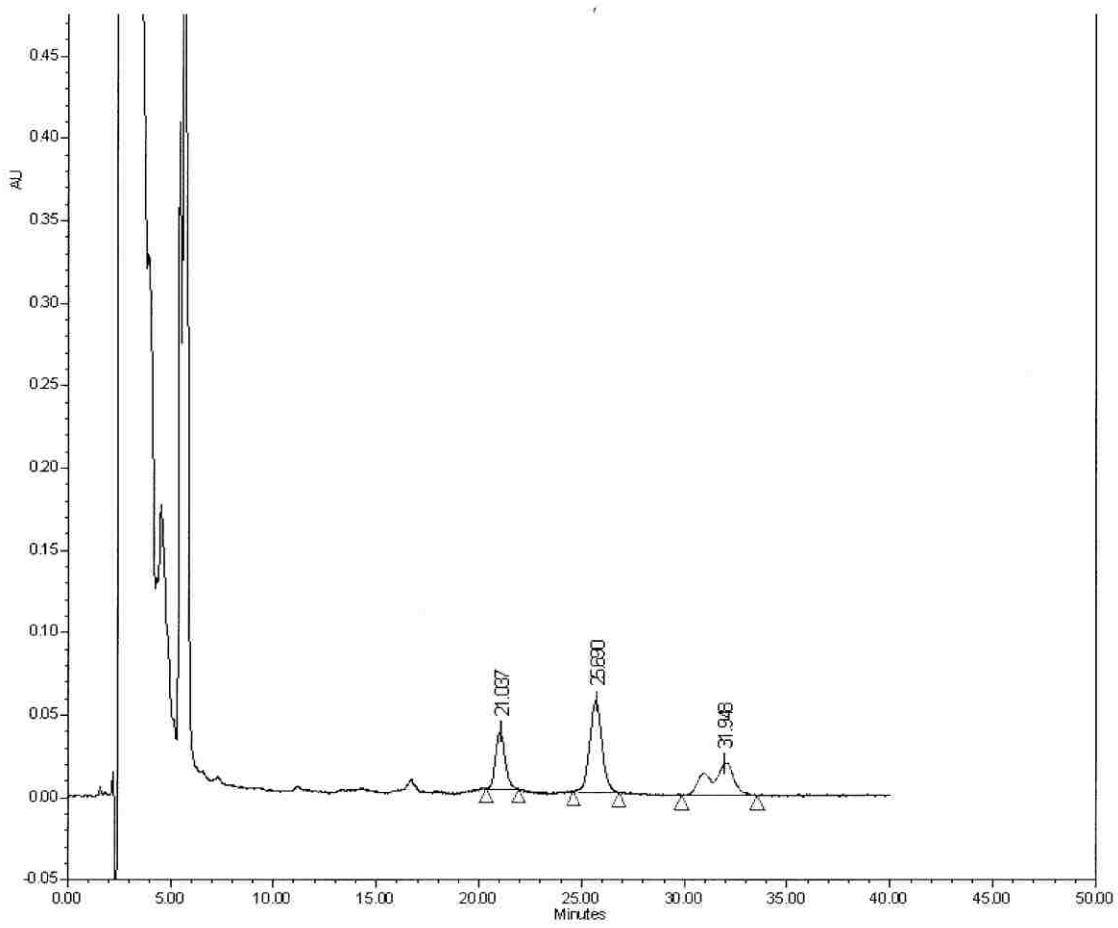

Figure 12: Typical HPLC chromatogram from the analysis of product mixtures in NNR reactions starting with heterodimer {**Pep1-cho**}.

In order to identify this extra peak, several samples were collected from an NNR reaction that was prepared using the standard conditions (see Section 5.2). The samples were then analyzed using an HPLC mobile phase that did not contain tetrabutyl ammonium acetate. A doublet of peaks with a retention time of ~31 minutes was observed, and fractions were manually collected from the HPLC detector in order to isolate a sample of each of the two peaks of the "doublet." The collected samples, along with samples of (*i*) pure {**Pep1-Pep1**} and (*ii*) a fraction collected from the HPLC detector when no peak was eluting (baseline), were analyzed by MALDI-MS to

determine molecular weight. The results of these analyses are shown in Table 1. In the sample of pure homodimer, only two peaks with m/z > 1000 were visible, at m/z of 1364.94 and 1380.96, corresponding to (M+Na) and (M+K). The samples collected from both HPLC peaks were identical.

Sample	Peaks Detected (m/z)
pure {**Pep1-Pep1**}	1364.94, 1380.96
baseline	-
peak 1	1364.89, 1380.87
peak 2	1365.00, 1380.90

Table 1: All peaks with m/z >1000 detected in MALDI analysis of fractions collected from NNR samples. Below 1000, it was not possible to distinguish matrix peaks from sample peaks.

The MS data shown in Table 1 suggests that the compounds present in **peak 1**and **peak 2** have identical molecular masses (*i.e.* are isomers). The most likely cause of isomerization of **Pep1** under NNR conditions would be epimerization at the cysteine residue. The mechanism of this epimerization is not presently understood. Potentially, it could occur as a result of deprotonation by the thiolate anions generated under NNR conditions, as shown in Figure 13.

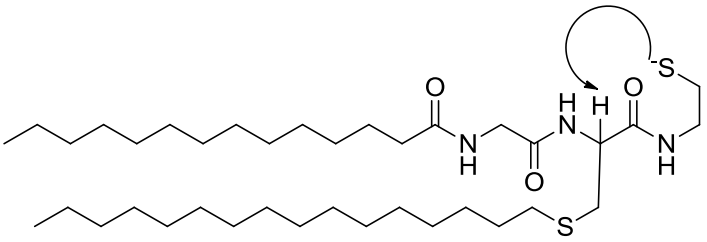

Figure 13: Hypothetical mechanism for epimerization of **Pep1**.

In order to confirm that these two peaks are due to the epimerization of the cysteine of **Pep1**, analogs of {**Pep1-Pep1**} and {**Pep1-cho**} and were synthesized starting from racemic cysteine. These dimers were then analyzed by HPLC and compared to the chromatogram shown in Figure 12. The results of these experiments are shown in Figures 14 and 15. Like the NNR samples, analogs of {**Pep1-Pep1**} that were

prepared from racemic cysteine produced a doublet of peaks, while the analog of {**Pep1-cho**} had a single peak.

Taken together with the MALDI results showing that both peaks of the doublet have identical molecular mass, the results of these experiments strongly suggest that the doublet of peaks evident for {**Pep1-Pep1**} in NNR samples is the result of epimerization. Since the {**Pep1-Pep1**} diastereomers are unlikely to have different molar absorbtivities, the doublets were integrated as one peak and the previously discussed calibration curve was applied to determine the concentration of {**Pep1-Pep1**} present in all NNR samples.

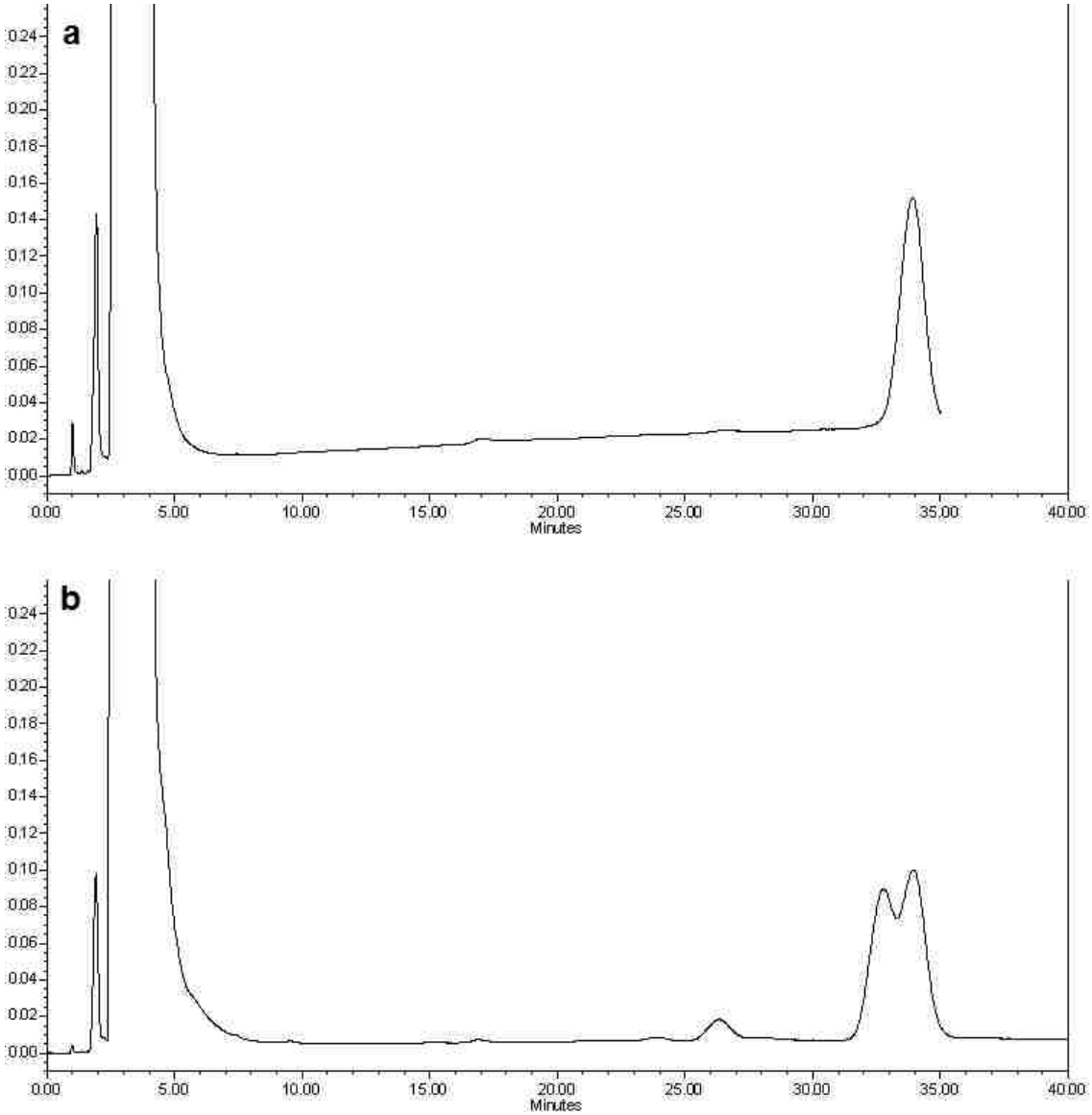

Figure 14: HPLC analysis of (**a**) {**Pep1-Pep1**} and (**b**) an analog of {**Pep1-Pep1**} synthesized from racemic cysteine

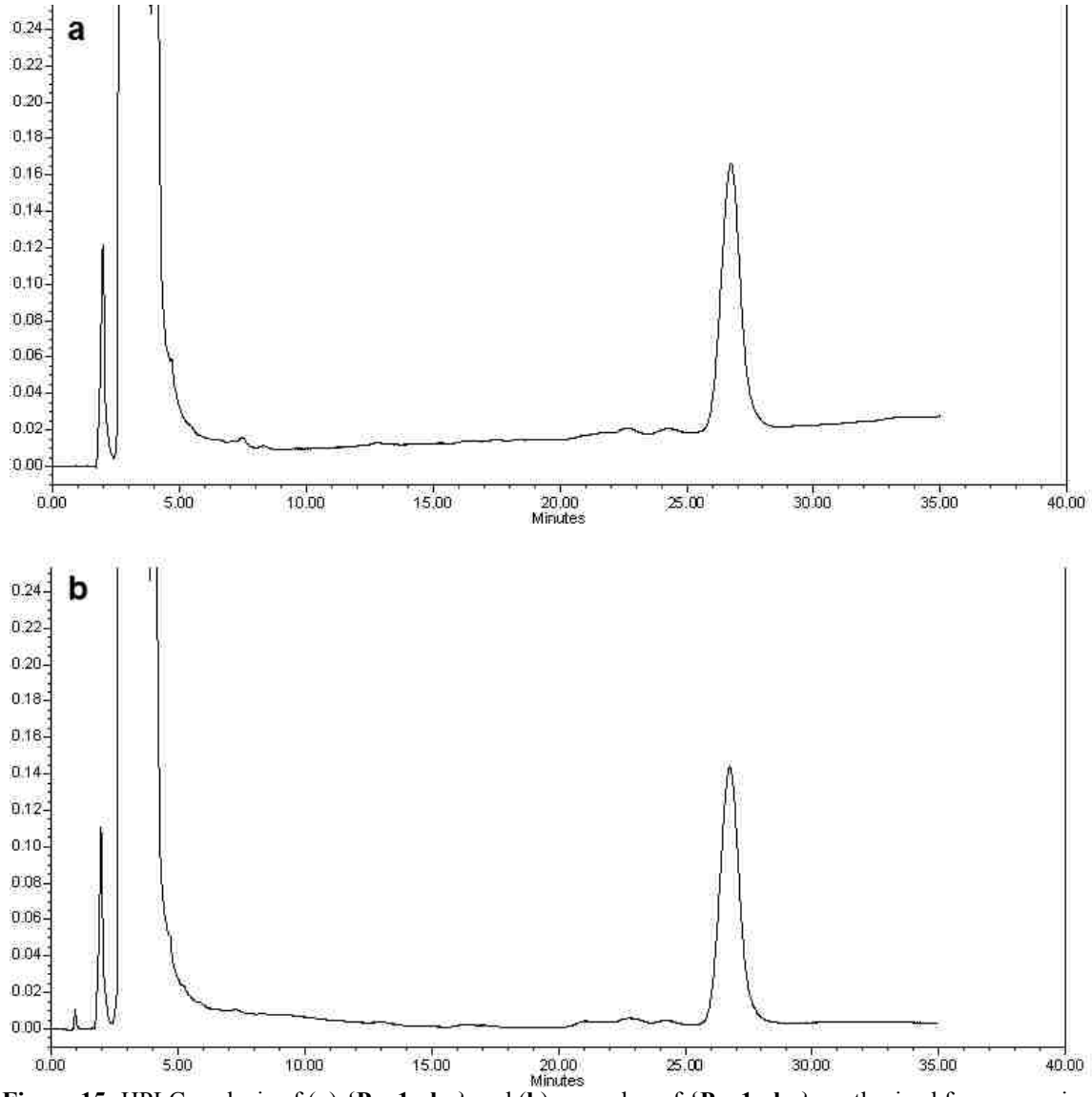

Figure 15: HPLC analysis of (**a**) {**Pep1-cho**} and (**b**) an analog of {**Pep1-cho**} synthesized from racemic cysteine

2.3.4 NNR Results

In order to obtain the Nearest Neighbor interaction energy (ω_{AB}) measurements necessary for Monte Carlo simulations, NNR experiments were carried out using the heterodimers {**16PL-cho**}, {**Pep1-cho**}, {**Pep1-16PL**}, {**Pep2-cho**}, and {**Pep2-16PL**} in l_d and l_o host membranes consisting of 5% exchangeable lipid and 95% DPPC (l_d) or a mixture of DPPC and cholesterol (l_o). For reactions using {**Pep1-cho}** or **{Pep2-cho}**,

2.5% 1,2-dipalmitoyl-*sn*-glycero-3-phosphoglycerol (DPPG) was included in the membrane to give all liposomes used in these studies the same net negative charge. For additional details regarding the composition and preparation of the liposomes used in these studies, see Section 5.2. Unless otherwise noted, Aldrithiol-2 was used during the preparation of HPLC samples from NNR reactions of {**Pep1-cho**}, {**Pep1-16PL**}, {**Pep2-cho**}, and {**Pep2-16PL**}, but was omitted from samples collected from {**16PL-cho**} reactions. The results of these NNR reactions are shown in Tables 2-13. The average K and ω_{AB} for each of these dimer pairs are summarized in Table 14.

In general, preliminary NNR reactions were conducted with samples collected at several time points, and the results were plotted to determine the time necessary to reach equilibrium (results not shown). In subsequent experiments, samples were withdrawn at two time points; one where equilibrium was expected to have been reached (based on the preliminary experiments) and a second time point ~12 hours later. If these two time points produced similar results, the reaction was considered to have reached equilibrium and the data from both time points were averaged. Thus, all of the reactions shown in Tables 2-13 contain data from samples collected at at least 2 time points.

For the equilibration of {**16PL-cho**} in l_d host membranes (Tables 2 and 3) there was significant difference between the two time points. Based on this, it was assumed that the reactions had not yet reached equilibrium after 12 hours, and the data from the 12 hour samples were not used. Because the 23 hour samples agreed with the results from preliminary experiments (not shown) and previously reported {**16PL-cho**} experiments,[19,21] the 23 hour results were used. For all other NNR reactions (Tables 4-13) equilibration was observed and all of the data were averaged.

The average vesicle size for each liposome preparation was measured before and after the NNR procedure, in order to verify that the liposomes remained intact. Those data are shown in Tables 15 and 16. Typical chromatograms from the analysis of NNR reaction product mixtures are presented in Figures 12 (page 28), and 16-19. For reasons that are not presently understood, the epimerization discussed in Section 2.3.3 was not observed in NNR reactions of {**Pep1-16PL**}, {**Pep2-cho**}, or {**Pep2-16PL**}.

Reaction	Reaction Time (h)	Dimer	R_T (min)	Peak Area	N (nmol)	K
1	12	**{16PL-16PL}**	11.15	2509780	5.25	3.91
		{16PL-cho}	17.01	5671667	10.65	
		{cho-cho}	31.65	3360075	5.52	
1	12	**{16PL-16PL}**	11.18	2579814	5.40	3.86
		{16PL-cho}	17.03	5819865	10.93	
		{cho-cho}	31.72	3487922	5.74	
1	23	**{16PL-16PL}**	11.20	2507409	5.25	3.52
		{16PL-cho}	17.09	5370991	10.09	
		{cho-cho}	31.76	3354369	5.51	
1	23	**{16PL-16PL}**	11.22	2471672	5.17	3.54
		{16PL-cho}	17.13	5323626	10.00	
		{cho-cho}	31.82	3323015	5.46	
1	23	**{16PL-16PL}**	11.25	2538360	5.31	3.58
		{16PL-cho}	17.18	5473361	10.28	
		{cho-cho}	31.90	3381364	5.56	
2	12	**{16PL-16PL}**	11.32	2507616	5.25	4.65
		{16PL-cho}	17.24	6182174	11.61	
		{cho-cho}	32.04	3363664	5.53	
2	12	**{16PL-16PL}**	11.36	2579734	5.40	4.62
		{16PL-cho}	17.30	6358257	11.94	
		{cho-cho}	32.14	3478508	5.72	
2	23	**{16PL-16PL}**	11.38	2780874	5.82	3.40
		{16PL-cho}	17.38	5795786	10.89	
		{cho-cho}	32.22	3635933	5.99	
2	23	**{16PL-16PL}**	11.45	2664372	5.57	3.50
		{16PL-cho}	17.47	5588222	10.50	
		{cho-cho}	32.33	3432769	5.65	
2	23	**{16PL-16PL}**	11.52	2847952	5.96	3.45
		{16PL-cho}	17.59	5949540	11.18	
		{cho-cho}	32.55	3687662	6.08	

Table 2: Data for {**cho-16PL**} equilibration in 2.5 mol% sterol LUVs at 45 °C using 0.8 equivalents of DTT (Reactions 1 and 2). Only 23 hour samples were used to calculate average *K*, as reaction had not yet reached equilibrium at 12 hours.

Reaction	Reaction Time (h)	Dimer	R_T (min)	Peak Area	N (nmol)	K
3	12	**{16PL-16PL}**	13.63	1483058	3.10	3.79
		{16PL-cho}	19.71	3378166	6.36	
		{cho-cho}	32.72	2124440	3.44	
3	12	**{16PL-16PL}**	13.67	1444816	3.02	4.04
		{16PL-cho}	19.77	3400178	6.40	
		{cho-cho}	32.80	2074445	3.35	
3	23	**{16PL-16PL}**	13.73	1389383	2.91	3.58
		{16PL-cho}	19.83	3088347	5.81	
		{cho-cho}	32.85	2010966	3.24	
3	23	**{16PL-16PL}**	13.73	1248334	2.61	3.68
		{16PL-cho}	19.85	2816810	5.30	
		{cho-cho}	32.87	1822690	2.93	
3	23	**{16PL-16PL}**	13.45	1399903	2.93	3.58
		{16PL-cho}	19.85	3138040	5.91	
		{cho-cho}	32.94	2058529	3.32	
4	12	**{16PL-16PL}**	13.82	1433026	3.00	3.72
		{16PL-cho}	19.97	3231017	6.08	
		{cho-cho}	33.09	2050948	3.31	
4	12	**{16PL-16PL}**	13.86	1379285	2.89	3.79
		{16PL-cho}	20.01	3115105	5.86	
		{cho-cho}	33.11	1951766	3.14	
4	23	**{16PL-16PL}**	13.92	1162704	2.43	3.49
		{16PL-cho}	20.11	2550957	4.81	
		{cho-cho}	33.21	1700225	2.72	
4	23	**{16PL-16PL}**	13.95	1253894	2.62	3.44
		{16PL-cho}	20.17	2622219	4.94	
		{cho-cho}	33.29	1689516	2.70	
4	23	**{16PL-16PL}**	14.00	1235744	2.59	3.49
		{16PL-cho}	20.24	2676294	5.04	
		{cho-cho}	33.35	1755506	2.81	

Table 3: Data for {**cho-16PL**} equilibration in 2.5 mol% sterol LUVs at 45 °C using 0.8 equivalents of DTT (Reactions 3 and 4). Only 23 hours samples were used to calculate average *K*, as reaction had not yet reached equilibrium at 12 hours

Reaction	Reaction Time (h)	Dimer	R_T (min)	Peak Area	N (nmol)	K
1	12	**{16PL-16PL}**	11.36	1428160	2.99	10.02
		{16PL-cho}	17.64	5233055	9.83	
		{cho-cho}	33.98	2002576	3.23	
1	16	**{16PL-16PL}**	11.40	1453197	3.04	9.96
		{16PL-cho}	17.67	5332490	10.02	
		{cho-cho}	34.06	2053687	3.32	
1	18	**{16PL-16PL}**	11.41	1353970	2.83	10.01
		{16PL-cho}	17.71	5122688	9.63	
		{cho-cho}	34.11	2023893	3.27	
1	20	**{16PL-16PL}**	11.64	1422840	2.98	10.04
		{16PL-cho}	18.05	5335479	10.02	
		{cho-cho}	34.59	2080007	3.36	
1	22	**{16PL-16PL}**	11.65	1416196	2.96	10.05
		{16PL-cho}	18.07	5292757	9.94	
		{cho-cho}	34.61	2056679	3.32	
2	12	**{16PL-16PL}**	12.28	1366107	2.86	9.96
		{16PL-cho}	18.73	4855303	9.12	
		{cho-cho}	34.83	1822288	2.93	
2	16	**{16PL-16PL}**	12.31	1314610	2.75	10.03
		{16PL-cho}	18.76	4823031	9.06	
		{cho-cho}	34.89	1854173	2.98	
2	18	**{16PL-16PL}**	12.35	1367810	2.86	9.90
		{16PL-cho}	18.80	4907340	9.22	
		{cho-cho}	34.89	1867776	3.00	
2	20	**{16PL-16PL}**	12.36	1288106	2.70	9.92
		{16PL-cho}	18.82	4680862	8.80	
		{cho-cho}	34.92	1803597	2.89	

Table 4: Data for {**cho-16PL**} equilibration in 40 mol% sterol LUVs at 45 °C using 0.8 equivalents of DTT (Reactions 1 and 2).

Reaction	Reaction Time (h)	Dimer	R_T (min)	Peak Area	N (nmol)	K
3	11	**{16PL-16PL}**	11.56	1564909	3.27	9.98
		{16PL-cho}	17.82	5608884	10.54	
		{cho-cho}	33.85	2101558	3.40	
3	11	**{16PL-16PL}**	11.62	1486861	3.11	10.31
		{16PL-cho}	17.88	5345242	10.04	
		{cho-cho}	33.89	1952812	3.15	
3	24	**{16PL-16PL}**	11.43	1510453	3.16	10.00
		{16PL-cho}	17.57	5523001	10.38	
		{cho-cho}	33.47	2106365	3.41	
3	24	**{16PL-16PL}**	11.46	1544369	3.23	9.74
		{16PL-cho}	17.60	5397989	10.14	
		{cho-cho}	33.46	2025715	3.27	
3	24	**{16PL-16PL}**	11.43	1629205	3.41	9.60
		{16PL-cho}	17.56	5751621	10.80	
		{cho-cho}	33.42	2201971	3.57	
4*	12	**{16PL-16PL}**	10.94	1470688	3.08	8.89
		{16PL-cho}	16.42	4850694	9.12	
		{cho-cho}	29.37	1889339	3.04	
4*	12	**{16PL-16PL}**	10.96	1442309	3.02	8.62
		{16PL-cho}	16.44	4768091	8.96	
		{cho-cho}	29.43	1917756	3.09	
4*	24	**{16PL-16PL}**	10.95	1414779	2.96	9.15
		{16PL-cho}	16.43	4731676	8.89	
		{cho-cho}	29.41	1818257	2.92	
4*	24	**{16PL-16PL}**	10.97	1382341	2.89	9.36
		{16PL-cho}	16.45	4706273	8.84	
		{cho-cho}	29.42	1801148	2.89	
4*	24	**{16PL-16PL}**	10.98	1374576	2.88	10.29
		{16PL-cho}	16.46	4867026	9.15	
		{cho-cho}	29.45	1763473	2.83	

Table 5: Data for {**cho-16PL**} equilibration in 40 mol% sterol LUVs at 45 °C using 0.8 equivalents of DTT (Reactions 3 and 4) *Aldrithiol-2 (8 equivalents relative to DTT was adding during preparation of HPLC samples)

Reaction	Reaction Time (h)	Dimer	R_T (min)	Peak Area	N (nmol)	K
		{cho-cho}	20.89	1568668	2.34	
1	15	**{Pep1-cho}**	25.57	3152714	3.54	3.40
		{Pep1-Pep1}	32.02	2297070	1.57	
		{cho-cho}	20.91	1491172	2.20	
1	15	**{Pep1-cho}**	25.63	2930782	3.24	3.03
		{Pep1-Pep1}	32.03	2296674	1.57	
		{cho-cho}	20.94	1372125	2.00	
1	24	**{Pep1-cho}**	25.67	2735311	2.98	3.38
		{Pep1-Pep1}	32.07	2036028	1.32	
		{cho-cho}	20.97	1397803	2.04	
1	24	**{Pep1-cho}**	25.69	2685431	2.91	3.03
		{Pep1-Pep1}	32.05	2081903	1.36	
		{cho-cho}	20.71	2520601	3.98	
2	15	**{Pep1-cho}**	25.28	4498039	5.33	2.75
		{Pep1-Pep1}	31.45	33328321	2.59	
		{cho-cho}	20.74	2510171	3.96	
2	15	**{Pep1-cho}**	25.31	4330008	5.10	2.62
		{Pep1-Pep1}	31.45	3243683	2.51	
		{cho-cho}	20.89	2351795	3.69	
2	24	**{Pep1-cho}**	25.50	4255424	5.00	2.83
		{Pep1-Pep1}	31.77	3135926	2.40	
		{cho-cho}	20.93	2336791	3.66	
2	24	**{Pep1-cho}**	25.54	3887591	4.52	2.62
		{Pep1-Pep1}	31.79	2857868	2.13	
		{cho-cho}	14.34	1677062	2.54	
3	24	**{Pep1-cho}**	15.92	2894584	2.86	2.41
		{Pep1-Pep1}	18.23	1998970	1.33	
		{cho-cho}	14.35	1667881	2.52	
3	24	**{Pep1-cho}**	15.94	2875665	2.83	2.32
		{Pep1-Pep1}	18.24	2038915	1.33	

Table 6: Data for {**Pep1-cho**} equilibration in 2.5 mol% sterol LUVs at 45 °C using 1.0 equivalents of DTT

Reaction	Reaction Time (h)	Dimer	R_T (min)	Peak Area	N (nmol)	K
1	15	**{cho-cho}**	20.76	927844	1.23	6.25
		{Pep1-cho}	25.41	2642361	2.86	
		{Pep1-Pep1}	31.78	1775891	1.06	
1	15	**{cho-cho}**	20.76	938919	1.25	6.10
		{Pep1-cho}	25.44	2561479	2.75	
		{Pep1-Pep1}	31.76	1704576	0.99	
1	24	**{cho-cho}**	20.78	926176	1.23	5.87
		{Pep1-cho}	25.45	2547746	2.73	
		{Pep1-Pep1}	31.79	1749358	1.04	
1	24	**{cho-cho}**	20.78	959906	1.29	5.84
		{Pep1-cho}	24.47	2425551	2.57	
		{Pep1-Pep1}	31.79	1590625	0.88	
2	15	**{cho-cho}**	20.61	1437920	2.11	5.30
		{Pep1-cho}	25.18	3323335	3.77	
		{Pep1-Pep1}	31.31	1983386	1.27	
2	15	**{cho-cho}**	20.69	1431611	2.10	4.91
		{Pep1-cho}	25.20	3274186	3.70	
		{Pep1-Pep1}	31.42	2044305	1.33	
2	24	**{cho-cho}**	20.75	1111352	1.55	5.67
		{Pep1-cho}	25.34	2852804	3.14	
		{Pep1-Pep1}	31.57	1836445	1.12	
2	24	**{cho-cho}**	20.79	1280725	1.84	5.36
		{Pep1-cho}	25.39	2927249	3.24	
		{Pep1-Pep1}	31.65	1776091	1.06	

Table 7: Data for {**Pep1-cho**} equilibration in 40 mol% sterol LUVs at 45 °C using 1.0 equivalents of DTT

Reaction	Reaction Time (h)	Dimer	R_T (min)	Peak Area	N (nmol)	K
		{16PL-16PL}	11.68	1468583	3.82	
1	15	**{Pep1-16PL}**	21.78	5596407	6.81	4.60
		{Pep1-Pep1}	44.24	3021457	2.64	
		{16PL-16PL}	11.76	1441823	3.75	
1	15	**{Pep1-16PL}**	21.91	5583514	6.80	4.58
		{Pep1-Pep1}	44.35	3076490	2.69	
		{16PL-16PL}	11.83	1346517	3.48	
1	24	**{Pep1-16PL}**	22.07	4984146	6.03	4.39
		{Pep1-Pep1}	44.45	2748803	2.38	
		{16PL-16PL}	11.89	1339278	3.46	
1	24	**{Pep1-16PL}**	22.22	4872834	5.88	4.29
		{Pep1-Pep1}	44.51	2704094	2.33	
		{16PL-16PL}	11.11	1572946	4.11	
2	15	**{Pep1-16PL}**	20.97	6314407	7.74	5.15
		{Pep1-Pep1}	43.76	3215506	2.83	
		{16PL-16PL}	11.14	1633964	4.28	
2	15	**{Pep1-16PL}**	20.98	6608247	8.11	5.11
		{Pep1-Pep1}	43.81	3404047	3.01	
		{16PL-16PL}	11.27	1691001	4.44	
2	24	**{Pep1-16PL}**	21.27	6669211	8.19	4.82
		{Pep1-Pep1}	44.09	3538274	3.14	
		{16PL-16PL}	11.30	1369611	4.30	
2	24	**{Pep1-16PL}**	21.37	6554686	8.04	5.01
		{Pep1-Pep1}	44.17	3406151	3.01	
		{16PL-16PL}	10.71	1529696	3.99	
3	24	**{Pep1-16PL}**	19.63	5979618	7.31	4.62
		{Pep1-Pep1}	41.55	3286918	2.89	
		{16PL-16PL}	10.69	1567496	4.10	
3	24	**{Pep1-16PL}**	19.64	5994065	7.32	4.35
		{Pep1-Pep1}	41.54	3405897	3.01	
		{16PL-16PL}	13.40	1644817	4.31	
4	15	**{Pep1-16PL}**	24.70	6816432	8.38	5.03
		{Pep1-Pep1}	45.48	3642892	3.24	
		{16PL-16PL}	13.47	1704481	4.48	
4	15	**{Pep1-16PL}**	24.80	6864943	8.44	4.72
		{Pep1-Pep1}	45.54	3785177	3.37	
		{16PL-16PL}	13.56	1638442	4.29	
4	24	**{Pep1-16PL}**	24.99	6583007	8.08	4.58
		{Pep1-Pep1}	45.66	3728445	3.32	
		{16PL-16PL}	13.67	1542800	4.03	
4	24	**{Pep1-16PL}**	25.18	6493601	7.97	5.17
		{Pep1-Pep1}	45.73	3446944	3.05	
		{16PL-16PL}	13.77	1523749	3.98	
4	24	**{Pep1-16PL}**	25.35	6163196	7.54	4.96
		{Pep1-Pep1}	45.85	3276312	2.88	

Table 8: Data for {**Pep1-16PL**} equilibration in 2.5 mol% sterol LUVs at 45 °C using 1.0 equivalent of DTT

Reaction	Reaction Time (h)	Dimer	R_T (min)	Peak Area	N (nmol)	K
1	15	**{16PL-16PL}**	11.48	887502	2.21	3.94
		{Pep1-16PL}	21.42	3247595	3.80	
		{Pep1-Pep1}	43.85	2004295	1.66	
1	15	**{16PL-16PL}**	11.49	898272	2.24	3.94
		{Pep1-16PL}	21.46	3306306	3.87	
		{Pep1-Pep1}	43.91	2046693	1.70	
1	24	**{16PL-16PL}**	11.52	847389	2.09	3.93
		{Pep1-16PL}	21.54	3182934	3.71	
		{Pep1-Pep1}	43.94	2020736	1.68	
1	24	**{16PL-16PL}**	11.59	885205	2.20	3.83
		{Pep1-16PL}	21.62	3137000	3.66	
		{Pep1-Pep1}	44.03	1926365	1.59	
2	15	**{16PL-16PL}**	11.07	1114527	2.84	4.11
		{Pep1-16PL}	20.91	4191505	5.01	
		{Pep1-Pep1}	43.61	2515718	2.15	
2	15	**{16PL-16PL}**	11.08	1069173	2.71	4.23
		{Pep1-16PL}	20.95	4013165	4.78	
		{Pep1-Pep1}	43.67	2348294	1.99	
2	24	**{16PL-16PL}**	11.19	1035050	2.62	4.11
		{Pep1-16PL}	21.16	3920981	4.66	
		{Pep1-Pep1}	43.85	2376613	2.02	
2	24	**{16PL-16PL}**	11.22	1107937	2.82	3.97
		{Pep1-16PL}	21.21	4113836	4.91	
		{Pep1-Pep1}	43.91	2519170	2.16	
3	15	**{16PL-16PL}**	13.12	1046008	2.65	4.23
		{Pep1-16PL}	24.32	4156429	4.96	
		{Pep1-Pep1}	45.05	2568589	2.20	
3	15	**{16PL-16PL}**	13.20	1068420	2.71	4.23
		{Pep1-16PL}	24.37	4184402	5.00	
		{Pep1-Pep1}	40.01	2548241	2.18	
3	24	**{16PL-16PL}**	13.23	1177348	3.01	3.70
		{Pep1-16PL}	24.42	4253370	5.09	
		{Pep1-Pep1}	45.16	2692814	2.32	
3	24	**{16PL-16PL}**	13.26	1183058	3.03	3.69
		{Pep1-16PL}	24.48	4268528	5.11	
		{Pep1-Pep1}	45.24	2707761	2.34	
2	24	**{16PL-16PL}**	13.31	1155534	2.95	3.99
		{Pep1-16PL}	24.59	4535480	5.45	
		{Pep1-Pep1}	45.30	2916304	2.54	

Table 9: Data for {**Pep1-16PL**} equilibration in 40 mol% sterol LUVs at 45 °C using 1.0 equivalent of DTT

Reaction	Reaction Time (h)	Dimer	R_T (min)	Peak Area	N (nmol)	K
1	18	**{cho-cho}**	20.89	1636534	3.04	2.83
		{Pep2-cho}	24.32	3047743	3.66	
		{Pep2-Pep2}	28.86	2537867	1.56	
1	18	**{cho-cho}**	20.92	1526852	2.79	3.20
		{Pep2-cho}	24.37	3127730	3.77	
		{Pep2-Pep2}	28.88	2568342	1.59	
1	24	**{cho-cho}**	20.94	1524012	2.78	2.67
		{Pep2-cho}	24.39	2833697	3.37	
		{Pep2-Pep2}	28.97	2497572	1.52	
1	24	**{cho-cho}**	20.95	1557946	2.86	2.74
		{Pep2-cho}	24.42	2932818	3.50	
		{Pep2-Pep2}	29.01	2544817	1.57	
1	24	**{cho-cho}**	20.97	1403241	2.51	3.16
		{Pep2-cho}	24.42	2693014	3.17	
		{Pep2-Pep2}	29.00	2242239	1.27	
2	18	**{cho-cho}**	24.27	2210245	4.32	2.23
		{Pep2-cho}	28.76	4211653	5.27	
		{Pep2-Pep2}	34.48	3861816	2.89	
2	18	**{cho-cho}**	24.15	2022522	3.90	2.57
		{Pep2-cho}	28.57	4017688	5.00	
		{Pep2-Pep2}	34.30	3469034	2.50	
2	24	**{cho-cho}**	24.11	2115256	4.11	2.52
		{Pep2-cho}	28.49	4230993	5.30	
		{Pep2-Pep2}	34.21	3687187	2.71	
2	24	**{cho-cho}**	24.06	2232175	4.37	2.50
		{Pep2-cho}	28.44	4410568	5.55	
		{Pep2-Pep2}	34.17	3793476	2.82	
2	24	**{cho-cho}**	24.09	2188602	4.27	2.43
		{Pep2-cho}	28.46	4263906	5.34	
		{Pep2-Pep2}	34.14	3726463	2.75	
3	18	**{cho-cho}**	19.59	1610371	2.98	2.72
		{Pep2-cho}	23.23	3022309	3.63	
		{Pep2-Pep2}	28.01	2598099	1.66	
3	18	**{cho-cho}**	19.65	1686870	3.15	2.59
		{Pep2-cho}	23.28	3143956	3.80	
		{Pep2-Pep2}	28.03	2741842	1.77	
3	24	**{cho-cho}**	19.67	1610073	2.98	2.74
		{Pep2-cho}	23.28	3052258	3.67	
		{Pep2-Pep2}	28.06	2627474	1.65	
3	24	**{cho-cho}**	19.69	1476728	2.68	3.03
		{Pep2-cho}	23.34	2757203	3.26	
		{Pep2-Pep2}	28.14	2286606	1.31	
3	24	**{cho-cho}**	19.73	1645247	3.06	2.71
		{Pep2-cho}	23.35	3080277	3.71	
		{Pep2-Pep2}	28.10	2634932	1.66	

Table 10: Data for {**Pep2-cho**} equilibration in 2.5 mol% sterol LUVs at 45 °C using 1.0 equivalent of DTT

Reaction	Reaction Time (h)	Dimer	R_T (min)	Peak Area	N (nmol)	K
1	18	**{cho-cho}**	20.71	1455056	2.63	4.97
		{Pep2-cho}	24.09	3671540	4.53	
		{Pep2-Pep2}	28.58	2543176	1.57	
1	18	**{cho-cho}**	20.80	1391508	2.49	4.68
		{Pep2-cho}	24.21	3642811	4.48	
		{Pep2-Pep2}	28.70	2702816	1.73	
1	24	**{cho-cho}**	20.80	1468489	2.66	4.70
		{Pep2-cho}	24.20	3780062	4.68	
		{Pep2-Pep2}	28.67	2725333	1.75	
1	24	**{cho-cho}**	20.86	1522040	2.78	4.64
		{Pep2-cho}	24.27	3900815	4.84	
		{Pep2-Pep2}	28.82	2795258	1.82	
1	24	**{cho-cho}**	20.85	1496257	2.72	4.72
		{Pep2-cho}	24.27	3891345	4.83	
		{Pep2-Pep2}	28.79	2791367	1.82	
2	18	**{cho-cho}**	24.53	1489497	2.71	5.36
		{Pep2-cho}	28.98	393957	4.90	
		{Pep2-Pep2}	34.75	2627428	1.65	
2	18	**{cho-cho}**	24.31	1497405	2.72	4.94
		{Pep2-cho}	28.74	3890068	4.83	
		{Pep2-Pep2}	34.45	2707348	1.73	
2	24	**{cho-cho}**	24.19	1521810	2.78	5.35
		{Pep2-cho}	28.60	4025985	5.02	
		{Pep2-Pep2}	34.29	2667567	1.69	
2	24	**{cho-cho}**	24.41	1493388	2.72	5.15
		{Pep2-cho}	28.84	3939318	4.90	
		{Pep2-Pep2}	34.63	2689828	1.73	
2	24	**{cho-cho}**	24.38	1473127	2.67	4.88
		{Pep2-cho}	28.83	3762291	4.65	
		{Pep2-Pep2}	34.59	2636651	1.66	
3	18	**{cho-cho}**	19.58	1273679	2.22	5.85
		{Pep2-cho}	23.21	3250644	3.94	
		{Pep2-Pep2}	27.96	2173029	1.20	
3	18	**{cho-cho}**	19.55	1309619	2.30	5.41
		{Pep2-cho}	23.17	3344632	4.07	
		{Pep2-Pep2}	27.90	2307285	1.33	
3	24	**{cho-cho}**	19.53	1388010	2.48	4.90
		{Pep2-cho}	23.17	3488717	4.27	
		{Pep2-Pep2}	27.90	2479001	1.50	
3	24	**{cho-cho}**	19.57	1327033	2.34	5.07
		{Pep2-cho}	23.19	3291093	4.00	
		{Pep2-Pep2}	27.94	2322463	1.35	
3	24	**{cho-cho}**	19.60	1264279	2.20	5.21
		{Pep2-cho}	23.23	3227374	3.91	
		{Pep2-Pep2}	27.96	2309331	1.33	

Table 11: Data for {**Pep2-cho**} equilibration in 40 mol% sterol LUVs at 45 °C using 1.0 equivalent of DTT

Reaction	Reaction Time (h)	Dimer	R_T (min)	Peak Area	N (nmol)	K
1	18	**{16PL-16PL}**	12.87	1431963	2.96	10.55
		{Pep2-16PL}	23.08	4952645	7.54	
		{Pep2-Pep2}	44.72	2252897	1.82	
1	18	**{16PL-16PL}**	12.87	1417138	2.92	10.51
		{Pep2-16PL}	23.08	4908069	7.47	
		{Pep2-Pep2}	44.75	2247037	1.81	
1	24	**{16PL-16PL}**	12.91	1366890	2.81	10.05
		{Pep2-16PL}	23.15	4556451	6.93	
		{Pep2-Pep2}	44.77	2131495	1.70	
1	24	**{16PL-16PL}**	12.95	1406100	2.90	9.91
		{Pep2-16PL}	23.18	4755153	7.23	
		{Pep2-Pep2}	44.80	2255986	1.82	
1	24	**{16PL-16PL}**	12.94	1440507	2.98	10.55
		{Pep2-16PL}	23.21	4876979	7.42	
		{Pep2-Pep2}	44.85	2182379	1.75	
2	18	**{16PL-16PL}**	20.18	1447609	3.00	9.84
		{Pep2-16PL}	32.90	5041223	7.67	
		{Pep2-Pep2}	53.71	2436892	2.00	
2	18	**{16PL-16PL}**	20.19	1498786	3.11	10.36
		{Pep2-16PL}	32.89	5342101	8.13	
		{Pep2-Pep2}	53.73	2491672	2.05	
2	24	**{16PL-16PL}**	20.19	1467423	3.04	10.13
		{Pep2-16PL}	32.90	5211314	7.93	
		{Pep2-Pep2}	53.73	2483378	2.04	
2	24	**{16PL-16PL}**	20.17	1537331	3.20	9.86
		{Pep2-16PL}	32.89	5419296	8.25	
		{Pep2-Pep2}	53.76	2600318	2.15	
2	24	**{16PL-16PL}**	20.17	1577682	3.30	9.32
		{Pep2-16PL}	32.90	5353106	8.15	
		{Pep2-Pep2}	53.79	2604991	2.16	
3	18	**{16PL-16PL}**	12.79	1511693	3.14	9.79
		{Pep2-16PL}	22.58	5611257	8.55	
		{Pep2-Pep2}	44.01	2826315	2.37	
3	18	**{16PL-16PL}**	12.74	1592945	3.33	9.54
		{Pep2-16PL}	22.48	5878642	8.95	
		{Pep2-Pep2}	43.93	2980061	2.52	
3	24	**{16PL-16PL}**	12.83	1621158	3.40	9.06
		{Pep2-16PL}	22.63	5832156	8.88	
		{Pep2-Pep2}	44.14	3022502	2.56	
3	24	**{16PL-16PL}**	12.84	1639915	3.44	8.57
		{Pep2-16PL}	22.65	5704906	8.69	
		{Pep2-Pep2}	44.14	3018201	2.56	
3	24	**{16PL-16PL}**	12.88	1572522	3.29	9.31
		{Pep2-16PL}	22.70	5851590	8.91	
		{Pep2-Pep2}	44.23	3057644	2.60	

Table 12: Data for {**Pep2-16PL**} equilibration in 2.5 mol% sterol LUVs at 45 °C using 1.0 equivalent of DTT

Reaction	Reaction Time (h)	Dimer	R_T (min)	Peak Area	N (nmol)	K
1	18	**{16PL-16PL}**	12.73	790886	1.46	9.34
		{Pep2-16PL}	22.96	2433678	3.68	
		{Pep2-Pep2}	43.60	1395634	0.99	
1	18	**{16PL-16PL}**	12.75	753095	1.37	10.29
		{Pep2-16PL}	22.87	2462433	3.72	
		{Pep2-Pep2}	43.96	1384618	0.98	
1	24	**{16PL-16PL}**	12.79	854748	1.61	8.90
		{Pep2-16PL}	22.94	2549529	3.86	
		{Pep2-Pep2}	44.39	1442794	1.04	
1	24	**{16PL-16PL}**	12.80	719586	1.29	10.22
		{Pep2-16PL}	23.02	2271574	3.43	
		{Pep2-Pep2}	44.48	1289208	0.89	
1	24	**{16PL-16PL}**	12.90	822421	1.53	9.18
		{Pep2-16PL}	23.11	2629641	3.98	
		{Pep2-Pep2}	44.60	1532138	1.12	
2	18	**{16PL-16PL}**	15.91	1279180	2.60	7.26
		{Pep2-16PL}	30.10	4145478	6.30	
		{Pep2-Pep2}	51.62	2546701	2.10	
2	18	**{16PL-16PL}**	20.32	1387044	2.85	7.79
		{Pep2-16PL}	33.08	4495410	6.84	
		{Pep2-Pep2}	53.91	2546701	2.10	
2	24	**{16PL-16PL}**	20.34	1490782	3.10	7.23
		{Pep2-16PL}	33.06	4619451	7.03	
		{Pep2-Pep2}	53.87	2652584	2.20	
2	24	**{16PL-16PL}**	20.34	1396364	2.88	7.61
		{Pep2-16PL}	33.02	4632398	7.05	
		{Pep2-Pep2}	53.83	2719604	2.27	
2	24	**{16PL-16PL}**	20.19	1307791	2.67	7.89
		{Pep2-16PL}	32.95	4380747	6.66	
		{Pep2-Pep2}	53.72	2551542	2.11	
3	18	**{16PL-16PL}**	12.76	1103240	2.19	7.32
		{Pep2-16PL}	22.60	3350508	5.10	
		{Pep2-Pep2}	43.87	2048319	1.62	
3	18	**{16PL-16PL}**	12.77	1051859	2.07	7.18
		{Pep2-16PL}	22.59	3281880	4.98	
		{Pep2-Pep2}	43.87	2095659	1.67	
3	24	**{16PL-16PL}**	12.76	1156501	2.31	6.51
		{Pep2-16PL}	22.61	3491473	5.30	
		{Pep2-Pep2}	43.89	2297144	1.86	
3	24	**{16PL-16PL}**	12.77	1116504	2.22	6.57
		{Pep2-16PL}	22.67	3408500	5.17	
		{Pep2-Pep2}	43.94	2266555	1.83	
3	24	**{16PL-16PL}**	12.80	1104174	2.19	6.54
		{Pep2-16PL}	22.68	3365931	5.11	
		{Pep2-Pep2}	44.00	2253226	1.82	

Table 13: Data for {**Pep2-16PL**} equilibration in 40 mol% sterol LUVs at 45 °C using 1.0 equivalent of DTT.

Dimer pair	l_o		l_d	
	K	**ω_{AB} (cal/mol)**	***K***	**ω_{AB} (cal/mol)**
cho-16PL	9.8 ± 0.5	-282 ± 15	3.5 ± 0.1	40 ± 7
Pep1-cho	5.7 ± 0.4	-110 ± 23	2.8 ± 0.4	108 ± 41
Pep1-16PL	4.0 ± 0.2	0.8 ± 14	4.8 ± 0.3	-55 ± 20
Pep2-cho	5.1 ± 0.3	-74 ± 21	2.7 ± 0.3	123 ± 31
Pep2-16PL	8.0 ± 1.3	-219 ± 51	9.8 ± 0.6	-284 ± 19

Table 14: Average *K* and ω_{AB} values from NNR reactions of **cho**, **16PL**, **Pep1**, and **Pep2**.

Dimer Pair	Host Mem-brane	time (h)	mean diameter (nm)
{Pep1-cho}	l_d	0	180.3 ± 70.3
		24	173.5 ± 76.3
{Pep1-cho}	l_d	0	165.1 ± 54.5
		24	160.3 ± 62.5
{Pep1-cho}	l_o	0	199.2 ± 59.8
		24	194.6 ± 75.9
{Pep1-cho}	l_o	0	191.8 ± 57.5
		24	194.3 ± 64.1
{Pep1-16PL}	l_d	0	182.1± 51.0
		24	178.4 ± 69.6
{Pep1-16PL}	l_d	0	174.4 ± 57.6
		24	173.1 ± 55.4
{Pep1-16PL}	l_d	0	173.0 ± 62.3
		24	167.9 ± 53.7
{Pep1-16PL}	l_o	0	201.9 ± 72.7
		24	187.7 ± 43.2
{Pep1-16PL}	l_o	0	194.8 ± 76.0
		24	200.3 ± 62.1
{Pep1-16PL}	l_o	0	192.7 ± 54.0
		24	188.0 ± 73.3

Dimer Pair	Host Mem-brane	time (h)	mean diameter (nm)
{Pep2-cho}	l_d	0	177.3 ± 63.8
		24	177.3 ± 62.1
{Pep2-cho}	l_d	0	158.6 ± 71.4
		24	150.5 ± 57.2
{Pep2-cho}	l_d	0	161.9 ± 47.0
		24	158.3 ± 68.1
{Pep2-cho}	l_o	0	180.6 ± 84.9
		24	198.7 ± 79.5
{Pep2-cho}	l_o	0	181.0 ± 65.2
		24	175.0 ± 63.0
{Pep2-cho}	l_o	0	186.7 ± 72.8
		24	185.8 ± 22.3
{Pep2-PL}	l_d	0	181.0 ± 63.5
		24	178.6 ± 44.7
{Pep2-PL}	l_d	0	178.9 ± 75.1
		24	169.3 ± 44.0
{Pep2-PL}	l_d	0	175.3 ± 57.8
		24	175.3 ± 61.4
{Pep2-PL}	l_o	0	180.6 ± 84.9
		24	198.7 ± 79.5
{Pep2-PL}	l_o	0	174.7 ± 36.7
		24	176.0 ± 77.4
{Pep2-PL}	l_o	0	191.8 ± 78.6
		24	179.3 ± 59.2

Table 15: DLS data for vesicles before and after NNR reactions involving **Pep1** and **Pep2**. Monomodal size distribution was observed in all cases

Dimer Pair	Host Membrane	time (h)	mean diameter (nm)
{cho-16PL}	l_d	0	169.0 ± 60.8
		23	163.7 ± 45.8
{cho-16PL}	l_d	0	169.7 ± 45.8
		23	159.6 ± 51.1
{cho-16PL}	l_d	0	178.8 ± 57.2
		24	163.3 ± 50.6
{cho-16PL}	l_d	0	181.7 ± 85.4
		24	160.9 ± 48.3
{cho-16PL}	l_o	0	185.6 ±70.5
		22	183.8 ± 58.8
{cho-16PL}	l_o	0	194.2 ± 56.3
		22	194.8 ± 58.4
{cho-16PL}	l_o	0	187.9 ± 52.6
		24	181.9 ± 56.4
{cho-16PL}	l_o	0	182.9 ± 56.7
		20	178.8 ± 46.5

Table 16: DLS data for vesicles before and after NNR reactions involving {**cho-16PL**}. Monomodal size distribution was observed in all cases.

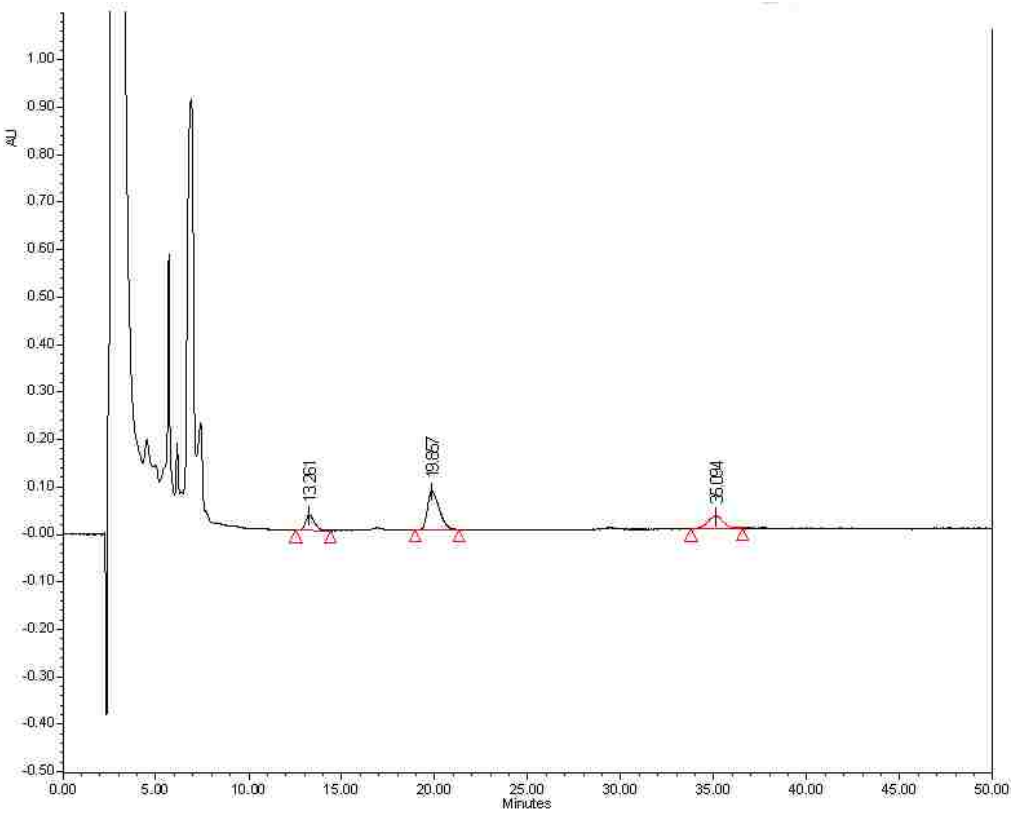

Figure 16: Typical HPLC chromatogram from the analysis of product mixtures in NNR reactions starting with heterodimer {**cho-16PL**}

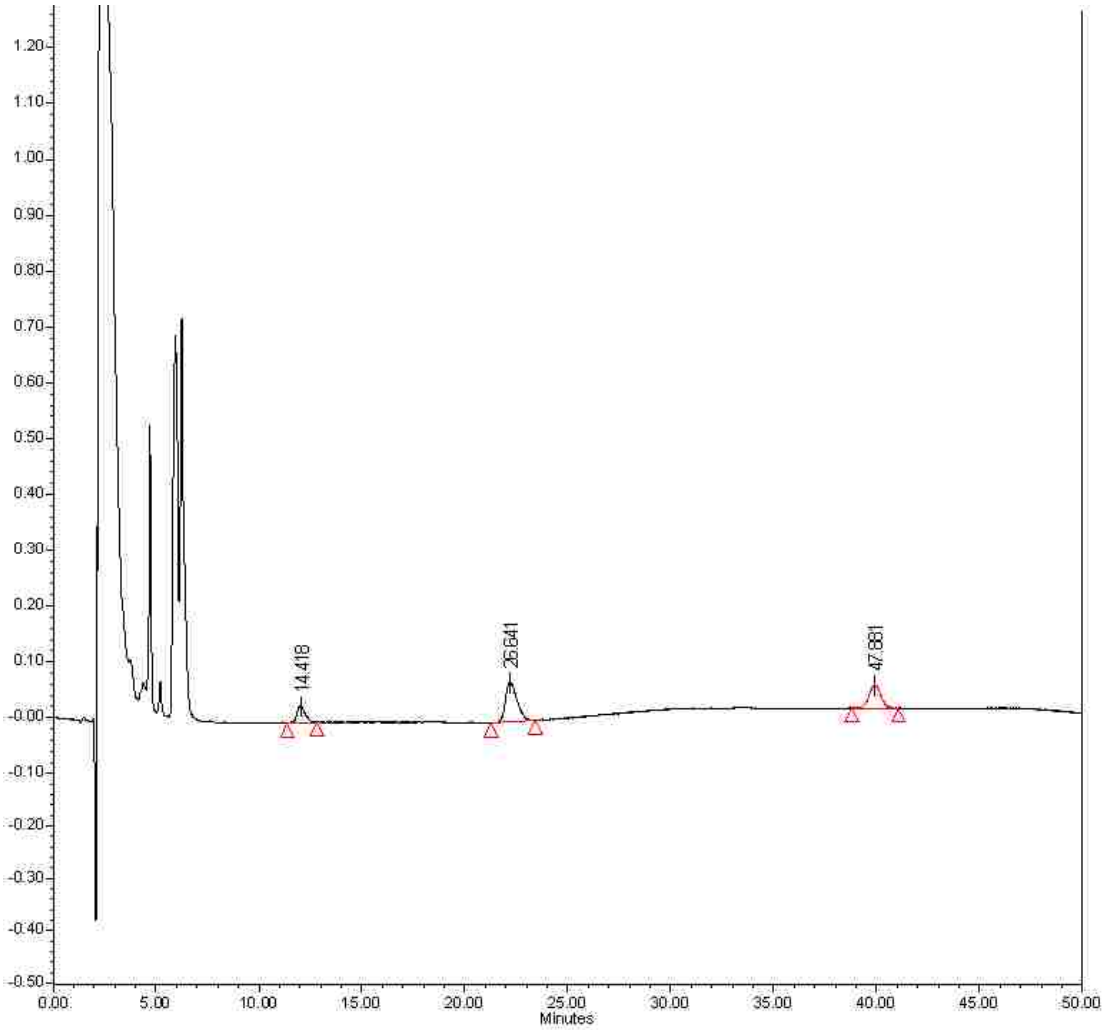

Figure 17: Typical HPLC chromatogram from the analysis of product mixtures in NNR reactions starting with heterodimer {**Pep1-16PL**}

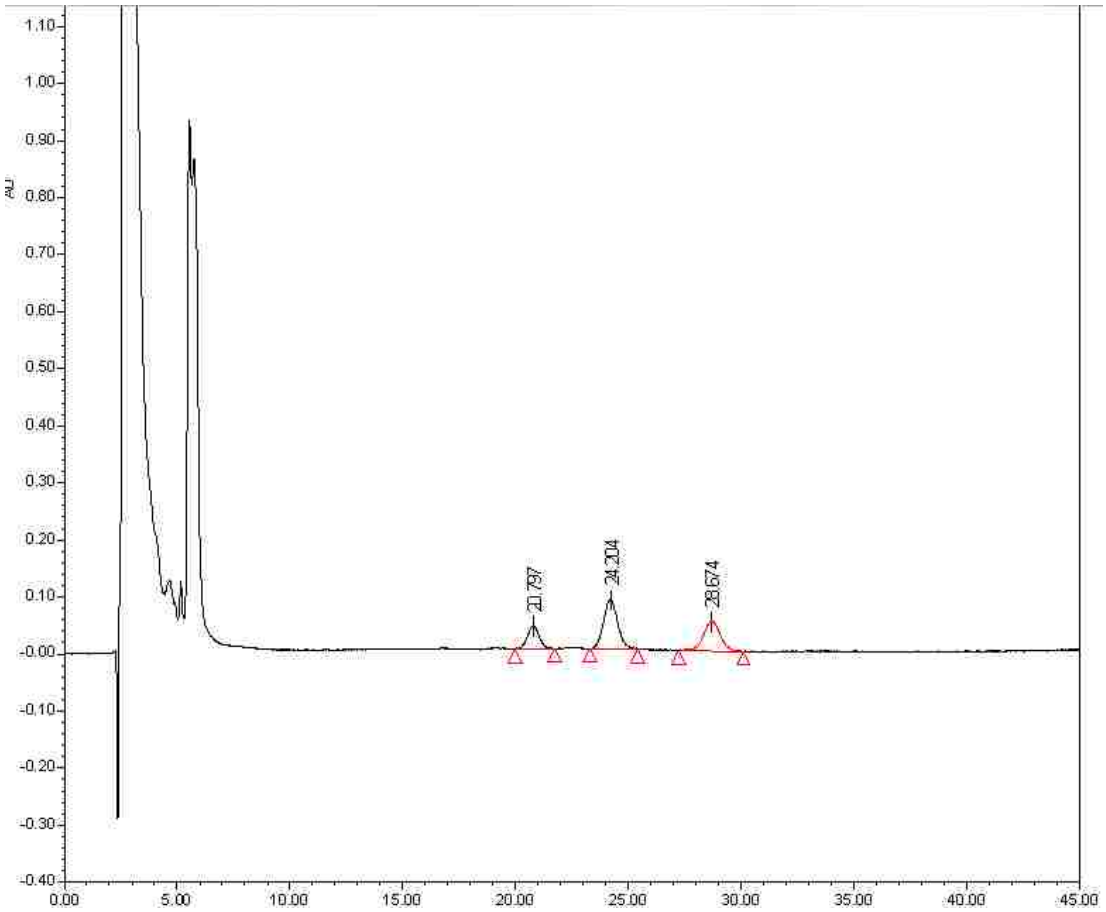

Figure 18: Typical HPLC chromatogram from the analysis of product mixtures in NNR reactions starting with heterodimer {**Pep2-cho**}

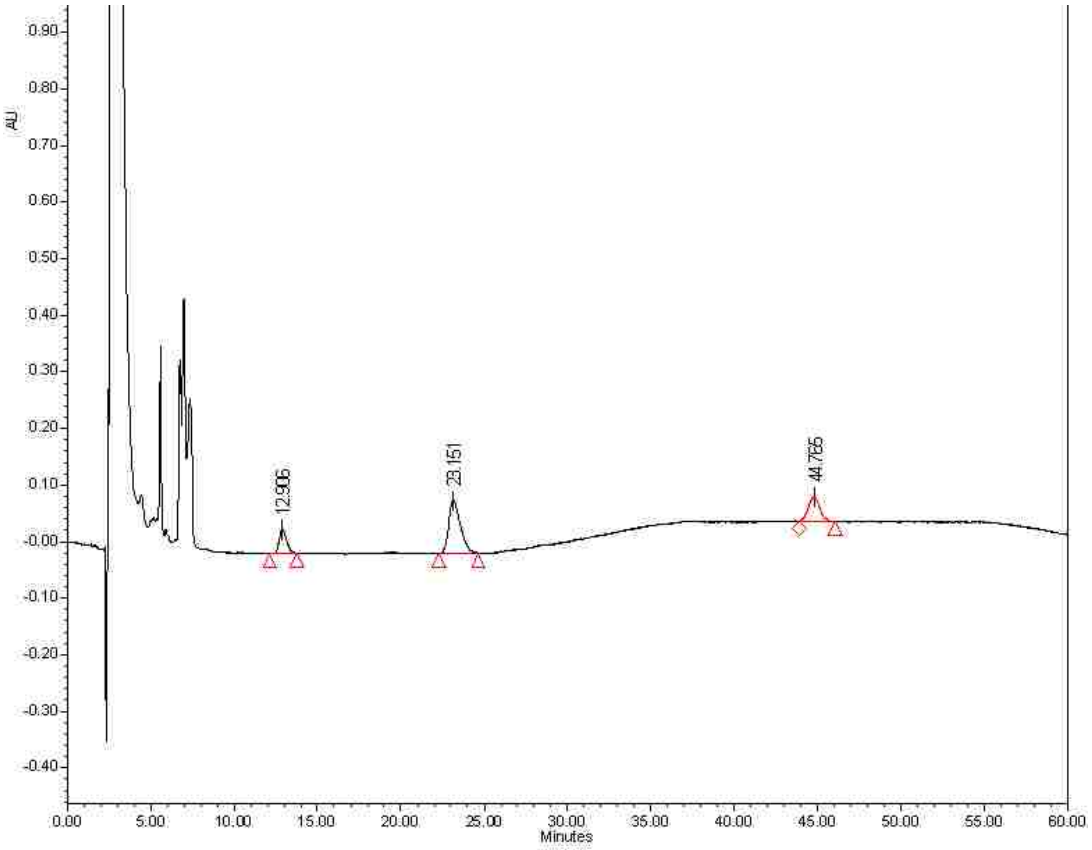

Figure 19: Typical HPLC chromatogram from the analysis of product mixtures in NNR reactions starting with heterodimer {**Pep2-16PL**}

2.3.5 DSC Results

Experimental results shown in this section were obtained by Prof. Paulo Almeida (University of North Carolina, Wilmington), additional preliminary experiments were performed at Lehigh University by Trevor Daly (results not shown).

In order to measure the phase transition properties of **Pep1** and **Pep2** by DSC, non-exchangeable mimics of each peptide, **Pep1a** and **Pep2a** (Figure 7, page 20), were synthesized by reduction of {**Pep1-Pep1**} or {**Pep2-Pep2**} by TCEP, followed by reaction with methyl iodide. Thin films of these monomers were then hydrated with MOPS buffer at 85 ^{o}C in order to prepare vesicles suspensions for DSC experiments. Monomer **Pep1a** remained completely insoluble in buffer at 85 ^{o}C, while **Pep2a** readily

formed a dispersion at that temperature. Examination of this dispersion by DSC showed a well-defined endotherm (Figure 20c) with a T_m of 61 ^oC. Due to uncertainty in determining the concentration of this dispersion, no enthalpy value could be determined from this analysis.

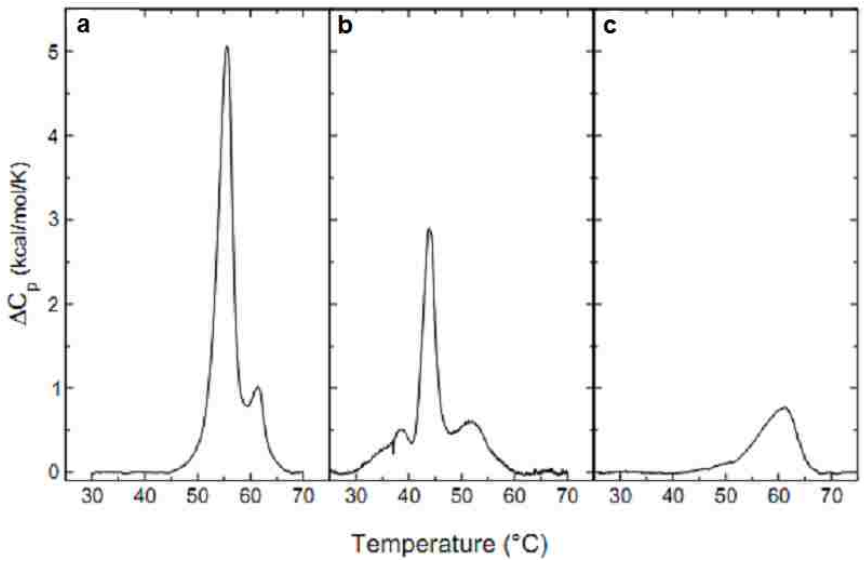

Figure 20: DSC scan of dispersions of (a) {**Pep1-16PL**}, (b) {**Pep2-16PL**}, and (c) **Pep2a**

As an alternate means to measuring the phase transition properties of **Pep1** and **Pep2**, dispersions of the heterodimers {**Pep1-16PL}** and **{Pep2-16PL}** were analyzed by DSC. Both heterodimers readily formed dispersions in MOPS buffer at 85 ^oC. Examination of {**Pep1-16PL**} by DSC revealed a main transition at 55 °C with an apparent $\Delta H \approx 24 \pm 3$ kcal/mol, while {**Pep2-16PL**} gave a broad and complex transition that was centered around 45 °C, with a significant dependence on the hydration temperature and thermal history (Figure 20a and 20b). All of these DSC data are summarized in Table 17. In addition, Table 17 contains relevant DSC data for lipids **14PL** and **18PL** (exchangeable mimics of 14 and 18 carbon phospholipids, see Figure 21), and their analogous phosphocholines, for comparison.[54, 58-66]

Lipid	T_m (^oC)	ΔH (kcal/mol)
DMPC	23.8	6.1
{14PL-14PL}[a]	22.7	14.7
DPPC	41.5	8.5
16PL[a,b]	39.9	9.3
{16PL-16PL}[a]	41.9	18.7
DSPC	54.8	10.9
{18PL-18PL}[a]	55.4	21.7
{14PL-16PL}[a]	31.2	16.7
{14PL-18PL}[a]	33.9	18.7
{Pep1-16PL}	55	~24
{Pep2-16PL}	45	~17
Pep1	(~80)	(~10)
Pep2	61[c]	(~7)

Table 17: Melting Behavior of Dimers and Monomers. The values given for phosphocholines, 1,2-myristoyl-sn-glycero-3-phosphocholine (DMPC), DPPC, and 1,2-stearoyl-sn-glycero-3-phosphocholine (DSPC) are from a combination of references 59-66). Numbers in parentheses are estimated values. [a]Taken from reference 54. [b]Value of a methyl thioether analog of **16PL**. [c]Value of **Pep2a**.

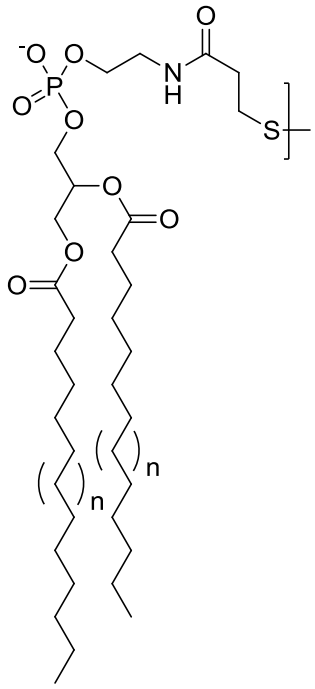

n = 2, **14PL**
n = 4, **16PL**
n = 6, **18PL**

Figure 21: Structures of exchangeable phospholipids used in DSC studies

Based on the data in Table 17, the enthalpies (ΔH) of dimers are nearly equivalent to the sum of their constituent monomers. The ΔH for **Pep1** and **Pep2** were therefore estimated by subtracting ΔH of **16PL** (9.3 kcal/mol) from the ΔH observed in the DSC experiments of the heterodimers **Pep1-16PL** and **Pep2-16PL**.

Unlike ΔH, the T_m data for dimers is not additive. Instead, the T_m of homodimers are nearly identical to the T_m of the monomer. The homodimer {**16PL-16PL**} for example, has a T_m of 41.9 ^oC, compared to 41.5 ^oC for DPPC (and 39.9 ^oC for the monomer **16PL**) . For heterodimers, the T_m is intermediate to the monomers, and is slightly closer to the T_m of the lower melting lipid. This bias towards the lower-melting lipid is analogous to what is known for phospholipids bearing two different acyl chains. For example, the T_m for 1-palmitoyl-2-oleyol-*sn*-glycero-3-phosphocholine (POPC), 1,2-dioleyol-*sn*-glycero-3-phosphocholine (DOPC), and DPPC are -3 °C, -13 °C, and 41.5 °C, respectively.[58]

Figure 22 shows the T_m of the dimers {**14PL-14PL**}, {**14PL-16PL**}, and {**14PL-18PL**}, plotted as a function of the T_m of the higher melting monomer. Based on the data shown in Figure 22, the T_m of a heterodimer can be approximated by Equation 1 (dashed line in Figure 22) where T_m^{low} and T_m^{high} are the T_m values for the low and high-melting monomers, respectively.

$$T_m^{dimer} = 0.65T_m^{low} + 0.35T_m^{high} \quad \text{eq.1}$$

Using equation 1, the T_m of **Pep1** was estimated to be ~80 °C, based on the experimentally observed T_m of {**Pep1-16PL**} and **16PL**. This high T_m can account for our difficulty dispersing the monomer **Pep1a** at 85 °C.

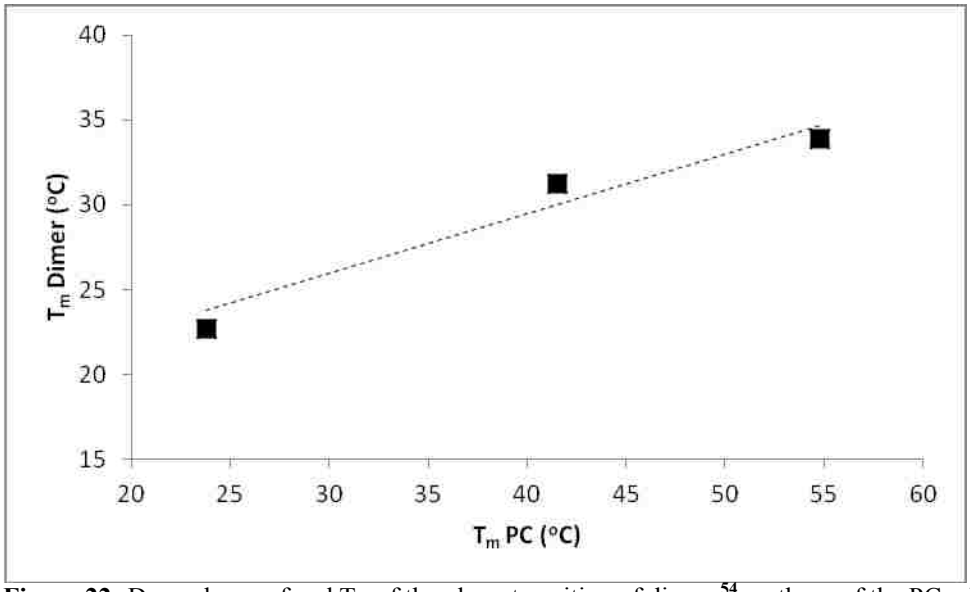

Figure 22: Dependence of and T_m of the phase transition of dimers[54] on those of the PC with the same acyl chain length.[58-66] Solid squares are for dimers of **14PL** with **14PL, 16PL,** and **18PL** as a function of the T_m of the PC that corresponds to the longer- or equivalent-chain monomer. The dashed line is the equation $y = 0.65\times23.8+0.35x$, which is eq. 1, with $T_m^{Low} = 23.8$ °C for DMPC

2.3.6 Monte Carlo Simulations

Based on the nearest neighbor interaction energies measured by NNR and the thermodynamic data measured in the DSC experiments, Monte Carlo simulations were performed by our collaborator, Professor Paulo Almeida (University of North Carolina, Wilmington). Lipid membranes were simulated as 100 × 100 triangular lattices, where each site represents a phospholipid, a lipidated peptide, or a sterol molecule. The phospholipids can exist in three states: gel, l_o, and l_d state. The l_o state is intermediate to the gel and l_d states in terms of its enthalpy, entropy, and chain order. Simulations were performed at the same temperature (45 °C) using NNR values that were experimentally determined in each phase, in addition to those previously used for DPPC/cholesterol.[67] Snapshots of the simulations are shown in Figure 23 for the l_d, l_o, and l_o/l_d (20 mol% cholesterol) coexistence regions. In addition, a fourth simulation was performed in which the DPPC/cholesterol interaction energy was changed from the experimental value of 40

cal/mol to an artificial value of 400 cal/mol. As expected, this led to a system approaching true phase separation (Figure 23-D). DPPC is shown in black (gel), white (l_d), or blue (l_o); cholesterol is shown in red, and **Pep1** is shown in green. No distinction is made between DPPC and **16PL**, or between cholesterol and **cho**. Similar simulations were also done using **Pep2** in place of **Pep1** (not shown).

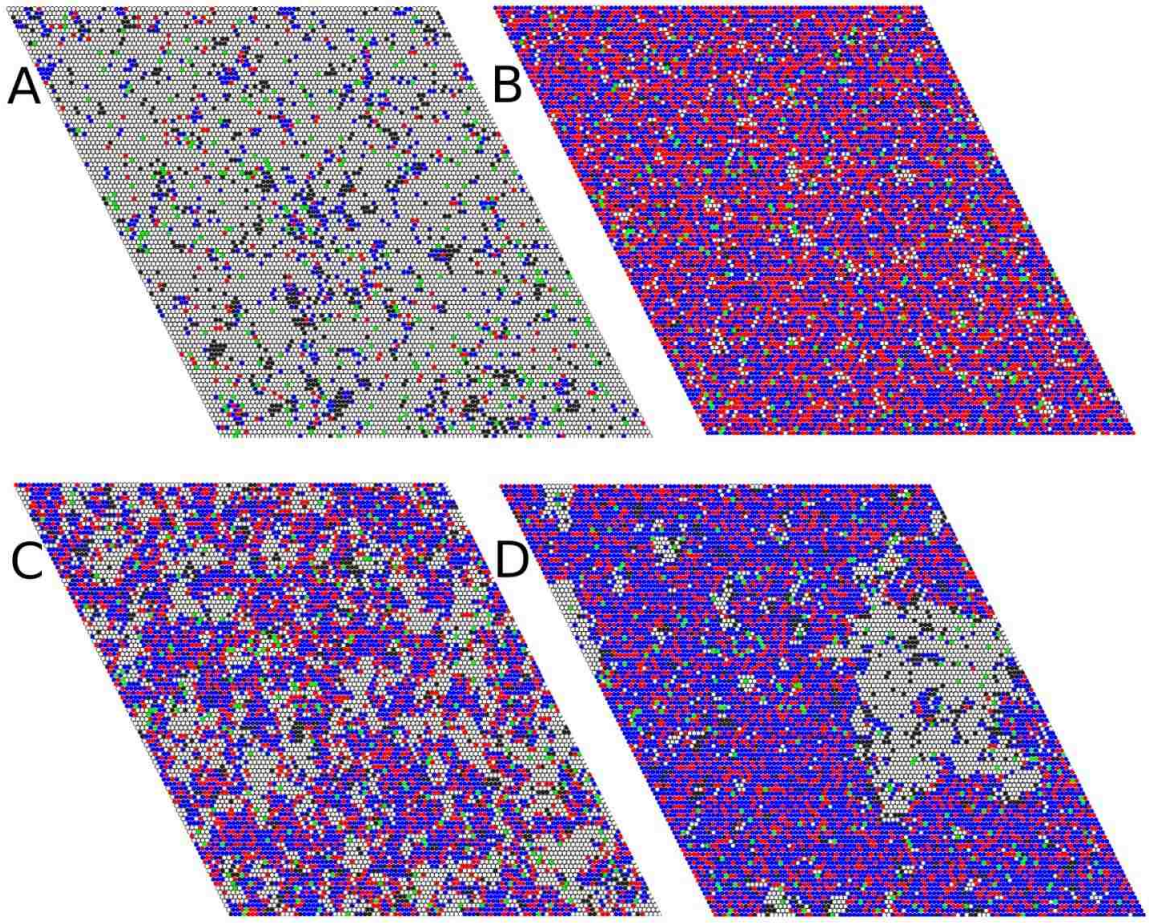

Figure 23: Snapshots of Monte Carlo simulations of mixtures of DPPC and cholesterol containing 2.5 mol% of **Pep1**: (A) l_d phase, DPPC/cholesterol/**Pep1**, 95/2.5/2.5 (mol/mol/mol), (B) l_o phase, DPPC/cholesterol/**Pep1**, 57.5/40/2.5 (mol/mol/mol), (C) l_d/l_o coexistence region, DPPC/cholesterol/**Pep1**, 77.5/20/2.5 (mol/mol/mol), (D) Same as C, except that $\omega^{d}_{\text{cho-16PL}}$ (i.e., nearest-neighbor interaction free energy between **cho** and **16PL** in the l_d phase) has been artificially set at 400 cal/mol instead of the observed value of 40 cal/mol. DPPC is shown in black (gel), white (l_d), or blue (l_o); cholesterol is shown in red; and 1 is shown in green. No distinction is made between DPPC and **16PL**, or between cholesterol and **cho**.

Figure 23-C shows a snapshot from the Monte Carlo simulation of 2.5% **Pep1** included in a host membrane containing coexisting l_d and l_o domains. While the peptides appear to be randomly distributed between l_d and l_o domains, a partition coefficient can be calculated based on Equation 2 to quantitatively measure the affinity of the peptide for each phase.

$$K_p = \frac{[pep]_o/[l_o]}{[pep]_d/[l_d]} \qquad \text{eq. 2}$$

Here, $[pep]_o$ and $[pep]_d$ represent the number of lipidated peptides (**Pep1** or **Pep2**) in the l_o and l_d regions, and $[l_o]$ and $[l_d]$ are the number of phospholipid sites belonging to each region. For these simulations, a lipidated peptide molecule was considered to be located in a l_o or l_d region according to the majority of nearest neighbor lipids surrounding it. In defining K_p, only phospholipid molecules were counted; the sites occupied by sterol were not counted for either phase. The results obtained for **Pep1** and **Pep2** in the l_d/l_o coexistence region (20 mol% cholesterol) are summarized in Table 18.

Peptide	Phase Behavior	$\omega_{cho\text{-}16PL}$ (cal/mol)	K_p (l_o/l_d)
Pep1	small domains	40	1.0
Pep1	phase separation	400	1.2
Pep2	small domains	40	0.46
Pep2	phase separation	400	0.46

Table 18: Partition coefficients determined from Monte Carlo simulations in membranes of DPPC/cholesterol/(pep) 77.5/20/2.5 (mol/mol/mol). No distinction is made between DPPC and **16PL**, and between cholesterol and **cho**.

2.4 Discussion

The results of the NNR reactions summarized in Table 14 (page 46) are shown graphically as an energy diagram in Figure 24. The light scattering data shown in Tables

15 & 16 demonstrate that vesicles used in these NNR reactions were stable over the timeframe of the experiments. The results shown in Figure 24 can be readily interpreted if one considers two factors: the favorable interactions between cholesterol and phospholipids (or lipidated peptides) that develop in the l_o phase, and unfavorable interactions that result from poor packing of kinked acyl chains in a planar bilayer. In explaining the trends observed in these energy levels, it is important to keep in mind that *our experimental values of ω_{AB} do not represent absolute energies for the interactions between **A** and **B**. Rather, they are a measure of the difference in energy associated with hetero-interactions and the average of the homo-interations.* The nearest neighbor interaction energy, ω_{AB} is thus defined by Equation 3, where ε_{AB} represents the contact (nearest-neighbor) interactions between lipids **A** and **B**.

$$\omega_{AB} = \varepsilon_{AB} - \frac{\varepsilon_{AA}+\varepsilon_{BB}}{2} \qquad \text{eq. 3}$$

Let us first consider the phospholipid-cholesterol and peptide-cholesterol interactions. In all cases, the lipid-sterol interactions become more favorable (*i.e.* ω_{AB} decreases) upon going from l_d to l_o. This favorable interaction between rigid planar sterols and condensed acyl chains is characteristic of the liquid ordered phase. Within experimental error, the interactions of the two peptides with **cho** are identical. While the mixing of **cho** and **16PL** is close to ideal in the l_d phase, the mixing of **cho** with either peptide favors homo-association in the same phase. This greater (more positive) value of ω_{AB} for the peptides relative to **16PL** carries over to the l_o phase, although in that phase all values of ω_{AB} are negative. The greater preference for hetero-association in **cho-16PL**

interactions (relative to **cho-Pep** interactions) in both phases is most likely a consequence of poor interactions between **cho** and the acyl chains of the peptides, which are farther apart, and thus more disordered, than those on the phospholipids.

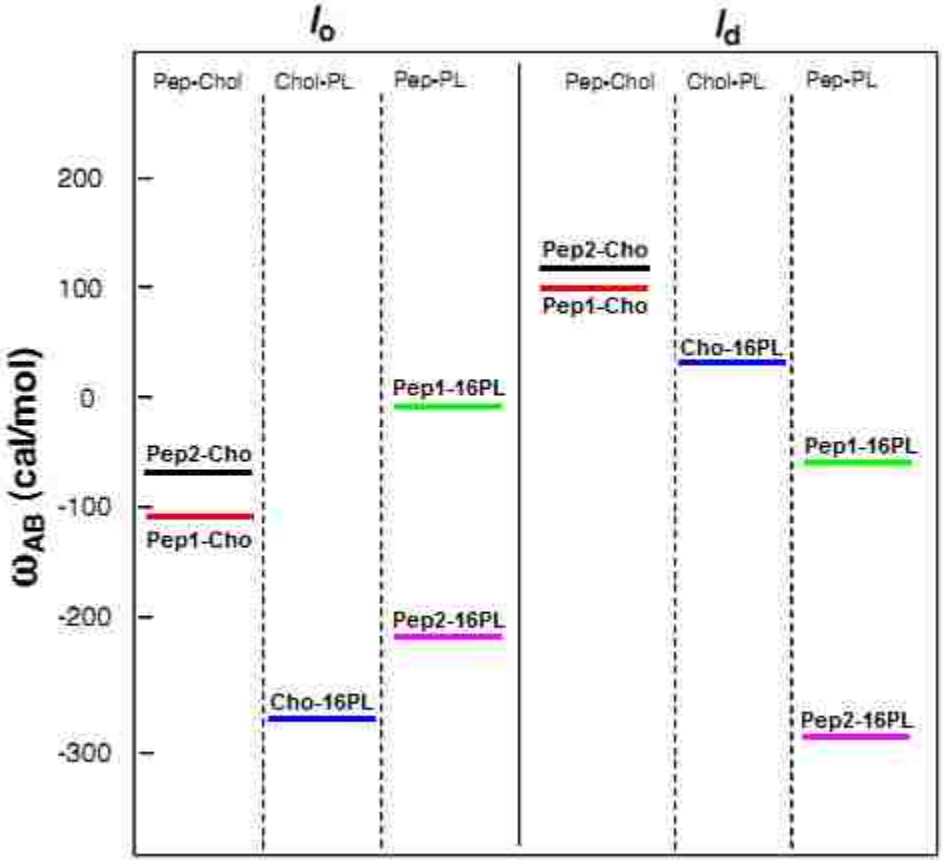

Figure 24: Energy diagram showing the nearest-neighbor interaction free energies, ω_{AB}, for various pair of lipids and lipidated peptides in the l_o phase (left) and the l_d phase (right), separated into peptide-cholesterol (Pep-Chol), cholesterol-phospholipid (Chol-PL) and peptide-phospholipid (Pep-PL) interactions

In considering the peptide-phospholipid interactions, the most dramatic trend is the large difference between **Pep1** and **Pep2** associating with **16PL**. The mixing of **Pep1** and **16PL** is close to ideal in both phases, implying that there are no significant hetero- or homo-interactions occurring in either phase. However, **Pep2** shows a strong preference for hetero-association with **16PL** in both phases. Since both peptides have the same headgroup, this large difference in their interactions with **16PL** must arise from the

presence of a kink in the acyl chains of **Pep2**. In light of the definition of ω_{AB}, the apparent favorable hetero-interaction between **Pep2** and **16PL** can be explained by a very weak homo-association between **Pep2** molecules. Apparently, the permanent kink in the acyl chain of **Pep2** inhibits efficient acyl chain packing when two **Pep2** molecules become nearest neighbors, resulting in poor homo-association. The slightly more negative value of ω_{AB} that is observed on going from l_o to l_d can therefore be accounted for by poor packing of neighboring **Pep2** molecules that becomes better tolerated in a disordered matrix.

Finally, note that unlike the **Pep2-16PL** interactions, large negative values ω_{AB} are not observed for the **Pep2-cho** interactions. Based on Equation 3, if the **Pep2-Pep2** homo-interactions are unfavorable (*i.e.* $\varepsilon_{Pep2\text{-}Pep2} > 0$), **Pep2-cho** interactions must also be unfavorable (*i.e.* $\varepsilon_{Pep2\text{-}cho} > 0$) in order for $\omega_{Pep2\text{-}Cho}$ to be positive in the l_d phase (or close to zero in the l_o phase). A careful examination of the energy level diagram in Figure 24 therefore leads to the conclusion that *nearest-neighbor interactions between two molecules of **Pep2**, and also between a molecule of **Pep2** interacting with a molecule of **cho**, are especially weak.*

The NNR measurements themselves thus provide new insight into the interaction of lipidated peptides with sterols and phospholipids. Further insight into the interaction of the peptides with membranes can be obtained from the Monte Carlo simulations. As shown in Table 18 (page 56), partition coefficients can be calculated from the Monte Carlo simulations to quantitatively measure the affinity of **Pep1** and **Pep2** for the l_o phase in membranes containing coexisting l_o and l_d domains. **Pep1** was chosen for these experiments because it was expected to strongly favor the liquid ordered phase, based on

the presence of two long saturated acyl chains. However, it was found to have no preference for either phase in these simulations ($K_p = 1$). As expected, the kinked acyl chain on **Pep2**, gives it a slight preference for l_d domains.

Pep1 is a mimic of a peptide that has previously shown a preference for l_o domains in model membranes made from DPPC, cholesterol, and POPC.[42] Such systems are known to exhibit phase separation into large domains, in contrast to the small transient domains thought to be present in binary mixtures of DPPC and cholesterol. To determine whether domain size is a key parameter in controlling the partitioning of lipidated peptides, the Monte Carlo simulations were repeated with $\omega_{16PL\text{-}Cho}$ in the l_d phase constrained to 400 cal/mol instead of the experimentally determined 40 cal/mol. As expected, this lead to large scale phase separation of l_d and l_o domains (Figure 23D, page 55). However, as shown in Table 18 (page 56), the change in phase behavior did not affect the partitioning of either peptide.

One particularly powerful method of interpreting the NNR data, and the resulting partition coefficients, was suggested to us by our collaborator, Prof. Paulo Almeida. In this approach, a "mean-field" approximation is used to represent the differences in peptide-phospholipid and peptide-cholesterol interactions experienced by the average peptide molecule upon going from the l_o to l_d domains as a weighted average of the measured interaction energies, as shown in Equations 4 and 5 below.

$$\Delta\omega_1 = \left(\omega^o_{Pep1-cho} f_c^o + \omega^o_{Pep1-16PL}(1 - f_c^o)\right) - \left(\omega^d_{Pep1-cho} f_c^d + \omega^d_{Pep1-16PL}(1 - f_c^d)\right) \quad \text{eq. 4}$$

$$\Delta\omega_2 = \left(\omega^o_{Pep2-cho} f_c^o + \omega^o_{Pep2-16PL}(1 - f_c^o)\right) - \left(\omega^d_{Pep2-cho} f_c^d + \omega^d_{Pep2-16PL}(1 - f_c^d)\right) \quad \text{eq. 5}$$

In these equations, ω^o and ω^d represent the measured nearest neighbor interaction energies in the l_o and l_d phase, respectively, and f_c^o and f_c^d are the mole fractions of cholesterol in the l_o and l_d phase. Note that f_c^o and f_c^d do not necessarily add up to one; they refer to the percentage of total lipid molecules in each phase that are cholesterol, not the percentage of total cholesterol molecules that are in a given phase. Because each lipid has 6 nearest-neighbors in the hexagonal array, the partition coefficient can be expressed in terms of $\Delta\omega$ as shown in Equation 6.

$$K_p = e^{-6\Delta\omega/RT} \qquad \text{eq. 6}$$

The only variables in Equations 4, 5, and 6 are the ω_{AB} values (which are experimentally determined in the NNR reactions) and f_c^o and f_c^d. Therefore, *the partition coefficient can be calculated directly from the experimental ω_{AB} values, if the mole fractions of cholesterol in each phase are known.* Based on the experimental ω_{AB} values and the K_p values of 1.0 and 0.46 for **Pep1** and **Pep2**, respectively (as determined by Monte Carlo simulation), the mole fractions of cholesterol in the l_o and l_d regions can be calculated to be $f_c^o = 0.36$ and $f_c^d = 0.08$. These values are reasonable, given a cholesterol content of 20 mol% in the host membrane and the phase diagram for DPPC/cholesterol.[50] Thus, NNR measurements can be used to determine the partition coefficients of other lipidated peptides in future experiments without the need for further Monte Carlo simulations by using these values of f_c^o and f_c^d, and Equations 4, 5, and 6, provided that the same host membranes are used.

2.5 Conclusions

The existence of lipid rafts in live cells, and as the role that lipid rafts may play in sorting of peripheral proteins remain controversial subjects. While techniques such as detergent resistance assays, fluorescence microscopy in GUV's, and AFM have been used to qualitatively gauge the partitioning of peripheral proteins into putative lipid rafts, these techniques suffer from several drawbacks and have largely been applied to specific proteins without regard to the more basic questions of what structural elements are key to lipid sorting on a molecular level. The studies presented here represent a new approach to the study of lipid sorting, which is unique in its ability to provide a quantitative, molecular level view of lipid sorting while probing domains of any size.

Nearest Neighbor Recognition experiments applied to lipidated peptides **Pep1** (a lipidated peptide based on the motif [(myristoyl)GlyCys(palmitoyl)Gly]) and **Pep2** (a similar peptide bearing a permanent kink in its 14 carbon chain) revealed that the interactions of both peptides with sterols and phospholipids were roughly similar, but the behavior of **Pep2** was largely dictated by poor packing of its kinked acyl chain in the planar bilayer. Interactions of **Pep2** molecules with cholesterol molecules, as well as with other molecules of **Pep2**, were found to be especially weak. The use of these NNR measurements in Monte Carlo simulations revealed that in membranes containing coexisting l_o and l_d domains, **Pep1** partitions randomly between both phases, while **Pep2** has a slight affinity for disordered domains. These results are qualitatively similar to those previously reported by Silvius *et al.* using similar peptides.[42] The observed partitioning coefficients were found to be independent of the size of the domains.

NNR measurement of nearest neighbor interaction energies, coupled with Monte Carlo simulation, provides a powerful new tool for measuring the partitioning of peripheral proteins between domains. This technique is unique in its ability to generate a quantitative partition coefficient without reliance on artificially large domains in model systems.

All of the variables in this study, including the choice of peptides, host membranes and reaction conditions, were anticipated to produce a marked affinity for the l_o phase ($K_p > 1$). The fact that **Pep1** did not exhibit such an affinity therefore suggests that the sorting of lipidated peripheral proteins based on the interaction of their hydrophobic anchors with the host membrane is less important than previously suggested, and that other factors, such as hydrogen bonding or specific protein-protein interactions may play a larger role in directing of peripheral proteins into lipid rafts.

Recent findings by Triffo *et al.* support the conclusion that that specific protein-protein or protein-lipid interactions may play a greater role in lipid sorting than sorting based on the packing of their hydrophobic anchors into phase separated membrane domains. Using an FCS technique called pulsed-interleaved excitation fluorescence cross-correlation spectroscopy (PIE-FCCS) in live cells, Triffo *et al.* observed the presence of two orthogonally composed membrane domains containing different lipid-anchored membrane proteins, as well as additional anchored proteins distributed evenly about the cell surface.[68] This level of complexity cannot be accounted for by sorting of proteins into lipid rafts by the packing of their fatty acid anchors. Instead, Triffo *et al.* favor a model in which, "lipid-anchored fluorescent proteins partition into pre-existing

clusters that are primarily defined by specific protein-protein and protein-lipid interactions among native cell membrane proteins." [68]

Now that the applicability of NNR and Monte Carlo simulations to the problem of measuring protein partitioning has been demonstrated, future work will involve the modification of this technique to allow the observation of molecular level interactions in a system that more closely mimics a biological membrane. Sphingomyelin, a lipid which has been shown to be a major component of lipid rafts in mammalian membranes, is of particular interest because the amide and hydroxyl groups in its headgroup could have significant hydrogen bonding interactions with peptides. Such hydrogen bonding interactions are not accounted for in DPPC/cholesterol host membranes. Performing NNR reactions in host membranes containing sphingomyelin (or a sphingomyelin mimic lacking a C-C double bond) could be used to assess the role of protein-lipid hydrogen bonding in lipid sorting.

Additionally, future experiments will involve the application of this technique to a wide variety of other peptides, in order to gain further insight into the structural elements necessary for effective peptide partitioning into l_o domains. Peptides with different spacing between chains, different chain lengths, and multiple unsaturations will all be considered. In addition, work on extending this technique to transmembrane peptide domains will also be considered.

CHAPTER 3

Cholesterol's Condensing Effect

3.1 Background

Cholesterol's condensing effect, defined as its ability to decrease the apparent molecular area occupied by fluid phase lipids, has been known for nearly a century.[69] This effect is typically observed in monolayer experiments at the air-water interface.[70-72] Despite the fact that the condensing effect presumably plays a large role in defining the structure of mammalian cell membranes (which are rich in both cholesterol and low-melting lipids), the molecular mechanism giving rise to lipid condensation is poorly understood.

The most widely accepted mechanism is the "umbrella model," proposed by Huang and Feigenson, in which the condensing effect is driven by the need for the relatively hydrophobic cholesterol molecule to fit underneath the phospholipid headgroups in order to minimize contact with water. In order to accommodate the cholesterol underneath the headgroups, the lipid acyl chains must, "become more tightly packed as cholesterol content increases, because they share limited space under phospholipid headgroups."[73]

This umbrella model is based on an effort at developing a theoretical model to account for the experimental observation that the maximum solubility of cholesterol in phosphatidylcholine (PC) membranes is 66 mol%, while the maximum solubility in phosphatidylethanolamine (PE) membranes is 51%.[74] A model of phospholipid-

cholesterol interaction must therefore account for solubility limits close to cholesterol/phospholipid mole ratios of both 2:1 and 1:1. Using Monte Carlo simulations to visualize membrane organization and calculate the chemical potential of cholesterol molecules in a simulated bilayer matrix, Huang and Feigenson observed that the only models which can produce sharp increases in chemical potential (which is necessary for cholesterol insolubility to occur) at both of the expected mole ratios are models which include increasingly steep energy penalties for multiple cholesterol molecules neighboring the same phospholipid.[73] In other words, the experimentally observed cholesterol solubility can be accounted for only in models in which phospholipid-cholesterol interactions become increasingly unfavorable with each additional cholesterol molecule contacting a given sterol. Such unfavorable interactions would arise in the case of an umbrella model, where the first cholesterol molecule neighboring a phospholipid is able to comfortably fit beneath the head group, but additional sterols are increasingly crowded out and exposed to water.

Work in the Regen group has lead to the proposal of an alternate mechanism to explain the condensing effect. This mechanism, which we call the "template model," is based on the finding that NNR reactions carried out using the exchangeable dimer {**cho-14PL**} (Figure 25), showed random mixing (*i.e.* K=4.0) across a range of cholesterol concentrations, while hetero-association (*i.e*. *K*>4.0) occurred for dimers {**cho-16PL**} and {**cho-18PL**} at physiologically relevant cholesterol concentrations.[55] This favorable interaction between sterol and phospholipid acyl chains suggests a "template mechanism" for the condensing effect, in which, "the uncoiling of the phospholipids is driven by hydrophobic interactions between their acyl chains and the rigid hydrophobic framework

of neighboring sterols."[55] The observed differences between the *K* of these three dimers suggest that the condensing effect is greatest when the acyl chain is long enough to complement, perfectly, the planar sterol core of cholesterol, thus maximizing hydrophobic contact.

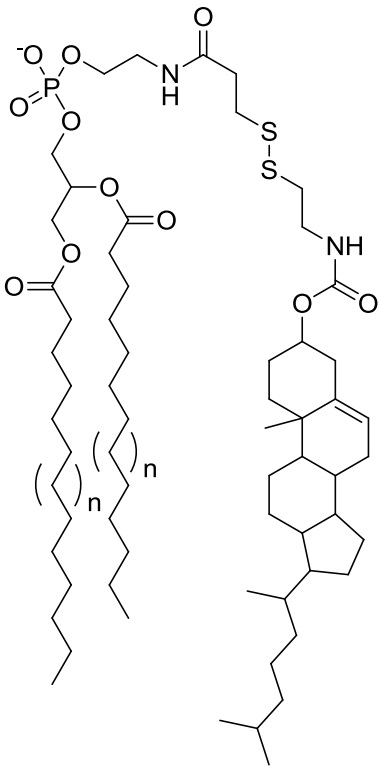

n = 2, {**cho-14PL**}
n = 4, {**cho-16PL**}
n = 6, {**cho-18PL**}

Figure 25: Exchangeable lipids {**cho-14PL**}, {**cho-16PL**}, and {**cho-18PL**}

Building upon this earlier work, the goal of the studies reported herein was to distinguish between the umbrella and template mechanisms for cholesterol's condensing effect by probing the interactions of cholesterol, and related structural analogs, with phospholipids using NNR.

3.2 Experimental Design

To differentiate between the "umbrella" and "template" models, we investigated the effects of coprostanol (Figure 26), a sterol that occupies a larger surface area in the monolayer state than cholesterol, due to the *cis* fusion of its A and B rings.[72] As depicted in Figure 27, a careful consideration of the template and umbrella models reveals that the two models differ in their predictions about the relative condensing power of coprostanol. By a template model, one would expect coprostanol to have a poor condensing effect, as it lacks the planar structure necessary to maximize hydrophobic contact with fully extended acyl chains. The umbrella model, however, would predict a stronger condensing effect for coprostanol than for cholesterol, since coprostanol's larger surface area would require tighter packing of the acyl chains in order for the sterol to fit completely under the headgroup. *Thus, a quantitative comparison of the condensing effects of these two sterols should distinguish between an umbrella and a template model.*

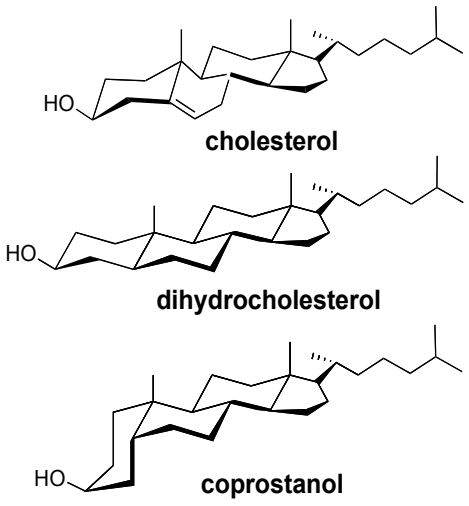

Figure 26: Structures of coprostanol, cholesterol, and dihydrocholesterol

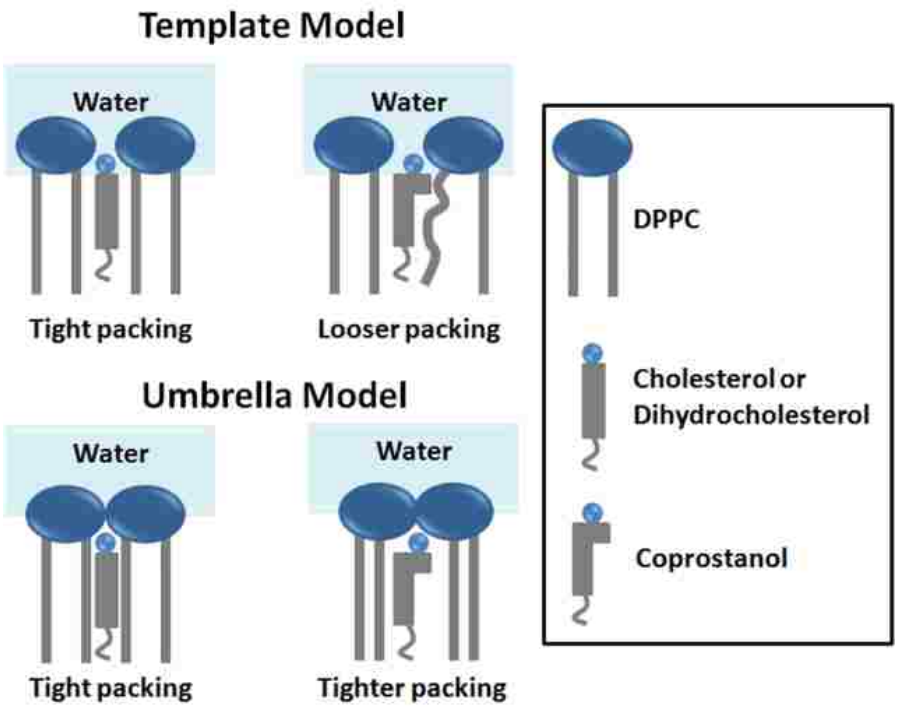

Figure 27: Cartoon depicting the "template" and "umbrella" models of cholesterol's condensing effect, and the predicted condensing effect of coprostanol

Dihydrocholesterol, which has a cross sectional area similar to cholesterol, but like coprostanol, lacks a double bond, would be expected to have a similar condensing effect to cholesterol based on both a template and umbrella model. It can be used to verify that the presence of a double bond is not crucial to cholesterol's condensing effect.

Previous efforts to compare the condensing effects of these sterols have had contradictory results. Previous NNR studies aimed at measuring the effects of a variety of sterols on the interaction of two exchangeable phospholipid mimics were unable to measure any difference between cholesterol and coprostanol.[75] Monolayer experiments have found that dihydrocholesterol has a similar condensing effect to cholesterol,[72,76] while coprostanol does not have a strong condensing effect, and fails to induce the formation of coexisting fluid phases.[72,77] It is not clear, however, whether these

monolayer measurements are relevant to biological systems. *An unambiguous measure of the condensing effect of coprostanol in a bilayer is necessary to clearly distinguish between the "template" and "umbrella" models of cholesterol's condensing effect.*

To measure the condensing effect of these three sterols, we used NNR as a chemical sensor (see Section 1.2) to measure the effect that replacing cholesterol with coprostanol or dihydrocholesterol has on the compactness of the bilayer. It has been previously shown that NNR reactions carried out using 2.5 mol % each of **cho** and **16PL** in host membranes made of non-exchangeable lipids (*i.e*. DPPC and cholesterol) can act as a "chemical sensor" to detect changes in the organization of the host membrane, with *K* increasing sharply as the host membrane becomes more condensed.[19] To assess the relative condensing power of cholesterol, dihydrocholesterol, and coprostanol, experiments were thus carried out using NNR reactions to measure the compactness of host membranes containing each of the three sterols. Specifically, thiolate-disulfide equilibration reactions were carried out at 45 ^{o}C in liposomes (~200 nm) made from DPPC/cholesterol/**X**/**cho**/**16PL** (here, **X** is coprostanol or dihydrocholesterol) having the following mole percentages: (*a*) 57.5/37.5/0/2.5/2.5, (*b*) 57.5/27.5/10/2.5/2.5, (*c*) 57.5/17.5/20/2.5/2.5, and (*d*) 57.5/0/37.5/2.5/2.5.

In a complementary set of experiments, studies aimed at directly measuring the interactions of several sterols with phospholipids by conducting NNR reactions using exchangeable analogs of coprostanol and dihydrocholesterol (among other sterols) were performed. The results of these experiments are discussed in Appendix 1.

Prior to performing NNR experiments, it was necessary to show that replacement of cholesterol with dihydrocholesterol or coprostanol does not alter the phase properties

of the membranes, *i.e.* to verify that all membranes used in these studies are in the liquid ordered phase. To do so, fluorescence measurements were carried out using the phase sensitive probe Laurdan (Figure 26). Laurdan generalized polarization (GP), given by $GP = (I_{440}-I_{490})/(I_{440}+I_{490})$ where I_{440} and I_{490} are the fluorescence emission intensity at 440 and 490 nm (λ_{ex}=350 nm), is highly sensitive to the polarity of the immediate environment of the probe.[78] Because a less compact membrane allows deeper penetration of water into the hydrophobic core, GP can be considered a measure of membrane compactness. Plots of GP as a function of temperature therefore reveal phase transitions as sharp changes in GP.

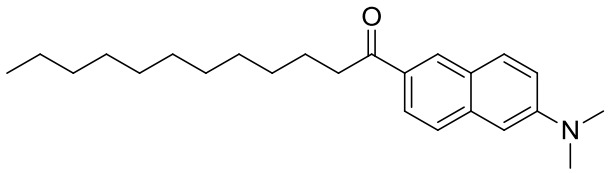

Figure 28: The structure of Laurdan

3.3 Results[79]

3.3.1 Laurdan Fluorescence Polarization Results

Laurdan generalized polarization measurements were used to examine the phase transition properties of liposomes containing cholesterol, coprostanol, and dihydrocholesterol. The results of these experiments are shown in Table 19, and plotted in Figure 29.

2.5 mol% Chol. 95 mol% DPPC 2.5 mol% DPPG		**40 mol% Chol. 57.5 mol% DPPC 2.5 mol% DPPG**		**20 mol% Cop. 20 mol% Chol. 57.5 mol% DPPC 2.5 mol% DPPG**	
T (°C)	**GP**	**T (°C)**	**GP**	**T (°C)**	**GP**
24.7	0.49	30.5	0.49	29.8	0.48
27.7	0.49	34.5	0.47	33.4	0.45
34.5	0.45	37.9	0.45	37.6	0.41
38.0	0.41	40.3	0.44	39.6	0.39
39.9	0.28	42.3	0.43	41.5	0.36
41.9	0.02	44.5	0.40	43.5	0.33
44.1	-0.05	46.4	0.39	45.9	0.31
46.1	-0.10	50.2	0.34	49.6	0.25
49.9	-0.17	54.4	0.30	54.0	0.19
54.4	-0.22				

37.5 mol% Cop. 2.5 mol% Chol. 57.5 mol% DPPC 2.5 mol% DPPG		**20 mol% Dihydro. 20 mol% Chol. 57.5 mol% DPPC 2.5 mol% DPPG**		**37.5 mol% Dihydro. 20 mol% Chol. 57.5 mol% DPPC 2.5 mol% DPPG**	
T (°C)	**GP**	**T (°C)**	**GP**	**T (°C)**	**GP**
29.6	0.43	29.7	0.49	30.0	0.48
33.4	0.37	33.4	0.47	33.4	0.47
37.7	0.31	37.2	0.45	37.4	0.45
39.6	0.28	39.5	0.44	39.4	0.43
41.4	0.25	41.4	0.42	41.5	0.41
43.5	0.21	43.4	0.40	43.9	0.39
45.8	0.18	45.8	0.38	45.7	0.37
49.7	0.12	49.3	0.34	49.7	0.32
53.8	0.06	54.5	0.28	54.5	0.27

Table 19: Laurdan GP values for all liposomes investigated in this study

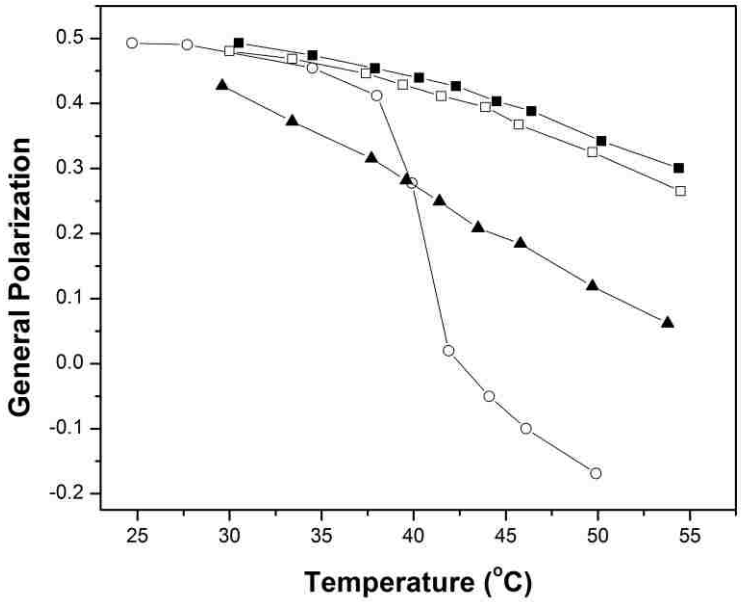

Figure 29: Plot of generalized polarization versus temperature for liposomes made from the following molar percentages of lipids: (○) DPPC/DPPG/cholesterol 95/2.5/2.5; (■) DPPC/DPPG/cholesterol 57.5/2.5/40; (□) DPPC/DPPG/cholesterol/dihydrocholesterol 57.5/2.5/2.5/37.5; and (▲) DPPC/DPPG/cholesterol/coprostanol 57.5/2.5/2.5/37.5

3.3.2 Results of NNR Experiments

In order to measure the condensing effects of cholesterol, coprostanol, and dihydrocholesterol, NNR reactions using {**cho-16PL**} were carried out in host membranes containing these three sterols. Specifically, NNR reactions were carried out in liposomes made from DPPC/cholesterol/**X**/**cho**/**16PL** (here, **X** is coprostanol or dihydrocholesterol) having the following mole percentages: (*a*) 57.5/37.5/0/2.5/2.5, (*b*) 57.5/27.5/10/2.5/2.5, (*c*) 57.5/17.5/20/2.5/2.5, and (*d*) 57.5/0/37.5/2.5/2.5. The results of the reactions containing only cholesterol (*i.e*. composition *a*) are shown in Section 2.3.4. The results for the other NNR reactions are shown in Tables 20-25, and summarized in Table 26 and Figure 30. In addition, DLS measurements of the size of the vesicles before and after NNR reactions for all of the experiments reported here are presented Table 27. Unless stated otherwise, aldrithiol-2 was not used in the preparation of samples for HPLC

analysis for all NNR reactions reported in this chapter (see Section 5.2 for a discussion of the sample preparation procedure).

Reaction	Reaction Time (h)	Dimer	R_T (min)	Peak Area	N (nmol)	K
1	12	**{16PL-16PL}**	11.46	1601680	3.35	9.80
		{cho-16PL}	17.75	5902559	11.09	
		{cho-cho}	34.20	2306896	3.74	
1	16	**{16PL-16PL}**	11.94	1410612	2.95	9.75
		{cho-16PL}	17.81	5240497	9.85	
		{cho-cho}	34.24	2084317	3.37	
1	18	**{16PL-16PL}**	11.48	1429628	2.99	9.71
		{cho-16PL}	17.80	5316417	9.99	
		{cho-cho}	34.25	2123605	3.43	
1	20	**{16PL-16PL}**	11.68	1471351	3.08	9.86
		{cho-16PL}	18.11	5385209	10.12	
		{cho-cho}	34.68	2086570	3.37	
1	22	**{16PL-16PL}**	11.73	1424513	2.98	10.11
		{cho-16PL}	18.15	5317250	9.99	
		{cho-cho}	34.76	2051154	3.31	

Table 20: Data for {**cho-16PL**} equilibration in 10 mol% dihydrocholesterol + 30 mol% cholesterol LUVs at 45 °C using 0.8 equivalents of DTT

Reaction	Reaction Time (h)	Dimer	R_T (min)	Peak Area	N (nmol)	K
1	12	**{16PL-16PL}**	11.52	1469550	3.07	10.28
		{cho-16PL}	17.85	5465099	10.27	
		{cho-cho}	34.29	2064445	3.33	
1	16	**{16PL-16PL}**	11.54	1403782	2.94	10.90
		{cho-16PL}	17.88	5389636	10.13	
		{cho-cho}	34.32	1986468	3.20	
1	18	**{16PL-16PL}**	11.56	1295224	2.71	10.55
		{cho-16PL}	17.93	4927691	9.26	
		{cho-cho}	34.39	1865654	3.00	
1	20	**{16PL-16PL}**	11.75	1346208	2.82	10.47
		{cho-16PL}	18.21	5094228	9.57	
		{cho-cho}	34.84	1930263	3.11	
1	22	**{16PL-16PL}**	11.77	1389339	2.91	10.40
		{cho-16PL}	18.24	5321970	10.00	
		{cho-cho}	34.86	2049025	3.31	
2	12	**{16PL-16PL}**	12.39	1294856	2.71	10.12
		{cho-16PL}	18.91	4456470	8.38	
		{cho-cho}	35.02	1606156	2.56	
2	16	**{16PL-16PL}**	12.44	1198310	2.51	10.89
		{cho-16PL}	18.94	4531307	8.52	
		{cho-cho}	35.13	1662635	2.66	
2	18	**{16PL-16PL}**	12.51	1086150	2.27	10.32
		{cho-16PL}	19.04	3947165	7.42	
		{cho-cho}	35.16	1480360	2.35	
2	20	**{16PL-16PL}**	12.47	1165140	2.44	10.52
		{cho-16PL}	19.03	4271552	8.03	
		{cho-cho}	35.27	1578928	2.51	
2	22	**{16PL-16PL}**	12.54	1206262	2.52	10.34
		{cho-16PL}	19.13	4489306	8.44	
		{cho-cho}	35.39	1705564	2.73	

Table 21: Data for {**cho-16PL**} equilibration in 20 mol% dihydrocholesterol +20 mol% cholesterol LUVs at 45 °C using 0.8 equivalents of DTT (Reactions 1 and 2)

Reaction	Reaction Time (h)	Dimer	R_T (min)	Peak Area	N (nmol)	K
		{16PL-16PL}	11.60	1524225	3.19	
1	12	**{cho-16PL}**	17.67	5521821	10.37	9.96
		{cho-cho}	34.49	2095396	3.39	
		{16PL-16PL}	11.63	1469070	3.07	
1	16	**{cho-16PL}**	18.01	5430197	10.20	10.03
		{cho-cho}	34.54	2089208	3.38	
		{16PL-16PL}	11.65	1341503	2.81	
1	18	**{cho-16PL}**	18.05	4959354	9.32	10.20
		{cho-cho}	34.56	1886607	3.03	
		{16PL-16PL}	11.80	1339188	2.80	
1	20	**{cho-16PL}**	18.30	5047761	9.48	10.50
		{cho-cho}	34.95	1900478	3.06	
		{16PL-16PL}	11.83	1402618	2.93	
1	22	**{cho-16PL}**	18.33	5295436	9.95	10.30
		{cho-cho}	34.98	2030087	3.28	
		{16PL-16PL}	12.58	1480248	3.10	
2	12	**{cho-16PL}**	19.17	5084391	9.55	9.47
		{cho-cho}	35.52	1932633	3.11	
		{16PL-16PL}	12.64	1443352	3.02	
2	16	**{cho-16PL}**	19.25	4828211	9.07	9.73
		{cho-cho}	35.68	1749254	2.80	
		{16PL-16PL}	12.71	1392584	2.91	
2	18	**{cho-16PL}**	19.35	4782586	8.99	9.40
		{cho-cho}	35.78	1837066	2.95	
		{16PL-16PL}	12.76	1284733	2.69	
2	20	**{cho-16PL}**	19.45	4450752	8.37	9.73
		{cho-cho}	35.82	1675237	2.68	
		{16PL-16PL}	12.86	1274545	2.67	
2	22	**{cho-16PL}**	19.60	4497639	8.45	9.46
		{cho-cho}	36.09	1766848	2.83	

Table 22: Data for {**cho-16PL**} equilibration in 37.5 mol% dihydrocholesterol + 2.5 mol% cholesterol LUVs at 45 °C using 0.8 equivalents of DTT (Reactions 1 and 2)

Reaction	Reaction Time (h)	Dimer	R_T (min)	Peak Area	N (nmol)	K
		{16PL-16PL}	11.69	1434498	3.00	
1	11	**{cho-16PL}**	17.98	4673266	8.78	8.67
		{cho-cho}	34.00	1845606	2.96	
		{16PL-16PL}	11.70	1333931	2.79	
1	11	**{cho-16PL}**	18.02	4366326	8.21	9.17
		{cho-cho}	33.95	1648698	2.63	
		{16PL-16PL}	11.45	1142870	2.39	
1	24	**{cho-16PL}**	17.65	3762546	7.08	8.35
		{cho-cho}	33.45	1575830	2.51	
		{16PL-16PL}	11.46	1203087	2.52	
1	24	**{cho-16PL}**	17.68	3859021	7.26	8.21
		{cho-cho}	33.44	1599076	2.55	
		{16PL-16PL}	11.48	1104068	2.31	
1	24	**{cho-16PL}**	17.71	3581069	6.74	8.61
		{cho-cho}	33.50	1440967	2.28	

Table 23: Data for {**cho-16PL**} equilibration in 10 mol% coprostanol + 30 mol% cholessterol LUVs at 45 °C using 0.8 equivalents of DTT (Reaction 1)

Reaction	Reaction Time (h)	Dimer	R_T (min)	Peak Area	N (nmol)	K
		{16PL-16PL}	11.75	1676350	3.51	
1	11	**{cho-16PL}**	18.10	4963874	9.33	7.76
		{cho-cho}	34.15	1983472	3.20	
		{16PL-16PL}	11.78	1447176	3.03	
1	11	**{cho-16PL}**	18.17	4285756	8.06	7.76
		{cho-cho}	34.20	1725175	2.76	
		{16PL-16PL}	11.49	1337467	2.80	
1	24	**{cho-16PL}**	17.72	4010051	7.54	7.36
		{cho-cho}	33.58	1723571	2.76	
		{16PL-16PL}	11.51	1198242	2.51	
1	24	**{cho-16PL}**	17.75	3860281	7.26	7.94
		{cho-cho}	33.54	1657473	2.65	
		{16PL-16PL}	11.51	1340493	2.80	
1	24	**{cho-16PL}**	17.77	3927432	7.39	7.04
		{cho-cho}	33.60	1726541	2.76	

Table 24: Data for {**cho-16PL**} equilibration in 20 mol% coprostanol + 20 mol% cholessterol LUVs at 45 °C using 0.8 equivalents of DTT (Reaction 1)

Reaction	Reaction Time (h)	Dimer	R_T (min)	Peak Area	N (nmol)	K
1	11	**{16PL-16PL}**	11.85	1584328	3.31	6.26
		{cho-16PL}	18.26	4392543	8.26	
		{cho-cho}	34.38	2034700	3.28	
1	11	**{16PL-16PL}**	11.89	1539091	3.22	6.50
		{cho-16PL}	18.31	4452380	8.37	
		{cho-cho}	34.49	2072355	3.35	
1	24	**{16PL-16PL}**	11.56	1154686	2.42	6.76
		{cho-16PL}	17.82	3451893	6.49	
		{cho-cho}	33.64	1618854	2.58	
1	24	**{16PL-16PL}**	11.58	1222506	2.56	6.43
		{cho-16PL}	17.84	3518862	6.62	
		{cho-cho}	33.63	1667751	2.66	
1	24	**{16PL-16PL}**	11.58	1152432	2.41	6.65
		{cho-16PL}	17.86	3374288	6.35	
		{cho-cho}	33.69	1577475	2.51	
2*	12	**{16PL-16PL}**	11.02	1321171	2.76	6.28
		{cho-16PL}	16.58	3666276	6.90	
		{cho-cho}	29.60	1713162	2.74	
2*	12	**{16PL-16PL}**	11.03	1436579	3.01	6.27
		{cho-16PL}	16.60	3939125	7.41	
		{cho-cho}	29.60	1814543	2.91	
2*	20	**{16PL-16PL}**	11.06	1354891	2.83	6.03
		{cho-16PL}	16.66	3629825	6.83	
		{cho-cho}	29.64	1705493	2.73	
2*	20	**{16PL-16PL}**	11.07	1330245	2.78	6.01
		{cho-16PL}	16.67	3611131	6.79	
		{cho-cho}	29.67	1723725	2.76	
2*	20	**{16PL-16PL}**	11.10	1403508	2.94	6.05
		{cho-16PL}	16.71	3712769	6.98	
		{cho-cho}	29.72	1714081	2.74	

Table 25: Data for {**cho-16PL**} equilibration in 37.5 mol% coprostanol + 2.5 mol% cholessterol LUVs at 45 °C using 0.8 equivalents of DTT (Reactions 1and 2). ***** Aldrithiol-2 (8 equivalents relative to DTT) was included in the HPLC sample preparation

% dihydro.	% coprostanol	% cholesterol	*K*	ω_{AB} (cal/mol)
0	0	40	9.8 ± 0.5	-282 ± 15
10	0	30	9.9 ± 0.2	-284 ± 5
20	0	20	10.5 ± 0.3	-304 ± 8
37.5	0	2.5	9.9 ± 0.4	-286 ± 12
0	10	30	8.6 ± 0.4	-243 ± 14
0	20	20	7.6 ± 0.4	-203 ± 15
0	37.5	2.5	6.3 ± 0.3	-145 ± 13

Table 26: Summary of {**cho-16PL**} equilibration in the presence of varying amounts of cholesterol, coprostanol, and dihydrocholesterol. Exchangeable lipid **cho** is included in the % cholesterol

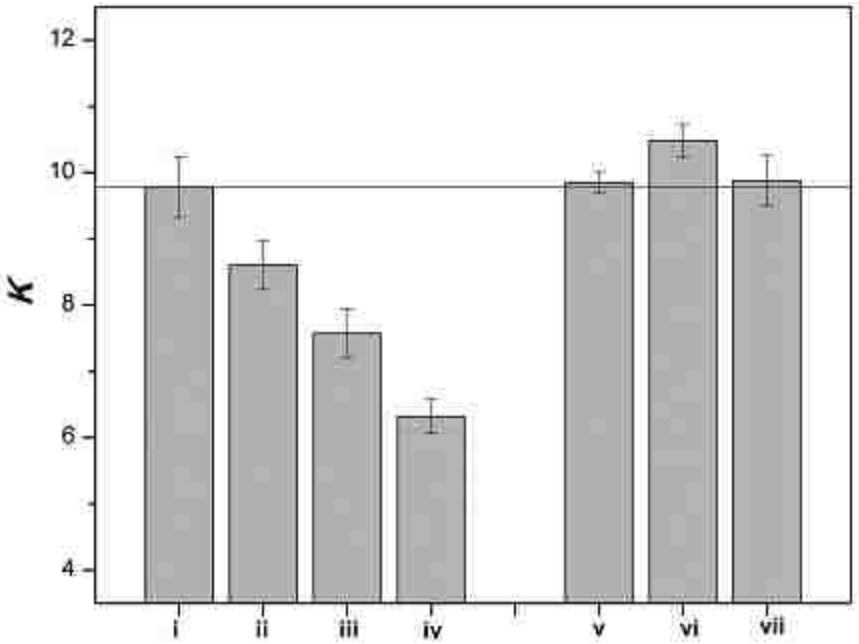

Figure 30: Bar graph showing *K* in liposomes containing (i) 40/0, (ii) 30/10, (iii) 20/20, (iv) 2.5/37.5 mole percentages of cholesterol/coprostanol and (v) 30/10, (vi) 20/20, and (vii) 2.5/37.5 mol percentages of cholesterol/dihydrocholesterol. Here, **cho** is included in the cholesterol count. Error bars represent one standard deviation

mol% dihydro	mol% cop	mol% cho	Time (h)	Diam. (nm)
10	0	30	0	186.3 ± 61.5
10	0	30	22	182.9 ± 49.4
20	0	20	0	188.3 ± 33.9
20	0	20	22	190.9 ± 61.1
20	0	20	0	179.2 ± 57.3
20	0	20	22	183.6 ± 44.1
37.5	0	2.5	0	188.9 ± 64.2
37.5	0	2.5	22	188.6 ± 60.4
37.5	0	2.5	0	175.3 ± 29.8
37.5	0	2.5	22	182.5 ± 74.8
0	10	30	0	162.9 ± 60.3
0	10	30	24	166.6 ± 43.3
0	20	20	0	181.2 ± 34.4
0	20	20	24	177.2 ± 40.8
0	37.5	2.5	0	178.6 ± 57.2
0	37.5	2.5	24	172.0 ± 60.2
0	37.5	2.5	0	169.2 ± 52.5
0	37.5	2.5	20	168.1 ± 55.5

Table 27: DLS data for vesicles before and after NNR reactions. Monomodal size distribution was observed in all cases

3.4 Discussion

The aim of the studies presented in this chapter was to distinguish between two competing models of cholesterol's condensing effect; the "template" and "umbrella" models. To do so, we investigated the condensing effects of cholesterol, dihydrocholesterol, and coprostanol using NNR as a chemical sensor to measure the compactness of a host membrane in which cholesterol has been replaced with dihydrocholesterol or coprostanol. By a template model, one would expect coprostanol to have a poor condensing effect, as it lacks the planar structure necessary to maximize hydrophobic contact with fully extended acyl chains. The umbrella model, however, would predict a stronger condensing effect for coprostanol than for cholesterol, since coprostanol's larger surface area would require tighter packing of the acyl chains in order for the sterol to fit completely under the headgroup. Thus, a quantitative comparison of the condensing effects of these two sterols should distinguish between an umbrella and a template model. Dihydrocholesterol, which has a cross sectional area similar to cholesterol, but like coprostanol, lacks a double bond, would be expected to have a similar condensing effect to cholesterol based on both a template and umbrella model, but will be used to verify that the presence of a double bond is not crucial to cholesterol's condensing effect.

Prior to measuring the condensing effect of these sterols, it was necessary to verify that replacement of cholesterol with dihydrocholesterol or coprostanol does not change the phase transition properties of the membrane, *i.e.* to make sure the host membrane for all NNR experiments will be in the l_o phase. To do so, the effects of cholesterol, dihydrocholesterol, and coprostanol on DPPC based liposomes were first

examined using the phase sensitive probe, Laurdan. Laurdan fluorescence, as measured by its generalized polarization (GP) where GP = $(I_{440}-I_{490})/(I_{440}+I_{490})$ and I_{440} and I_{490} are the emission intensities at these wavelengths (λ_{ex} = 350 nm), is highly dependent on the polarity of its microenvironment. A higher GP measurement is indicative of a less polar microenvironment around the Laurdan molecule, and therefore less penetration of water into the hydrophobic core and a more tightly packed membrane. As shown in Figure 29 (page 73), a DPPC based liposome containing 2.5% cholesterol (open circles) exhibits a sharp decrease in GP near the DPPC phase transition temperature of ~41 ^{o}C. A liposome containing 40% cholesterol (filled squares) shows a gradual decline in GP as temperature increases, showing the presence of a l_o phase across all temperatures. Liposomes containing 40% dihydrocholesterol or 40% coprostanol (open squares and filled triangles, respectively) also show similar "l_o-like" profiles, indicating that the replacement of cholesterol with dihydrocholesterol or coprostanol does not alter the phase properties of the membrane. The coprostanol containing liposomes, however, have significantly lower GP values than either of the other sterols, suggesting that coprostanol containing membranes are not as tightly packed as those rich in cholesterol or dihydrocholesterol.

In order to assess the relative condensing power of cholesterol, dihydrocholesterol, and coprostanol, experiments were carried out using NNR in its "chemical sensor" application to measure the compactness of host membranes containing each of the three sterols. Thiolate-disulfide exchange reactions were carried out at 45 ^{o}C in liposomes made from DPPC/cholesterol/**X/cho**/**16PL** (here, **X** is coprostanol or dihydrocholesterol) having the following mole percentages: (a) 57.5/37.5/0/2.5/2.5, (b) 57.5/27.5/10/2.5/2.5, (c) 57.5/17.5/20/2.5/2.5, and (d) 57.5/0/37.5/2.5/2.5. The results of

these experiments are shown graphically in Figure 30 (page 79). The incremental replacement of cholesterol with coprostanol resulted in a steady decrease in *K*, indicating a decrease in the compactness of the host membrane. In contrast, replacement of cholesterol with dihydrocholesterol did not result in a statistically significant change in *K*. Taken together, the results of these NNR experiments show that while cholesterol and dihydrocholesterol have similar condensing effects, coprostanol is a weaker condensing agent.

The Laurdan fluorescence results, which show coprostanol containing bilayers to be significantly less compact than bilayers containing cholesterol or dihydrocholesterol, combined with the NNR experiments showing coprostanol to be a weaker condensing agent than the other sterols, provide compelling evidence that coprostanol's curved structure and large surface area make it a *weaker* condensing agent than cholesterol. These findings agree with previously reported monolayer experiments,[72] as well as similar monolayer experiments conducted in our own laboratoy.[79]

3.5 Conclusions

The finding that coprostanol is a weaker condensing agent than cholesterol argues against the long-held "umbrella model" for cholesterol's condensing effect, which would predict that coprostanol, with its large surface area, would induce greater condensing of phospholipid acyl chains in order to accommodate the bulky sterol underneath the phospholipid headgroup. Instead, these results are strong evidence for a "template model," wherein the planar sterol nucleus of cholesterol acts as a template to promote the straightening of the acyl chains in order to maximize hydrophobic contact. Such a model

would predict the observed weak condensing effect of coprostanol, as a sterol with a curved hydrophobic core could not compliment the acyl chains as perfectly as planar cholesterol molecules.

Other recent findings from our laboratory shed more light on the structural features of a sterol necessary for efficient condensing of acyl chains. Using a similar approach to what was reported here for coprostanol, it has been shown that 7β-hydroxycholesterol (7β-OH, see Figure 31 for structure) has a greater condensing effect than cholesterol.[24] This observation can best be explained if one assumes that 7β-OH orients itself in the bilayer in such a way as to expose both hydroxyl groups to water. Doing so would require the sterol nucleus of 7β-OH to occupy more space closer to the surface of the bilayer. It has been shown that in fluid bilayers, the phospholipid headgroups occupy only about half of the surface area of membrane, with the remainder occupied by partially solvated methylene groups of the acyl chains.[80,81] When cholesterol is added to the membrane, some of this excess surface area is occupied by the cholesterol hydroxyl group, freeing the acyl chains to penetrate into the hydrophobic core. A sterol like 7β-OH, which occupies more surface area (while still preserving the planar nucleus necessary for a template effect), can therefore be expected to condense acyl chains to a greater extent than cholesterol.

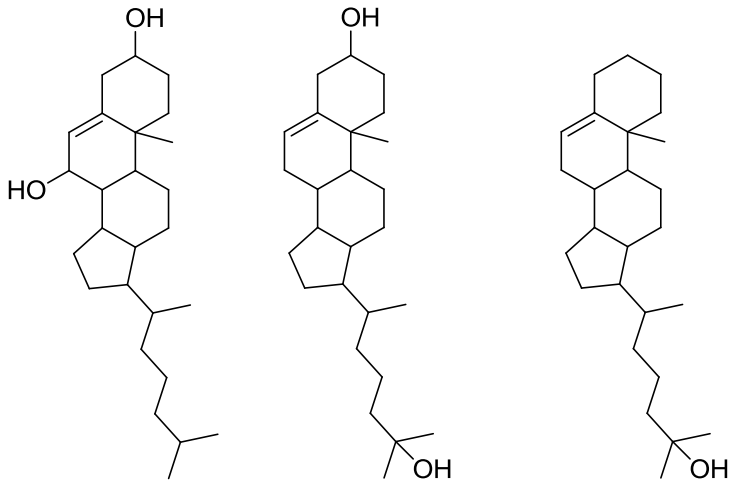

Figure 31: Structure of 7β-OH, 25-OH and "upside down" cholesterol

Further evidence for the importance of surface occupancy comes from NNR studies measuring the condensing effects of 25-hydroxycholesterol (**25-OH**) and "upside down" cholesterol (**25-OH'** Figure 31). Using similar methods to those reported here for coprostanol and dihydrocholesterol, both of these sterols were found to be weaker condensing agents than cholesterol.[27,82] The hydroxyl groups located on the acyl chain of both of these sterols allow them to orient themselves in the membrane with the sterol nucleus penetrating deep into the hydrophobic core. Both of these sterols thus occupy less area at the membrane surface than cholesterol, resulting in a weaker condensing effect.

Considering the strong evidence in support of a template effect and the importance of surface occupancy, a cohesive mechanism for cholesterol's condensing effect emerges. Cholesterol's hydroxyl headgroup occupies area at the membrane surface, displacing methylene groups of the phospholipid acyl chains and freeing them to make hydrophobic contact with the sterol nucleus. The planar structure of cholesterol then acts as a template to condense the acyl chains.

Work towards confirming or refining this template model is ongoing in our laboratory. Specifically, we are interested in measuring the condensing effects of demethylated cholesterol. As shown in Figure 26 (page 68), cholesterol has two methyl groups protruding from its sterol core, giving it one "smooth" planar face (the α face) and one "bumpy" face (the β face). Removing these two methyl groups would produce a sterol with two planar faces. From a template model point of view, demethylated cholesterol, with two planar faces capable of acting as templates for acyl chain condensation, would have a stronger condensing effect than cholesterol. Recent molecular dynamics studies, however, indicate that demethylated cholesterol is not a good condensing agent.[83] Obtaining experimental measurements of the condensing effects of demethylated cholesterol will, therefore, be a critical test of the "template" model of cholesterol's condensing effect.

Chapter 4

Conclusions

The studies presented in this thesis illustrate the potential for NNR to be used to probe important biologically relevant problems that were previously difficult to approach. Because of the unique ability of Nearest Neighbor Recognition to quantify the molecular level interaction energies of membrane components, it is an ideal tool for examining basic questions about membrane structure.

Chapter 2 of this thesis details the use of NNR to measure the interaction of two lipidated peptides, **Pep1** and **Pep2** with membrane lipids in liquid ordered and liquid disordered membranes. The resulting data were then used in Monte Carlo simulations to develop a physical picture of membrane organization in a membrane containing coexisting l_d and l_o domains. From these Monte Carlo simulations, a quantitative partition coefficient was calculated to describe the distribution of the peptides in the membrane. In addition, it was found that through the use of a mean field approximation, the partition coefficients can be calculated directly from the experimental ω_{AB} measurement without the need for Monte Carlo simulations, if the cholesterol content of each phase in the membrane is known. The dipeptide **Pep1**, with its two saturated acyl chains, was expected to exhibit an affinity for l_o domains, but was shown to mix ideally in both phases. This finding suggests that interactions between lipid anchors on peripheral proteins and the membrane lipids alone are not as important as previously suggested in driving lipid sorting, and that some other factor which was not accounted for in our model, such as hydrogen bonding or specific protein-protein interactions may play a

larger role. These findings are in agreement with recently reported results from fluorescence experiments in live cells which show a level of complexity in lipid sorting that cannot be explained by differences in lipid anchor structure alone.[68]

The success of this study in determining quantitative partition coefficients based on NNR measurements demonstrated that the combination of NNR experiments and Monte Carlo simulations is a powerful new tool for examining lipid sorting. Among the tools commonly used to examine the lateral distribution of membrane proteins, including detergent resistance experiments, fluorescence microscopy experiments in GUVs, and AFM, this approach is unique in its ability to provide quantitative partition coefficients in model systems with domains of any size. Continued use of this powerful new tool to investigate the partitioning of several other peptide motifs will be invaluable in sorting out the "ground rules" that dictate how lipidated protein structure dictates partitioning between coexisting phases.

In the third chapter, NNR was applied to a long unsolved mystery of membrane biophysics, the origin of cholesterol's condensing effect. Despite the fact that cholesterol has been known to condense the acyl chains of neighboring phospholipids for nearly a century, the molecular mechanism for this biologically important phenomenon remained unknown. By comparing the condensing power of cholesterol to that of two other sterols, dihydrocholesterol and coprostanol, we were able to distinguish between the commonly held "umbrella model" and an alternative "template model." Our findings strongly support the template model, in which cholesterol's planar sterol core acts as a template to guide the straightening of the phospholipid acyl chains. Ongoing work aimed at

confirming or refining our understanding of the origin of cholesterol's condensing effect includes an examination of the condensing effect of demethylated cholesterol.

Taken together, the results presented in this thesis represent novel applications of NNR chemistry to develop molecular level understanding of well known, but poorly understood, properties of biological membranes. Nearest Neighbor Recognition is an important tool for basic science research into membrane organization, and continues to produce valuable insight into important biologically relevant questions.

Chapter 5

Experimental

5.1 General

Unless stated otherwise, all reagents and chemicals were obtained from Sigma-Aldrich or VWR and used without further purification. Boc protected cysteine was purchased from Chem Impex International (Wood Dale, IL, USA). 1,2-Dihexadecanoyl-*sn*-glycero-3-phosphoethanolamine (DPPE), 1,2-dipalmitoyl-*sn*-glycero-3-phosphocholine (DPPC), and 1,2-dipalmitoyl-*sn*-glycero-3-phosphoglycerol (DPPG, sodium salt) were purchased from Avanti Polar Lipids (Alabaster, AL, USA) and used as obtained. Dithiothreitol and dihydrocholesterol were purchased from Alfa Aesar (Ward Hill, MA, USA). Aldrithiol-2 (2,2'-dipyridyldisulfide) and EDTA (ethylenediaminetetraacetic acid) were obtained from Acros (Waltham, MA, USA). Coprostanol was obtained from Steraloids, Inc. (Newport, RI, USA). House-deionized water was purified using a Millipore Milli-Q filtering system containing one carbon and two ion-exchange stages.

Silica gel (EMS, silica gel 60) was used for all column chromatographic separations. Preparative TLC was done on 1.0 mm EMD silica gel 60 plates purchased from VWR. Analytical TLC was done on EMD silica gel 60 plates or 250 micron Analtech silica gel plates purchased from VWR, with detection by a combination of sulfuric acid (10% in water), I_2, ninhydrin, and UV (254 and 365 nm).

All ^{1}H NMR spectra were recorded on a Bruker Avance 500 MHz instrument. Chemical shifts are reported in parts per million relative to residual solvent. Unless stated otherwise (Section 5.3) all mass spectrometry measurements were performed at the

University of California, Riverside Mass Spectrometry facility using either an Agilent LCTOF high resolution TOF analyzer or a PE Biosystems DE-STR MALDI TOF system.

5.2 Procedures Used for NNR Experiments

5.2.1 Preparation of Vesicle Dispersion

Thin films of lipid were prepared by evaporating a chloroform solution containing the desired lipids under a stream of argon while rapidly rotating the tube, resulting in a thin film uniformly covering the inner surface of the tube up to approximately 1/2 of the height of the tube. Typically, < 2mL of chloroform solution and 13 x 100 mm test tubes were used. For the exact composition of the thin films used for all NNR reactions reported in this thesis, see Tables 28 and 29. After drying the thin film overnight under reduced pressure (0.4 mm Hg), 2.0 mL of a 10 mM Tris-HCl buffer (10 mM Tris, 150 mM NaCl, 2 mM NaN_3, 1 mM EDTA, pH = 7.4) was added the dried film. The mixture was then vortexed for 30 seconds, incubated for 5 min at 60 °C, vortexed for an additional 30 seconds, and incubated for an additional 30 min at 60 °C with intermittent vortexing. The dispersions were then subjected to six freeze/thaw cycles (liquid nitrogen/60 °C water bath) and extruded 20 times through a 200 nm pore diameter polycarbonate (Nuclepore, Whatman Inc.) filter using argon at a pressure of ~100 psi.

Host Membrane	µmol Pep1 or Pep2	µmol cho	µmol 16PL	µmol DPPC	µmol DPPG	µmol cholesterol
l_o	0.3	0.3	-	6.6	0.3	4.5
l_o	0.3	-	0.3	6.6	-	4.8
l_d	0.3	0.3	-	11.1	0.3	-
l_d	0.3	-	0.3	11.1	-	0.3

Table 28: Composition of lipid films used for the preparation of vesicle dispersions for lipid sorting studies

µmol cho	µmol 16PL	µmol DPPC	µmol cholesterol	µmol coprostanol or dihydro chol.
0.3	0.3	6.9	4.5	-
0.3	0.3	6.9	3.3	1.2
0.3	0.3	6.9	2.1	2.4
0.3	0.3	6.9	-	4.5

Table 29: Composition of lipid films used for the preparation of vesicle dispersions for NNR experiments including non-exchangeable dihydrocholesterol and coprostanol

5.2.2 NNR Experiments

An aliquot of the vesicle dispersion (typically 1600 µL) was heated to 45 °C, oxygen was removed by purging with argon, and thiolate-disulfide interchange reactions were initiated by adding dithiothreitol (typically 0.8-1.0 equivalents with respect to disulfide content, added as a ~20 mM solution in pH 7.4 Tris buffer) and sufficient amounts of 0.1 M NaOH to bring the pH to 7.4 at 45 °C. Aliquots (250 µL) were withdrawn as a function of time. The exchange reactions were quenched by adding 25 µL of 8.3 M acetic acid to the test tubes containing these aliquots, vortexing, and quickly freezing in liquid nitrogen. Aliquots were stored at -20 °C until HPLC analysis was carried out.

To each thawed aliquot was then added 1000 µL of $CHCl_3$/MeOH (2/1, v/v) and aldrithiol-2 (30 µL of a 10 mM solution in $CHCl_3$), the tubes were vortexed, centrifuged, and the aqueous phases removed using a Pasteur pipette. The organic phase was then concentrated under reduced pressure using a Savant SVC-100 SpeedVac concentrator equipped with a cold trap and vacuum pump (~1 hr at ~ 0.4 torr). The lipids were then dissolved in a mixture of $CHCl_3$ and mobile phase A (see Table 30 for the compositions of mobile phases A and B). For samples containing **Pep1** or **Pep2**, 30 µL of $CHCl_3$ and

70 μL of mobile phase were used. For all other samples, 20 μL of $CHCl_3$ and 80 μL of mobile phase were used.

Mobile Phase	Ethanol (mL)	Water (mL)	hexanes (mL)
A	76	130	100
B	77.5	11	11

Table 30: Composition of mobile phases A & B. All mobile phases consisted of 10mM *n*-Bu_4NOAc in ethanol/water/hexane mixtures given here.

These samples were then analyzed by HPLC using either a Waters Alliance HPLC system consisting of a Waters 2690 Separation Module and a Waters 996 Photodiode Array Detector or a Waters Breeze HPLC system consisting of a Waters 717plus Autosampler, Waters 1515 Binary Pump, and Waters 2187 Dual λ Absorbance Detector. A 5 μ, 80 Å, 4.6 x 250 mm Ultrasphere ODS C18 column (Hichrom, Reading, England) was used, with a flow rate of 0.9 mL/minute, and 70 μL injections. The column was maintained at 31 °C and the components were monitored at 203 nm. Values of K (K=[**AB**]^2/([**AA**]×[**BB**])) were calculated from peak areas obtained from the HPLC chromatograms using appropriate calibration curves. NNR reactions using {**cho-16PL**} were analyzed using mobile phase A isocratically. NNR reactions using {**Pep1-cho**} or {**Pep2-cho**} were analyzed using mobile phase B isocratically. The gradient used for the analysis of product mixtures from NNR reactions using {**Pep1-16PL**} or {**Pep2-16PL**} is shown in Table 31.

time (min)	%A	%B
0	100	0
20	100	0
30	0	100
50	0	100
60	100	0

Table 31: Gradient used for HPLC analysis of product mixtures containing {**Pep1-16PL**} or {**Pep2-16PL**}

5.2.3 DLS Measurements

The effect of NNR reactions and vesicle composition on vesicle size was investigated using a Nicomp Model 270 Submicron Particle Sizer. Typically, 60 μL aliquots were taken from each vessel before and after the exchange reaction. These aliquots were diluted with 400 μL of Tris buffer (pH = 7.4) and analyzed at 23 °C assuming a sample viscosity of 0.9325 centipoise. The photopulse rate was adjusted to ~300 kHz. Vesicle size was evaluated through Gaussian analysis. At least 100000 scans were performed.

5.3 MALDI Analysis of {Pep1-Pep1}

Samples were collected from an NNR reaction of {**Pep1-cho**} in a l_o host membrane, following the procedure outlined in Section 5.2. Samples from this reaction were analyzed using the typical HPLC procedure, with tetrabutyl ammonium acetate omitted from the mobile phase. From each of seven injections, fractions were collected thusly: two thirty second collections taken at randomly selected times when no peak was eluting (these fractions, that are henceforth called **baseline**, were combined immediately after collection), one thirty second collection (**peak1**) taken as soon as the first of the peaks with retention time near 32 minutes began to elute, and one thirty second collection (**peak2**) taken near the end of the elution of the second peak. All collected fractions were taken to dryness under reduced pressure using a Savant SVC-100 SpeedVac concentrator equipped with a cold trap and vacuum pump (~1 hr at ~ 0.4 torr). Each sample was dissolved in 100 μL $CHCl_3$. In addition, a solution of {**Pep1-Pep1**} in $CHCl_3$ (1.5 mg/mL) was prepared to use as a standard.

An α-cyano matrix (a saturated solution of α-cyano-4-hydroxy cinnamic acid in 670 μL water, 330 μL acetonitrile, and 1 μL trifluoroacetic acid) was prepared, and 5 μL was deposited on a MALDI target plate. The solvent was evaporated and {**Pep1-Pep1**} standard (1 μL) or a sample of **baseline**, **peak1**, or **peak2** (5 μL) was deposited on top. Samples were analyzed using a Bruker Daltonics MicroFlex MALDI-MS.

5.4 Generalized Polarization Analysis

Liposomes made from 40/0/0/57.5/2.5, 2.5/0/0/95/2.5, 20/20/0/57.5/2.5, 2.5/37.5/0/57.5/2.5, 20/0/20/57.5/2.5, and 2.5/0/37.5/57.5/2.5 cholesterol/coprostanol/dihydrocholeterol/DPPC/DPPG (mol/mol/mol/mol, 12 μmol total lipid) plus Laurdan (0.5 mol% with respect to total lipid) were prepared from thin lipid films using methods similar to those used in NNR experiments (see Section 5.2.1). Liposomal dispersions were placed in sealed fluorescence cuvettes and the fluorescence of each sample was measured as a function of temperature using a Perkin Elmer LS50B Luminescence Spectrometer employing a temperature controlled cell holder. An excitation wavelength of 350 nm was used, along with an excitation slit width of 6.5 nm. Fluorescence emissions were recorded from 350 to 600 nm using an emission slit width of 6.5 nm. To correct for light scattering, a vertical polarizer was placed on the excitation beam and a horizontal polarizer was placed on the emission beam. Generalized Polarization (GP) values were calculated using the equation: $GP=(I_{440} - I_{490})/(I_{440} + I_{490})$, where I_{440} and I_{490} are fluorescence emission intensities at 440 and 490 nm respectively.

5.5 Differential Scanning Calorimetry

DSC experiments were performed using one of two procedures. In the first procedure, performed by Professor Paulo Almeida (University of North Carolina, Wilmington), suspensions of lipidated peptide samples (heterodimers {**Pep1-16PL**} and {**Pep2-16PL**}, and **Pep2a**, the methyl sulfide derivative of **Pep2**) were prepared by hydrating the lipid film at 85-95 °C in buffer, pH 7.5 (10 mM Potassium Phosphate or 20 mM MOPS, 0.1 mM EGTA, 0.02% NaN_3, and 100 mM KCl). Concentrations were estimated by weight and (for phosphate-containing dimers) by a modified Bartlett phosphate method.[84,85] The heat capacity of the aqueous suspensions (degassed under vacuum of 500 mm Hg for 10 min) was measured using a high sensitivity Nano DSC (TA Instruments, New Castle, DE), equipped with 300-mL twin gold capillary cells, under a slight pressure (set once to 3 atm). The scan rate was 0.1 °C/min. The DSC curves were corrected by baseline subtraction as previously described.[86] This technique was used to obtain the data shown in Section 2.3.5.

In additional preliminary experiments, performed by Trevor Daly, dispersions of {**Pep1-16PL**} and {**Pep2-16PL**} (1.56 μmol) were prepared using the procedure described in Section 5.2.1. The resulting dispersions were filtered through glass wool to remove any suspended solids. Several aliquots (10 μL each) of the dispersions were set aside for concentration measurement. The lipid concentration was determined using HPLC procedures similar to those used for NNR samples (see Section 5.2.2). The remaining vesicle dispersions were placed in the sample cell of a Microcal MC-2 Scanning Calorimeter, with TRIS buffer in the reference cell. Five scans were performed

for each sample, with an initial temperature of 10 ^{o}C, a final temperature of 60 ^{o}C, a scan rate of 30 ^{o}C/hour, and a resting time of 90 minutes between scans.

5.6 Monte Carlo Simulations

Monte Carlo simulations were performed by Professor Paulo Almeida (University of North Carolina, Wilmington) using the model and methods recently described for DPPC/Cholesterol,[67] with standard Monte Carlo procedures.[87-89] The lipid membrane was represented by a triangular lattice, with skew-periodic boundary conditions, where each site is occupied by a phospholipid, a lipidated peptide, or a cholesterol molecule. Equilibrium configurations of the lattice were generated using two types of steps: a non-nearest-neighbor Kawasaki step,[90] in which lipids are exchanged by randomly selecting partners on the lattice, and a Glauber step,[91] in which the lipid is switched between gel, l_d and l_o states. Cholesterol is considered to have only one state. The choice between attempted moves is aleatory. Acceptance is based on the Metropolis criterion[92] with a move probability that depends exponentially on the free energy change,[67,87-88,92] using a random number for the decision.[93] The simulations were performed in 100×100 lattices, but it was previously shown that simulations in lattices of 200×200 and 300×300 sites yield equivalent results in this type of system.[67,94] A Monte Carlo cycle is defined as a number of attempted moves identical to the number of lattice sites. The calculations included a pre-equilibration period of 5×10^4 Monte Carlo cycles followed by a period of 10^6 acquisition cycles, which were more than sufficient to obtain equilibrium properties. One lipid–lipid interaction parameter (ω_{AB}) is used for each pair of possible states (gel, l_o and l_d) and lipid species (**Pep1**, **Pep2**, **cho**, and **16PL**) present in the system, which is

defined by Equation 3 (page 57).[15] Except in the cases determined here experimentally by nearest-neighbor recognition measurements, the ω_{AB} interaction parameters were the same as those previously used for DPPC/cholesterol.[85] Namely, for gel-l_o and l_d-l_o interactions ω_{AB} = +330 cal/mol, and for gel-l_d interactions ω_{AB} = +360 cal/mol, where A and B are any phospholipids (**16PL**) or lipidated peptides (**Pep1 or Pep2**). The complete set of parameters is listed in Table 32.

Lipids		ω_{AB} (cal/mol)								
		DPPC (**16PL**)			Lipidated Peptide **Pep1**			Lipiddated Peptide **Pep2**		
	State	gel	l_o	l_d	gel	l_o	l_d	gel	l_o	l_d
DPPC (**16PL**)	gel	0	+330	+360	+140	+330	+360	+140	+330	+360
	l_o	+330	0	+330	+330	**0**	+330	+330	**-220**	+330
	l_d	+360	+330	0	+360	+330	**-55**	+360	+330	**-285**
Cholesterol (**cho**)		+350	**-280**	**+40**	+350	**-110**	**+110**	+280	**-75**	**+120**

Table 32: Lipid-Lipid interaction parameters ω_{AB} used in the Monte Carlo simulations. The values from NNR experiments (in **bold**) were rounded to the nearest 5 cal/mol.

In addition, the simulations use the experimental values of the enthalpy (ΔH) and the transition temperatures (T_m) of the main phase transition of the phospholipids and lipidated peptides to calculate the probabilities of changing the lipid state. The model of Almeida[67] was used for DPPC and **16PL**. In this model, the phospholipid accesses essentially only the gel and the l_d states in the absence of cholesterol, but has one more accessible thermodynamic state, l_o, which is intermediate in enthalpy and entropy, in the presence of cholesterol. The enthalpy of the l_o state is assumed to lie at 40% of the way between those of the gel and l_d.[67] Because lipidated peptides **Pep1** and **Pep2** resemble phospholipids, having a polar headgroup and two hydrocarbon chains, we have assumed that they behave similarly to DPPC and its analogue **16PL**. Namely, they exhibit gel-to-fluid phase transitions. The T_m and ΔH values of the chain-melting transition for **Pep1** and **Pep2** were estimated from DSC experiments, as described above (see Sections 2.3.5

and 5.5). The thermodynamic values used in the simulations are shown in Table 33. It should be noted that, although there is some uncertainty about the ΔH values for the monomer **Pep1** and **Pep2**, it has been shown that this level of uncertainty has a negligible effect on the outcome of the Monte Carlo simulations.[94]

	DPPC/16PL			Pep1			Pep2		
Transition	**ΔH**	**ΔS**	**T_m**	**ΔH**	**ΔS**	**T_m**	**ΔH**	**ΔS**	**T_m**
gel - l_d	8.7	27.65	41.5	10.0	28.33	80	7.0	20.96	61
gel - l_o	3.5	10.15		4.0	10.45		2.8	7.65	
l_o - l_d	5.2	17.5		6.0	17.88		4.2	13.31	

Table 33: Phase transition enthalpies (in kcal/mol), entropies (in cal/mol/K) and temperatures (in ^oC) used in the Monte Carlo simulations

5.7 Synthetic Procedures

S-Hexadecyl boc-cysteine (**1**) Procedures that were used for the alkylation of cysteine were similar to those previously described.[95] Freshly cut sodium (857mg, 37.28 mmol) was dissolved in ethanol (100 mL) under an argon atmosphere. Boc-cysteine (3.00g, 13.56 mmol) and 1-bromohexadecane (4.56 mL, 14.92 mmol) were added and the solution was refluxed for 6 h under an argon atmosphere. After cooling to room temperature, the solvent was removed under reduced pressure, and the resulting solid was dissolved in ethyl acetate (75 mL), washed with 5% NaH_2PO_4 (2 x 75 mL) and brine (75 mL), and dried with anhydrous $MgSO_4$. Purification by column chromatography [silica gel, $CHCl_3$/MeOH (8/1, v/v)] yielded **1** (5.842 g, 97%) as a yellow solid having R_f 0.49 [silica gel, $CHCl_3$/MeOH (8/1, v/v)]; ^1H NMR ($CDCl_3$, 500 MHz) δ 5.39 (bs, 1 H), 4.51 (bs, 1 H), 3.00 (bs, 2 H), 2.56 (t, J=7.45 Hz, 2 H), 1.58 (m, 2 H), 1.47 (s, 9 H), 1.40-1.20 (26 H), 0.89 (t, J=6.94 Hz, 3 H); and HR-ESI MS for $C_{24}H_{47}NO_4NaS$ ($[M+Na]^+$) Calculated: 486.3124, found: 486.3101.

N_1,N_2-Bis[S-(hexadecyl)cysteinyl]cystadiamide (2) To a solution of cystamine (74 mg, 0.49 mmol, prepared by washing a suspension of cystamine dihydrochloride in $CHCl_3$ with 1 M NaOH and removing solvent under reduced pressure) in CH_2Cl_2 (20 mL), was added 1 (500 mg, 1.12mmol), EDC (215 mg, 1.12 mmol), HOBt (172 mg, 1.12 mmol), and DIPEA (600 μL), and the resulting mixture was stirred overnight under an argon atmosphere, affording a clear solution. After adding $CHCl_3$ (30 mL), the resulting solution was washed with 5% NaH_2PO_4 (2 x 50 mL), and the aqueous layers extracted with $CHCl_3$. The combined organic layers were washed with saturated $NaHCO_3$ (50 mL) and brine (50 mL), and dried with anhydrous $MgSO_4$. Purification by column chromatography [silica gel, $CHCl_3$/MeOH (95/5, v/v)] afforded a yellow solid, which was then dissolved in TFA (3 mL). After stirring for 20 min, the solvent was removed under reduced pressure, and the resulting solid was dissolved in $CHCl_3$ (50 mL), washed with saturated $NaHCO_3$ (2 x 50 mL) and brine (50 mL), and dried over anhydrous $MgSO_4$. Removal of the solvent under reduced pressure yielded afforded **2** (303 mg, 77%) as a white solid having R_f 0.43 [silica gel, $CHCl_3$/MeOH (8/1, v/v)]; ^{1}H NMR ($CDCl_3/D_2O$, 500 MHz) δ 3.58 (m, 4 H), 3.49 (m, 2 H), 3.05 (m, 2 H), 2.83 (t, J=6.45 Hz, 4 H), 2.66 (m, 2 H), 2.51 (t, J=7.46 Hz, 4 H), 1.58 (m, 4 H), 1.41-1.19 (52 H), 0.88 (t, J=6.73 Hz, 6 H); and HR-ESI MS for $C_{42}H_{87}N_4O_2S_4$ ($[M+H]^+$) Calculated: 807.5712, found 807.5704.

N-Myristoyl glycine (3) To a solution that was made from t-butyl glycine hydrochloride (100 mg, 0.60 mmol), DIPEA (364 μL), and CH_2Cl_2 (10 mL), was added, dropwise, a solution made from myristoyl chloride (324 μL, 1.19 mmol) and CH_2Cl_2 (10 mL) with stirring at 0 ^{o}C under an argon atmosphere. After stirring for 3.5 h, $CHCl_3$ (50 mL) was added, and the solution was washed, sequentially, with 5% NaH_2PO_4 (2 x 50

mL) and brine (50 mL), and then dried over $MgSO_4$. The solvent was removed under reduced pressure, and TFA (5 mL) was added. After stirring for 20 min, the solvent was removed under reduced pressure. Trituration of the resulting solids with hexanes afforded **3** (146 mg, 86%) as a white powder having R_f 0.24 [silica gel, $CHCl_3$/MeOH (4/1, v/v)]; ^{1}H NMR ($MeOD_3$, 500 MHz) δ 3.89 (bs, 2 H), 2.23 (m, 2 H), 1.60 (m, 2 H), 1.37-1.22 (20 H), 0.89 (t, J=6.83 Hz, 3 H); and HR-ESI MS for $C_{16}H_{32}NO_3$ ($[M+H]^+$) Calculated: 286.2382, found: 286.2380.

N_1,N_2-Bis{[(myristoyl)glycyl]-S-(hexadecyl)cysteinyl}cystadiamide ({Pep1-Pep1}) To a solution of **2** (100 mg, 0.12 mmol) in CH_2Cl_2 (5 mL), was added **3** (84 mg, 0.30 mmol), EDC (57 mg, 0.30 mmol), HOBt (46 mg, 0.30 mmol) and DIPEA (130 µL). After stirring the mixture overnight, the solvent was removed under reduced pressure and the residue recrystallized from a mixture of $CHCl_3$ and MeOH to give **{Pep1-Pep1}** (116 mg, 70 %) as a white solid having R_f 0.81 [silica gel, $CHCl_3$/MeOH (6/1, v/v)]; ^{1}H NMR ($CDCl_3$/CD_3OD, 500 MHz) δ 4.60 (t, J=6.54, 2 H), 3.91 (m, 4 H), 3.54 (m, 4 H), 2.96-2.80 (8 H), 2.54 (t, J=6.90, 4 H), 2.26 (t, J=7.41 Hz, 4 H), 1.67-1.52 (8 H), 1.41-1.21 (96 H), 0.89 (t, J=6.64 Hz, 12 H); and HR-MALDI-TOF MS for $C_{74}H_{144}N_6O_6NaS_4$ ($[M+Na]^+$) Calculated: 1363.9922, found 1363.9902.

O-(N-succinimidyl)-O-cholesteryl carbonate (10) To a solution that was made from cholesterol (1.00 g, 2.59 mmol), $CHCl_3$ (15 mL), and NEt_3 (5 mL), was added di-(*N*-succinimidyl)carbonate (2.98 g, 11.64 mmol). After stirring the solution overnight at 45 ^{o}C, the solvent was removed under reduced pressure, and the residue was dissolved in $CHCl_3$ (100 mL) and washed with water (2 x 50 mL). The aqueous layers were extracted with $CHCl_3$ (2 x 50 mL), and the organic layers were combined, dried over anhydrous

$MgSO_4$, and the solvent was removed under reduced pressure. Purification by column chromatography [silica gel, $CHCl_3/CH_3CN$ (95/5, v/v)] yielded **10** (1.162 g, 85%) as a yellow-white solid having R_f 0.49 [silica gel, $CHCl_3/CH_3CN$ (95/5, v/v)]; ^1H NMR ($CDCl_3$, 500 MHz) δ 5.39 (m, 1H), 4.58 (m, 1H), 2.81 (s, 4H), 2.46 (m, 2H), 2.04-0.77 (38H), 0.66 (s, 3H).

N_1-(Cholesteryl)cystamide carbamate (4) To a solution of cystamine (1.154 g, 7.58 mmol, prepared by washing a suspension of cystamine dihydrochloride in $CHCl_3$ with 1 M NaOH and removing solvent under reduced pressure) and DIPEA (1.32 µL) in $CHCl_3$ (50 mL) was added a solution of **10** (1.00 g, 1.89 mmol) in $CHCl_3$ (30 mL) while stirring at 0 ^oC. After stirring for 90 minutes, the solution was diluted with $CHCl_3$ (100 mL) and washed, sequentially, with saturated $NaHCO_3$ (2 x 50 mL), H_2O (50 mL), 0.5 M HCl (150 mL), and brine (150 mL). Removal of the solvent under reduced pressure followed by column chromatography [silica gel, $CHCl_3$/MeOH (8/1, v/v)] afforded **4** (540 mg, 47%) as a white solid having R_f 0.13 [silica gel, $CHCl_3$/MeOH (8/1, v/v)]; ^1H NMR ($CDCl_3$, 500 MHz) δ 5.37(bs, 1H), 5.03 (bs, 1H), 4.50 (bs, 1H), 3.51 (m, 2H), 3.02 (t, J=6.23 Hz, 2 H), 2.77 (m, 4H), 2.06-0.76 (40H), 0.67 (s, 3H); and HR-ESI MS for $C_{32}H_{57}N_2O_2S_2$ ($[M+H]^+$) Calculated: 565.3861, found 565.3858.

O-(cholesteryl)-N_2-6-carbamoyl-3,4-dithia-N_1-hexylamide (5) To a solution of **1** (222 mg, 0.50 mmol) in CH_2Cl_2 (15 mL), were added EDC (97 mg, 0.50 mmol), HOBt (76 mg, 0.50 mmol), and DIPEA (525 µL). After stirring under an argon atmosphere for 1 h, **4** (250 mg, 0.42 mmol) was added and the solution stirred overnight. The solution was then washed with 5% NaH_2PO_4 (2 x 50 mL), and the aqueous layers were extracted with $CHCl_3$. Subsequently the organic layers were combined, washed with saturated

$NaHCO_3$ (50 mL) and brine (50 mL), and dried over anhydrous $MgSO_4$. Purification by column chromatography [silica gel, ethyl acetate/hexanes (20/80, v/v)] afforded a cloudy white oil, which was dissolved in TFA (4 mL). After stirring for 20 min, the solvent was removed under reduced pressure, and the residue was dissolved in $CHCl_3$, washed with saturated $NaHCO_3$ (2 x 50 mL) and brine (50 mL), and dried over anhydrous $MgSO_4$. Removal of the solvent under reduced pressure yielded **5** (107 mg, 29%) having R_f 0.65 [silica gel, $CHCl_3$/MeOH (8/1, v/v)]; ^{1}H NMR ($CDCl_3$, 500 MHz) δ 7.81 (bs, 1 H), 5.37 (m, 1 H),5.16 (m, 1 H), 4.49 (m 1 H), 3.59 (m, 2 H), 3.50 (m, 3H), 3.05 (m, 1 H), 2.82 (m, 4 H), 2.67 (m, 1 H), 2.51 (t, J=7.42 Hz, 2 H), 2.34 (m, 1 H), 2.27 (m, 1 H), 2.03-0.80 (71 H), 0.67 (s, 3 H); and HR-ESI MS for $C_{51}H_{94}N_3O_3S_3$ ($[M+H]^+$) Calculated: 892.6457, found 892.6463.

(Myristoyl)glycinyl-S-(hexadecyl)cysteinyl-O-(cholesteryl)-N_2-6-carbamoyl-3,4-dithia-N_1-hexylamide ({Pep1-cho}) To a solution that was made from **5** (152 mg, 0.17 mmol) in CH_2Cl_2 (15 mL), was added **3** (58 mg, 0.20 mmol), EDC (39 mg, 0.20 mmol), HOBt (31 mg, 0.20 mmol), and DIPEA (177 μL). After stirring overnight, removal of the solvent under reduced pressure followed by recrystallization from a mixture of $CHCl_3$ and MeOH afforded **{Pep1-cho}** (110 mg, 56 %) as a yellow solid having R_f 0.73 [silica gel, $CHCl_3$/MeOH (8/1, v/v)]; ^{1}H NMR ($CDCl_3$/CD_3OD, 500 MHz) δ 5.37 (bs, 1 H), 4.45 (m, 1 H), 3.88 (m, 2 H), 3.54 (m, 1 H), 3.43 (m, 2 H), 2.98-2.74 (7 H), 2.53 (t, J=7.38 Hz, 2 H), 2.34 (m, 2 H), 2.27 (t, J=7.94), 2 H), 2.05-0.79 (92 H), 0.69 (s, 3 H); and HR-ESI MS for $C_{67}H_{123}N_4O_5S_3$ ($[M+H]^+$) Calculated: 1159.8656, found 1159.8628.

3-(2-pyridinyldithio)porpionyl-dipalmitoyl phosphatidylethanolamine sodium salt (**6**) To a solution that was made from 1,2-dihexadecanoyl-*sn*-glycero-3-phosphoethanolamine (DPPE, 250 mg, 0.36 mmol) in $CHCl_3$ (5 mL), MeOH (5 mL), and H_2O (1 mL) was added DIPEA (125 μL) and BPDP (169 mg, 0.47 mmol). See Reference 96 for a discussion of the preparation and use of BPDP. After stirring under an argon atmosphere for 4 h, $CHCl_3$ (50 mL) was added. The solution was then washed with 5% NaH_2PO_4 (2 x 50 mL), and the aqueous layers were extracted with $CHCl_3$ (2 x 50 mL). The organic layers were combined and dried over anhydrous $MgSO_4$. Purification by column chromatography [silica gel, $CHCl_3$/MeOH (4/1, v/v)] yielded **6** (281 mg, 85%) as a yellow solid having R_f 0.65 [silica gel, $CHCl_3$/MeOH (4/1, v/v)]; ^1H NMR ($CDCl_3$, 500 MHz) δ 8.30 (bs, 1H), 7.86 (bs, 1H), 7.60 (bs, 1H), 7.16 (bs, 1H), 5.19 (m, 1H), 4.54 (m, 1H), 4.34 (m, 1H), 4.16-4.03 (2H), 3.92 (m, 4H), 3.81 (m, 1H), 3.57-3.35 (4H), 3.04-2.76 (6H), 2.58 (t, J=6.81 Hz, 2 H), 2.48 (t, J=7.43 Hz, 2 H), 2.30-2.18 (6H), 1.63-1.15 (114H), 0.85 (t, J=6.85 Hz, 12H); and HR-ESI MS for $C_{45}H_{80}N_2O_9PS_2$ ([M]-) Calculated: 887.5048, found: 887.5031.

(Myristoyl)glycyl-S-(hexadecyl)cysteinyl-4,5-dithia-7-aminoheptanoyl-dipalmitoyl phosphatidylethanolamine, sodium salt (**{Pep1-16PL}**) To a solution that was made from {**Pep1-Pep1**}(40 mg, 0.03 mmol) in $CHCl_3$ (20 mL), and MeOH (20 mL) and heated to 55 °C was added a solution of TCEP (34 mg, 0.12 mmol) in 0.19M aqueous NaOH (1.6 mL). After stirring at 55 °C under an argon atmosphere for 4 h, the solution was washed with brine (50 mL), the aqueous layer was extracted with $CHCl_3$/MeOH (3/1 v/v, 3 x 25 mL), and the organic layers were combined and dried over anhydrous $MgSO_4$. The resulting material was purified by column chromatography

[silica gel, $CHCl_3$/MeOH (9/1, v/v)]. Solvent was removed from the collected fractions under reduced pressure, and the resulting white residue was immediately dissolved in 25 mL $CHCl_3$/MeOH (2/1, v/v) and added to a flask containing **6** (68 mg, 0.07 mmol). After stirring under an argon atmosphere for 48 h, purification by preparative TLC [$CHCl_3$/MeOH/H_2O (4/1/0.1, v/v)] afforded {**Pep1-16PL**} (54 mg, 62%) as a white solid having R_f 0.74 [silica gel, $CHCl_3$/MeOH (4/1, v/v)]; ^{1}H NMR ($CDCl_3$MeOD, 500 MHz) δ 8.36 (m, 1H), 7.81-7.73 (2H), 7.16 (m, 1H), 5.17 (m, 1H), 4.38 (m, 1H), 4.14 (m, 1H), 3.93 (t, J=5.80, 2H), 3.86 (m, 2H), 3.68 (m, 1H), 3.17 (m, 1H), 3.04 (t, J=7.26 Hz, 2H), 2.60 (t, J=7.20 Hz, 2H), 2.27 (m, 4H), 1.56 (bs, 4H), 1.48-1.10 (48), 0.85 (t, J=7.01 Hz, 6H); and HR-ESI MS for $C_{77}H_{148}N_4O_{12}PS_3$ ([M]-)Calcd: 1447.9999, Found: 1448.0052.

***Cis*-9,10-methylenetetradecanoic acid (7)** Procedures that were used for the synthesis of **7** were similar to those previously described.[57] To a solution of 2,4,6-trichlorophenol (1.61g, 8.16 mmol) in anhydrous CH_2Cl_2 (36 mL); which was maintained at -40 °C, was added a 1M hexane solution of diethyl zinc (8.16 mL). After stirring for 15 minutes at -40 °C under an Ar atmosphere, CH_2I_2 (658µL, 8.16 mmol) was added. The solution was then stirred another 15 minutes at -40 °C, and myristeoleic acid (462 mg, 2.04 mmol) was added. After stirring overnight at room temperature, $CHCl_3$ (150 mL) was added and the mixture was washed with 10% HCl (2 x 75 mL). The aqueous layers were combined and extracted with $CHCl_3$ (3 x 50 mL). The organic layers were combined, washed with brine (100 mL) and dried over anhydrous $MgSO_4$. Purification by flash chromatography [silica gel, $CHCl_3$/MeOH (20/1, v/v)] afforded **7**, (190 mg, 39%) having R_f 0.76 [silica gel, $CHCl_3$/MeOH (8/1, v/v)]; ^{1}H NMR ($CDCl_3$, 500 MHz) δ 2.31 (t, J=7.56 Hz, 2H), 1.60 (m, 2H), 1.39-1.20 (14H), 1.10 (bs, 2H), 0.86 (t, J=7.01 Hz,

3H), 0.60 (bs, 2H), 0.53 (m, 1H), -0.37 (m, 1H); and HR-ESI MS for $C_{15}H_{27}O_2$ ($[M-H]^-$) Calculated: 239.2017, Found: 239.2015.

N_1,N_2-Bis[N-glycyl-S-(hexadecyl)cysteinyl]cystadiamide (8) To a solution of **2** (100 mg, 0.12 mmol) in CH_2Cl_2 (40 mL) was added DIPEA (170 µL), boc-glycine (48 mg, 0.27 mmol), EDC (52 mg, 0.27 mmol), and HOBt (41 mg, 0.27 mmol) and the resulting mixture was stirred overnight under an argon atmosphere. The resulting solution was washed with 5% NaH_2PO_4 (2 x 25 mL), saturated $NaHCO_3$ (2 x 25 mL) and brine (25 mL), and dried with anhydrous $MgSO_4$. Purification by preparative TLC [$CHCl_3$/MeOH (12/1, v/v)] afforded a white solid, which was then dissolved in $CHCl_3$ (3 mL) and TFA (3 mL). After stirring for 45 min, the solvent was removed under reduced pressure, and the resulting solid was dissolved in $CHCl_3$ (50 mL), washed with saturated $NaHCO_3$ (2 x 50 mL) and brine (50 mL), and dried over anhydrous $MgSO_4$. Removal of the solvent under reduced pressure afforded **8** (63 mg, 55%) as a white solid having R_f 0.20 [silica gel, $CHCl_3$/MeOH (4/1, v/v)]; ^{1}H NMR ($CDCl_3$, 500 MHz) δ 8.03 (d, J=6.26 Hz, 1H), 7.36 (bs, 1H), 4.61 (m, 2H), 3.54 (m, 4H), 3.38 (s, 4H), 2.90 (m, 8H), 2.78 (t, J=6.48 Hz, 4H), 2.53 (t, J=7.45, 4H), 1.83 (bs, 4H), 1.54 (m, 4H), 1.38-1.34 (52H), 0.84 (t, J=6.98Hz, 6H); and HR-ESI MS for $C_{46}H_{93}N_6O_4S_4$($[MH]^+$) Calculated: 921.6136, Found: 921.6115.

N_1,N_2-Bis-(*cis*-9,10-methylenetetrdecanoyl)glycyl-S-(hexadecy)cysteinyl cystadiamide {**Pep2-Pep2**} To a solution of **8** (53 mg, 0.06 mmol) in CH_2Cl_2 (10 mL) was added DIPEA (60 µL), **7** (30 mg, 0.13 mmol), EDC (24 mg, 0.13 mmol), and HOBt (19 mg, 0.19 mmol) and the resulting mixture was stirred overnight under an argon atmosphere. Removal of solvent under reduced pressure followed by preparative TLC

[$CHCl_3$/MeOH (10/1 v/v)] afforded **{Pep2-Pep2}** (55 mg, 70%) as a white solid having R_f 0.58 [silica gel, $CHCl_3$/MeOH (8/1, v/v)]; ^{1}H NMR ($CDCl_3$, 500 MHz) δ 7.49 (d, J=8.43, 2H), 7.42 (bs, 2H), 7.02 (bs, 2H), 4.73 (m, 2H), 4.01 (m, 4H), 3.57 (m, 4H), 2.81 (m, 8H), 2.55 (m, 4H), 2.22 (t, J=7.63, 4H), 1.71-1.02 (96H), 0.86 (m, 12H), 0.61 (bs, 4H), 0.53 (m, 2H), -0.36 (m, 2H); and HR-ESI MS for $C_{76}H_{144}N_6O_6S_4Na([MNa]^+)$ Calculated: 1387.9922, Found: 1387.9890.

2-(2-Pyridinyldithio)-ethanamine (9) A solution of cysteamine hydrochloride (516 mg, 4.54 mmol) was added, drop wise, to a solution of 2,2`-dithiopyridine (1.100g, 4.99 mmol) in methanol (10 mL). After stirring for 90 minutes at room temperature, removal of solvent under reduced pressure followed by purification by column chromatography [silica gel, $CHCl_3$/MeOH (10/1, v/v)] yielded **9** (575 mg, 57%) as a yellow solid having ^{1}H NMR ($CDCl_3$/MeOD, 500 MHz) δ 8.55 (m, 1H), 7.72 (m, 1H), 7.53 (m, 1H), 7.28 (m, 1H), 3.29 (t, J=6.41 Hz, 2H), 3.16 (t, J=6.16 Hz, 2H).

N-[2-(2-pyridinyldithioethyl)]-O-cholesteryl carbamate (11) To a solution of **9** (297 mg, 1.30 mmol) and DIPEA (1.36 mL) in $CHCl_3$ (45 mL) was added **10** (686 mg, 1.30 mmol). After stirring overnight at room temperature, purification by column chromatography [silica gel, $CHCl_3$/MeOH (99/1, v/v)] afforded **11** (1.08g, 100%) as a yellow oil having R_f 0.85 [silica gel, $CHCl_3$/MeOH (95/5, v/v)]; ^{1}H NMR ($CDCl_3$, 500 MHz) δ 5.37 (bs, 1H), 5.03 (bs, 1H), 4.50 (bs, 1H), 3.51 (m, 2H), 3.02 (t, J=6.23 Hz, 2H), 2.77 (m, 4H), 2.06-0.76 (40H), 0.67 (s, 3H); and HR-ESI MS for $C_{35}H_{55}N_2O_2S_2([MH]^+)$ Calculated: 599.3700, Found: 599.3703.

(*Cis*-9,10-methylenetetradecanoyl)glycyl-S-(hexadecyl)cysteienyl-O-(cholesteryl)N_2-6-carbanoyl-3,4-dithia-N_1-hexylamide ({**Pep2-cho**}) To a solution that

was made from {**Pep2-Pep2**}(25 mg, 0.02 mmol) in $CHCl_3$ (25 mL), and MeOH (25 mL) and heated to 55 °C was added a solution of TCEP (21 mg, 0.07 mmol) in 0.18 M aqueous NaOH (1.0 mL). After stirring at 55 °C under an argon atmosphere for 4.5 h, the solution was washed with brine (50 mL), the aqueous layer was extracted with $CHCl_3$/MeOH (3/1 v/v, 3 x 25 mL), and the organic layers were combined and dried over anhydrous $MgSO_4$. The resulting material was purified by column chromatography [silica gel, $CHCl_3$/MeOH (9/1, v/v)]. Solvent was removed from the collected fractions under reduced pressure, and the resulting white residue was immediately dissolved in 25 mL $CHCl_3$/MeOH (2/1, v/v) and added to a flask containing **11** (27 mg, 0.05 mmol). After stirring under an argon atmosphere for 45 h, purification by preparative TLC [$CHCl_3$/MeOH (8/1, v/v)] afforded **{Pep2-cho}** (8 mg, 37%) as a white solid having R_f 0.68 [silica gel, $CHCl_3$/MeOH (4/1, v/v)]; ^{1}H NMR ($CDCl_3$, 500 MHz) δ 7.19 (bs, 1H), 7.07 (d, J=8.01Hz, 1H), 6.37 (bs, 1H), 5.35 (m, 1H), 5.20 (m, 1H), 4.56 (m, 1H), 4.47 (m, 1H), 3.93 (m, 2H), 3.56 (d, J=5.57 Hz, 2H), 3.44 (m, 2H), 3.00 (m, 2H), 2.89-2.70 (5H), 2.51 (m, 2H), 2.32 (m, 1H), 2.24 (t, J=7.49 Hz, 2H), 2.05-0.74 (93H), 0.71-0.57 (5H), 0.54 (m, 1H), 0.36 (m, 1H); HR-ESI MS for $C_{68}H_{122}N_4O_5NaS_3$([M-Na]$^+$) Calculated: 1193.8470, Found: 1193.8464.

(*Cis*-9,10-methylenetetradecanoyl)glycyl-S-(hexadecyl)cysteinyl-4,5-dithia-7-aminoheptanoyl-dipalmitoyl phosphatidylethanolamine, sodium salt (**{Pep2-16PL}**)
To a solution that was made from {**Pep2-Pep2**}(56 mg, 0.04 mmol) in $CHCl_3$ (27.5 mL), and MeOH (27.5 mL) and heated to 55 °C was added a solution of TCEP (47 mg, 0.16 mmol) in 0.23M aqueous NaOH (1.8 mL). After stirring at 55 °C under an argon atmosphere for 4 h, the solution was washed with brine (50 mL), the aqueous layer was

extracted with $CHCl_3$/MeOH (3/1 v/v, 3 x 25 mL), and the organic layers were combined and dried over anhydrous $MgSO_4$. The resulting material was purified by column chromatography [silica gel, $CHCl_3$/MeOH (9/1, v/v)]. Solvent was removed from the collected fractions under reduced pressure, and the resulting white residue was immediately dissolved in 25 mL $CHCl_3$/MeOH (2/1, v/v) and added to a flask containing **6** (93 mg, 0.10 mmol). After stirring under an argon atmosphere for 48 h, purification by preparative TLC [$CHCl_3$/MeOH/H_2O (4/1/0.1, v/v)] afforded **{Pep2-16PL}** (36 mg, 59%) as a white solid having R_f 0.47 [silica gel, $CHCl_3$/MeOH/ H_2O (4/1/0.1, v/v)]; ^1H NMR ($CDCl_3$, 500 MHz) δ 8.30 (bs, 1H), 7.78 (bs, 1H), 7.60 (bs, 1H), 7.12 (bs, 1H), 5.20 (m, 1H), 4.54 (m, 1H), 4.35 (m, 1H), 4.10 (m, 2H), 3.92 (m, 4H), 3.82 (m, 1H), 3.58-3.35 (4H), 3.05-2.75 (6H), 2.58 (t, J=6.98 Hz, 2H), 2.49 (t, J=7.46 Hz, 2H), 2.25 (m, 6H), 1.63-1.04 (98H), 0.85 (t, J=6.90 Hz, 12H), 0.61 (bs, 2H), 0.53 (m, 1H), -0.36 (m, 1H); HR-ESI MS for $C_{78}H_{148}N_4O_{12}PS_3([M]^-)$ Calculated: 1459.9999, Found: 1460.0033.

N-[(*cis*-9,10-methylenetetradecanoyl)glycyl-S-(hexadecy)cysteinyl-2-(methylthio)ethyl]amide (**Pep1a**) To a solution made from **{Pep1-Pep1}** (22 mg, 0.016 mmol) in $CHCl_3$ (10 mL), and MeOH (10 mL) and heated to 55 °C was added a solution of TCEP (19 mg, 0.07 mmol) in 0.40M aqueous NaOH (0.4 mL). After stirring at 55 °C under an argon atmosphere for 4 h, the solution was washed with brine (50 mL), the aqueous layer was extracted with $CHCl_3$/MeOH (3/1 v/v, 3 x 25 mL), and the organic layers were combined and dried over anhydrous $MgSO_4$. The resulting material was purified by column chromatography [silica gel, $CHCl_3$/MeOH (9/1, v/v)]. To a flask containing the collected fractions from the column (~15 mL) was added a solution of CH_3I (5.0 μL, 0.08 mmol) in 0.1 M methanolic NaOH solution (300 μL). After stirring

overnight, purification by preparative TLC [$CHCl_3$/MeOH (9/1, v/v)] afforded **Pep1a** (9 mg, 40%) as a white solid having R_f 0.81 [silica gel, $CHCl_3$/MeOH (6/1, v/v)]; ^{1}H NMR ($CDCl_3$, 500 MHz) δ 4.27 (t, J=6.50 Hz, 1H), 3.63 (m, 2H), 3.19 (m, 2H), 2.96 (m, 1H), 2.67 (t, J=5.54 Hz, 2H), 2.41 (t, J=6.95 Hz, 2H), 2.30 (t, J=7.43, Hz, 2H), 2.04 (t, J=7.73 Hz, 2H), 1.89 (s, 3H), 1.45-1.28 (5H), 1.63-0.97 (44H), 0.65 (t, J=6.95 Hz, 6H); HR-ESI MS for $C_{38}H_{76}N_3O_3S_2$ ($[MH]^+$) Calculated: 686.5323, Found 686.5338.

N-[(myristoyl)glycyl-S-(hexadecy)cysteinyl-2-(methylthio)ethyl]amide (**Pep2a**) To a solution made from **{Pep2-Pep2}** (17 mg, 0.012 mmol) in $CHCl_3$ (10 mL), and MeOH (10 mL) and heated to 55 °C was added a solution of TCEP (13 mg, 0.05 mmol) in 0.30M aqueous NaOH (0.4 mL). After stirring at 55 °C under an argon atmosphere for 4 h, the solution was washed with brine (50 mL), the aqueous layer was extracted with $CHCl_3$/MeOH (3/1 v/v, 3 x 25 mL), and the organic layers were combined and dried over anhydrous $MgSO_4$. The resulting material was purified by column chromatography [silica gel, $CHCl_3$/MeOH (9/1, v/v)]. To a flask containing the collected fractions from the column (~15 mL) was added a solution of CH_3I (3.8 µL, 0.06 mmol) in 0.1 M methanolic NaOH solution (300 µL). After stirring overnight, purification by preparative TLC [$CHCl_3$/MeOH (9/1, v/v)] afforded **Pep2a** (14 mg, 81%) as a white solid having R_f 0.50 [silica gel, $CHCl_3$/MeOH (9/1, v/v)]; ^{1}H NMR ($CDCl_3$, 500 MHz) δ 4.41 (t, J=6.50 Hz, 1H), 3.79 (m, 2H), 3.35 (t, J=6.91 Hz, 2H), 2.81 (bs, 2H), 2.55 (bs, 2H), 2.44 (t, J=7.34 Hz, 2H), 2.18 (t, J=7.69 Hz, 2H), 2.03 (s, 3H), 1.61-1.41 (4H), 1.33-0.95 (43H), 0.79 (m, 6H), 0.55 (bs, 2H), 0.47 (m, 1H), -0.43 (m, 1H); HR-ESI MS for $C_{39}H_{76}N_3O_3S_2$ ($[MH]^+$) Calculated: 698.5323, Found 698.5336.

Appendix 1

Additional NNR Studies Using Exchangeable Sterol Dimers

A1.1 Introduction

In a complementary approach to the experiments discussed in Chapter 3, we sought to gain additional insight into sterol-phospholipid interactions by directly measuring the nearest neighbor interaction energies between **16PL** and several exchangeable sterols. Despite the importance that sterol-phospholipid interactions have in membrane structure, little is known about the energetics of these interactions, especially in the biologically important l_o phase. In an attempt to investigate the effects of variations in sterol structure on sterol-phospholipid interactions, we conducted a series of NNR experiments using the lipids shown in Figure 32.

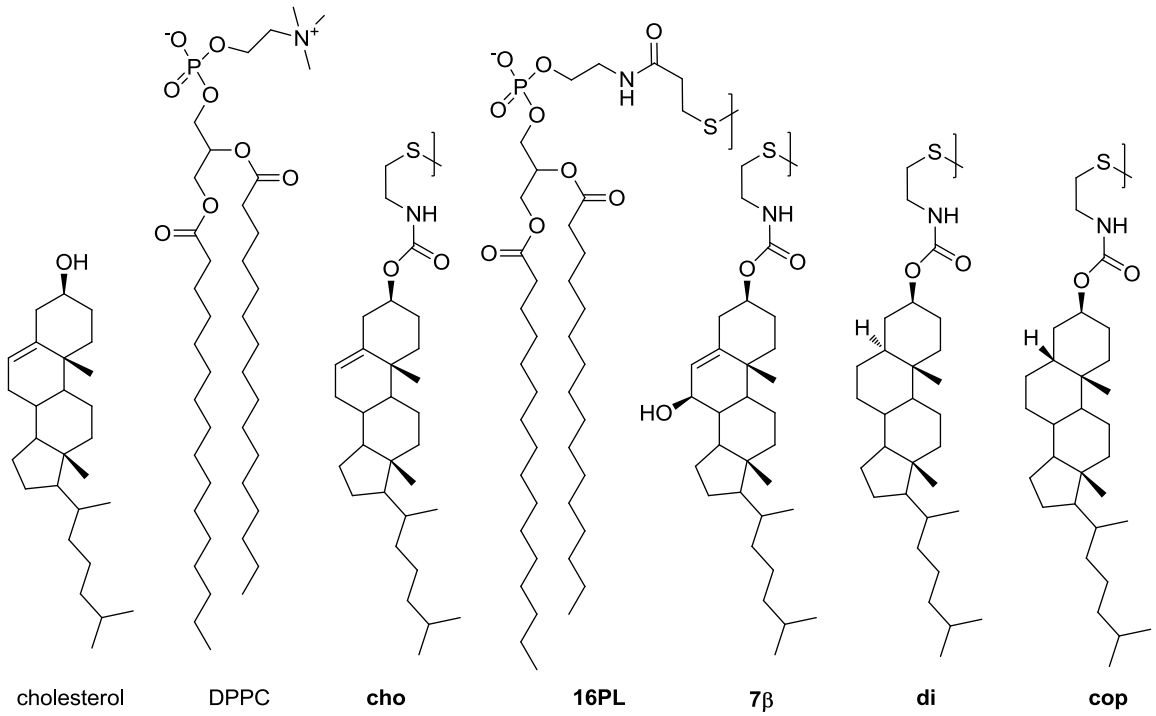

Figure 32: Structures of exchangeable lipids used in exchangeable sterol studies

Lipids **cho** and **16PL** are exchangeable mimics of cholesterol and DPPC, respectively (see Section 2.2 for a discussion of the properties of these lipids). Lipid **7β** is an exchangeable mimic of 7β-hydoxycholesterol (7β-OH). This sterol was chosen to investigate the effect of the addition of a polar group to the sterol core. Lipids **di** and **cop** are exchangeable mimics of dihydrocholesterol and coprostanol, respectively. Both dihydrocholesterol and coprostanol are structural analogs of cholesterol lacking the double bond found in cholesterol's B ring. Dihydrocholesterol and coprostanol differ only in the stereochemistry at carbon 5; coprostanol's structure at this position results in a *cis* fusion of its A and B rings, giving the sterol core a curved three dimensional structure (see Figure 26, page 68). Dihydrocholesterol has a planar core similar to cholesterol. A sterol with a non-planar nucleus cannot make the perfect contact with fully extended acyl chains that is necessary (by a template model) to maximize sterol-phospholipid interaction in the l_o phase. Sterol **cop** is therefore expected to show less affinity for **16PL** than **di** does, mirroring its weaker condensing effect compared to cholesterol or dihydrocholesterol (as discussed in Chapter 3).

To quantitatively measure the interactions of the four sterols with **16PL** in the liquid-ordered phase, NNR reactions were performed using the exchangeable lipids shown in Figure 32 in host membranes of DPPC and cholesterol. All NNR reactions were done in membranes containing 40 mol% sterol. Such membranes are in the l_o phase, where sterol-phospholipid interactions are expected to be greatest. Specifically, thiolate-disulfide equilibration reactions were carried out at 45 ^{o}C in liposomes (~200 nm) made from 57.5/37.5/2.5/2.5 mol% DPPC/cholesterol/X/**16PL** (here, X is **cho**, **7β**, **di**, or **cop**).

A1.2 Results

A1.2.1 Synthesis of Dimers for NNR Reactions

The exchangeable dimers {**di-di**}, {**di-16PL**}, and {**7β -7β**}, as well as the7β-OH used as a starting material to synthesize {**7β -7β}**, were synthesized in our laboratory by Dr. Wen-Hua Chen. Dimers {**cop-cop**} and {**cop-16PL**} were synthesized by Destinee Zablocki. The heterodimer {**7β -16PL**} was synthesized by Trevor Daly. As discussed in Section 2.3.1, {**cho-16PL**}, {**16PL-16PL**}, and {**cho-16PL**} were synthesized as previously reported.[19,55]

The synthesis of the dihydrocholesterol dimers {**di-di**} and {**di-16PL**} is shown in Scheme 7. In brief, dihydrocholesterol was activated with N,N' disuccinimdyl carbonate and condensed with cystamine to generate the homodimer. The activated sterol was condensed with 3-(2-aminoethyldithio)propanoic acid hydrochloride salt (AEDP), followed by coupling with 1,2-dipalmitoyl-*sn*-glycero-3-phosphoethanolamine (DPPE), affording the corresponding heterodimer.

The coprostanol dimers ({**cop-cop**} and {**cop-16PL**}) were synthesized similarly, beginning with coprostanol rather than dihydrocholesterol. The 7β-OH homodimer ({**7β -7β**}) was also synthesized via N,N' disuccinimidyl carbonate activation and condensation with cystamine, beginning with 7β-OH cholesterol prepared from cholesterol as shown in Scheme 8.

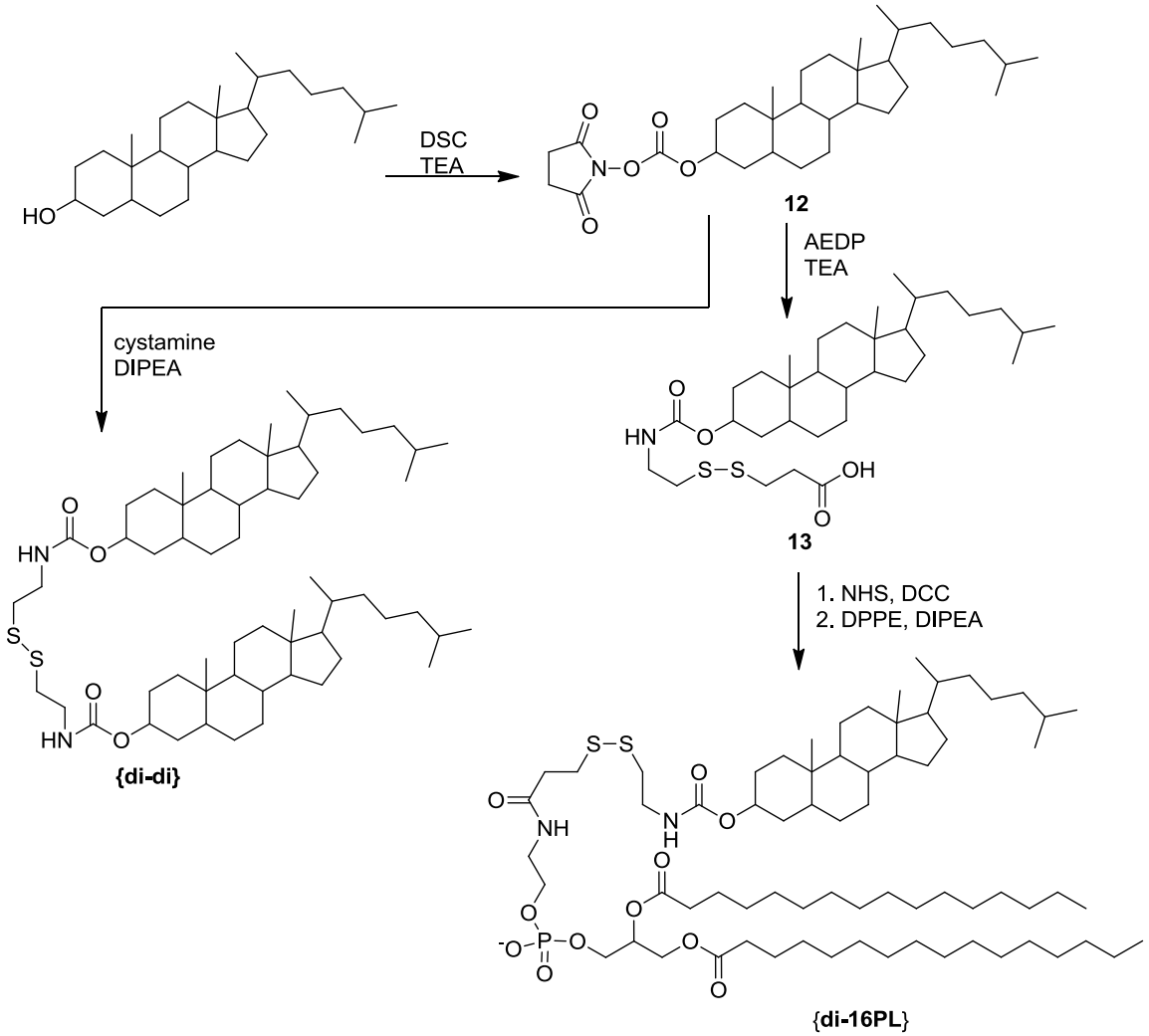

Scheme 7: Synthesis of dimers {**di-di**} and {**di-16PL**}

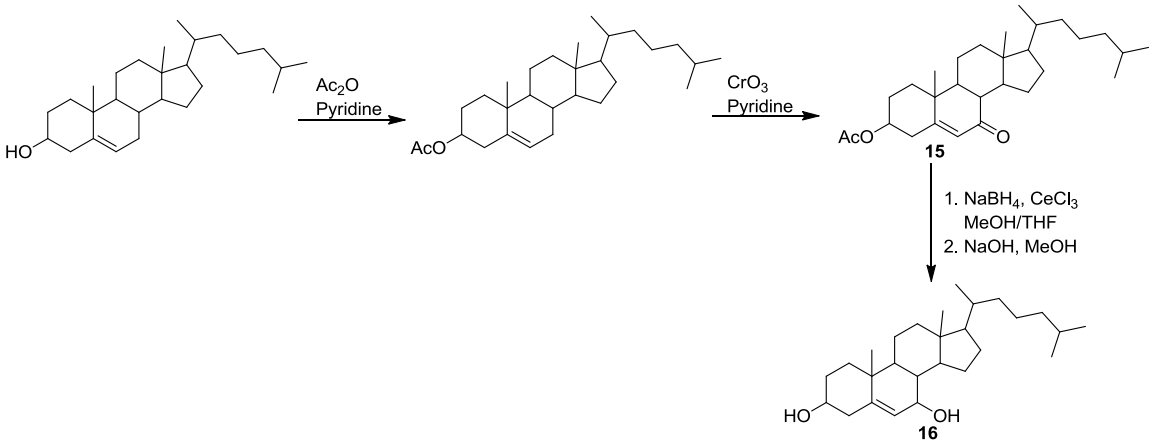

Scheme 8: Synthesis of 7β-OH cholesterol

An attempted synthesis of the 7β-OH-phospolipid heterodimer ({**7β-16PL**}) using methods similar to those used for the other heterodimers failed to produce product of sufficiently high purity. Instead, {**7β -16PL}** was prepared as shown in Scheme **9**. A catalytic amount of TCEP was added to a mixture of {**7β-7β**} and {**16PL-16PL**} under basic pH to initiate thiolate-disulfide exchange. Preparative thin layer chromatography was used to separate the resulting heterodimer from the homodimers, which were then subjected to an additional round of thiolate-disulfide exchange to generate additional heterodimer.

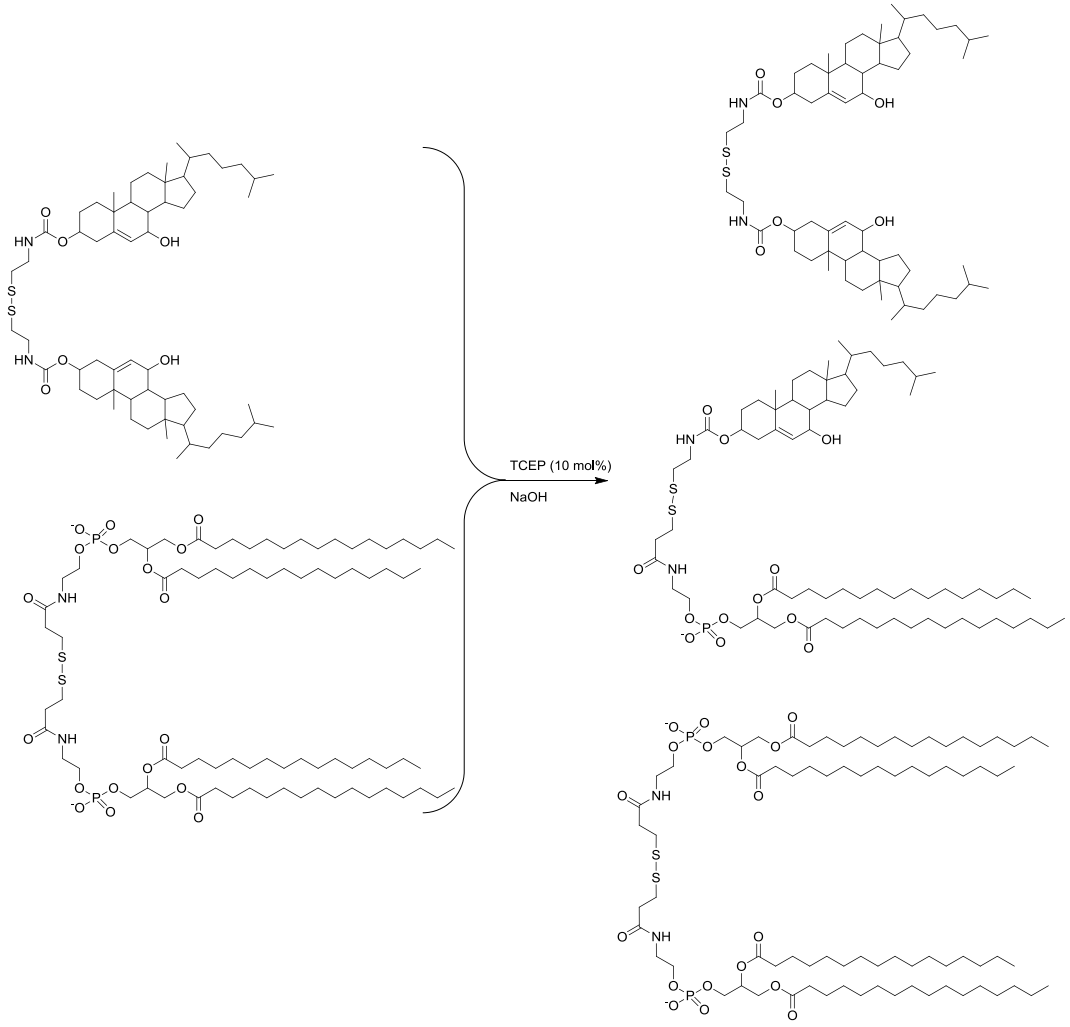

Scheme 9: Synthesis of {**7β-16PL**} via thiloate-disulfide exchange

A1.2.2 Calibration of Chromatographic Systems

In order to analyze NNR product mixtures by HPLC, it was first necessary to develop appropriate calibration curves. As noted in Section 2.3.2, all NNR reactions performed using {**cho-16PL**} were analyzed using the previously published calibration curve.[21] For the other dimer pairs, the chromatographic systems were calibrated by repeating the NNR sample preparation technique using samples of known dimer concentration. The HPLC conditions were identical to those used for NNR reaction analysis, see Section A1.5 for the specific conditions used for the HPLC analysis of each pair of dimers. The calibration curve obtained for {**7β-16PL**} and related dimers is shown in Figure 33. For the chromatographic system used for **{7β-16PL}** reactions, the system was found to respond as follows: for {**7β-7β**}, 723370 x $n\{_{7\beta\text{-}7\beta}\}$ + 19294 = *Signal* (R^2= 0.9974); for **{7β-16PL}** *648646 x* $n\{_{7\beta\text{-}16PL}\}$ *+ 1461.1 = Signal n* (R^2 =0.9981); for **{16PL-16PL}** *554675 x* $n\{_{16PL\text{-}16PL}\}$ *- 90368 = Signal* (R^2 = 0.9976) where *signal* is the area of the chromatographic peaks for the dimers and *n* is the number of moles of dimers.

The calibration curves for the dimers containing **di** and **cop** are shown in Figures 34 and 35, respectively. Because the chromatographic system used in these reactions is identical to that used in previously reported experiments, it was not necessary to prepare a new calibration curve for {**16PL-16PL**} under these conditions, so it is not included in the figures. For the chromatographic system used for **{di-16PL}** and **{cop-16PL}** reactions, the system was found to respond as follows: for **{di-16PL}**, 340730 x $n\{_{di\text{-}16PL}\}$ + 44454 = *Signal* (R^2= 0.9958); for **{di-di}** *159102 x* $n\{_{di\text{-}di}\}$ *– 5345.6 = Signal n* (R^2

=0.9961); for **{cop-16PL}** *295492 x* $n_{\{cop\text{-}16PL\}}$ + 117225 = *Signal* (R^2 = 0.9946), and for **{cop-cop}** *157225 x* $n_{\{cop\text{-}cop\}}$ + 42112 = *Signal* (R^2 = 0.9899).

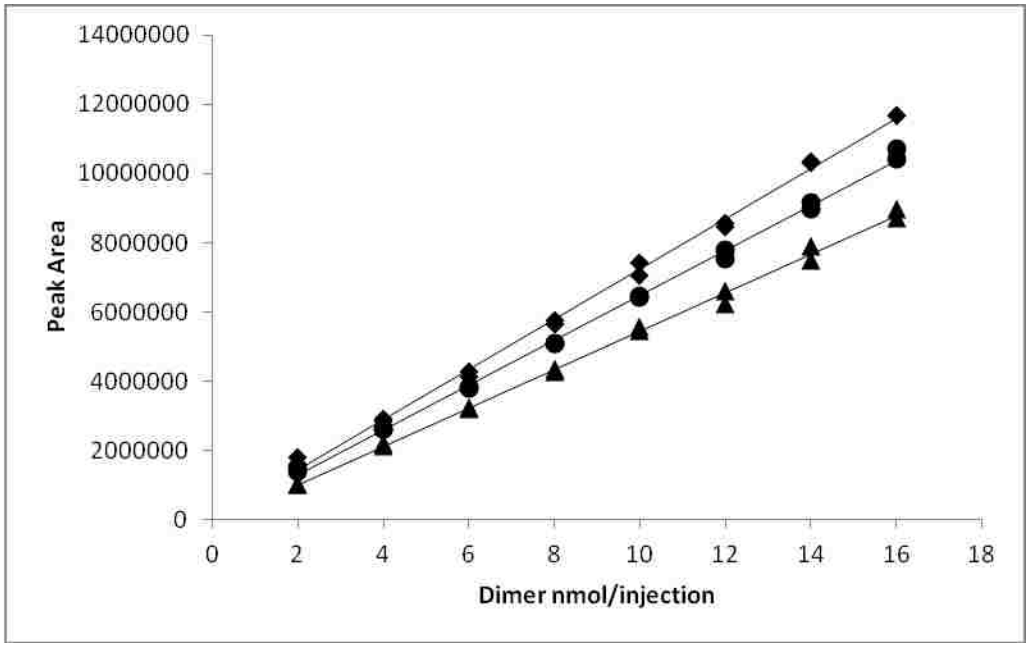

Figure 33: Peak area plotted as a function of nmol/injection for dimers {**7β-7β**} (♦),{**7β-16PL**} (●), and {**16PL-16PL**} (▲)

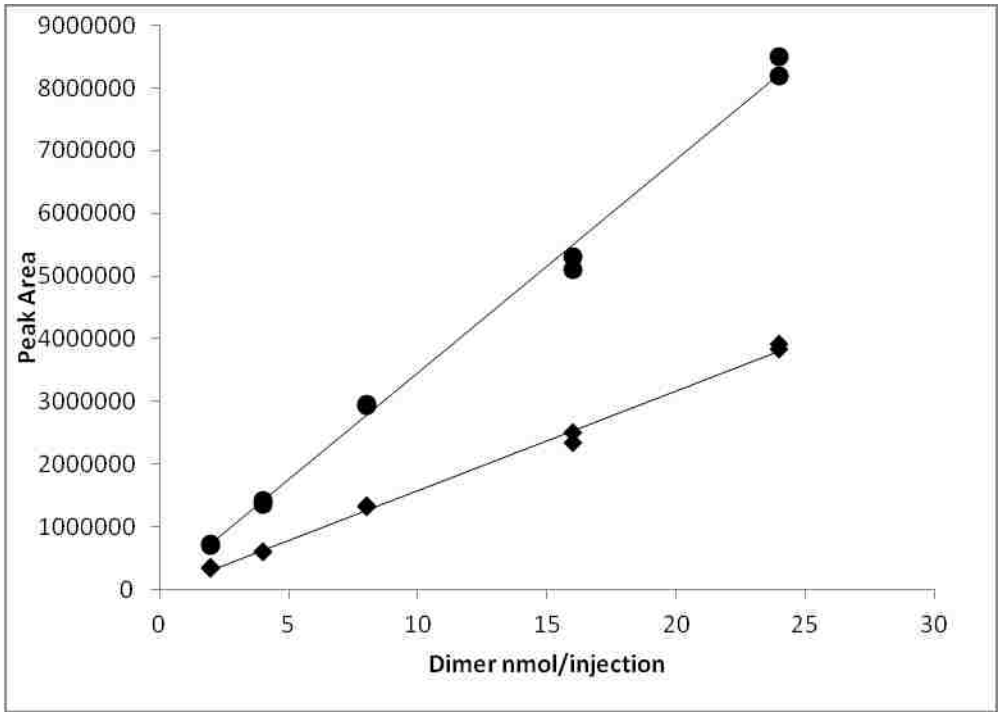

Figure 34: Peak area plotted as a function of nmol/injection for dimers {**di-di**} (♦) and {**di-16PL**} (●)

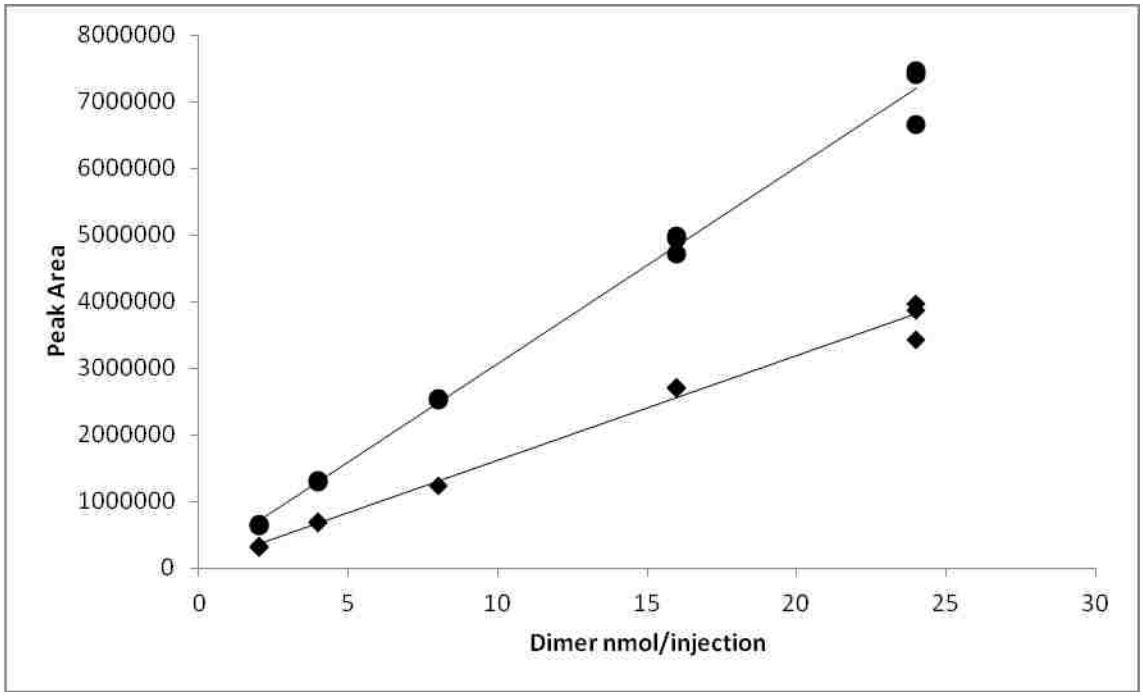

Figure 35: Peak area plotted as a function of nmol/injection for dimers {**cop-cop**} (♦) and {**cop-16PL**} (●)

A1.2.3 Results of NNR Experiments Using Exchangeable Sterols

For the results of NNR reactions using {**cho-16PL**}, see Section 2.3.4. The results of individual NNR reactions using {**7β-16PL**}, {**di-16PL**}, and {**cop-16PL**} are shown in Tables 34-37. Refer to Figure 32 (page 110) for the structures of these exchangeable lipids. The average K and ω_{AB} for each of these dimer pairs are summarized in Table 38. In addition, the average vesicle size for each liposome preparation was measured before and after the NNR procedure, in order to verify that the liposomes remained intact. Those data are shown in Table 39. Typical chromatograms from the analysis of NNR reaction product mixtures are presented in Figures 36-38.

NNR results for samples from {**7β-16PL**} are shown in Table 34, below. These data represent the results from only one NNR reaction, and therefore should be

considered approximate results and are presented only for comparison to the NNR values obtained for the other dimer pairs. In addition, it should be noted that because the {**7β-7β**} peak overlaps with an unknown impurity peak (see the representative chromatogram, Figure 36) for these samples *K* was approximated as $K \approx [\{\textbf{7β-16PL}\}]^2/[\{\textbf{16PL-16PL}\}]^2$.

Reaction	Reaction Time (h)	Dimer	R_T (min)	Peak Area	N (nmol)	K
1	12	**{7β-16PL}**	28.51	4918321	7.58	
1	12	**{16PL-16PL}**	33.72	1662160	3.16	5.76
1	16	**{7β-16PL}**	28.57	4984098	7.68	
1	16	**{16PL-16PL}**	33.72	1720393	3.26	5.54
1	18	**{7β-16PL}**	28.64	4930195	7.60	
1	18	**{16PL-16PL}**	33.83	1710500	3.25	5.48
1	20	**{7β-16PL}**	28.72	4967288	7.66	
1	20	**{16PL-16PL}**	33.90	1707549	3.24	5.58
1	22	**{7β-16PL}**	28.80	5077526	7.83	
1	22	**{16PL-16PL}**	33.98	1756866	3.33	5.52

Table 34: Data for {**7β-16PL**} equilibration in 40 mol% sterol LUVs at 45 ^{o}C using 0.8 equivalents of DTT

Reaction	Reaction Time (h)	Dimer	R_T (min)	Peak Area	N (nmol)	K
		{16PL-16PL}	12.85	1569031	3.28	
1	12	**{di-16PL}**	20.61	3350550	9.70	8.09
		{di-di}	43.11	558650	3.54	
		{16PL-16PL}	12.87	1369067	2.86	
1	16	**{di-16PL}**	20.68	2918754	8.44	7.92
		{di-di}	43.14	493707	3.14	
		{16PL-16PL}	12.90	1352906	2.83	
1	18	**{di-16PL}**	20.71	2938809	8.49	8.82
		{di-di}	43.30	454753	2.89	
		{16PL-16PL}	12.93	1314669	2.75	
1	20	**{di-16PL}**	20.76	2872427	8.30	7.96
		{di-di}	43.25	495036	3.15	
		{16PL-16PL}	12.94	1375007	2.88	
1	22	**{di-16PL}**	20.78	2953287	8.54	7.83
		{di-di}	43.39	509216	3.23	
		{16PL-16PL}	12.94	2008393	4.20	
2	12	**{di-16PL}**	20.74	4100554	11.90	9.34
		{di-di}	43.56	568938	3.61	
		{16PL-16PL}	12.91	2013996	4.21	
2	16	**{di-16PL}**	20.79	4069564	11.81	9.11
		{di-di}	43.50	573069	3.64	
		{16PL-16PL}	12.99	2130895	4.46	
2	18	**{di-16PL}**	20.82	4268169	12.40	9.19
		{di-di}	43.71	591575	3.75	
		{16PL-16PL}	13.03	2082062	4.36	
2	20	**{di-16PL}**	20.88	4184820	12.15	9.31
		{di-di}	43.71	573724	3.64	
		{16PL-16PL}	13.06	2173343	4.55	
2	22	**{di-16PL}**	20.94	4307414	12.51	8.73
		{di-di}	43.83	622251	3.94	

Table 35: Data for {**di-16PL**} equilibration in 40 mol% sterol LUVs at 45 ^{o}C using 0.8 equivalents of DTT. (Reactions 1 and 2)

Reaction	Reaction Time (h)	Dimer	R_T (min)	Peak Area	N (nmol)	K
1	12	**{16PL-16PL}**	11.66	1376505	2.88	8.35
		{di-16PL}	18.85	2905390	8.40	
		{di-di}	39.77	460838	2.93	
1	16	**{16PL-16PL}**	11.67	1356624	2.84	8.07
		{di-16PL}	18.87	2832348	8.18	
		{di-di}	39.81	459878	2.92	
1	18	**{16PL-16PL}**	11.69	1294586	2.71	8.01
		{di-16PL}	18.90	2733830	7.89	
		{di-di}	39.99	451682	2.87	
1	20	**{16PL-16PL}**	11.72	1297343	2.71	8.06
		{di-16PL}	18.95	2747802	7.93	
		{di-di}	39.91	452168	2.88	
1	22	**{16PL-16PL}**	11.74	1287155	2.69	8.11
		{di-16PL}	18.99	2755287	7.96	
		{di-di}	40.02	455506	2.90	
2	12	**{16PL-16PL}**	11.84	1621373	3.39	8.05
		{di-16PL}	19.12	3414506	9.89	
		{di-di}	40.31	5644485	3.58	
2	16	**{16PL-16PL}**	11.87	1460650	3.06	8.15
		{di-16PL}	19.19	3140692	9.09	
		{di-di}	40.37	522062	3.31	
2	20	**{16PL-16PL}**	11.90	1431664	3.00	8.44
		{di-16PL}	19.23	3035384	8.78	
		{di-di}	40.38	479682	3.05	
2	22	**{16PL-16PL}**	11.94	1469769	3.08	8.37
		{di-16PL}	19.28	3061067	8.85	
		{di-di}	40.52	478923	3.04	

Table 36: Data for {**di-16PL**} equilibration in 40 mol% sterol LUVs at 45 ^{o}C using 0.8 equivalents of DTT (Reactions 3 and 4)

Reaction	Reaction Time (h)	Dimer	R_T (min)	Peak Area	N (nmol)	K
1	12	**{16PL-16PL}**	11.63	1276120	2.67	23.17
		{cop-16PL}	17.65	4148346	13.64	
		{cop-cop}	41.04	515127	3.01	
1	16	**{16PL-16PL}**	11.66	1247174	2.61	23.28
		{cop-16PL}	17.73	4020901	13.21	
		{cop-cop}	41.20	493865	2.87	
1	18	**{16PL-16PL}**	11.72	1325243	2.77	23.84
		{cop-16PL}	17.79	4233830	13.93	
		{cop-cop}	41.38	503737	2.94	
1	20	**{16PL-16PL}**	11.77	1330530	2.78	24.02
		{cop-16PL}	17.89	4235515	13.94	
		{cop-cop}	41.51	498778	2.90	
1	22	**{16PL-16PL}**	11.85	1294205	2.71	25.36
		{cop-16PL}	18.01	4163583	13.69	
		{cop-cop}	41.68	471498	2.73	
2	12	**{16PL-16PL}**	11.75	1201637	2.51	24.50
		{cop-16PL}	17.75	3869950	12.70	
		{cop-cop}	40.81	453828	2.62	
2	16	**{16PL-16PL}**	11.77	1231174	2.58	23.81
		{cop-16PL}	17.77	3968086	13.03	
		{cop-cop}	40.84	477418	2.77	
2	18	**{16PL-16PL}**	11.76	1198559	2.51	26.89
		{cop-16PL}	17.82	3838822	12.59	
		{cop-cop}	40.95	411884	2.35	
2	20	**{16PL-16PL}**	11.80	1225525	2.56	23.65
		{cop-16PL}	17.81	3924415	12.88	
		{cop-cop}	40.95	472564	2.74	
2	22	**{16PL-16PL}**	11.81	1220376	2.55	24.45
		{cop-16PL}	17.83	3903061	12.81	
		{cop-cop}	40.97	455314	2.63	
3	12	**{16PL-16PL}**	11.84	1301231	2.72	25.46
		{cop-16PL}	17.87	4165991	13.70	
		{cop-cop}	41.15	467914	2.71	
3	16	**{16PL-16PL}**	11.87	1308954	2.74	26.23
		{cop-16PL}	17.91	4058596	13.34	
		{cop-cop}	41.25	431466	2.48	
3	18	**{16PL-16PL}**	11.88	1223807	2.56	25.10
		{cop-16PL}	17.96	3847920	12.63	
		{cop-cop}	41.26	432012	2.48	
3	20	**{16PL-16PL}**	11.91	1245795	2.61	24.52
		{cop-16PL}	17.99	3983929	13.09	
		{cop-cop}	41.38	463383	2.68	
3	22	**{16PL-16PL}**	11.95	1282741	2.68	25.60
		{cop-16PL}	18.05	4114851	13.53	
		{cop-cop}	41.49	460946	2.66	

Table 37: Data for {**cop-16PL**} equilibration in 40 mol% sterol LUVs at 45 ^{o}C using 0.8 equivalents of DTT

Dimer Pair	*K*	ω_{AB} (cal/mol)
{**cho-16PL**}	9.77 ± 0.47	-282.0 ± 15.2
{**7β-16PL**}	5.57 ± 0.11	-104.6 ± 6.2
{**di-16PL**}	8.42 ± 0.51	-235.0 ± 19.1
{**cop-16PL**}	24.66 ± 1.09	-574.3 ± 14.0

Table 38: Summary of NNR data from exchangeable sterols

Dimer Pair	Reaction Number	Time (h)	Mean Diameter (nm)
{**7β-16PL**}	1	0	167.2 ± 60.2
		22	170.1 ± 45.9
{**di-16PL**}	1	0	183.6 ± 42.2
		22	183.7 ± 29.4
{**di-16PL**}	2	0	165.6 ± 39.7
		22	169.2 ± 60.9
{**di-16PL**}	3	0	188.3 ± 60.3
		22	181.7 ± 56.3
{**di-16PL**}	4	0	181.9 ± 40.0
		22	189.8 ± 66.4
{**cop-16PL**}	1	0	183.4 ± 23.8
		22	177.4 ± 56.8
{**cop-16PL**}	2	0	168.1 ± 50.4
		22	173.9 ± 57.4
{**cop-16PL**}	3	0	163.5 ± 37.6
		22	168.3 ± 52.2

Table 39: DLS data for vesicles before and after NNR reactions. Monomodal size distribution was observed in all cases. DLS data for reactions involving {**cho-16PL**} is reported in Section 2.3.4

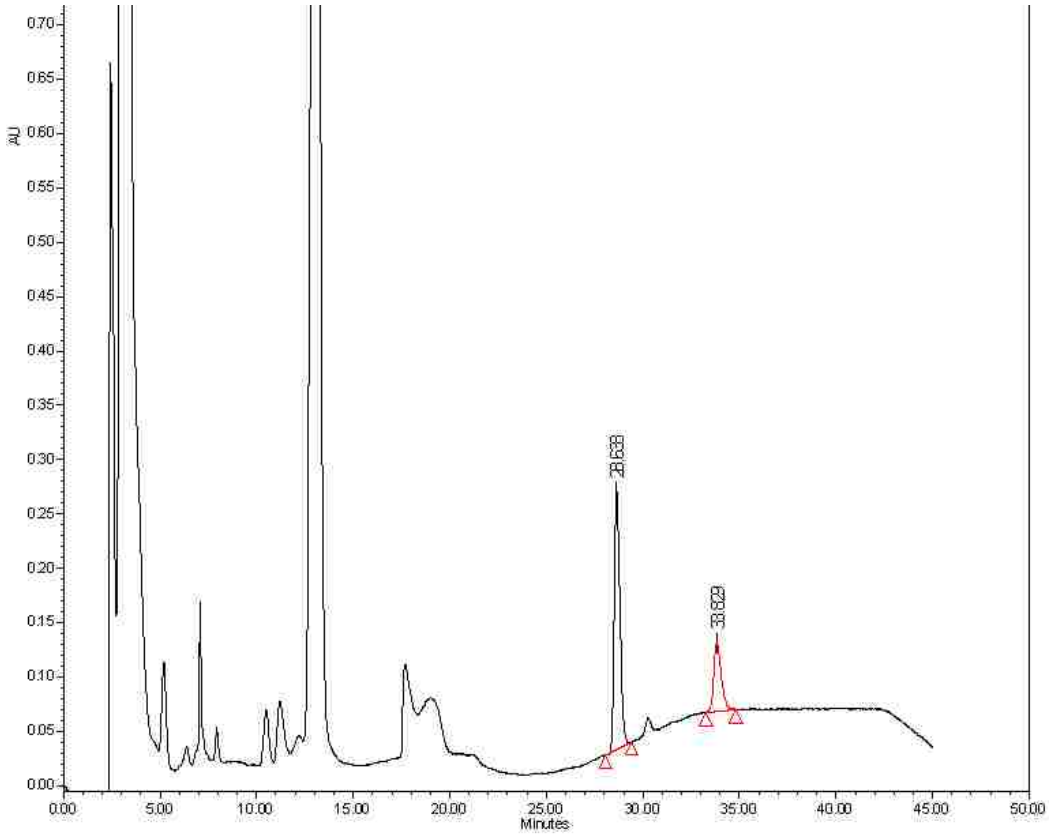

Figure 36: Typical HPLC chromatogram from the analysis of product mixtures in NNR reactions starting with heterodimer {**7β-16PL**}

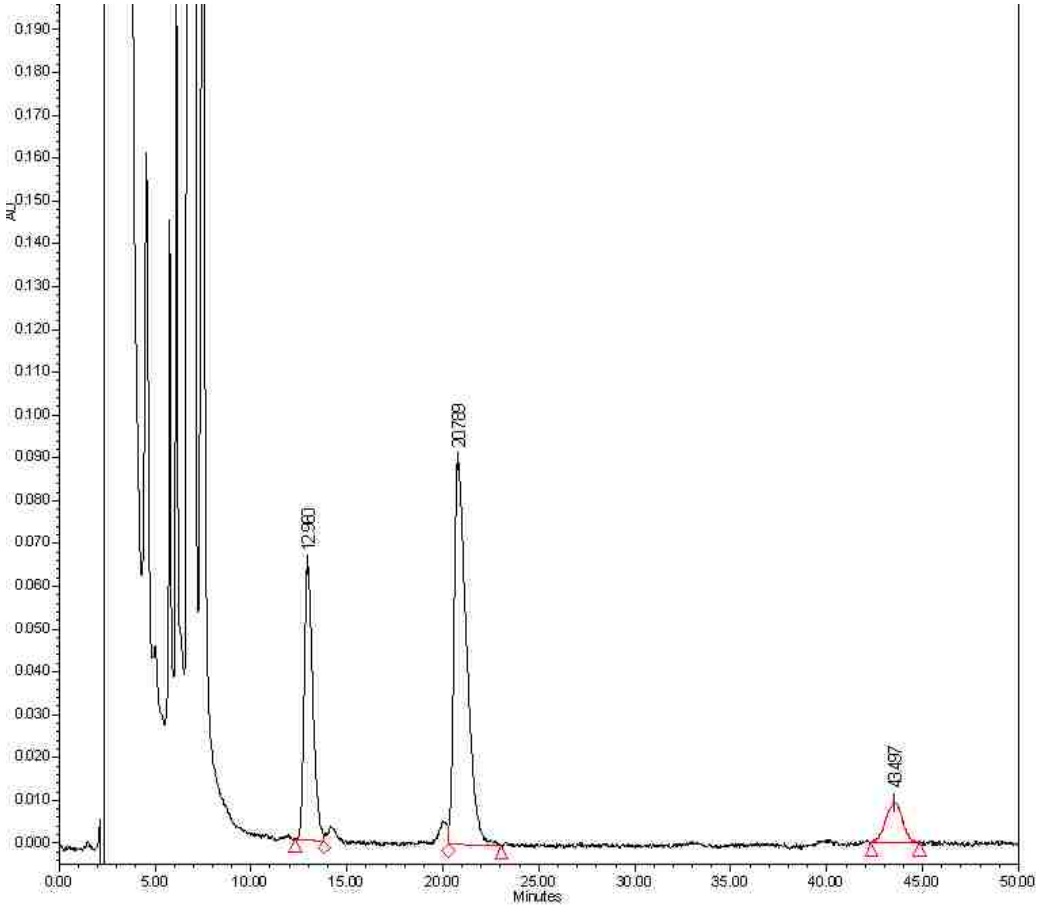

Figure 37: Typical HPLC chromatogram from the analysis of product mixtures in NNR reactions starting with heterodimer {**di-16PL**}

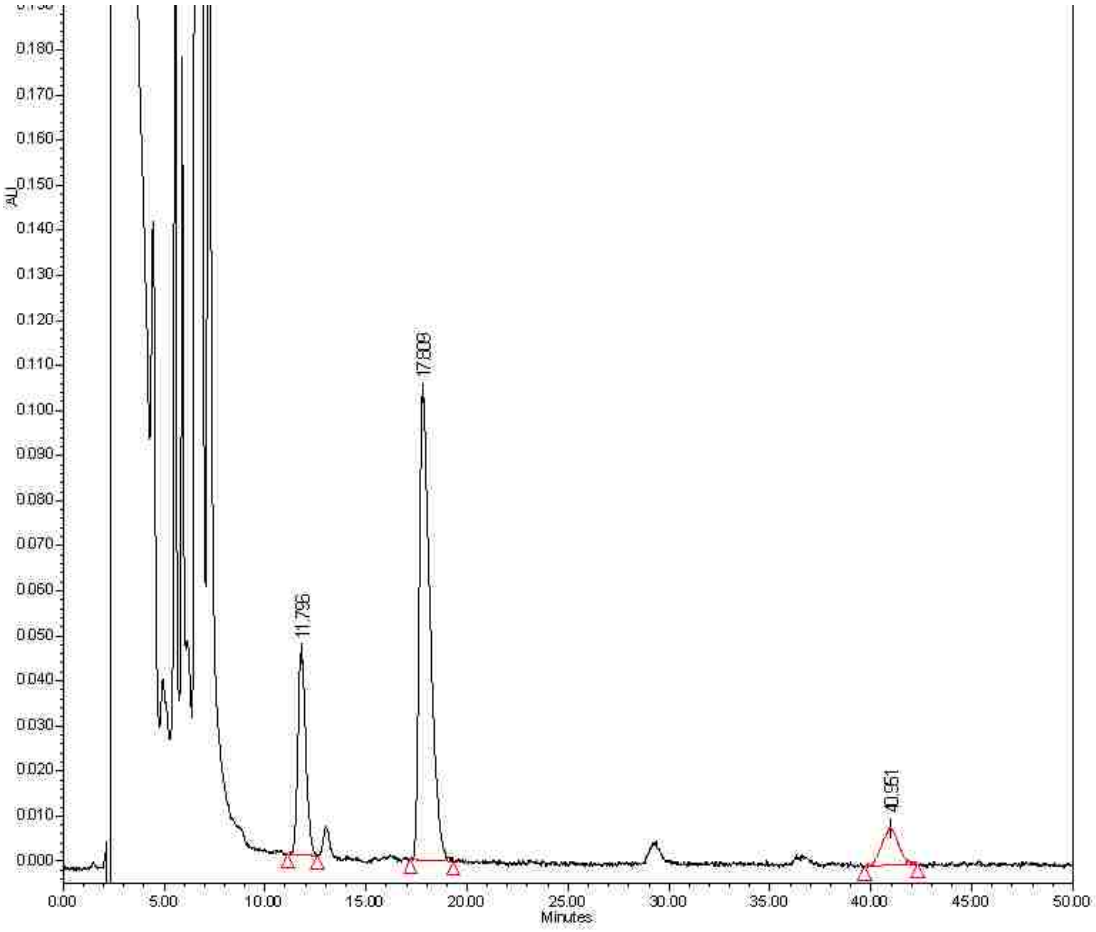

Figure 38: Typical HPLC chromatogram from the analysis of product mixtures in NNR reactions starting with heterodimer {**cop-16PL**}

A1.3 Discussion

In order to directly measure the nearest neighbor interaction energies of cholesterol, 7β-OH, dihydrocholesterol, and coprostanol with a DPPC, exchangeable mimics of these lipids (see Figure 32, page 110) were synthesized and used in NNR reactions. The results of these reactions are shown in Table 38 (page 122).

All four of the exchangeable sterols interact favorably with **16PL** in the l_o phase (*i.e.* $\omega_{AB} < 0$). The affinity of **cho** for **16PL** in membranes has been previously reported,[19,55] and is a result of the favorable interactions between the hydrophobic sterol and the ordered acyl chains of the phospholipid. For a more detailed discussion of the interactions of **cho** and **16PL**, see Section 2.4. The similarity in structure between **cho** and **di** leads to very little difference in their interactions with **16PL**.

In interpreting the interaction energies of the other sterols, it is important to remember that *our experimental values of ω_{AB} do not represent absolute energies for the interactions between **A** and **B**. Rather, they are a measure of the difference in energy associated with hetero-interactions and the average of the homo-interations (eq. 3, page 57).*

The most striking feature of Table 38 is the high *K* (and corresponding low ω_{AB}) observed for **cop**, the coprostanol mimic. This result is analogous to the low ω_{AB} observed for **Pep2-16PL** (see Section 2.4). In that case, the kinked structure of **Pep2** led to poor homo-association, making the heterodimer more stable than the corresponding homodimers. Coprostanol, and the exchangeable lipid **cop**, also have kinked structures, due to the *cis* fusion of their A and B rings. The inefficient packing of coprostanol molecules in a bilayer thus leads to poor homo-association, and a correspondingly high *K*.

The weak affinity between **7β** and **16PL** lends itself to two possible explanations. One possibility is that the low *K* value is a consequence of strong homo-association between molecules of **7β** due to the increased hydrogen bonding made possible by the additional hydroxyl group. The other possibility is that the presence of a hydroxyl group

at the 7 position of the sterol core disrupts the close hydrophobic contact between the sterol nucleus and the saturated acyl chains. To distinguish between these possibilities, let us consider other recent findings applying NNR as a chemical sensor (*i.e.* using NNR measurements of {**cho-16PL**} to probe the state of the host membrane).

When {**cho-16PL**} affinity was measured in l_o host membranes containing varying amounts of (non-exchangeable) 7β-OH, it was found that replacing cholesterol with 7β-OH resulted in a more compact membrane,[24] indicating that 7β-OH forms a more stable l_o phase than cholesterol itself. It is therefore unlikely that the low *K* value observed in NNR reactions of {**7β-16PL**} is indicative of a weakening of sterol-phospholipid association in the l_o phase due to the presence of a hydroxyl group on the hydrophobic nucleus of the peptide. Rather, the NNR results can best be explained as hydrogen bonding between **7β** molecules resulting in strong homo-association.

The *K* values and interaction energy measurements reported in Table 38 can thus be readily interpreted in terms of the sterol structures, the well known affinity of cholesterol for phospholipid acyl chains in l_o membranes, the poor packing of coprostanol molecules in a bilayer, and the favorable hydrogen bonding interaction between 7β-OH cholesterol molecules. However, because these NNR measurements reflect the *relative* stability of the heterodimers compared to the average stability of the homodimers, rather than the *absolute* stability of the heterodimers, we cannot directly measure the affinity of each sterol for phospholipids in liquid-ordered membranes. These data, therefore cannot distinguish between the "umbrella" and "template" models for sterol-phospholipid interactions.

A1.4 Conclusions

Directly measuring the nearest neighbor interactions between **16PL** and the exchangeable sterols **cho**, **di**, **7β**, and **cop** via NNR measurements in l_o phase host membranes reveals a strong tendency for homo-association between molecules of **7β** (most likely a result of increased hydrogen bonding due to the presence of a second hydroxyl group) and a high *K* value for **cop-16PL** interactions (which reflects the poor homo-association between molecules of **cop**, as a result of the poor packing of their non-planar sterol cores in a condensed bilayer). Because these results are largely dictated by the strong (positive or negative) homo-interactions, however, they fail to provide insight into how variations in sterol core structure affect the energetics of hetero-interactions between sterols and **16PL**. For this reason, the approach of using exchangeable sterols to measure sterol-phospholipid interactions was abandoned in favor of the more informative, and less synthetically demanding method of using NNR as a chemical sensor, as discussed in Chapter 3.

A1.5 Experimental

A1.5.1 NNR Procedures

Vesicle preparation, NNR reactions, and particle size analysis were all conducted according to the procedures provided in Section 5.2. Table 40 shows the compositions of the 40 mol% sterol vesicle dispersions used in all NNR reactions.

µmol cop, di, or 7β	µmol cho	µmol 16PL	µmol DPPC	µmol cholesterol
0.3	-	0.3	6.9	4.5
-	0.3	0.3	6.9	4.5

Table 40: Composition of lipid films used for the preparation of vesicle dispersions for NNR experiments using **cop**, **di**, and **7β**

The product mixtures from NNR reactions were analyzed using similar conditions to those described in Section 5.2. Aldrithiol-2 was not used in the preparation of HPLC samples from reactions containing {**7β-16PL**}, {**cop-16PL**}, or {**di-16PL**}. Samples containing {**cho-16PL**}, {**cop-16PL**}, or {**di-16PL**} were analyzed using mobile phase A isocratically (see Table 41 for the compositions of mobile phases). The gradient used for the analysis of product mixtures from NNR reactions using {**7β-16PL}** is shown in Table 42.

Mobile Phase	Ethanol (mL)	Water (mL)	hexanes (mL)
A	76	130	100
C	77	18	6

Table 41: Composition of all the mobile phases used in analysis of exchangeable sterol NNR reaction mixtures. All mobile phases consisted of 10mM *n*-Bu_4NOAc in ethanol/water/hexane mixtures given here

time (min)	%A	%C
0	0	100
12	0	100
27	100	0
39	100	0
45	0	100

Table 42: Gradient used for HPLC analysis of product mixtures containing {**7β-16PL**}

A1.5.2 Synthetic Procedures

O-(N-succinimidyl)-O-dihydrocholesteryl carbonate (12) To a solution of dihydrocholesterol (1.0 g, 2.57 mmol) and Et_3N (5.0 mL) in $CHCl_3$ (20 mL) was added di-(*N*-succinimidyl)carbonate (2.96 g, 11.55 mmol). After stirring at 45 ^oC for 6 h, the reaction mixture was concentrated, re-dissolved in $CHCl_3$ (100 mL), washed with water (2 x 100 mL) and dried over anhydrous sodium sulfate. After the solvent was removed under reduced pressure, the residue obtained was purified by chromatography on a silica-

gel column ($CHCl_3$) to give **12** (1.10 g, 81%) having ^{1}H NMR (500 MHz, $CDCl_3$) δ 4.66 (m, 1 H), 2.81 (s, 4 H), 1.95-0.81 (m, 43 H), 0.62 (s, 3 H).

{di-di} homodimer Cystamine dihydrochloride (150 mg, 0.67 mmol) was suspended in $CHCl_3$ (5 mL), followed by addition of DIPEA (0.7 mL). After stirring for 10 minutes, **12** (760 mg, 1.40 mmol) was added as powder. The reaction mixture was stirred overnight at room temperature, and then concentrated under reduced pressure. Purification by column chromatography [silica gel, $CHCl_3$/hexanes, (1/1 v/v) and $CHCl_3$/EtOAc (10/1 v/v)] gave {**di-di**} (562 mg, 86%) having ^{1}H NMR (500 MHz, $CDCl_3$) δ 5.13 (br, 2 H), 4.55 (m, 2 H), 3.86 (br, 2 H), 3.47 (br, 4 H), 2.77 (t, 4 H), 1.94~0.78 (m, 86 H), 0.62 (s, 6 H); and HR-ESI MS for $C_{60}H_{105}N_2O_4S_2$ ($[M+H]^+$) Calculated: 981.7510, found: 981.7494.

***N*-[1-(Carboxyethyldithio)-2-ethyl]dihydrocholesteryl carbamate (13)** To a mixture of 3-(2-aminoethyldithio)propanoic acid hydrochloride salt (AEDP, 100 mg, 0.46 mmol) and Et_3N (200 μL) in $CHCl_3$ (10 mL) was added **12** (250 mg, 0.46 mmol) in one portion. The resulting solution was stirred overnight at room temperature, and then diluted with $CHCl_3$ (50 mL), washed with water (100 mL, pH 3, HCl). The organic phase was dried over sodium sulfate, and concentrated under reduced pressure. Purification by column chromatography [silica gel, $CHCl_3$/MeOH (15/1 v/v)] afforded **13** (232 mg, 85%) having ^{1}H NMR (500 MHz, $CDCl_3$/MeOD, *ca* 10/1 v/v) δ 4.48 (br, 1 H), 3.40 (br, 2 H), 2.87 (t, 2 H), 2.72 (t, 2 H), 2.68 (t, 2 H), 1.91-0.75 (m, 43 H), 0.58 (s, 3 H); and HR-ESI MS for $C_{33}H_{58}NO_4S_2$ ($[M+H]^+$) Calculated: 596.3802, found: 596.3789.

{di-16PL} heterodimer To a solution of **13** (225 mg, 0.38 mmol) and *N*-hydroxysuccinimide (NHS) (49 mg, 0.43 mmol) in $CHCl_3$ (5 mL) was added DCC (115

mg, 0.56 mmol). After stirring for 5 h at room temperature, 1,2-dipalmitoyl-sn-glycero-3-phosphoethanolamine (DPPE, 255 mg, 0.37 mmol) and DIPEA (200 µL) were added. After stirring overnight at room temperature, the solution was diluted with $CHCl_3$ (50 mL) and washed, sequentially, with water (pH ~2-3, HCl, 50 mL) and brine (50 mL). The organic layer was then separated, dried over anhydrous sodium sulfate and concentrated under reduced pressure. Purification by column chromatography [silica-gel, $CHCl_3$/MeOH (25/1, v/v) and $CHCl_3$/MeOH/H_2O (50/10/1, v/v)] afforded {**di-16PL**} (132 mg, 28%) having ^{1}H NMR (500 MHz, $CDCl_3$/MeOD, *ca* 10/1, v/v) δ 5.15 (1H), 4.45 (m, 1 H), 4.31 (m, 1 H), 4.08 (m, 1H), 3.92 (m, 4 H), 3.38 (br, 4 H), 2.87 (t, 2 H), 2.73 (t, 2 H), 2.57 (t, 2 H), 2.27-2.21 (m, 4 H), 1.90-0.73 (m, 103 H), 0.58 (s, 3 H); and HR-ESI MS for $C_{70}H_{129}N_2O_{11}PS_2Na$ ($[M+Na]^+$) calculated: 1291.8668, found: 1291.8647.

O-(N-succinimidyl)-O-coprostanyl carbonate To a solution of coprostanol (40.0 mg, 0.103 mmol) and Et_3N (0.25 mL) in $CHCl_3$ (1.0 mL) was added di-(*N*-succinimidyl)carbonate (263.86 mg, 1.03 mmol). After stirring at 45 ^{o}C for 48 h, the reaction mixture was concentrated, re-dissolved in $CHCl_3$ (10 mL), washed with water (2 x 50 mL), and dried over anhydrous magnesium sulfate. After the solvent was removed under reduced pressure, the residue obtained was purified by column chromatography [silica-gel, $CHCl_3$] to give O-(N-succinimidyl)-O-coprostanyl carbonate (39.0 mg, 72%) having ^{1}H NMR (500 MHz, $CDCl_3$) δ 5.07 (m, 1 H), 2.80 (s, 4 H), 2.03-0.79 (m, 43 H), 0.62 (s, 3 H); and HR-ESI MS for $C_{53}H_{55}N_2O_5$ ($[M+NH_4]^+$). Calculated: 547.4106, found: 547.4103.

{cop-cop} homodimer Cystamine dihydrochloride (10.3 mg, 0.0457 mmol) was suspended in $CHCl_3$ (4 mL), followed by addition of DIPEA (39.8 μL). After stirring for 10 minutes, O-(N-succinimidyl)-O-coprostanyl carbonate (44.0 mg, 0.0831 mmol) was added as powder. The reaction mixture was stirred overnight at room temperature, and then concentrated under reduced pressure. Purification by column chromatography [silica gel hexanes/EtOAc (3/1, v/v)] and preparative TLC using 5% CH_3OH in $CHCl_3$ afforded {**cop-cop**} (35.0 mg, 43%) having ^{1}H NMR (500 MHz, $CDCl_3$) δ 4.84 (s, 1 H), 3.33 (t, 2 H, J=6.62 Hz), 3.25 (m, 2 H), 3.10 (m, 2 H), 2.72 (t, 2 H, J=6.55 Hz), 1.94~0.71 (m, 53 H), 0.56 (s, 3 H) ; and HR-ESI MS for $C_{60}H_{105}N_2O_4S_2$ ($[MH]^+$). Calculated: 981.7510, found: 981.7498.

***N*-[1-(Carboxyethyldithio)-2-ethyl]coprostanyl carbamate** To a mixture of 3-(2-aminoethyldithio)propanoic acid hydrochloride salt (AEDP, 37.1 mg, 0.171 mmol) and DIPEA (105.2 μL) in $CHCl_3$ (13.0 mL) was added O-(N-succinimidyl)-O-coprostanyl carbonate (82.0 mg, 0.155 mmol) in one portion. The resulting solution was stirred overnight at room temperature, and then diluted with $CHCl_3$ (50.0 mL) and washed with water (2 x 50 mL, pH 2, HCl). The organic phase was dried over magnesium sulfate, and concentrated under reduced pressure. Purification by column chromatography [silica gel, $CHCl_3$/MeOH (15/1, v/v) and $CHCl_3$/MeOH (5/1, v/v)] yielded *N*-[1-(carboxyethyldithio)-2-ethyl]coprostanyl carbamate (58.0 mg, 62.8%) having ^{1}H NMR (500 MHz, $CDCl_3$, *ca* 10/1 v/v) δ 4.92 (s, 1 H), 3.43 (s, 2 H), 2.88 (t, 2 H, J=7.15 Hz), 2.74 (m, 4 H), 2.68 (t, 2 H), 1.97-0.73 (m, 43 H), 0.58 (s, 3 H); and HR-ESI MS for $C_{33}H_{58}NO_4S_2$ ($[MH]^+$). Calculated: 596.3802. Found: 596.3795.

{cop-16PL} heterodimer To a solution of *N*-[1-(carboxyethyldithio)-2-ethyl]coprostanyl carbamate (58 mg, 0.097 mmol) and *N*-hydroxysuccinimide (NHS) (12.7 mg, 0.110 mmol) in $CHCl_3$ (1.5 mL) was added DCC (29.5 mg, 0.143 mmol). After stirring for 5 h at room temperature, 1,2-dipalmitoyl-sn-glycero-3-phosphoethanolamine (DPPE, 65.3 mg, 0.094 mmol) and DIPEA (51.2 μL) were added. After stirring overnight at room temperature, the solution was diluted with $CHCl_3$ (50 mL) and washed, sequentially, with water (pH ~2-3, HCl, 50 mL) and brine (50 mL). The organic layer was then separated, dried over anhydrous magnesium sulfate and concentrated under reduced pressure. The product was purified by column chromatography [silica gel, $CHCl_3$/MeOH (5/1, v/v)], followed by preparative TLC [$CHCl_3$/MeOH (5/1, v/v) with 1% water]. This afforded {**cop-16PL**} (31.0 mg, 24.7%) having ^{1}H NMR (500 MHz, $CDCl_3/CD_3OD$, *ca* 10/1 v/v) δ 5.14 (s, 1 H), 4.83 (s, 1 H), 4.33 (m, 1 H), 4.10 (m, 1 H), 3.90 (m, 4 H), 3.34 (m, 4 H), 2.86 (t, 2 H, J=6.82 Hz), 2.73 (t, 2 H, J=6.45 Hz), 2.55 (t, 2 H, J=7.00 Hz), 2.24 (m, 4 H), 1.97-0.65 (m, 107 H), 0.57 (s, 3 H); and HR-ESI MS for $C_{70}H_{128}N_2O_{11}PS_2$ ($[M]^-$). Calculated: 1267.8703, found: 1267.8713.

3-Acetoxy-cholesterol (14) To a solution of cholesterol (5.25 g, 13.56 mmol) in anhydrous pyridine (40 mL) was added acetic anhydride (15 mL). The resulting solution was stirred overnight at room temperature. The reaction mixture was concentrated to about 20 mL, and then was poured into cold water (250 mL). The resulting precipitate was collected by filtration, washed with water and dried under reduced pressure to quantitatively give **14** (5.82 g) having ^{1}H NMR (500 MHz, $CDCl_3$) δ 5.35 (d, 1H), 4.58 (m, 1H), 2.29 (m, 2H), 2.00-0.83 (m, 41 H), 0.65 (s, 3H).

3-Acetoxy-7-oxo-cholesterol (15) To dichloromethane (200 mL) was added chromium trioxide (13.6 g), followed by addition of pyridine (22 mL). The mixture was stirred for 30 minutes and **14** (6.8 g) in dichloromethane (100 mL) was added. The mixture was refluxed for 3 days and diethyl ether (100 mL) was added and stirred for another 20 minutes. After filtration through a short silica gel column, the filtrate was concentrated under reduced and purified by column chromatography [silica gel, hexanes/EtOAc (10/1 v/v)] to give **15** (3.7 g, 52.8%) having ^{1}H NMR (500 MHz, $CDCl_3$) δ 5.68 (d, 1H), 4.70 (m, 1H), 2.54-2.18 (m, 4H), 2.03-0.83 (m, 37 H), 0.65 (s, 3 H).

7β-hydroxycholesterol (16) To a mixture of **15** (6.5 g) and $CeCl_3 \cdot 7H_2O$ (5.2 g) in a THF (150 mL) and MeOH (75 mL) was added $NaBH_4$ (1.3 g). After stirring at room temperature for 30 min, HCl (65 mL, 1 N) was added and the solvent was removed under reduced pressure. The obtained residue was partitioned between $CHCl_3$ (150 mL) and water (150 mL). The organic layer was separated and the aqueous layer was washed with $CHCl_3$ (2 x 100 mL). The organic layer was combined and washed, sequentially, with aqueous $NaHCO_3$ (100 mL), brine (100 mL) and water (100 mL). Removal of solvent under reduced pressure afforded the crude *3-acetoxy-7β-hydroxycholesterol* (6.5 g) which was hydrolyzed without further purification. Crude *3-acetoxy-7β-hydroxycholesterol* (1.5 g) was dissolved in THF (35 mL) and NaOH (270 mg) in MeOH/H_2O (12 mL, 5/1 v/v) was added. After stirring at room temperature for 2 h, the reaction mixture was concentrated under reduced pressure. The obtained residue was partitioned between $CHCl_3$ (100 mL) and water (100 mL). The organic layer was separated and the aqueous layer was washed with $CHCl_3$ (2 x 50 mL). The organic layers were combined, dried over hydrous sodium sulfate, and concentrated under reduced pressure. Purification by column

chromatography [silica gel, EtOAc/hexanes (3/2 v/v)] afforded 7β-hydroxycholesterol **16** (1.34 g, 98%) having ^{1}H NMR (500 MHz, $CDCl_3$) δ 5.26 (1H, m), 3.83-3.81 (1H), 3.46 (m, 1H), 2.33-2.19 (m, 2H), 2.02-0.83 (m, 36H), 0.67 (s, 3H).

O-(N-succinimidyl)-O-7βhydroxycholesteryl carbonate To a solution of **16** (1.10 g, 2.74 mmol) and Et_3N (10 mL) in a mixture of $CHCl_3$ (25 mL) and CH_3CN (25 mL) was added di-(*N*-succinimidyl)carbonate (2.10 g, 8.20 mmol). After stirring at 45 ^oC for 3 h, another portion of di-(*N*-succinimidyl)carbonate (2.10 g, 8.20 mmol) was added, and the stirring continued for another 3 h. The reaction mixture was concentrated under reduced pressure and partitioned between $CHCl_3$ (200 mL) and water (200 mL). The organic layer was separated and dried over anhydrous sodium sulfate. Concentration under reduced pressure and purification by column chromatography [silica gel, hexanes/EtOAc (2/1 v/v)] gave O-(N-succinimidyl)-O-7βhydroxycholesteryl carbonate (686 mg, 46%) having ^{1}H NMR (500 MHz, $CDCl_3$) δ 5.33 (1H), 4.59 (m, 1H), 3.83-3.81 (1H), 2.80 (s, 4H), 2.47 (2H, m), 2.06-0.82 (m, 36 H), 0.66 (s, 3H).

{7β-7β} homodimer Cystamine dihydrochloride (75 mg, 0.33 mmol) was suspended in $CHCl_3$ (10 mL), followed by addition of DIPEA (500 uL, 2.61 mmol). After stirring for 10 minutes, O-(N-succinimidyl)-O-7βhydroxycholesteryl carbonate (386 mg, 0.71 mmol) was added as powder. The reaction mixture gradually became clear to yellowish, and was stirred overnight at room temperature. The solvent then removed under reduced pressure and the residue was purified by column chromatography [silica gel, hexanes/EtOAc (3/2 v/v)] to give {**7β-7β**} (318 mg, 95%) having ^{1}H NMR (500 MHz, $CDCl_3$) δ 5.29 (s, 2H), 5.19 (br, 2H), 4.51 (m, 2H), 3.84-3.82 (2H), 3.48 (m, 4H),

2.79 (t, 4H), 2.39-2.26 (m, 4H), 2.01-0.84 (m, 72H), 0.67 (s, 6H); and HR-ESI MS for $C_{60}H_{100}N_2O_6NaS_2$ ($[M+Na]^+$) calculated: 1031.6915, found: 1031.6891.

{**7β-16PL**} **heterodimer** To a solution of {**16PL-16PL**}(25 mg, 24.8 μmol) in $CHCl_3$ (1 mL) and MeOH (1 mL) was added {**7β-7β**} (37 mg, 24.8 μmol), TCEP (5 μmol, 235 μL of a 21.1 mM aqueous solution), and NaOH (15 μmol, 15 μL of a 1M aqueous solution). The solution was allowed to stir under argon for 48 h, during which time a white precipitate appeared. The solvent was removed under reduced pressure, and the resulting residue was dissolved in $CHCl_3$ and purified by preparative TLC, affording **{7β -16PL}** (8 mg) as a white solid. From the rest of the TLC plate, 58 mg of yellow solid were collected. This material was dissolved in $CHCl_3$ (1 mL) and MeOH (1 mL), and additional TCEP (5 μmol) and NaOH (15 μmol) were added, and the solution was stirred under argon for 48 h. Purification by preparative TLC and combination with the previously purified products afforded **{7β -16PL}** (22 mg, 34%) as a white powder having ^{1}H NMR (500 MHz, $CDCl_3$) δ 5.28 (s, 1H), 5.17 (1 H), 4.46 (m, 1H), 4.36 (m, 1H), 4.11 (m, 1H), 3.84 (m, 5H), 3.43 (4H), 2.92 (2H), 2.78 (2H), 2.60 (2H), 2.36-2.24 (m, 6H), 2.00-0.83 (94 H), 0.66 (s, 3H) and HR-ESI MS for $C_{70}H_{127}N_2O_{12}NaPS_2$ ($[M+H]^+$) calculated: 1305.8460, found: 1305.8447.

Appendix 2

NMR Spectra

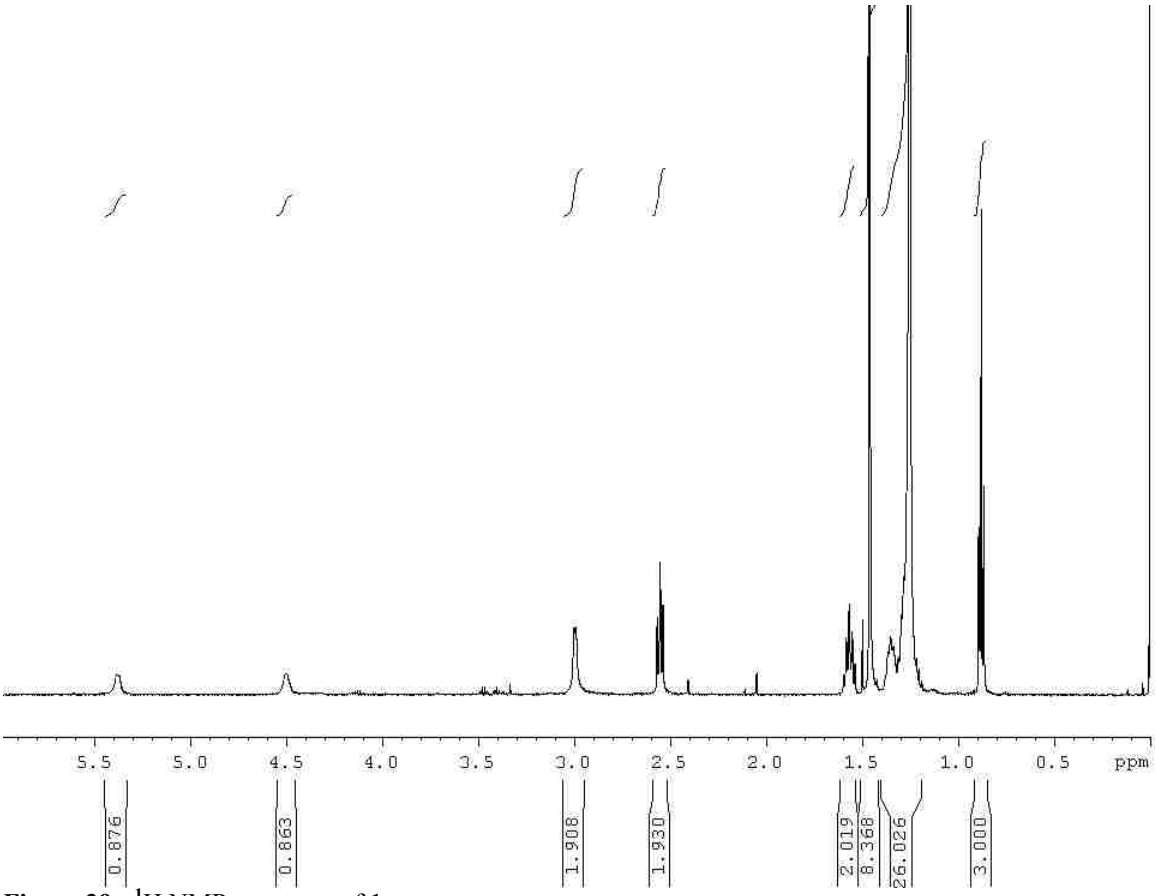

Figure 39: ^{1}H NMR spectrum of **1**

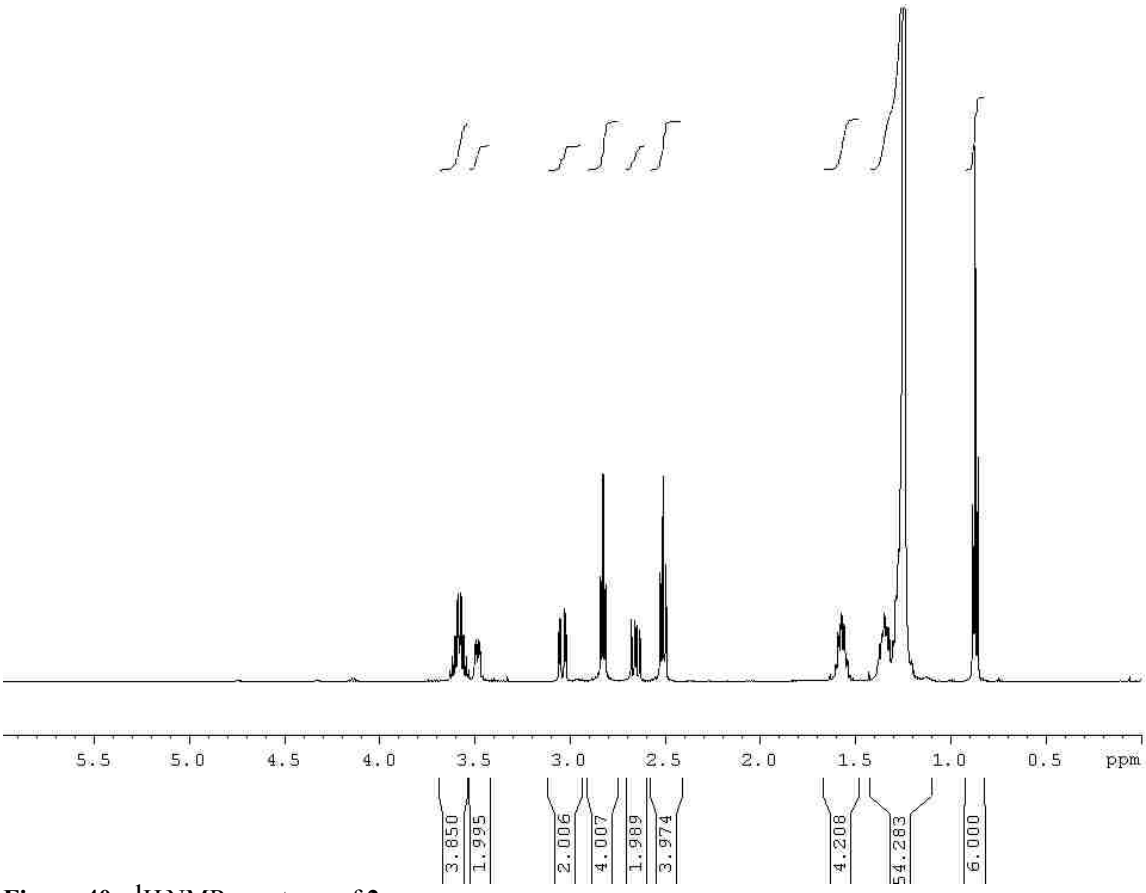

Figure 40: ^{1}H NMR spectrum of **2**

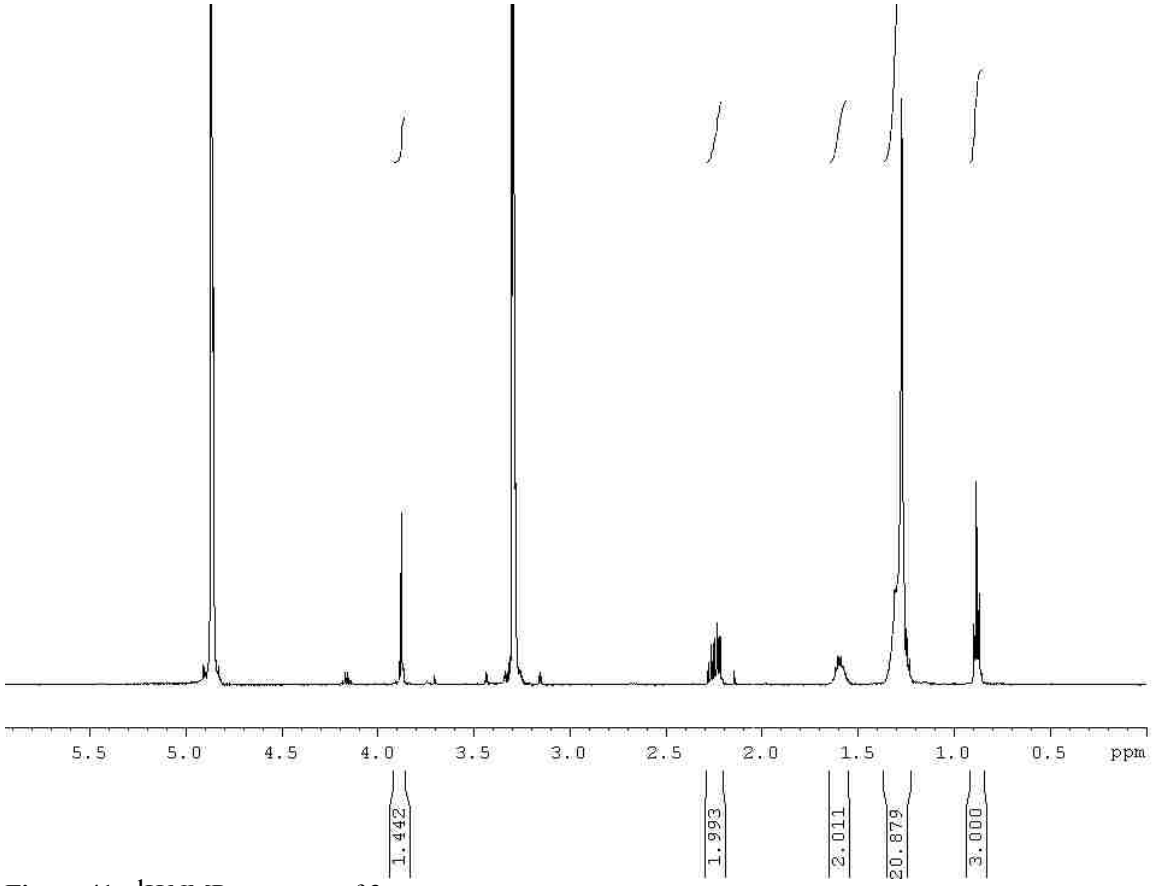

Figure 41: ^{1}H NMR spectrum of **3**

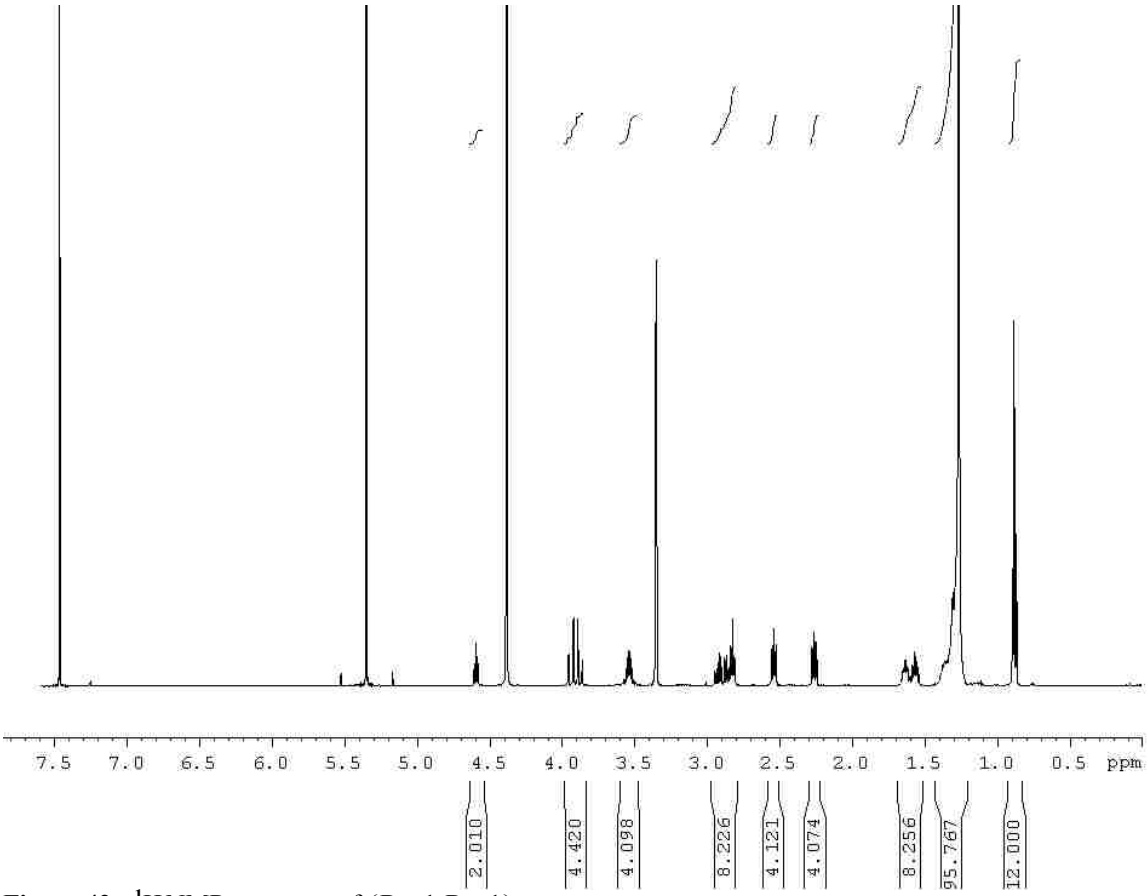

Figure 42: ^{1}H NMR spectrum of {**Pep1-Pep1**}

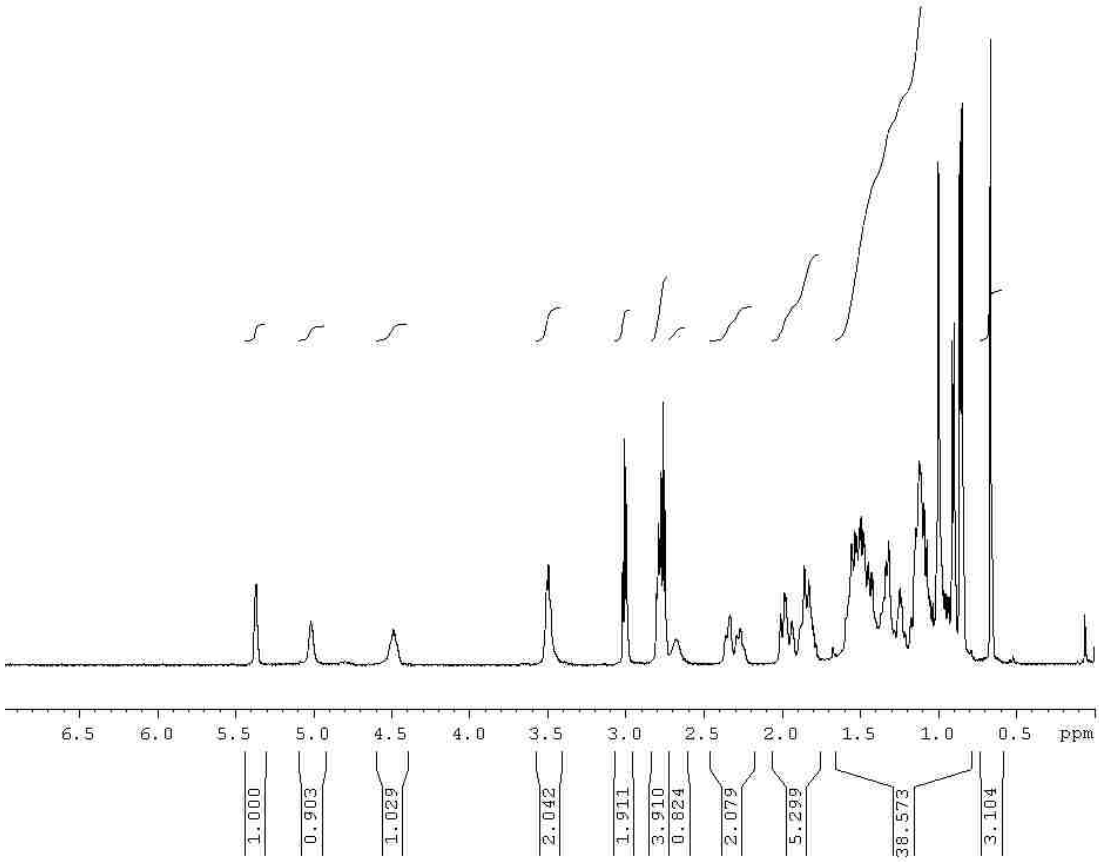

Figure 43: ^{1}H NMR spectrum of **4**

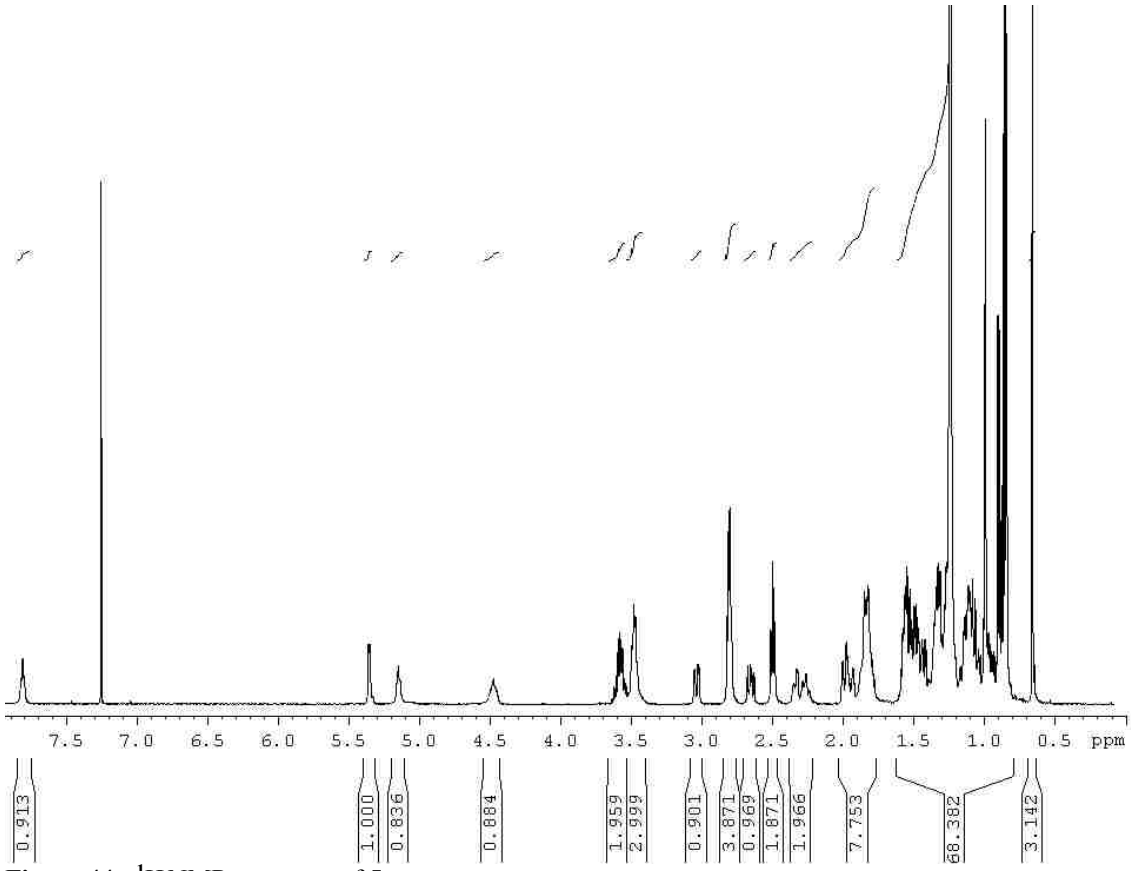

Figure 44: ^{1}H NMR spectrum of **5**

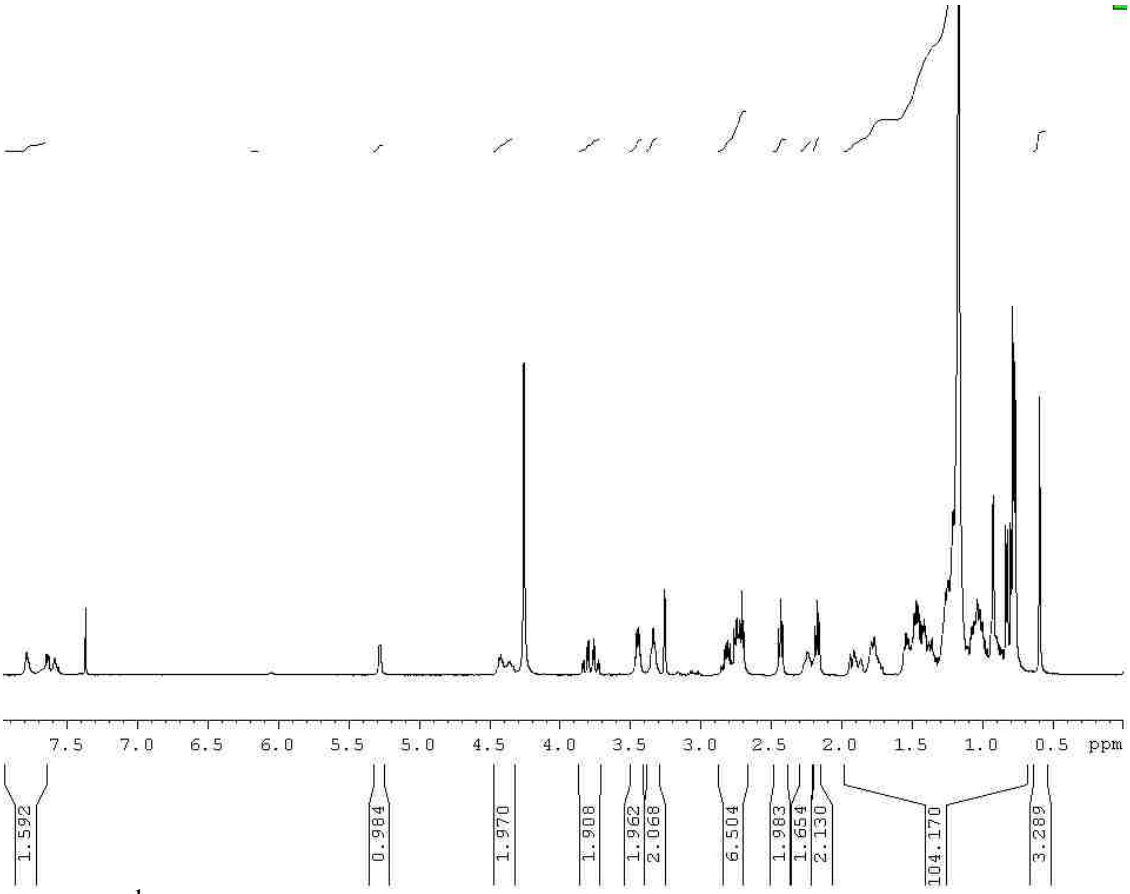

Figure 45: ^{1}H NMR spectrum of {**Pep1-cho**}

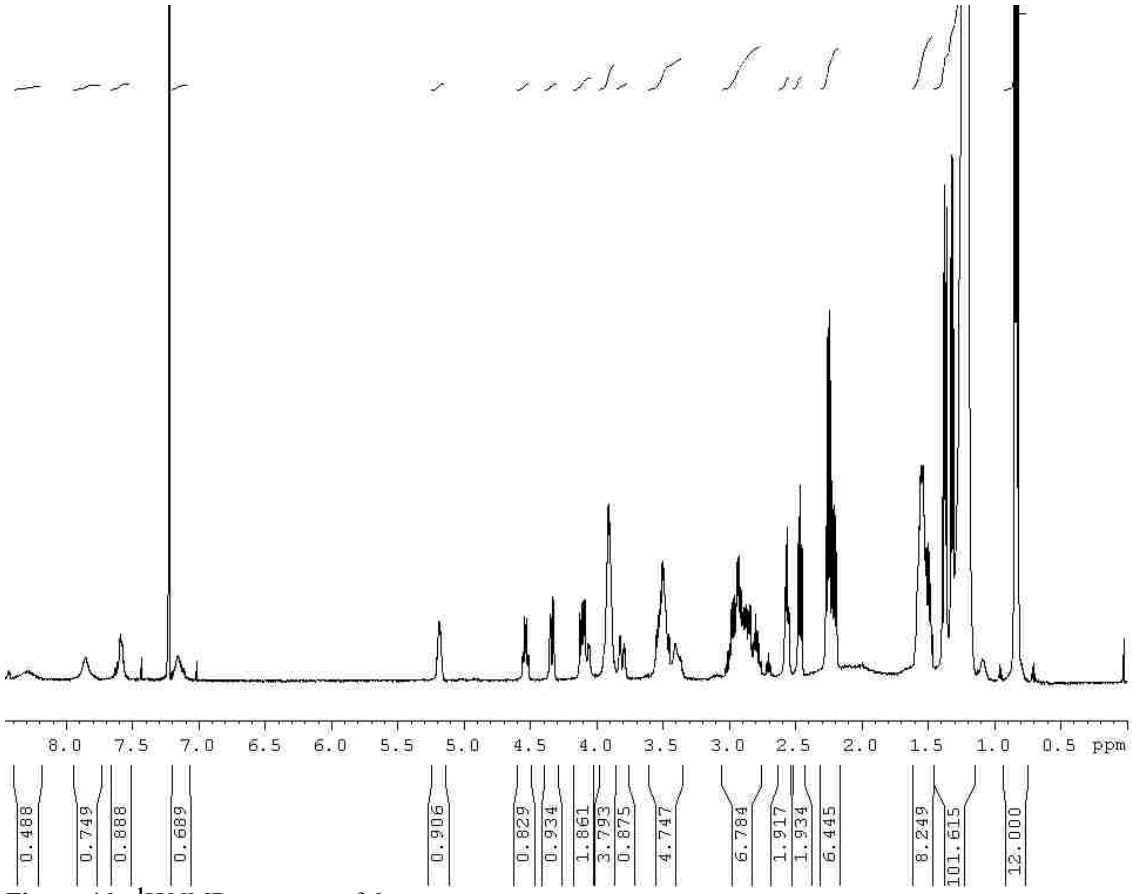

Figure 46: ^{1}H NMR spectrum of **6**

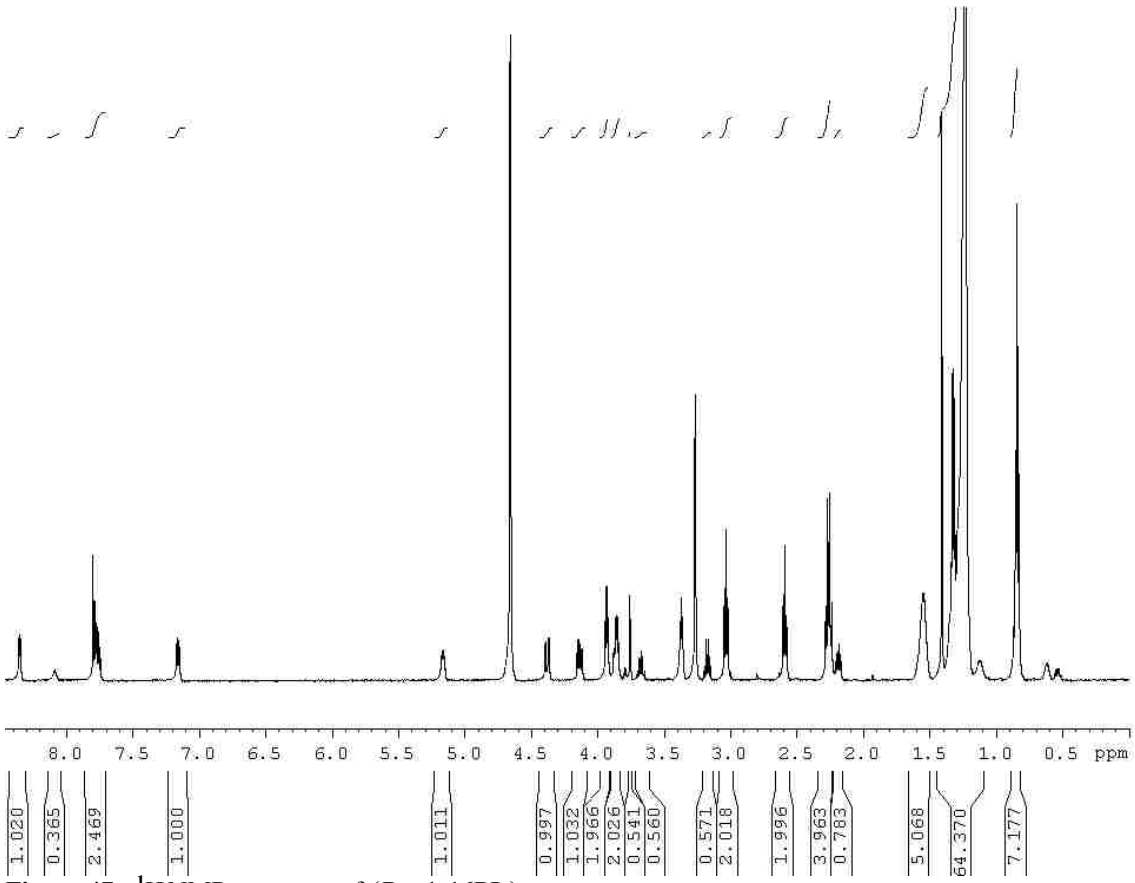

Figure 47: ^{1}H NMR spectrum of {**Pep1-16PL**}

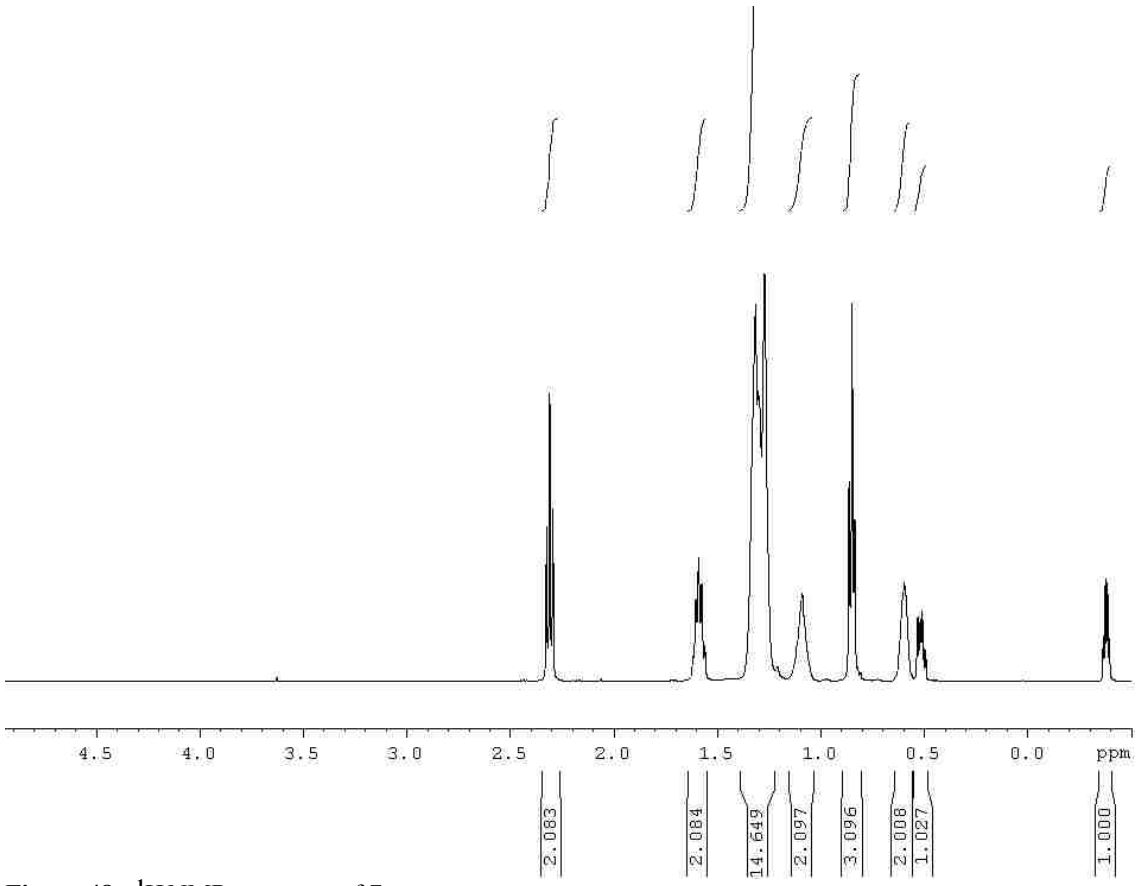

Figure 48: ^{1}H NMR spectrum of **7**

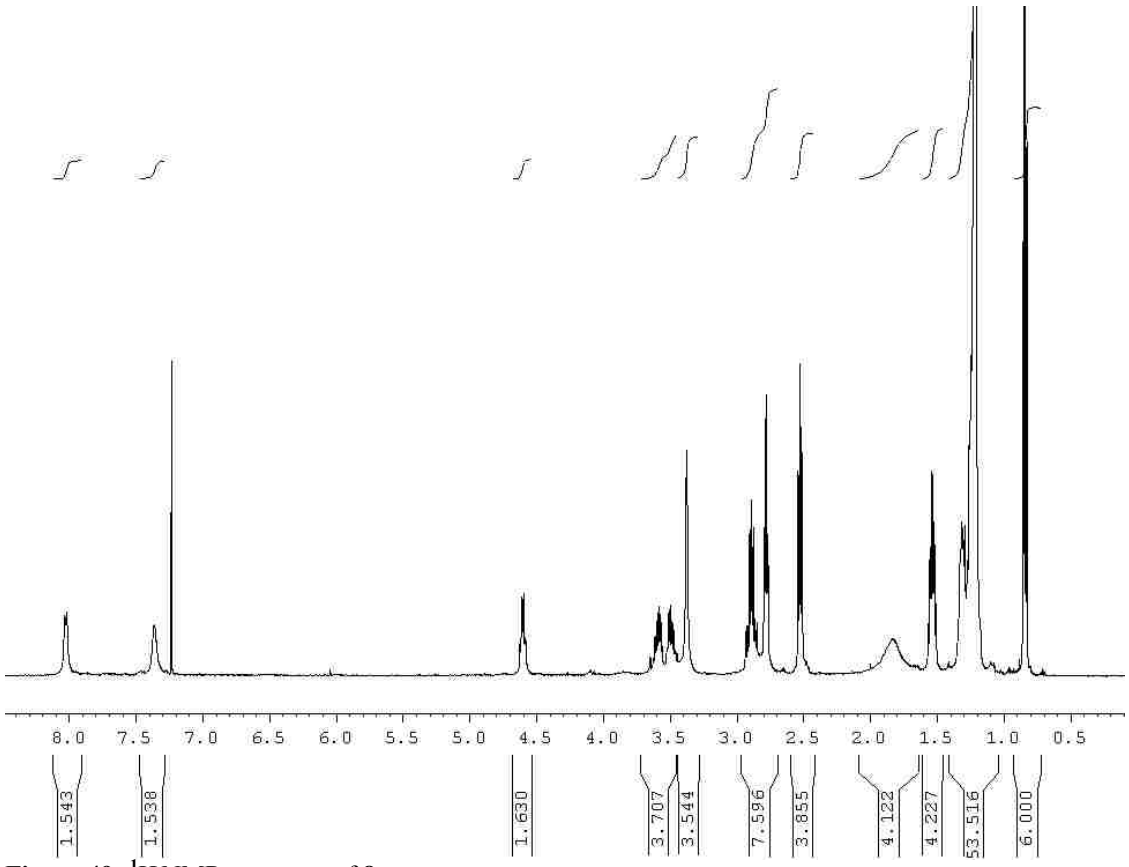

Figure 49: ^{1}H NMR spectrum of **8**

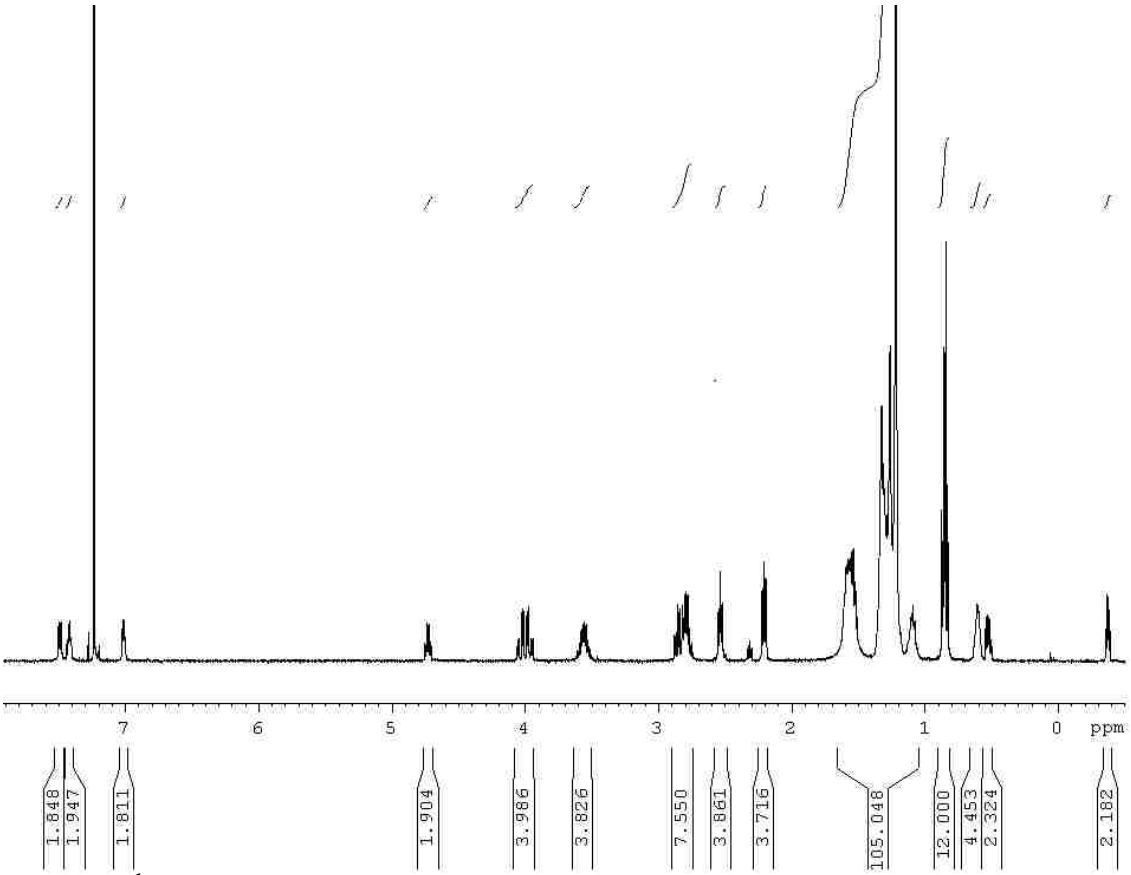

Figure 50: ^{1}H NMR spectrum of {**Pep2-Pep2**}

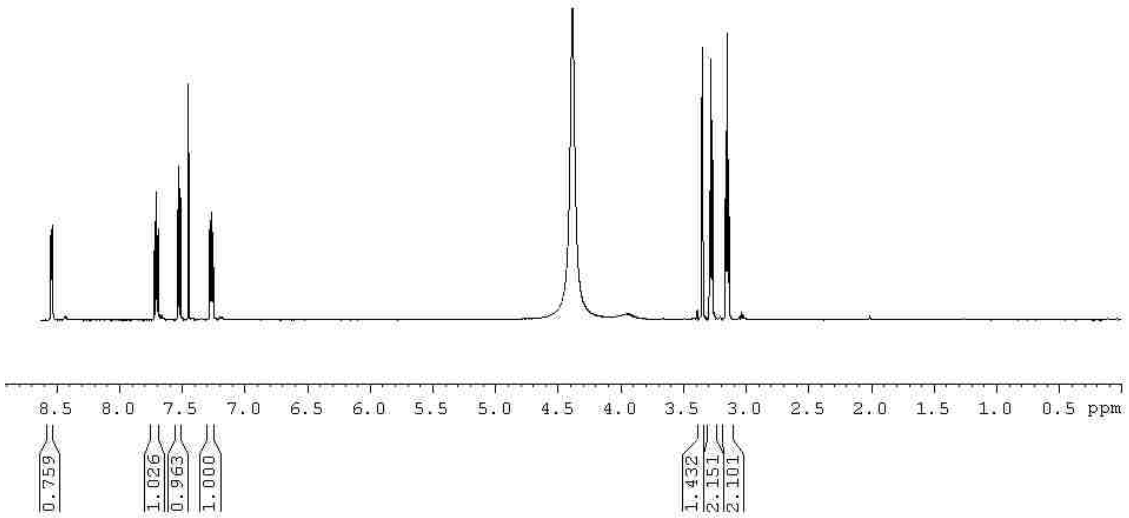

Figure 51: ^{1}H NMR spectrum of **9**

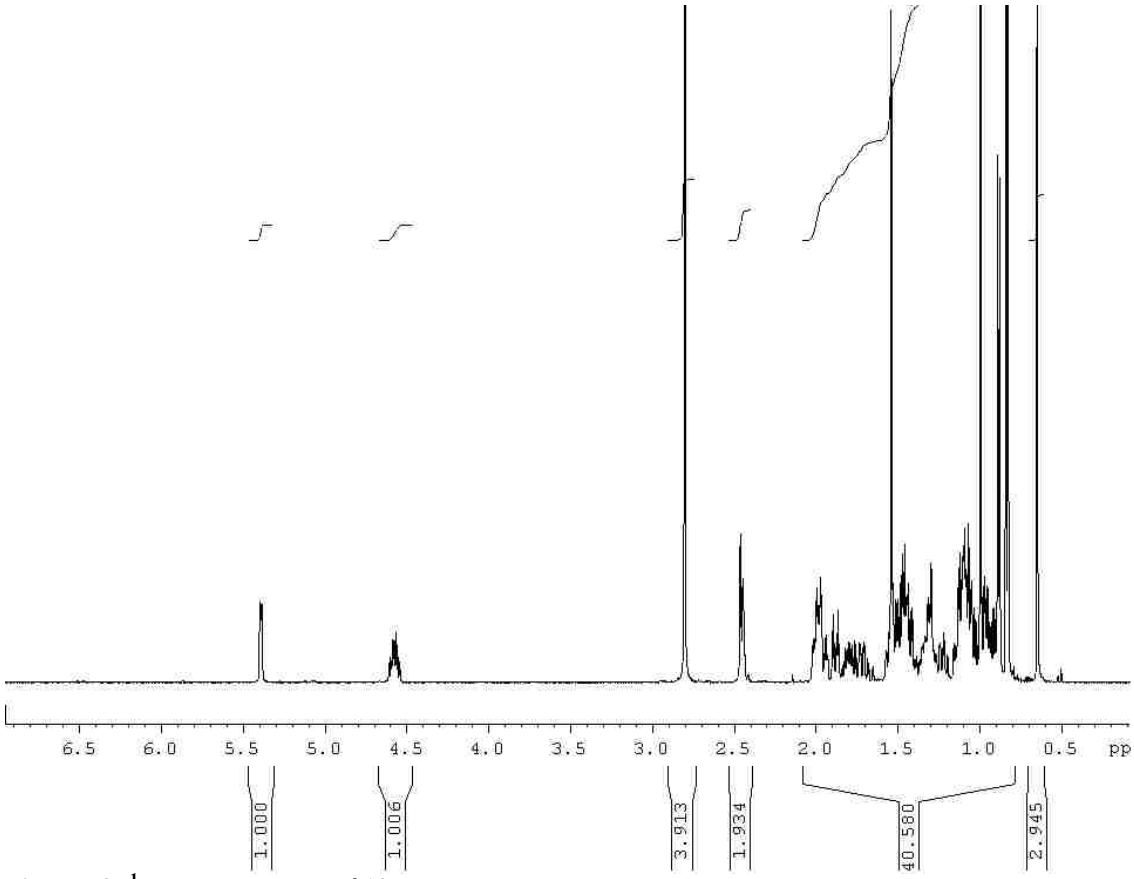

Figure 52: ^{1}H NMR spectrum of **10**

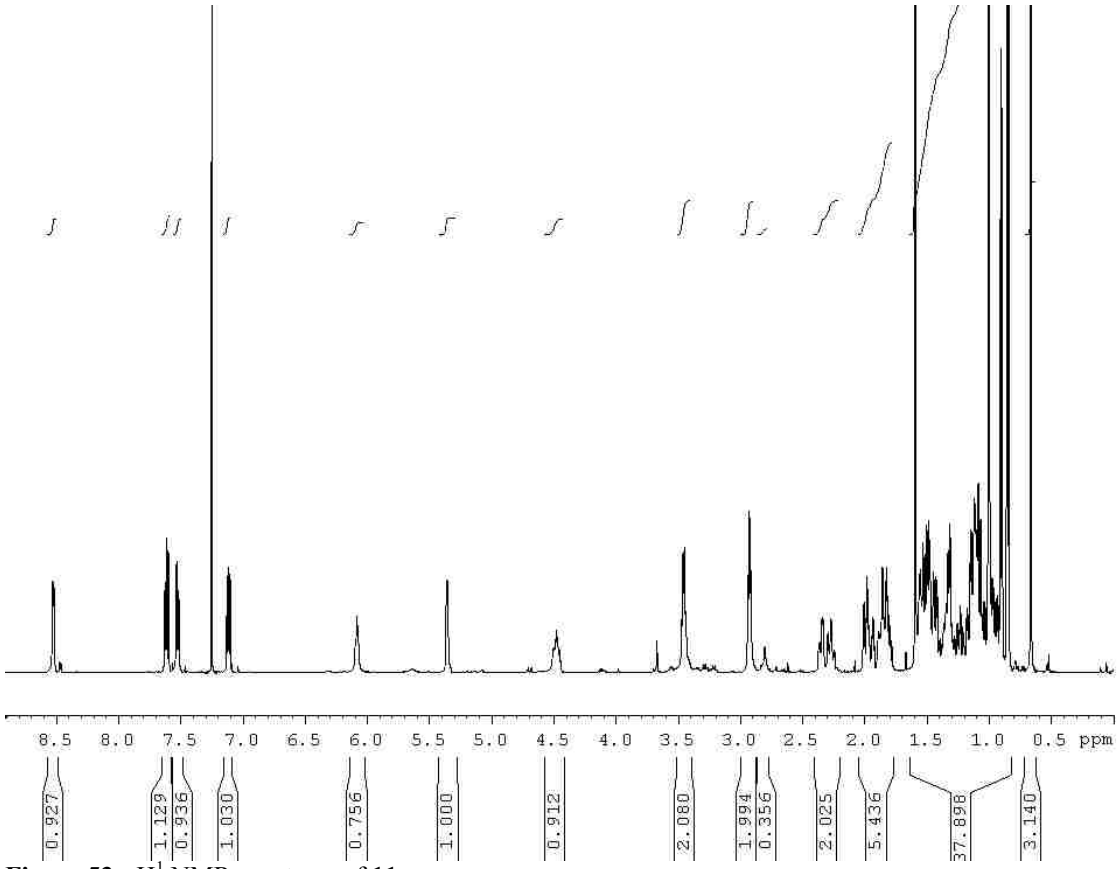

Figure 53: H^1 NMR spectrum of **11**

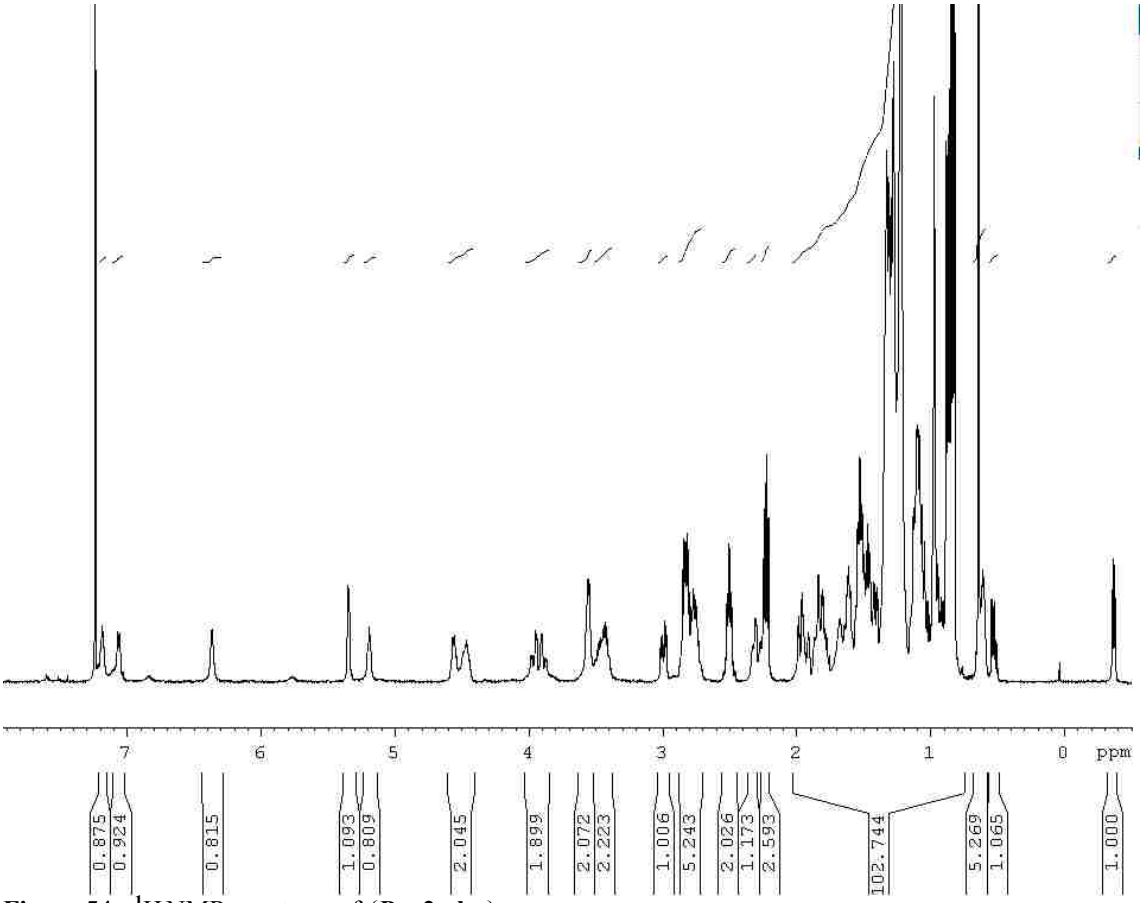

Figure 54: ^{1}H NMR spectrum of {**Pep2-cho**}

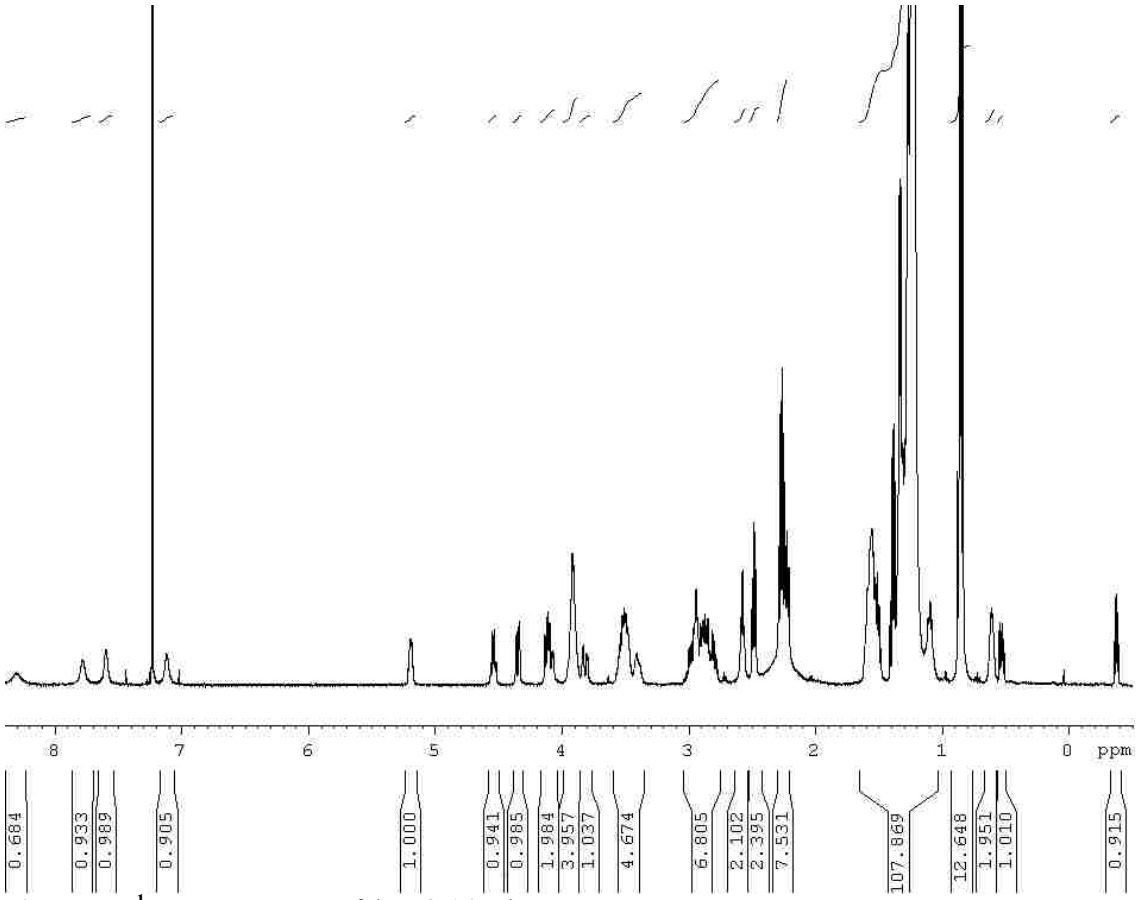

Figure 55: ^{1}H NMR spectrum of {**Pep2-16PL**}

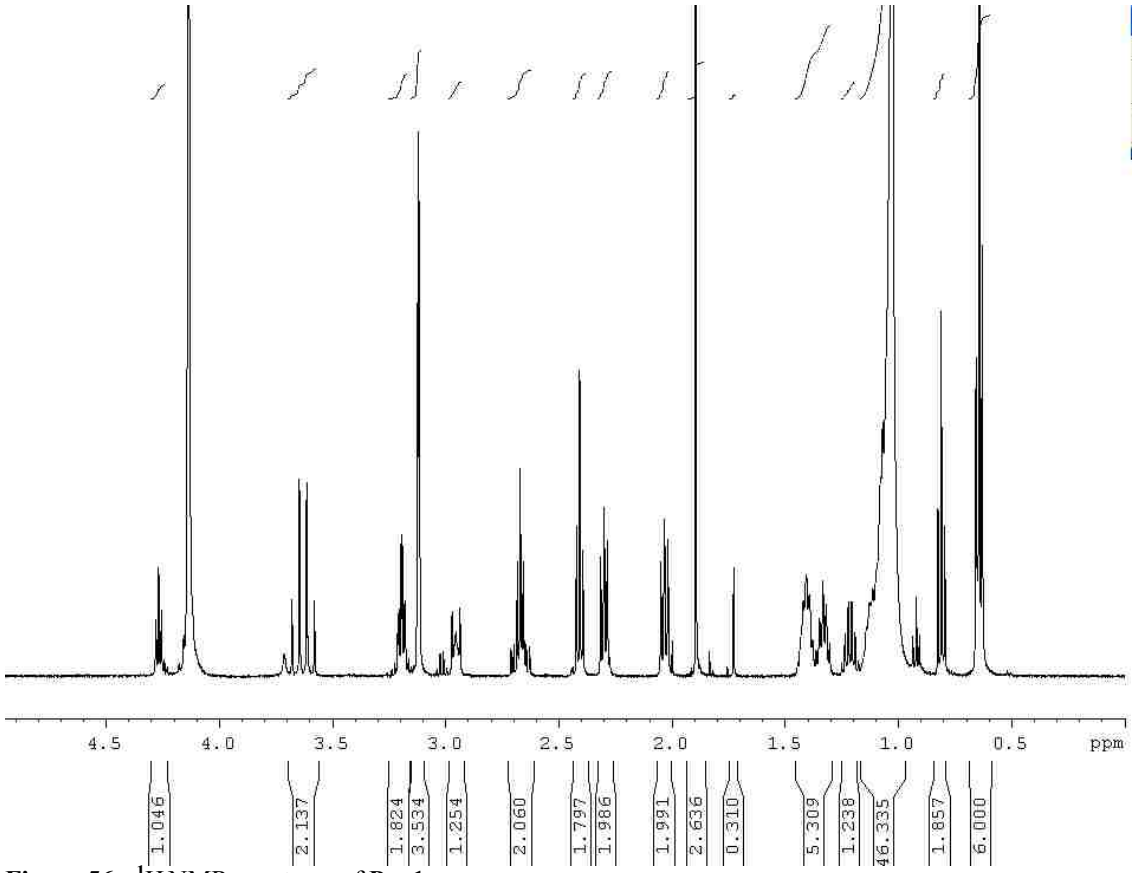

Figure 56: ^{1}H NMR spectrum of **Pep1a**

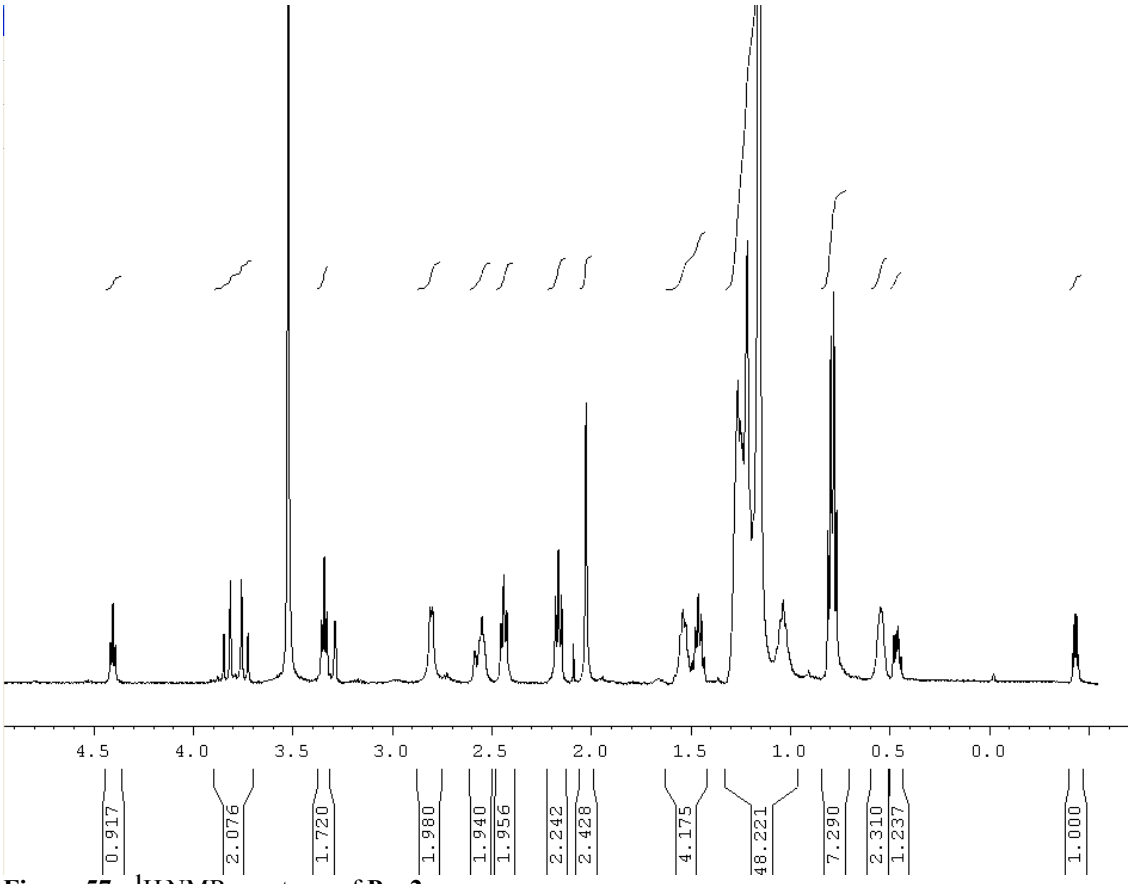

Figure 57: ^{1}H NMR spectrum of **Pep2a**

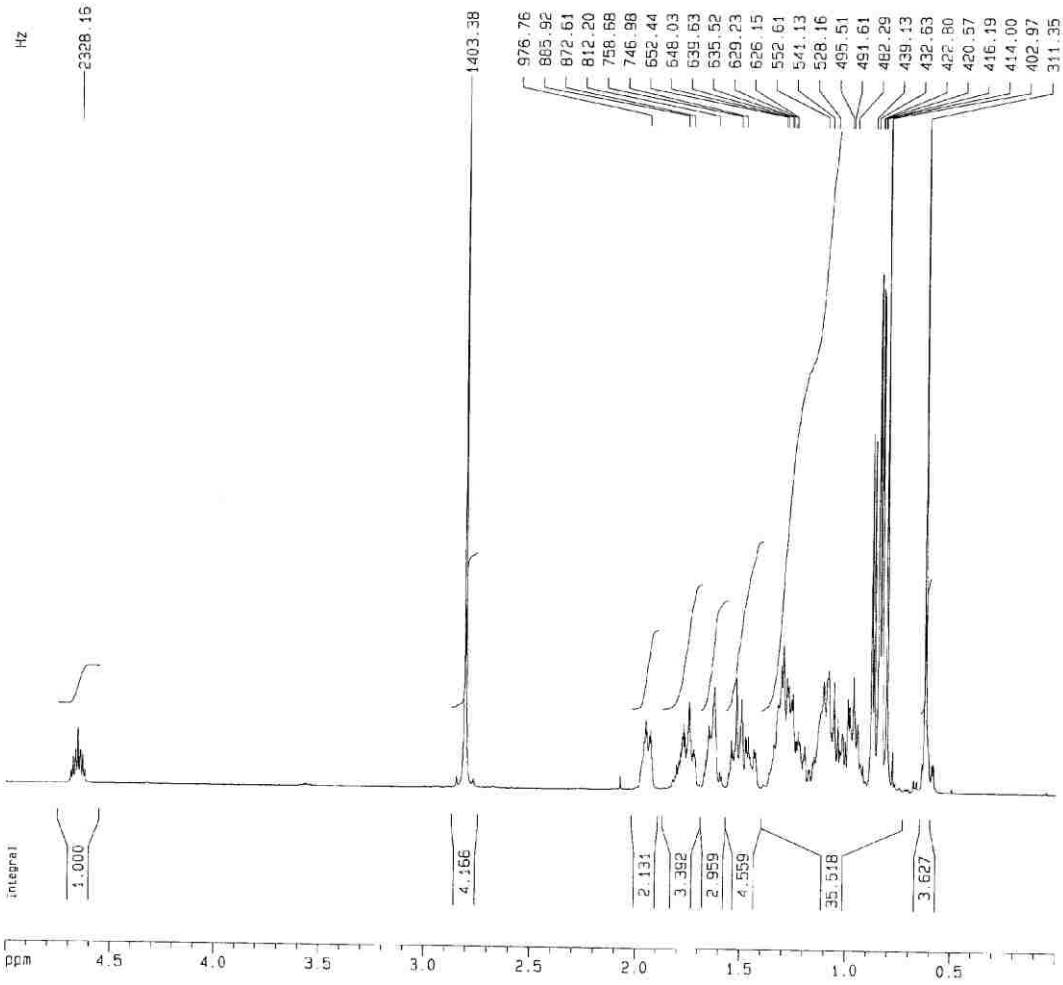

Figure 58: ^{1}H NMR spectrum of **12**

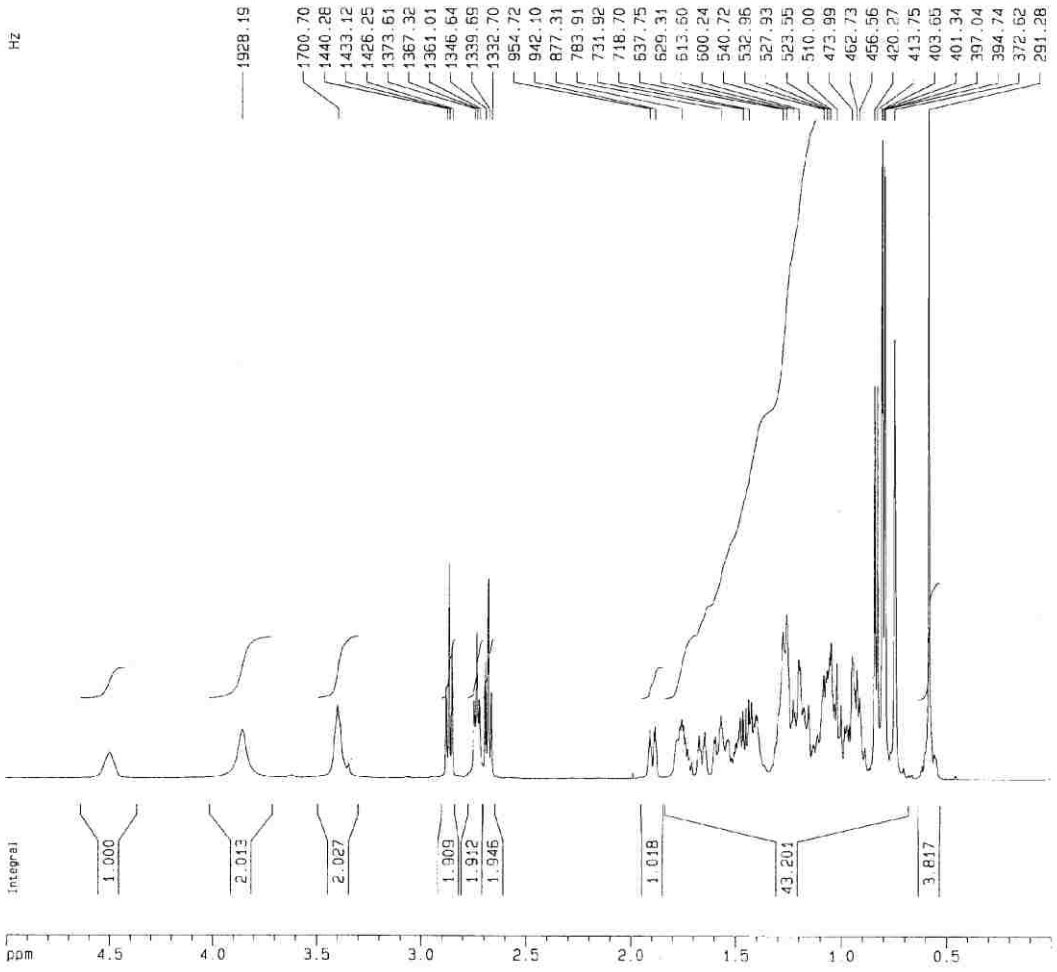

Figure 59: ^{1}H NMR spectrum of **13**

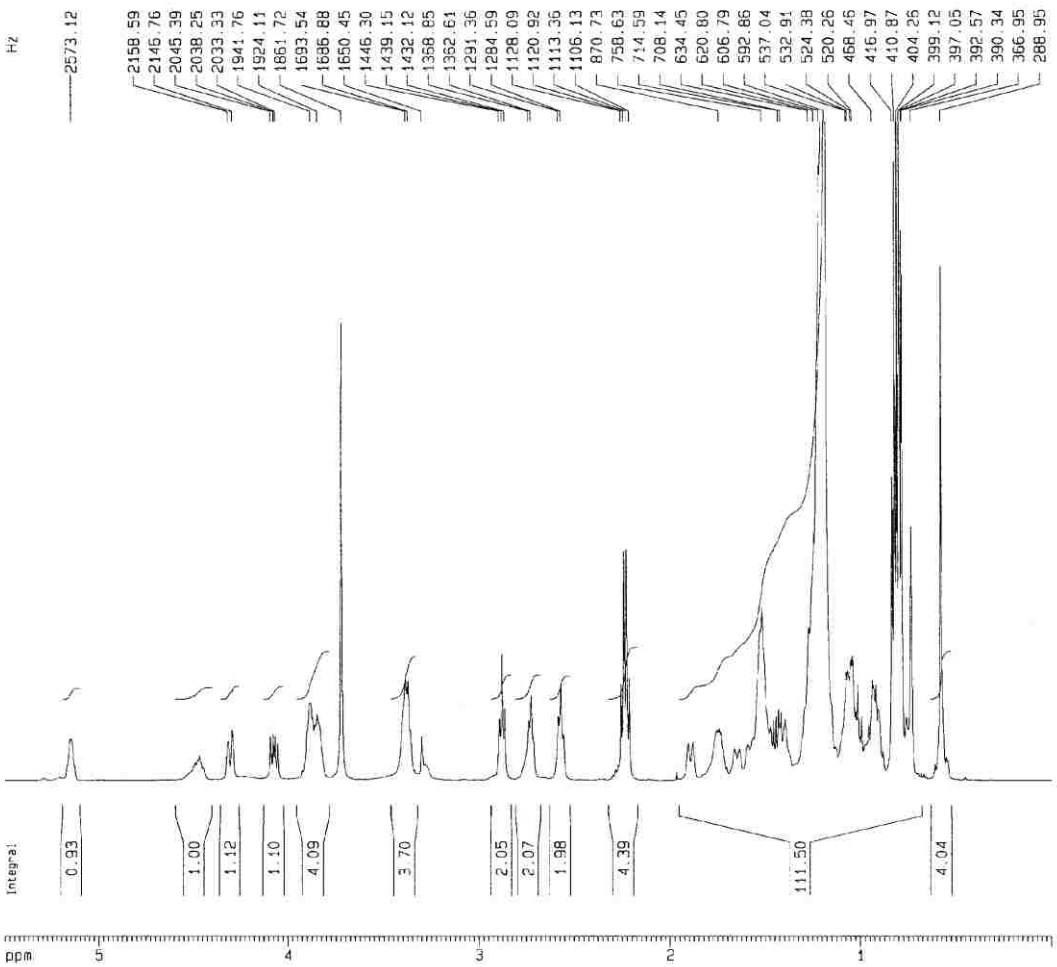

Figure 60: ^{1}H NMR spectrum of **{di-16PL}**

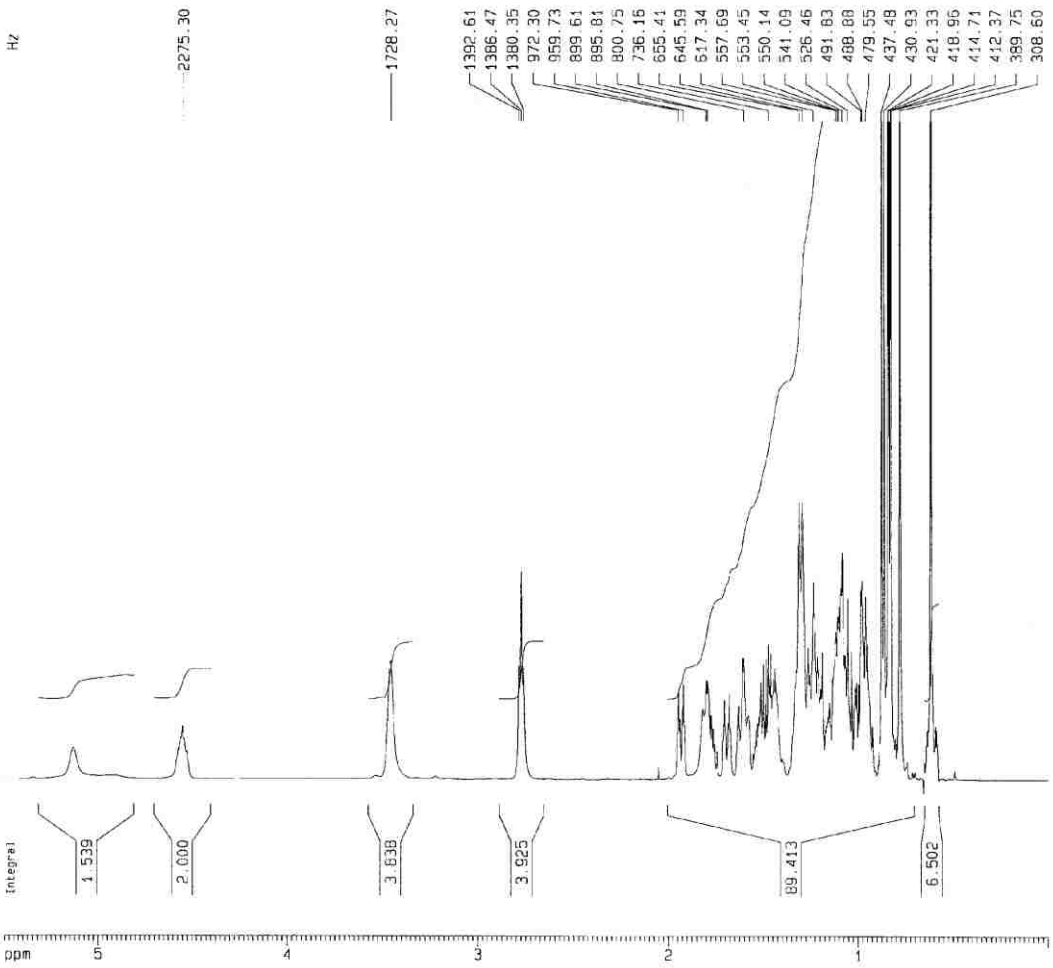

Figure 61: ^{1}H NMR spectrum of **{di-di}**

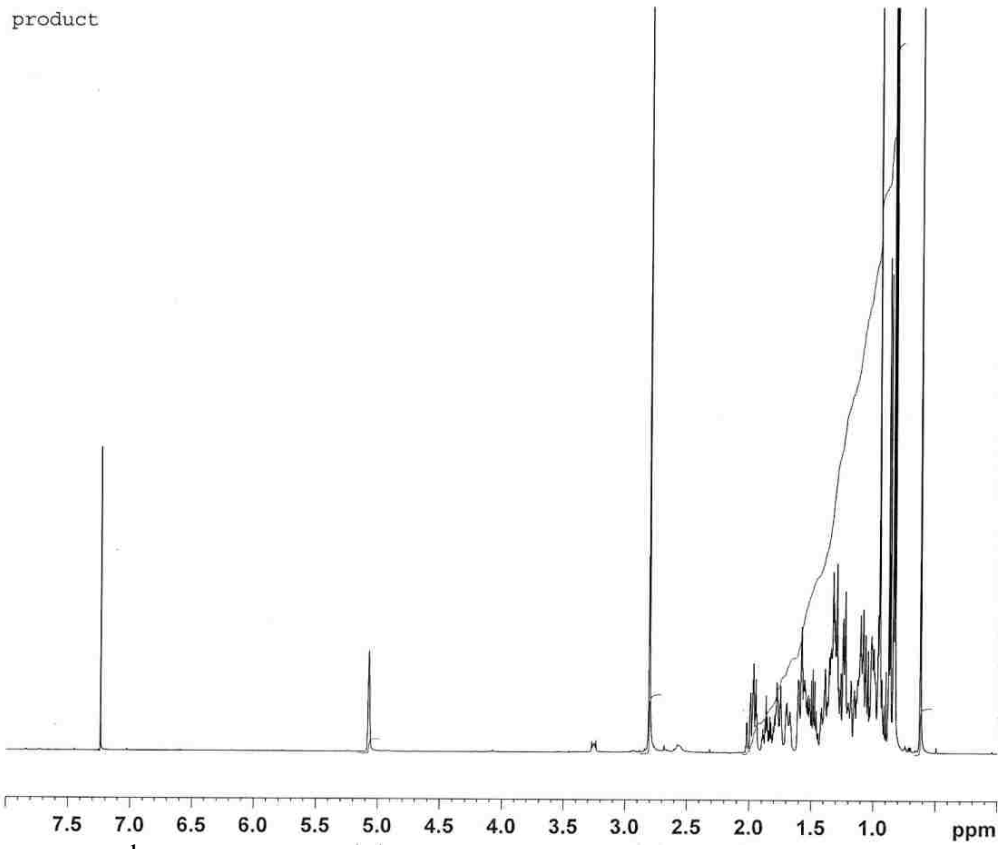

Figure 62: ^{1}H NMR spectrum of O-(N-succinimidyl)-O-coprostanyl carbonate

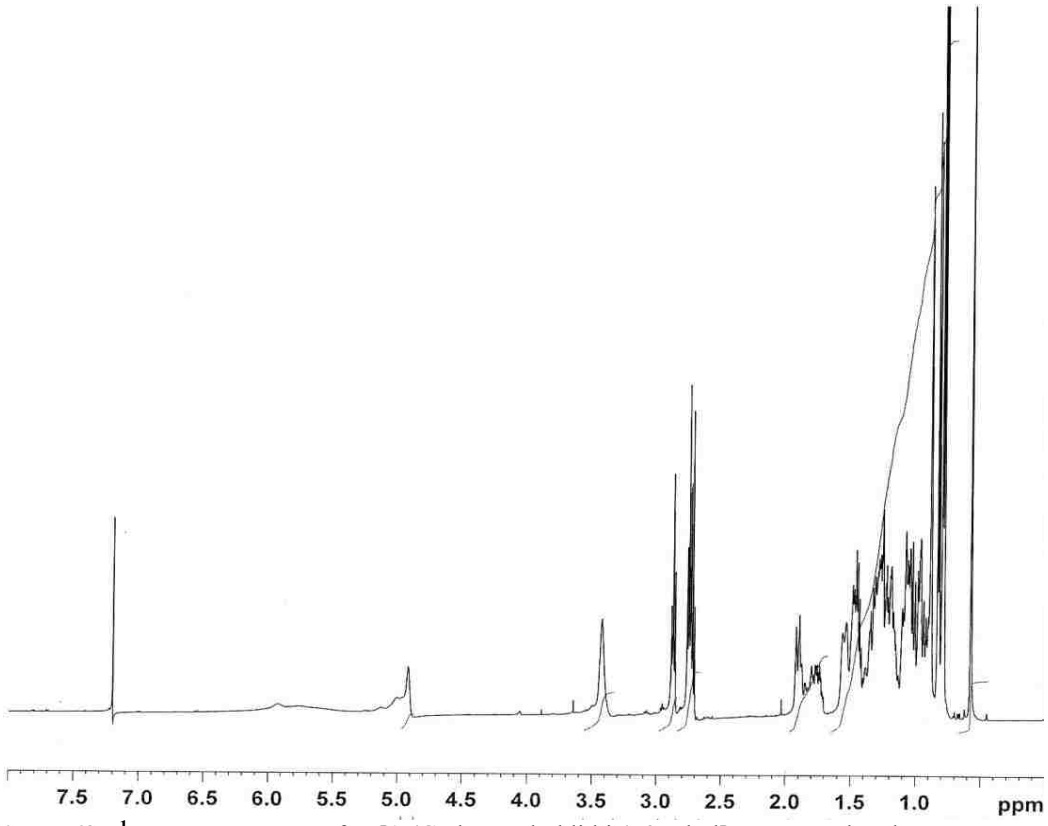

Figure 63: ^{1}H NMR spectrum of *N*-[1-(Carboxyethyldithio)-2-ethyl]coprostanyl carbamate

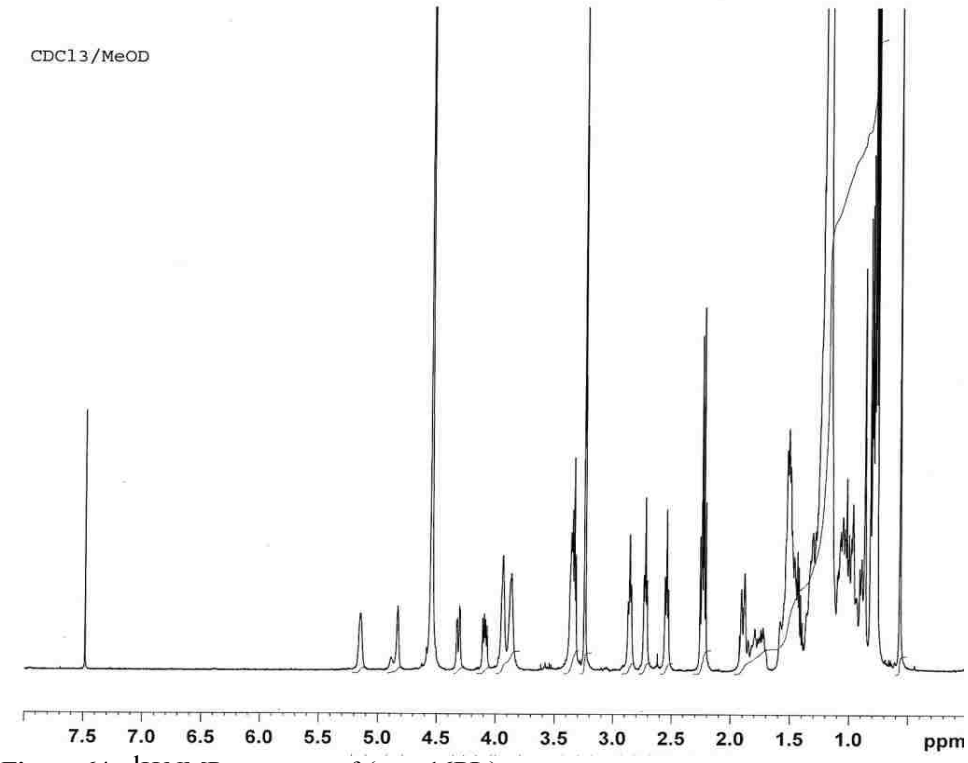

Figure 64: ^{1}H NMR spectrum of {**cop-16PL**}

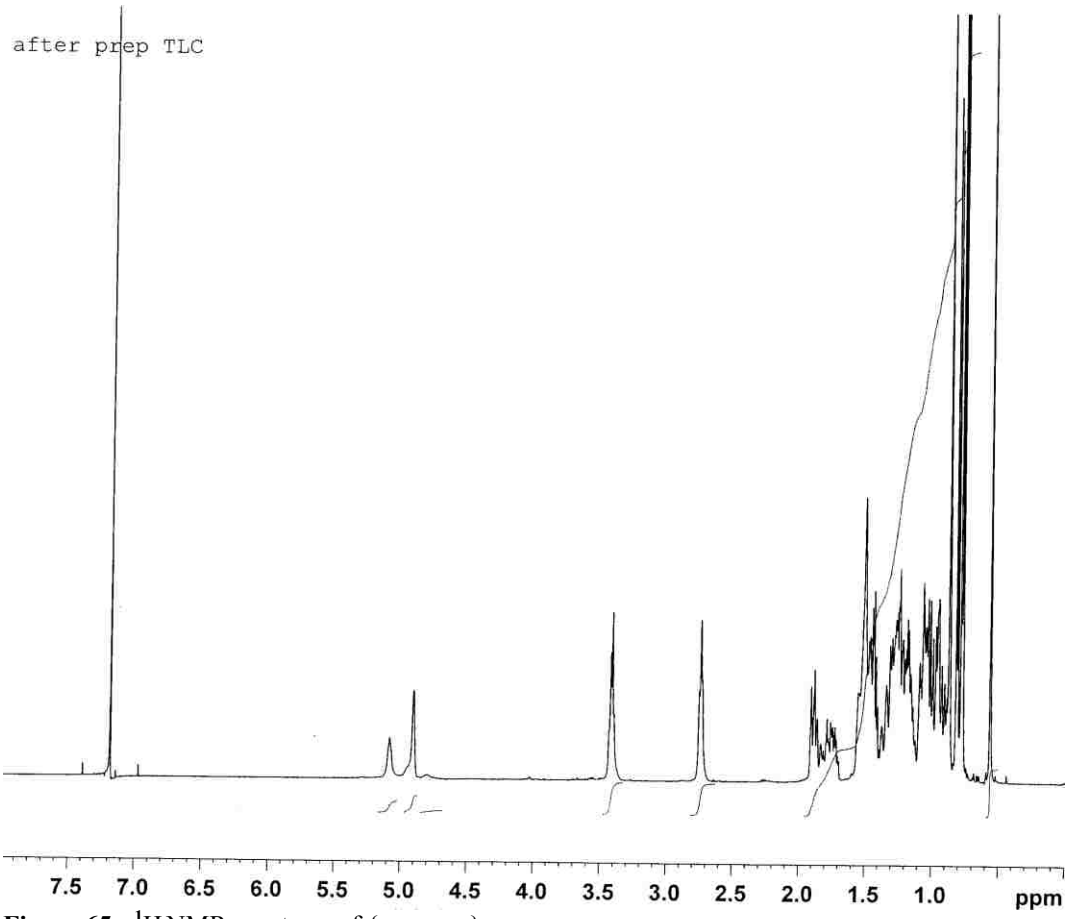

Figure 65: ^{1}H NMR spectrum of {**cop-cop**}

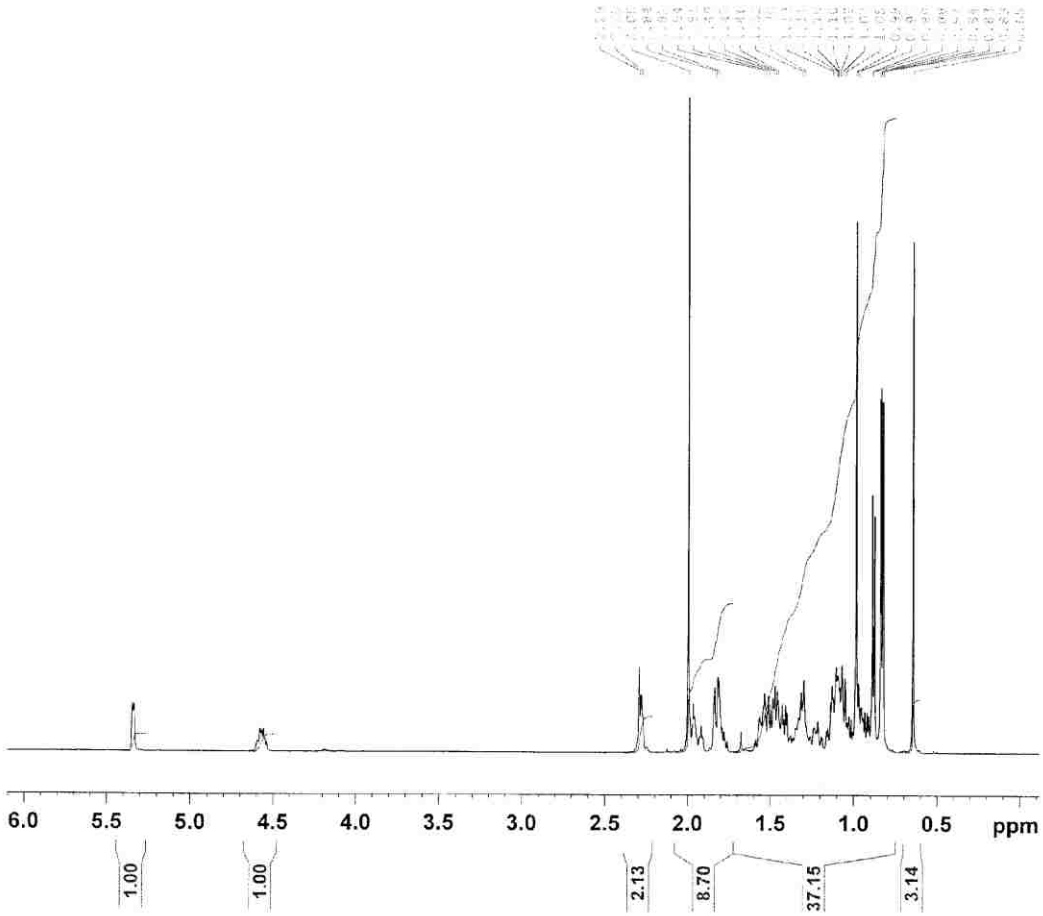

Figure 66: ^{1}H NMR spectrum of **14**

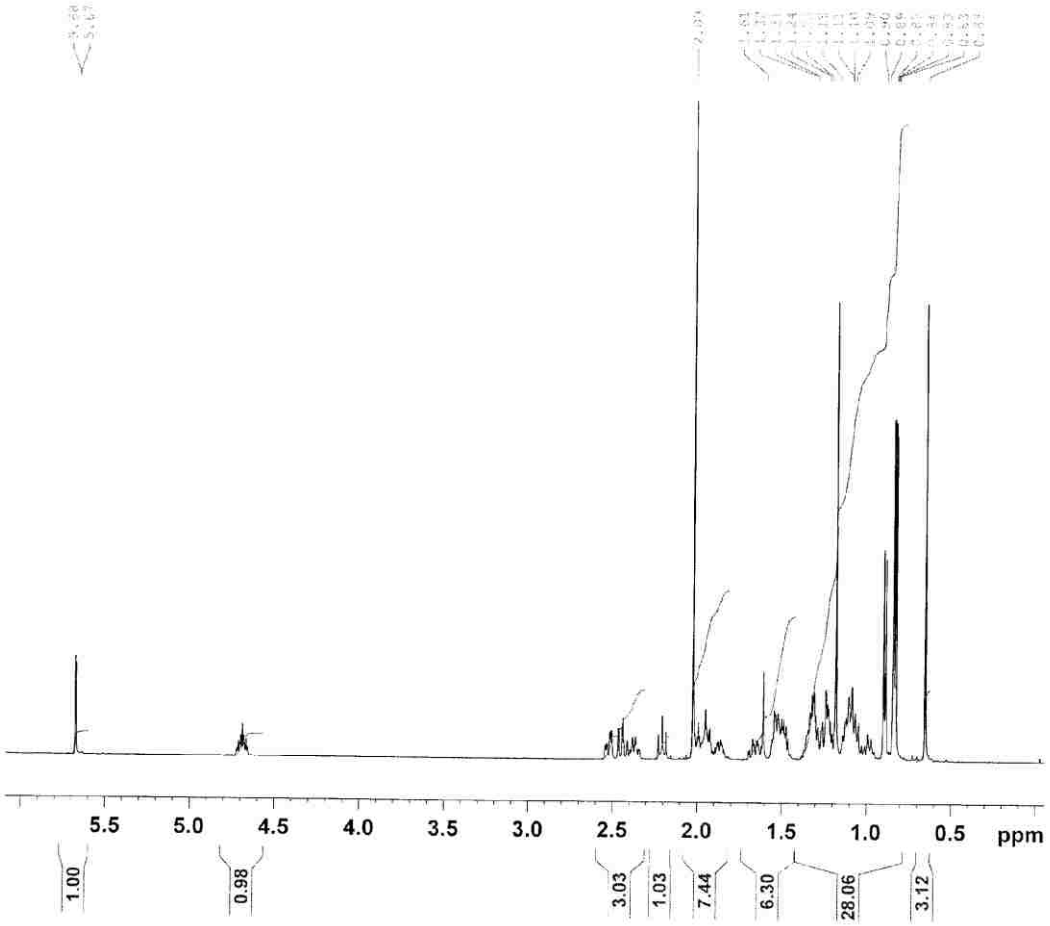

Figure 67: ^{1}H NMR spectrum of **15**

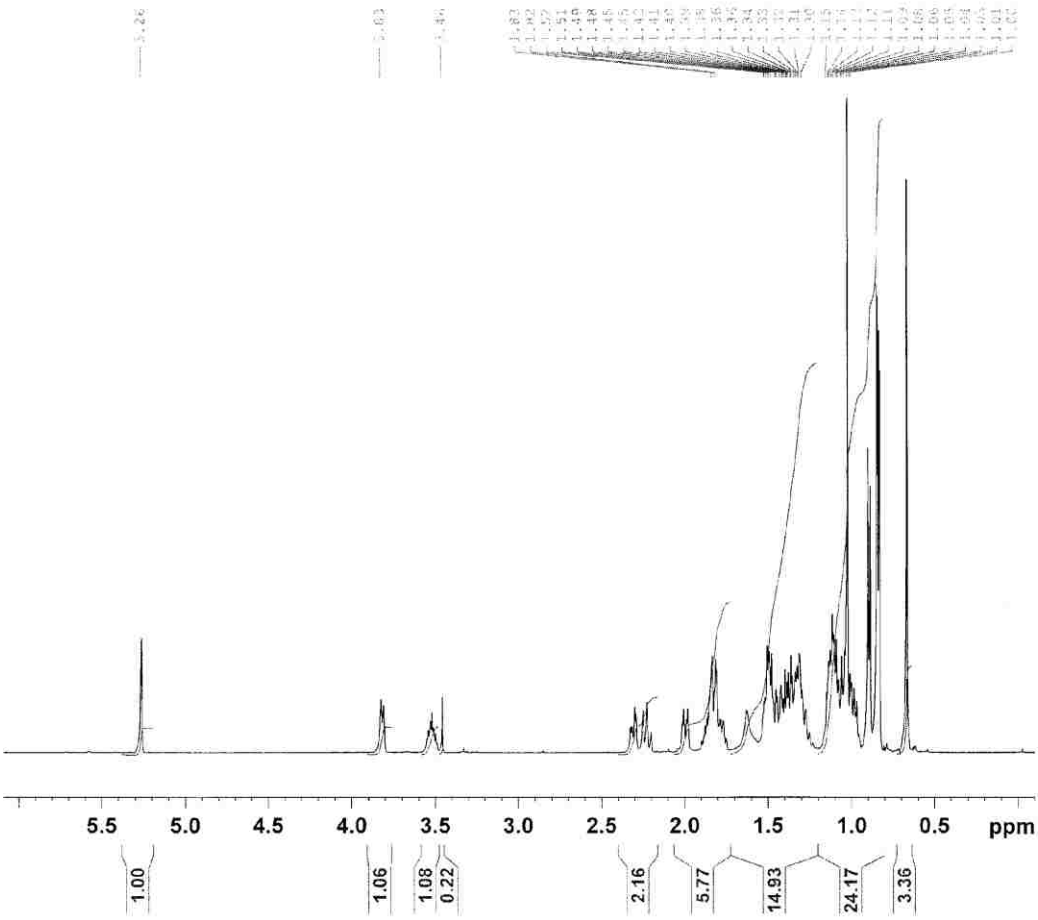

Figure 68: ^{1}H NMR spectrum of **16**

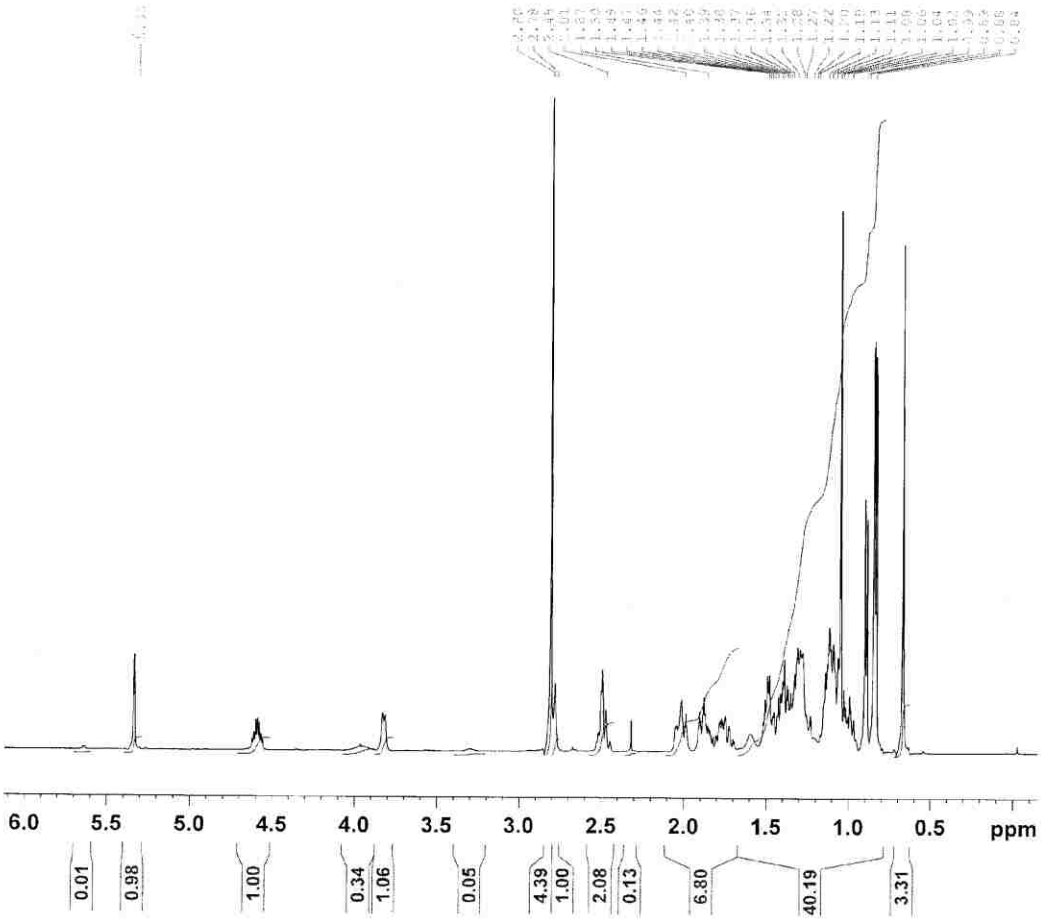

Figure 69: ^{1}H NMR spectrum of O-(N-succinimidyl)-O-7βhydroxycholesteryl carbonate

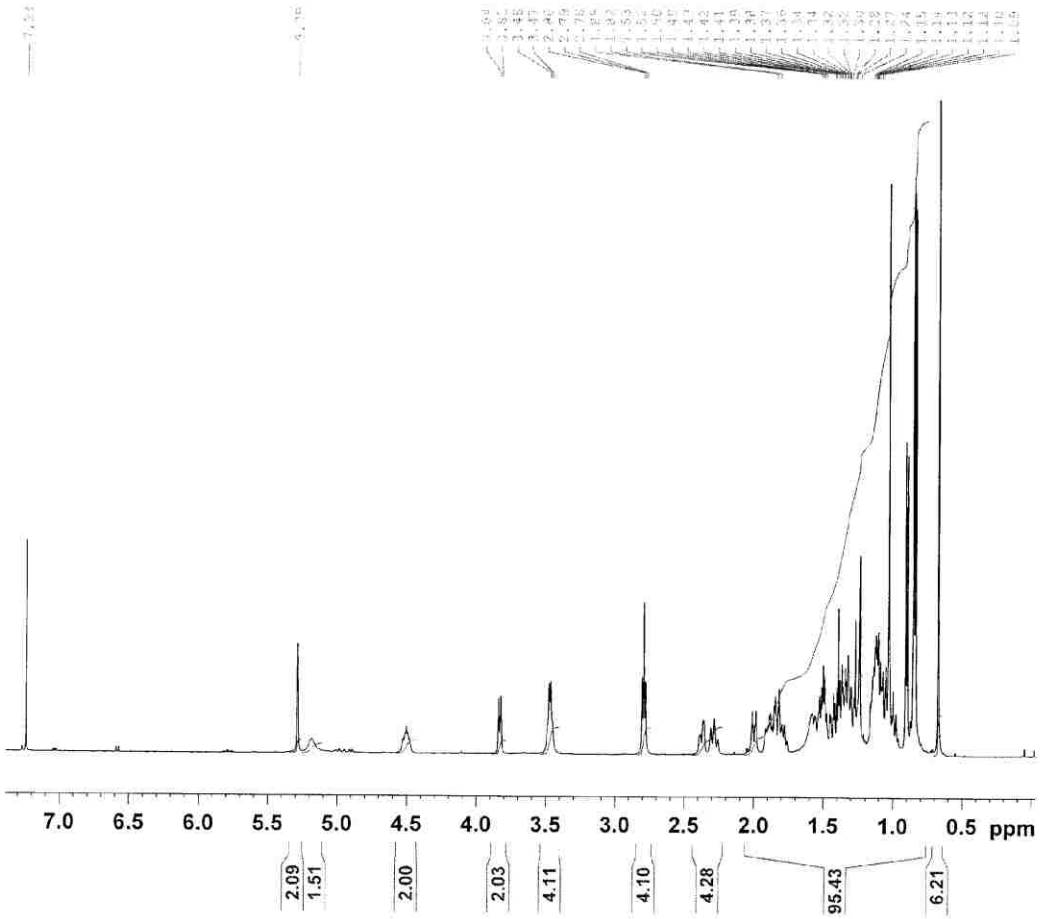

Figure 70: ^{1}H NMR spectrum of {**7β-7β**}

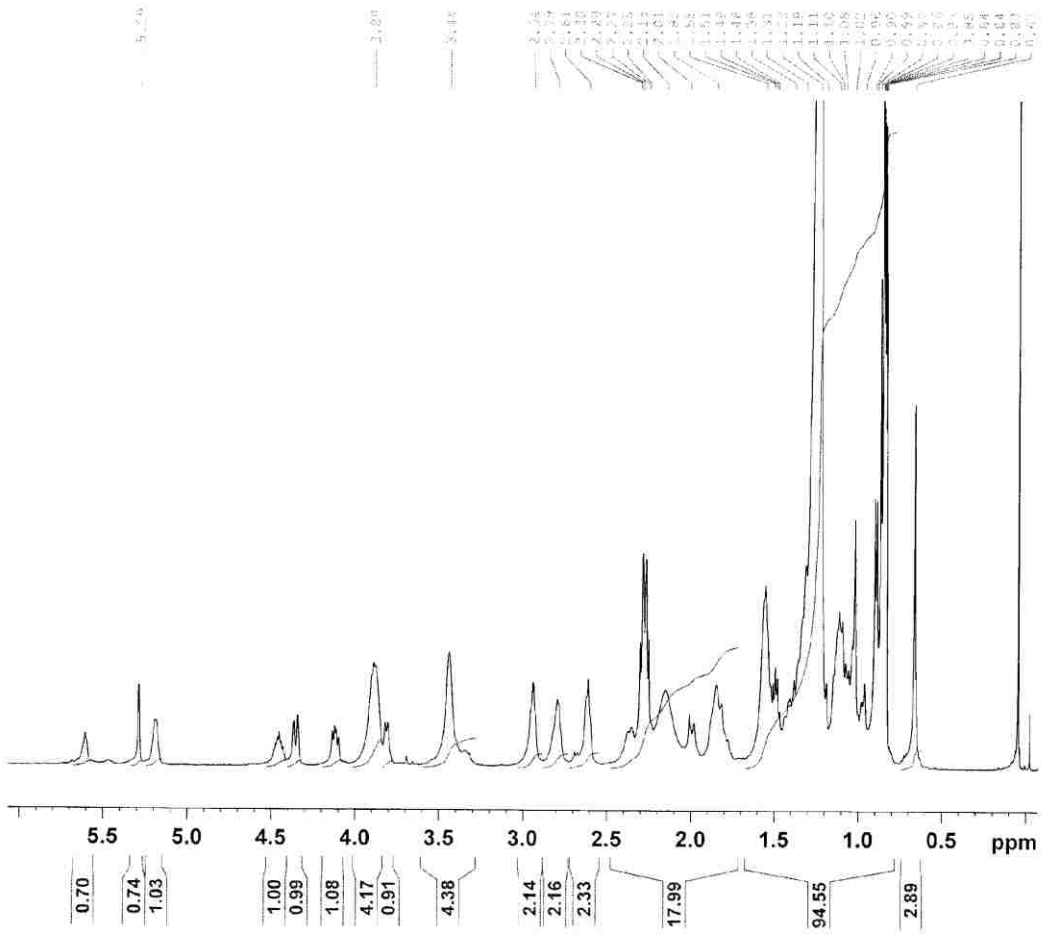

Figure 71: ^{1}H NMR spectrum of {**7β-16PL**}

References

1. Singer, S. J., and Nicholson, G. L. (1972). The fluid mosaic model of the structure of cell membranes. *Science*, *175*, 720-731.
2. Simons, K., and Ikomen, E. (1997). Functional rafts in cell membranes. *Nature*, *387*, 569-572.
3. Lingwood, D., and Simons, K. (2010). Lipid rafts as a membrane-organizing principle. *Science*, *327*, 46-50.
4. Simons, K., and Toomre, D. (2000). Lipid rafts and signal transduction. *Nat. Rev. Mol. Cell Biol.*, *1*, 31-39.
5. Prieschl, E. E., and Baumruker, T. (2000). Sphingolipids: second messengers, mediators, and raft constituents in signaling. *Immunol. Today*, *21*, 555-560.
6. Brown, D.A., and Rose, K. J. (1992). Sorting of GPI-anchored proteins to glycolipid- enriched membrane subdomains during transport to the apical cell surface. *Cell, 68,* 533-544.
7. Schroeder,R., London, E., and Brown, D. (1994). Interactions between saturated acyl chains confer detergent resistance on lipids and glycosylphosthatidylinositol (GPI)-anchored proteins: GPI-anchored proteins in liposomes and cell show similar behavior. *Proc. Nat. Acad. Sci. U.S.A.*, *91*, 12130– 12134.
8. Schroeder, R. J., Ahmed, S. N., Zhu, Y., London, E., and Brown, D. (1998). Cholesterol and sphingolipid enhance the Triton X-100 insolubility of glycosylphosthatidylinositol-anchored proteins by promoting the formation of detergent-insoluble ordered membrane domains. *J. Biol.Chem*., *273*, 1150– 1157.

9. Lichtenberg, D., Goni, F. M., and Heerklotz, H. (2005). Detergent-resistant membranes should not be identified with membrane rafts. *Trends Biochem. Sci., 30*, 430-436.
10. Cambi, A. and Lidke, D. S. (2012). Nanoscale membrane organization: where biochemistry meets advances microscopy. *Chem. Biol*., *7*, 139-149.
11. Eggeling, C., Ringemann, C., Medda, R., Schwarzmann, G., Sandhoff, K., Polyakova, S., Belov, V. N., Hein, B., von Middendorff, C., Schonle, A., and Hell, S. W. (2009). Direct observation of the nanoscale dynamics of membrane lipids in a living cell. *Nature,* **2009**, *457*, 1159-1163.
12. Manzo, C., van Zanten, T. S., and Garcia-Parajo, M. F. (2011). Nanoscale fluorescence correlation spectroscopy on intact living cell membranes with NSOM probes. *Biophys. J., 100,* L08-L10.
13. Sharma, P., Varma, R., Sarasij, R. C., Ira, Gousset, K., Krishnamoorthy, G., Rao, M., and Mayor, S. (2004). Nanoscale organization of multiple GPI-anchored proteins in living cell membranes. *Cell, 116,* 577-589.
14. Brameshuber, M., Weghuber, J., Ruprecht, V., Gombos, I., Horvarth, I., Vigh, L., Eckerstorfer, P., Kiss, E., Stockinger, H., and Schutz, G. J. (2010). Imaging of mobile long-lived nanoplatforms in the live cell plasma membrane. *J. Biol. Chem., 285*, 41765-41771.
15. Almeida, P. F. F. (2009). Thermodynamics of lipid interactions in complex bilayers. *Biochim. Biophys. Acta, 1788,* 72-85.
16. Hammond, A. T., Heberle, F. A., Baumgart, T., Holowka, D., Baird, B., and Feigenson, G. W. (2005). Crosslinking a lipid raft component triggers liquid

ordered-liquid disordered phase separation in model plasma membranes. *Proc. Nat. Acad. Sci. U.S.A., 102,* 6320-6325.

17. Kalvodova, L., Kahya, N., Schwille, P., Ehehalt, R., Verkade, P., Drechel, D., and Simons, K. (2005). Lipids as modulators of proteolytic activity of BACE. *J. Biol. Chem.*, *44,* 36815-36823.
18. Davidson, S.K.M., and Regen, S. L. (1997). Nearest-neighbor recognition in phospholipid membranes. *Chem. Rev.*, *97*, 1269-1280.
19. Cao, H., Zhang, G., Jing, B., and Regen, S. L. (2005). A chemical sensor for the liquid-ordered phase. *J. Am. Chem. Soc.*, *127*, 8813-8816.
20. Zhang, J., Jing, B., Janout, V., and Regen, S. L. (2007). Detecting cross talk between two halves of a phospholipid bilayer. *Langmuir*, *23*, 8709-8712.
21. Turkyilmaz, S., Chen, W.-H., Mitomo, H., and Regen, S. L. (2009). Loosening and reorganization of fluid phospholipid bilayers by chloroform. *J. Am. Chem. Soc.*, *131*, 5068-5069.
22. Turkyilmaz, S., Mitomo, H., Chen, W.-H., and Regen, S. L. (2010). Phospholipid complexation of general anestheics in fluid bilayers. *Langmuir, 26*, 5309-5311.
23. Turkyilmaz, S., Almeida, P. F., and Regen, S. L. (2011). Effects of isoflurane, halothane, and chloroform on the interactions and lateral organization of lipids in the liquid-ordered phase. *Langmuir*, *27*, 14380-14385.
24. Mitomo, H., Chen, W.-H., and Regen, S. L. (2009). Oxysterol induced rearrangement of the liquid-ordered phase: a possible link to Alzheimer;s disease?. *J. Am. Chem. Soc.*, *131,* 12354-12357.

25. Stevens, T. J., and Arkin, I. T. (2000). Do more complex organisms have a greater proportion of membrane proteins in their genomes?. *Proteins, 39*, 417-420.

26. Aicart-Ramos, C., Valero, R. A., and Rodriguez-Crespo, A. (2011). Protein palmitoylation and subcellular trafficking. *Biochim. et Biophys. Acta, 1808,* 2981-2994.

27. Orlean, P., and Menon, A.K. (2007). GPI-anchoring of protein in yeast and mammalian cells, or: how we learned to stop worrying and love glycophospholipids. *J. Lipid Res., 48*, 993-1011.

28. Levental, I., Grzybek, M., and Simons, K. (2010). Greasing their way: lipid modifications determine protein association with membrane rafts. *Biochemistry*, *49*, 6305-6316.

29. Fiedler, K., Kobayashi, T., Kurzchalia, T. V., and Simons, K.(1993). Glycosphingolipid-enriched, detergent insoluble complexes in protein sorting in epithelial cells. *Biochem.,* 32, 6365-6373.

30. Veatch, S. L., and Keller, S. L. (2003). Separation of Liquid Phases in Giant Vesicles of Ternary Mixtures of Phospholipids and Cholesterol. *Biophys. J., 85*, 3074-3083.

31. Lingwood, D., Reis, J., Schwille, P., and Simons, K. (2008). Plasma membranes are poised for activation of raft phase coalescence at physiological temperature. *Proc. Nat. Acad. Sci. U.S.A, 105*, 10005-10010.

32. Weise, K., Kappor, S., Denter, C., Nikolaus, J., Opitz, N., Koch, S., Triola, G., Merrmann, A., Waldmann, H., and Winter, R. (2011). Membrane-mediated

induction and sorting of K-Ras microdomain signaling platforms. *J. Am. Chem. Soc., 133*, 880-887.

33. Weise, K., Triola, G., Janosch, S., Waldmann, H., and Winter, R. (2010). Visualizing association of lipidated signaling proteins in heterogeneous membranes-Partitioning into subdomains, lipid sorting, interfacial adsorption, and protein association. *Biochim. Biophys. Acta, 1798,* 1409-1417.
34. Kaiser, H.-J., Orlowski, A., Rog, T., Nyholm, T. K. M., Chai, W., Feizi, T., Lingwood, D., Vattulainen, I., and Simons, K.(2011). Lateral sorting in model membranes by cholesterol mediated hydrophobic mismatch. *Proc. Nat. Acad. Sci. U.S.A.,108,* 16628-16633.
35. Schafer, L. V., de Jong, D. H., Holt, A., Rzeplela, A. J., de Vries, A. H., Poolman, B., Killian, J. A., and Marrink, S. J. (2011). Lipid packing drives the segregation of transmembrane helices into disordered lipid domains in model membranes. *Proc. Nat. Acad. Sci. U.S.A., 108*, 1343-1348.
36. Horton, M. R., Rädler, J., and Gast, A. P. (2006). Phase behavior and the partitioning of caveolin-1 scaffolding domain peptides in model lipid bilayers. *J. Colloid. and Interface Sci., 304*, 67-76.
37. Kahya, N., Brown, D. A., and Schwille, P. (2005). Raft partitioning and dynamic behavior of human placental alkaline phosphotase in giant unilamellar vesicles. *Biochemistry, 44,* 7479-7489.
38. Buamgardt, T., Hammond, A. T., Sengupta, P., Hess, S. T., Holowka, D. A., Baird, B. A., and Webb, W. W. (2007). Structural determinants for partitioning of

lipids and proteins between coexisting fluid phases in giant plasma membrane vesicles. *Proc. Nat. Acad. Sci. U.S.A. , 104*, 3154-3170.

39. Levental, I., Grzybek, M., and Simons, K. (2011). Raft domains of variable properties and compositions in plasma membrane vesicles. *Proc. Nat. Acad. Sci. U.S.A., 108*, 11411-11416.
40. Johnson, S.A., Stinson, B. M., Go, M. S., Carmona, L. M., Reminick, J. I., Fang, X., and Baumgart, T. (2010). Temperature-dependent phase behavior and protein partitioning in giant plasma membrane vesicles. *Biochim. Biophys. Acta, 1798*, 1427-1435.
41. Weise, K., Triola, G., Brunsveld, L., Waldmann, H., and Winter, R. (2009). Influence of the lipidation motif on the partitioning and association of N-Ras in model membrane subdomains. *J. Am. Chem. Soc., 131*, 1557-1564.
42. Wang. T.-Y., Leventis, R., and Silvius, J. R. (2001). Partitioning of lipidated peptides sequences into liquid-ordered lipid domains in model and biological membranes. *Biochemistry, 40*, 13031-13040.
43. Chao, L., and Daniel, S. (2011). Measuring the partitioning kinetics of membrane biomolecules using patterned two-phase coexistent lipid bilayers. *J. Am. Chem. Soc.*, *133*, 15625-15643.
44. Campbell, S. L., Khosravi-Far, R., Rossman, K. L., Clark, G. J., and Der, C. J. (1998). Increasing complexity of Ras signalling. *Oncogene, 17,* 1395-1413.
45. Prior, I. A., Harding, A., Yan, J., Sluimer, J., Parton, R. G., and Hancock, J. F. (2001). GTP-dependent segregation of H-Ras from lipid rafts is required for biological activity. *Nat. Cell Biol., 3*, 368-375.

46. Prior, I. A., Muncke, C., Parton, R. G., and Hancock, J. F. (2003). Direct visualization of Ras protiens in spatially distinct cell surface microdomains. *J. Cell Biol.*, *160*, 165-170.

47. Gohlke, A., Triola, G., Waldmann, H., and Winter, R. (2010). Influence of the lipid anchor motif of N-Ras on the interaction with lipid membranes: a surface plasmon resonance study. *Biophys. J., 98,* 2226-2235.

48. Webb, Y., Hermida-Matsumoto, L., and Resh, M. D. (2000). Inhibition of protein palmitoylation, raft localization, and T cell signaling by 2-bromopalmitate and polyunsaturated fatty acids. *J. Biol. Chem., 275,* 261-270.

49. Jing, B., Tokutake, N., McCullough III, D. H., and Regen, S. L. (2004). A quantitative assessment of the influence of permanent kinks on the mixing behavior of phospholipids in cholesterol-rich bilayers. *J. Am. Chem. Soc*., *126*, 15344-15345.

50. Chiang, Y. –W., Costa-Filho, A. J., and Freed, J. H. (2007). Dynamic molecular structure and phase diagram of DPPC-cholesterol binary mixtures: a 2D-EDLOR study. *J. Phys. Chem. B, 111,* 11260-11270.

51. Recktenwald, D. J., and McConnell, H. M. (1981). Phase equilibria in binary mixtures of phosphatidylcholine and cholesterol. *Biochemistry*, *20*, 4505-4510.

52. Subramaniam, S., and McConnell, H. M. (1987). Critical mixing in monolayer mixtures of phospholipid and cholesterol. *J. Phys. Chem.*, *91*, 1715-1718.

53. Collins, M. D., and Keller, S. L. (2008). Tuning lipid mixtures to induce or suppress domain formation across leaflets of unsupported asymmetric bilayers. *Proc. Nat. Acad. Sci. U.S.A.*, *105*, 124-128.

54. Kristovitch, S. M., and Regen, S. L. (1992). Nearest neighbor recognition in phospholipid membranes: a molecular-level approach to the study of membrane suprastructure. *J. Am. Chem. Soc., 114*, 9828–9835.

55. Sugahara, M., Uragami, M., Yan, X., and Regen, S. L. (2001) The structural role of cholesterol in biological membranes. *J. Am. Chem. Soc., 123*, 7939–7940.

56. Daly, T. A., Almeida, P. F., and Regen, S. L. (2012) Sorting of lipidated peptides in fluid bilayers: a molecular-level investigation. *J. Am. Chem. Soc., 134,* 17245-17252.

57. Charette, A. B., Sebastien, F., Martel, J., and Wilb, N. (2000) New family of cyclopropanating reagents: synthesis, reactivity, and stability of iodomethylzinc phenoxides. *Angew. Chem., Int. Ed.*, *39*, 4539-4542.

58. Ivanova, V. P., and Heimburg, T. (2001). Histogram method to obtain heat capacities in lipid monolayers, curved bilayers, and membranes containing peptides. *Phys. Rev. E.*, *63*, 041914-041925.

59. Phospholipids Handbook; Cevc. G., Ed.; Marcel Dekker: New York, 2001; 939-956.

60. Hac, A. E., Seeger, H. M., Fidorra, M., and Heimburg, T. (2005). Diffusion in two-component lipid membranes – a fluorescence correlation spectroscopy and Monte Carlo simulation study. *Biophys. J.*, *88*, 317-333.

61. Suurkuusk, J., Lentz, B. R., Barenholz, Y., Biltonen, R. L., and Thompson, T. E. (1976). A calorimetric and fluorescent probe study of the gel-liquid crystalline in small, single-lamellar dipalmitoylphosphotidylcholine vesicles. *Biochemistry*, *15*, 1393-1401.

62. Mabrey, S., and Sturtevant, J. (1976). Investigation of phase transitions of lipids and lipid mixtures by sensitivity differential scanning calorimetry. *Proc. Natl. Acad. Sci. U.S.A.*, *73*, 3862-3866.

63. Estep, T.N., Mountcastle, D. B., Biltonen, R. L., and Thompson, T. E. (1978). Studies on the anomalous thermotropic behavior of aqueous dispersion of dipalmitoylphosphtidycholine-cholesterol mixtures. *Biochemistry*, *17*, 1984-1989.

64. Blume, A. (1983). Apparent molar heat capacities of phospholipids in aqueous dispersions. Effects of chain lengths and head group structure. *Biochemistry*, *22*, 5436-5442.

65. Marsh, D. CRC Handbook of Phospholipid Bilayers; CRC Press: Boca Raton, FL, 1990, 149.

66. Koyonova, R., and Caffrey, M. (1998). Phases and phase transitions of the phosphotidylcholines. *Biochim. Biophys. Acta*, *1376*, 91-145.

67. Almeida, P.F. (2011). A simple thermodynamic model of the liquid-ordered state and the interactions between phospholipids and cholesterol. *Biophys. J., 100*, 420-429.

68. Triffo, S. B., Huang, H. H., Smith, A. W., Chou, E. T., and Groves, J. T. (2012). Monitoring lipid anchor organization in cell membranes by PIE-FCCS. *J. Am. Chem. Soc.*, *134*, 10833-10842

69. Leathes, J. B. (1925). On the role of fats in vital phenomena. *Lancet, 208*, 853–856.

70. Stockton, G.W., and Smith, I. C. P. (1976). A deuterium nuclear magnetic resonance study of the condensing effect of cholesterol on egg phosphotidyl

choline bilayer membranes. I. Perdueterated fatty acid probes. *Chem. Phys. Lipids, 17*, 251–261.

71. Demel, R. A., van Deenen, L. L. M., and Pethica, B. A. (1967). Monolayer interactions of phospholipids and cholesterol. *Biochim. Biophys. Acta*, *135*, 11–19.
72. Sottrup, B. L., and Keller, S. L. (2006). Phase behavior of lipid monolayers containing DPPC and cholesterol analogs. *Biophys. J.*, *90*, 3176-3183.
73. Huang, J., and Feigenson, G. W. (1999). A microscopic interaction model of maximum solubility of cholesterol in lipid bilayers. *Biophys. J.*, *76*, 2142-2157.
74. Huang, J., Buboltz, J.T., and Feigenson, G.W. (1999). Maximum solubility of cholesterol in phosphatidylcholine and phosphatidylethanolamine bilayers. *Biochim. Biophys Acta, 1417*, 89-100.
75. Cao, H., Tokutake, N., and Regen, S. L. (2003). Unraveling the mystery surrounding cholesterol's condensing effect. *J. Am. Chem. Soc.,125,* 16182-16183.
76. Hagen, J. P., McConnell, H. M., (1997). Liquid-liquid immiscibility in lipid monolayers. *Biochim. Biophys. Acta*, *1329*, 7-11.
77. Demel, R. A., Bruckdorfer, K. R., and van Deenen, L. L. M. (1972). Structural requirements of sterols for the interaction with lecithin at the air-water interface. *Biochim. Biophys. Acta*, *255*, 311-320.
78. Parassi, T., DiStefano, M., Loiero, M., Ravagnan, G., and Gratton, E. (1994). Influence of cholesterol on phospholipid bilayers phase domains as detected by Laurdan fluorescence. *Biophys. J.*, *66*, 120–132.

79. Daly, T. A., Wang, M., and Regen, S. L. (2011). The origin of cholesterol's condensing effect. *Langmuir*, *27*, 2159-2161.

80. Kauffman, K., Westerman, P. W., and Carey, M . C. (2000). Flurocholesterols, in contrast to hydroxycholesterols, exhibit interfacial properties similar to choelsterol. *J. Lipid Res.*, *41*, 991-1003.

81. Cantor, R. S. (1997) The lateral preesure profile in membranes: a physical mechanism of general anesthesia. *Biochemistry*, *36*, 2339-2344.

82. Janout, V., Turkyilmaz, S., Wang. M., Wang, Y., Manaka, Y., and Regen, S. L. (2010). An upside down view of cholesterol's condensing effect: does surface occupancy play a role. *Langmuir*, *26,* 5316-5318.

83. Rog, T., Pasenkiewicz-Gierula, M., Vattulainen, I., and Karttunen, M. (2007). What happens if cholesterol is made smoother? *Biophys. J.*, *92*, 3346-3357.

84. Bartlett, G.R. (1955). Phosphorus assay in column chromatography. *J. Biol. Chem.*, *234,* 466-468.

85. Pokorny, A., Birkbeck, T.H., and Almeida, P.F.F. (2002). Mechanism and kinetics of δ-lysin interaction with phospholipid vesicles. *Biochemistry, 41*, 11044–11056.

86. Pokorny, A., Yandek, L.E., Elegbede, A.I, Hinderliter, A., and Almeida, P.F.F. (2006). Temperature and composition dependence of the interaction of δ-lysin with ternary mixtures of sphingomyelin/cholesterol/POPC. *Biophys. J.*, *91*, 2184-2197.

87. Heimburg, T. Thermal Biophysics of Membranes; Wiley-VCH: Weinheim, Germany, 2007; 123-140.

88. Sugar, I.P., Biltonen, R. L., and Mitchard, N. (1994). Monte Carlo simulations of membranes: phase transitions of small unilamellar dipalmitoylphosphatidylcholine vesicles. *Methods Enzymol., 240,* 569-593.

89. Binder, K.; Heerman, D.W. *Monte Carlo Simulations in Statistical Physics,* 3rd ed.; Springer: New York, 1997.

90. Kawasaki, K. Kinetics of Ising Models. In *Phase Transitions and Critical Phenomena*; Domb, C., Green, M.S., Ed.; Academic Press: New York, 1972; Vol. 2, 443-501.

91. Glauber, R. J. (1963). Time dependent statistics of the Ising model. *J. Math. Phys., 4,* 294-307.

92. Metropolis, N., Rosenbluth, A. W., Rosenbluth, W. N., Teller, A. H., and Teller, E. (1953). Equation of state calculations by fast computing machines. *J. Chem. Phys., 21,* 1087-1092.

93. Press, W. H.; Teukolsky, S. A.; Vetterling, W. T.; Flannery, B. P. *Numerical Recipes in FORTRAN: The Art of Scientific Computing,* 2nd ed.; Cambridge University Press: Cambridge UK, 1994.

94. Svetlovics, J. A., Wheaten, S. A., and Almeida, P. F. (2012). Phase separation and fluctuations in mixtures of a saturated and an unsaturated phospholipid. *Biophys. J., 102*, 2526–2535.

95. Perrey, D. A., and Uckun, F. M. (2001). An improved method for cysteine alkylation. *Tetrahedron Lett.*, *42,* 1859-1861.

96. Janout, V., Lanier, M., and Regen, S. L. (1999). *N*-[O-1,2,3-benzotriazin-4(3H)one-yl]-3,(2-pyridyldithio)propionate: A more reactive alternative to SPDP. *Tetrahedron Lett.*, *40*, 1107-1108.

Vita

EDUCATION AND EXPERIENCE

Lehigh University, Bethlehem, PA *Ph.D.* 2013
Doctor of Philosophy, Organic Chemistry *M.S.* 2009
Advisor: Dr. Steven Regen

- Researched lateral organization of lipids in model membranes using Nearest-Neighbor-Recognition chemistry (NNR)
- Synthesized, purified, and characterized phospholipids, sterols, and small peptides for NNR experiments
- Extensively used NMR, HPLC, fluorescence, and UV-Vis spectrophotometry to characterize products
- Mentored undergraduate students in organic synthesis and analytical chemistry

Norwich Pharmaceuticals, Norwich, NY 2006-2007
Analytical Chemistry Intern

- Performed quality control analysis of pharmaceutical raw materials, finished products, and stability samples using a variety of techniques, including UV-Vis spectroscopy, IR spectroscopy, Karl Fischer titrations, and Raman spectroscopy in a cGMP environment
- Produced databases of past analytical results to improve the statistical analysis of trends

Colgate University, Hamilton, NY 2006
Bachelor of Arts, Chemistry, Magna Cum Laude
Advisor: Dr. Ernest Nolen
Honors Thesis: "Towards the Synthesis of a C-linked Galactosyl Serine Mimic"

- Synthesized and purified glycosylated amino acid analogs
- Characterized products by MALDI-TOF mass spectrometry and NMR

TEACHING EXPERIENCE

Teaching Assistant for Organic Chemistry Laboratories (Lehigh University) 2010-2011
Teaching Assistant for Organic Chemistry Laboratories (Colgate University) 2005-2006
Organic Chemistry Tutor (Colgate University) 2005-2006

PUBLICATIONS AND PRESENTATIONS

Daly, T. A., Almeida, P. F., Regen, S. L., (2012) Sorting of Lipidated Peptides in Fluid Bilayers: A Molecular-Level Investigation. *J. Am. Chem. Soc.*, *134,* 17245-17252.

Daly, T. A., Almeida, P. F., Regen, S. L., "A Molecular Level View of Lipid Sorting in a Model Membrane" 244th ACS National Meeting, August 2012 in Philadelphia, PA.

Janout, V., **Daly, T. A.**, Cline, L. L., Kulp, L. J., Regen, S. L., (2012) Stimulated Release of Cholesterol from Liposomal Membranes by a PEGylated Phospholipid. *Bioconjugate Chem.*, *23*, 336-339.

Daly, T. A., Wang, M., Regen, S. L., "The Origin of Cholesterol's Condensing Effect" Biophysical Society Regional Networking Meeting, November 2011 in Hershey, PA.

Daly, T. A., Wang, M., Regen, S. L., (2011) The Origin of Cholesterol's Condensing Effect. *Langmuir*, *27*, 2159-2161.

Nolen, E. G., Donahue, L. A., Greaves, R., **Daly, T. A.,** Calabrese, D. R., (2008) Synthesis of α- and β-C-Glucopyranosyl Serines from a Common Intermediate. *Organic Lett., 10,* 4911-4914.

Daly, T.A. and Nolen, E. G. "Ring Closing Metathesis Approach to the Synthesis of a C-linked Galactosyl Serine Mimic" 231st ACS National Meeting, March 2006 in Atlanta, GA.

AWARDS AND AFFILIATIONS

Lehigh University Fellowship (2007-2009)

Colgate University Honors in Chemistry

Colgate University Distinction in the Liberal Arts CORE Curriculum

Phi Eta Sigma National Honor Society

American Chemical Society Member (2007-Present)

.